HAL
open science

Carbon cycling across the human-impacted Seine River basin : from the modeling of carbon dioxide outgassing to the assessment of greenhouse gas emissions

Audrey Marescaux

To cite this version:

Audrey Marescaux. Carbon cycling across the human-impacted Seine River basin : from the modeling of carbon dioxide outgassing to the assessment of greenhouse gas emissions. Hydrology. Sorbonne Université, 2018. English. NNT : 2018SORUS479 . tel-02924855v2

HAL Id: tel-02924855

https://theses.hal.science/tel-02924855v2

Submitted on 28 Aug 2020

HAL is a multi-disciplinary open access archive for the deposit and dissemination of scientific research documents, whether they are published or not. The documents may come from teaching and research institutions in France or abroad, or from public or private research centers.

L'archive ouverte pluridisciplinaire **HAL**, est destinée au dépôt et à la diffusion de documents scientifiques de niveau recherche, publiés ou non, émanant des établissements d'enseignement et de recherche français ou étrangers, des laboratoires publics ou privés.

Sorbonne Université

ED 398 - Géosciences Ressources Naturelles et Environnement

FR 636 IPSL / UMR 7619 METIS

Carbon cycling across the human-impacted Seine River basin:

from the modeling of carbon dioxide outgassing

to the assessment of greenhouse gas emissions

Audrey Marescaux

Thèse de doctorat de Biogéochimie

Dirigée par Josette Garnier et encadrée par Vincent Thieu

Présentée et soutenue publiquement le 11.12.2018

Devant un jury composé de :

Steven Bouillon	Pr. Katholieke Universiteit Leuven	Rapporteur
Damien Cardinal	Pr. Sorbonne Université (Paris)	Examinateur
Alexandra Coynel	MC Université de Bordeaux	Examinatrice
Josette Garnier	DR CNRS (Paris)	Directrice de thèse
Emmanuel Soyeux	Expert Veolia VERI (Maisons-Laffitte)	Examinateur
Vincent Thieu	MC Sorbonne Université (Paris)	Encadrant de thèse
Julien Tournebize	Ingénieur Chercheur (Antony)	Rapporteur
Lauriane Vilmin	Dr Utrecht University	Examinatrice

Except where otherwise noted, this work is licensed under
http://creativecommons.org/licenses/by-nc-nd/3.0/

Carbon cycling across the human-impacted Seine River basin

from the modeling of carbon dioxide outgassing to the assessment of greenhouse gas emissions

Audrey Marescaux

UMR 7619 – METIS
Case courrier 105
4 place Jussieu75252
Paris cedex 05

Sorbonne Université
Ecole doctorale GRNE
Campus Jussieu
75252 Paris cedex 05

Version compilée le 10 janvier 2019

Remerciements

Embarquée dans le tourbillon de cette thèse, ces trois belles années ont filé. Lors de cette course folle, j'ai pu compter sur d'innombrables soutiens : les vieilles branches depuis toujours, les nouvelles personnes rencontrées et celles qui bouleversent ma vie. Je tiens à remercier toutes les personnes qui ont contribué à la réalisation de ma thèse ainsi que toutes celles qui m'ont soutenue.

Tout d'abord, je remercie mon jury de thèse pour l'intérêt et le regard critique qu'il a porté sur mes travaux de thèse : Steven Bouillon, Damien Cardinal, Alexandra Coynel, Josette Garnier, Emmanuel Soyeux, Vincent Thieu, Julien Tournebize, Lauriane Vilmin.

Je voudrais remercier Josette Garnier et Vincent Thieu qui m'ont dirigée et encadrée avec une énergie, une disponibilité et une patience mémorables. Josette, après ces trois années, je reste impressionnée par ta connaissance dans tant de domaines ainsi que ta rapidité à établir des liens entre eux. Je te remercie d'avoir eu la patience que j'apprenne à mon rythme. Vincent, je te remercie pour ta sérénité, ta tolérance et ta simplicité à décrire des processus complexes. Ta pédagogie et ton humour m'ont apaisée et aidée à progresser. Votre complémentarité combinée à vos exigences scientifiques ont fait de moi la chercheuse que je suis devenue. Proche de cet encadrement, toujours discret mais bien présent, je remercie mon compatriote Gilles qui a toujours pris le temps de répondre à mes questions avec le sourire.

Cette thèse n'aurait pas pu être réalisée sans le travail de terrain effectué avec Benjamin, Sébastien, Abdel et Anun. Je vous remercie pour toutes ces campagnes de terrain inoubliables. Merci de m'avoir accueillie dans l'équipe et formée à de nouvelles techniques. J'ai passé de très bons moments avec vous, en échantillonnant sous la neige ou le soleil. Je remercie également Anun d'avoir géré le laboratoire et les analyses comme une fée.

J'ai eu la chance, humainement et scientifiquement, de travailler avec Goulven, je te remercie énormément pour ton investissement dans nos travaux.

Ma thèse s'est déroulée dans le cadre des programmes PIREN-Seine et C-CASCADES. Ces programmes ont enrichi ma thèse grâce aux différents échanges scientifiques et humains. I would like to thank all the members of the C-CASCADES program, and especially all the 14 PhD students (Adam, Anna, Anna, Andre, Asa, Domitille, Fabrice, Hélène, Jens, Jo, Marie, Matteo, Philip, Simon), and Emily, and Pierre[2]. Our meetings, workshops, and summer school were and would not have as enjoyable without your company. I look forward to working with you in the future (TOTEM forever). Je remercie également Nathalie Gypens et Alberto Borges pour leur collaboration scientifique.

Je suis reconnaissante à l'école doctorale, Dovy Tristani dont l'aide et la bienveillance m'ont été précieuses, et les directeurs qui se sont succédés : François Baudin et Loïc Labrousse. Je remercie également les membres du personnel de METIS (dont Alban, Aurélien, Bénédicte, Christophe, Nadine, Valérie) et de l'IPSL (Sophie, Mehdi) ainsi que le directeur de l'UMR METIS Jean-Marie Mouchel.

Je remercie également tous les autres membres du laboratoire. Mélanie qui m'a accueillie dès mon premier jour et guidée dans le labyrinthe de Jussieu. Tous nos trajets à vélo m'ont permis de relâcher

la pression. Marie et ses valeurs encrées ainsi que sa gentillesse m'ont souvent aiguillée dans mes décisions. Je te remercie d'avoir été là et de m'avoir soutenue à travers toutes mes phases. J'en profite pour notifier que Cyril et François ont été indispensables lors de nos présentations à Hawaii. Je remercie également Philipe et Virginie qui m'auront fait découvrir le Teddy's. Julia, j'ai apprécié nos dégustations de bières donnant lieu à des discussions mémorables. Antsiva, ta bonne humeur aura égayé ma thèse. Alexandre, Agnès, Beyoncée, Fabrice, Elsa, Marc, Paul, Nicolas, Raphaël et Sylvain, je vous remercie pour vos gestes de soutien (dont les pâtisseries, bonbons et chocolats !). A tous les cyclistes, la Loire à vélo restera un moment phare de ma thèse.

Je souhaite une excellente poursuite de thèse aux doctorants en cours et qui m'ont particulièrement soutenue ce dernier mois. Je remercie donc Diane (je te lègue la charge BD et l'expression « faire une Audrey ») ; la calme Salma qui aime les sensations fortes ; Mohammed pour son sourire colgate; Noëlie qui a les bacs piscine pour la prochaine canicule ; Ningxin et le meilleur thé du monde ; Ardalan à qui je souhaite le meilleur ; et Mounir et ses fous rires.

Je remercie également Danièle, Florence, Ludo, Matthieu, Michel, Nicolas, Pierre, Sylvie, Thomas, Valérie pour tous ces midis partagés à parler de sciences ou de vacances. Ainsi qu'Hafida et Thushanty, qui ont permis qu'on travaille toujours dans un environnement impeccable.

Je voudrais également remercier ma famille pour leur soutien inconditionnel. Ma petite maman qui sauta plus d'une fois dans un Thalys pour un verre de rouge et un souper improvisé pour me réconforter, me motiver ou juste pour profiter d'être ensemble. Ma sœur (et Juju), que j'admire pour la façon dont elle gère sa vie et ses ambitions, et dont les valeurs plus que tout le reste nous rapprochent. Je remercie mon frère Robin (et Pépito), pour leur regard décalé sur la vie, et ma grand-mère, pour m'avoir hébergée et nourrie pendant les périodes intenses de mes études. Je suis reconnaissante à Pierre, de prendre soin de moi de loin. Je remercie Cerise et Adrien qui malgré mon emploi du temps, m'ont accordé leur confiance. Léonie, il me tarde de rattraper le temps avec toi. Je remercie également mon père qui me déposa il y a 20 ans sous la Tour Eiffel. Amoureux de la littérature, de la peinture, de la musique, nos discussions m'auront donné une bouffée d'air vital pendant ces trois années.

Je remercie mes colocs Charlotte, Marianne, Marie, Maud, Sarah et presque colocs (Hari, Lies, Max) qui font que la vie à Paris est plus douce. Je remercie La Fondation Biermans Lapôtre pour son soutien et toutes les personnes que j'y ai rencontrées (dont Loïc et Joël). Je remercie particulièrement Sarah qui m'a accompagnée depuis mes premiers jours à Paris dans un marché de Noël danois (merci Marie), à aujourd'hui.

Je remercie la Belgique et tous les amis que j'ai hâte de revoir un peu plus. Carole et Jil, mes deux amies dont les questionnements me perdent et me réorientent. Carole, je te remercie pour ton super schéma. Cédric, Claire, Laëticia, Cédric, Pou, Sarah, Alizée, Jérôme, Aurore, Sébastien et Lily, je vous remercie d'avoir accepté de moins me voir mais de toujours répondre présent. Enfin, je remercie Pico d'avoir autant pris soin de moi, te découvrir fut l'imprévu transcendant.

Et Chopin, pour sa musique,

Résumé

Le cycle du carbone dans le bassin anthropisé de la Seine :

de la modélisation du dioxyde de carbone à l'évaluation des émissions des gaz à effet de serre.

Des études récentes ont souligné l'importance des émissions de dioxyde de carbone (CO_2) par les eaux continentales, replaçant ainsi l'hydro-système comme compartiment actif du bilan carbone. Un premier objectif de cette thèse a été de comprendre et quantifier la dynamique du C aquatique le long du continuum aquatique de la Seine, empreint d'une très forte activité anthropique. Pour cela, un module de carbone inorganique (CI) a été développé au sein du modèle de fonctionnement biogéochimique des écosystèmes aquatiques, Riverstrahler, permettant de simuler les variations spatio-temporelles du C. Le second objectif était de quantifier les émissions aquatiques et terrestres afin de proposer une évaluation conjointe des trois principaux gaz à effet de serre (GES: CO_2, méthane – CH_4, protoxyde d'azote- N_2O) à l'échelle du bassin.

Les mesures de la pression partielle de CO_2 (pCO_2) dans des rivières drainant différentes occupations du sol, à différentes saisons, attestent que l'hydro-système Seine est sursaturé et une source d'émission de CO_2 vers l'atmosphère. Le principal facteur de contrôle de pCO_2 est la concentration en carbone organique dissout (COD) ($R^2 = 0,56$, $p < 0,05$), modulée par les conditions hydro-climatiques et les contributions d'eaux souterraines. Dans les rivières amont, les concentrations en COD semblent reliées au stock de CO des sols, alors que sur l'axe principal de la Seine, elles dépendent des effluents de stations d'épuration. Sur le long terme (1970-2015) la pCO_2 a clairement évolué conjointement à l'amélioration du traitement des eaux usées.

Les bilans par modélisation (moyenne 2010-2013) montrent l'importance du CI apporté à l'hydro-système Seine (1138 ktC an^{-1}) et une faible contribution des processus biogéochimiques (27 ktC an^{-1}). Si une grande part du CI est exportée vers l'estuaire (69%), les émissions de CO_2 dépassent 360 ktC an^{-1} (soit 30%). Les apports de carbone organique ne représentent que 104 ktC an^{-1}. La production nette de l'écosystème (NEP) apparait négative, et indique le caractère hétérotrophe de la Seine. Cette nouvelle version du modèle Riverstrahler a été couplée au modèle estuarien C-GEM afin de proposer une description complète de la cascade du carbone dans le continuum rivière-estuaire. L'estuaire représente 34 % de la surface miroir de la Seine et contribue à hauteur de 23% des émissions aquatiques de CO_2 du bassin, estimée à 445 kt C (année 2010).

Les émissions de CO_2 complétées par celles de N_2O et CH_4 montrent que les émissions aquatiques de GES représentent 3.7% des émissions totales du bassin de la Seine (2,276 kt CO_2 équivalent an^{-1} dont 95,3% de CO_2). Les émissions agricoles (14,295 ktCO_2 équivalent an^{-1}) et urbaines (44,713 ktCO_2 équivalent an^{-1}) contribuent respectivement pour 23.3 et 73.0%. Une reconstruction historique des émissions agricoles en France montre une augmentation par 4 de 1850 à 2014, soit 114,000 kt CO_2 équivalent an^{-1} actuellement (CO_2:22%, CH_4:49%, N_2O: 29%). Un scénario prolongeant la tendance actuelle à la spécialisation et l'intensification à l'horizon 2040, prédit une augmentation par 1.5 des émissions agricoles, alors qu'un second scenario, proposant un changement profond de l'agriculture française, réduirait les émissions actuelles de 50%.

Mots clés: *Cycle du carbone, CO_2, CH_4, N_2O, émissions de GES, Modélisation des écosystèmes aquatiques, Bassin de la Seine, Impacts humains, continuum aquatique*

Abstract

Carbon cycling across the human-impacted Seine River basin:

from the modeling of carbon dioxide outgassing to the assessment of greenhouse gas emissions

Several recent studies have highlighted significant fluxes of carbon dioxide (CO_2) from inland waters in the global carbon cycling. The first main objective of this thesis was to quantify and understand carbon dynamics in the Seine River basin, which is deeply impacted by human activities. For this purpose a new inorganic carbon (IC) module was implemented in the biogeochemical Riverstrahler model, to simulate spatial and temporal variations in carbon forms in the drainage work. A second major objective was to size both aquatic and terrestrial emissions as a part of a joint assessment of three main GHGs (CO_2, methane –CH_4, and nitrous oxide –N_2O).

Field campaigns in rivers draining various land uses in different hydrological seasons, showed a supersaturation in CO_2 of the Seine hydrosystem leading to CO_2.emissions to the atmosphere. The main factor controlling the CO_2 partial pressure (pCO_2) was the concentration of dissolved organic carbon (DOC) (R^2=0.56, n=119, $p<0.05$), modulated by hydro-climatic conditions and groundwater contribution. In small streams, DOC concentrations were dependent on the soil organic carbon stock. For the main stem, a long-term analysis (1970-2015) showed that pCO_2 tracked urban pollution, decreasing from the 2000s after improvement of wastewater treatment.

The validation of the IC module newly implemented in Riverstrahler showed that IC inputs to the Seine River dominated the overall carbon budget (1138 ktC yr^{-1} on average for the period 2010-2013) of which less than 2% was produced from biogeochemical processes (27 ktC yr^{-1}). In addition, CO_2 outgassing represented 30% of IC outputs while exports to the estuary represented 69% of IC outputs. OC inputs were comparatively lower, accounting only for 104 ktC yr^{-1}. Analysis of the biogeochemical processes of the Seine River showed a negative net ecosystem production (NEP), the river being mostly heterotrophic.

In order to complete the modeling of the fate of carbon in the Seine River, the Riverstrahler model was combined with the estuarine C-GEM model, towards an integrated approach to the Land-to-Ocean Aquatic continuum. Representing 34% of the river mirror area, the estuary thus contributes ~23% of the CO_2 emitted from the whole estuary-river aquatic continuum (estimated at 445 kt C for the year 2010).

In addition, analyses of available institutional databases and measurements of other GHGs (CH_4 and N_2O) enabled estimation of aquatic emissions at 3.7% of the Seine basin total emissions (2,276 ktCO_2 equivalent yr^{-1}), dominated by CO_2 (95.3%), while agricultural (14,295 ktCO_2 equivalent yr^{-1}) and urban emissions (44,713 ktCO_2 equivalent yr^{-1}) accounted for 23.3% and 73.0%, respectively. A historical reconstruction of agricultural emissions for the whole of France (1850-2014) estimated that, among the 114,000 ktCO_2 equivalent yr^{-1} emitted by the agricultural sector, 22% were represented by CO_2, 49% by CH_4 and 29% by N_2O. Finally, two contrasting scenarios were explored (horizon 2040). The first, characterized by the current trend towards specialization and intensification, predicted an almost 1.5-fold increase in agricultural emissions. While the second, characterized by a transition to organic agriculture and dietary change, would reduce current emissions by about 50%.

Keywords: *Carbon cycling, CO_2, GHG emissions, aquatic ecosystem modeling, Seine River basin.*

Foreword

This PhD thesis manuscript is composed of two parts and study axes. The first part: "*Carbon dioxide in the Seine aquatic continuum: Observations and modeling*" focuses on the hydrosystem and reports on the understanding of CO_2 dynamics and the quantification of the outgassing. This part includes one published scientific article in *Scientific Reports*, and two papers in preparation for submission, one to *Water Research* and one to *Frontiers* forming respectively Chapters 1, 2 and 3.

The second part of the manuscript: "*Greenhouse gas (CO_2, CH_4, N_2O) emissions from the Seine basin*" compares CO_2 with CH_4 and N_2O concentrations and emissions in the hydrosystem but also from agricultural and nonagricultural areas. The first article in this part was published in *Science of the Total Environment*, and focused on the comparison of the different sources in the Seine basin. The second article has also been accepted to *Science of the Total Environment*. These two papers form the Chapters 4 and 5. A general conclusion and future perspectives are proposed.

The C-CASCADES project (https://c-cascades.ulb.ac.be/) of which this thesis is part, received funding from the European Union's Horizon 2020 research and innovation program under the Marie Sklodowska-Curie grant agreement No. 643052.

Table of contents

LIST OF FIGURES ..... **XI**

LIST OF TABLES ..... **XIX**

INTRODUCTION **1**

0.1. Overview of the global carbon cycle *2*

0.2. New paradigm of inland water as an active component of the carbon cycle *5*

0.3. Carbon dioxide evasion as a result of cascades of biogeochemical and physical processes *6*

0.3.1. Carbon from terrestrial landscapes 6

0.3.2. Understanding CO_2 evasion processes 9

0.4. Carbon dynamics along the aquatic continuum: *13*

0.5. Lesson learned from contrasted regional climates about CO_2 evasion *15*

0.5.1. Sub-tropical regions: a hotspot of aquatic CO_2 emission 15

0.5.2. Artic regions: slowly releasing CO_2 sequestered in permafrost 16

0.6. Focus on carbon dioxide evasion control in temperate hydrosystems imprinted by human activities . *18*

0.6.1. Hydrological influence 18

0.6.2. Land use and impact of modern agricultural practices 18

0.6.3. Organic pollution from urban effluents 19

0.6.4. River management 19

0.7. Replacing CO_2 evasion as a part of regional GHG emissions *20*

0.7.1. GHG riverine emissions 21

0.7.2. GHG direct emissions 23

0.8. The Seine river basin: a temperate system highly impacted by humans *24*

0.8.1. Key features of the regional Seine basin 24

0.8.2. State of research on carbon dynamics in the Seine River 26

0.8.3. Ecological functioning of the Seine River: the Riverstrahler model 27

0.9. Objectives of the thesis research *30*

CARBON DIOXIDE IN THE SEINE AQUATIC CONTINUUM: OBSERVATIONS AND MODELING **33**

1 SEASONAL AND SPATIAL VARIABILITY OF THE PARTIAL PRESSURE OF CARBON DIOXIDE IN THE HUMAN-IMPACTED SEINE RIVER IN FRANCE 37

1.1. Introduction *39*

1.2. Materials and methods *40*

1.2.1. Study site 40

1.2.2. Sampling strategy, physical-chemical analysis and direct measurements of pCO_2 42

1.2.3. pCO_2 calculations from existing data 43

1.2.4. Determination of gas transfer velocities 44

1.2.5. Statistical tests 46

1.3. Results *46*
1.3.1. Measured versus calculated pCO_2 46
1.3.2. Field campaign dataset overview 47
1.3.3. Variability in pCO_2 48
1.3.4. pCO_2 environmental controls 54
1.4. Discussion *56*
1.4.1. pCO_2 supersaturation of the Seine hydrosystem 56
1.4.2. Hydro-climatic controls on pCO_2 57
1.4.3. Control of pCO_2 by the soil organic carbon stock 58
1.4.4. Control of pCO_2 by urban effluents: long term evidence 59
1.4.5. Limits of the approach 60
1.5. Conclusions *61*
1.6. Annex *63*
1.6.1. Annex 1-1: Location of sampling stations used during the field campaigns in 2016-2017 63
1.6.2. Annex 1-2 : Direct pCO2 measured during the four field campaigns vs nutrients 64
2 MODELING INORGANIC CARBON DYNAMICS IN THE SEINE RIVER CONTINUUM IN FRANCE 67
2.1. Introduction *69*
2.2. Material and methods *71*
2.2.1. Description of the Seine basin 71
2.2.2. The pyNuts-Riverstrahler model and its biogeochemical model, RIVE 75
2.2.3. Development of an inorganic carbon module 76
2.2.4. Documenting input constraints of the pyNuts-Riverstrahler model 80
2.2.5. Observations data 84
2.3. Results *85*
2.3.1. Validation of spatial and seasonal variations of pCO_2 85
2.3.2. Inorganic and organic carbon budgets 88
2.3.3. Carbon aquatic processes 89
2.4. Discussion *92*
2.4.1. Validation of the model 92
2.4.2. Export fluxes 93
2.4.3. Metabolism 94
2.5. Conclusion *96*
2.6. Annex *98*
2.6.1. Annex 2-1 : List of state variables of the Rive model 98
2.6.2. Annex 2-2: Kinetics and parameters of the Rive model (updated from Garnier et al., 2002). 99
2.6.3. Annex 2-3: Modeling objects of the Seine basin 101
2.6.4. Annex 2-4: Description of the inorganic carbon module implemented in pyNuts-Riverstrahler 102
2.6.5. Annex 2-5 Representation of superficial MESO water bodies 108
2.6.6. Annex 2-6: Sampling strategies and protocol for the sampling of wastewater treatment plants sampled in the Seine Basin 110
2.6.7. Annex 2-7: Relationships between alkalinity and water discharges or phytoplankton 111

2.6.8. Annex 2-8: Impact of the choice of the gas transfer velocity formalisms and the water effluent discharges on the main stem CO2 concentrations. ... 111

3 CARBON DYNAMICS ALONG THE SEINE RIVER NETWORK: INSIGHT FROM A COUPLED ESTUARINE/RIVER MODELING APPROACH 113

3.1. Introduction ... 115

3.2. Methods ... 117

3.2.1. Study area ... 117

3.2.2. Modeling strategy ... 118

3.2.3. Modeling chain description ... 120

3.2.4. Simulations Set-up ... 126

3.3. Results ... 128

3.3.1. Model validation ... 128

3.3.2. Carbon dynamics ... 136

3.4. Discussion ... 140

3.4.1. Interests and weaknesses of the approach ... 140

3.4.2. A carbonate module in the land-ocean aquatic continuum. ... 141

3.4.3. Features and fates of Carbon in LOAC at regional scale ... 142

3.5. Conclusions ... 143

GREENHOUSE GAS (CO_2, CH_4, N_2O) EMISSIONS FROM THE SEINE BASIN ... 147

4 CARBON DIOXIDE, METHANE AND NITROUS OXIDE EMISSIONS FROM THE HUMAN-IMPACTED SEINE WATERSHED IN FRANCE ... 151

4.1. Introduction ... 155

4.2. Material and methods ... 157

4.2.1. Study site ... 157

4.2.2. Sampling strategies ... 158

Eleven field campaigns were conducted at 23 sampling locations over a distance of 700 km (exact locations in Annex 1-6). Sampling sites were selected to account for the spatial variability of the upstream basin along the Marne River, upstream and downstream from the main WWTPs, including Paris, and along the lower Seine. The 11 field campaigns at low water were conducted in 2010 (May 3–4 May; July 5–7; October 2–6 2010), in 2011 (May 17–19; August 23–28), in 2012 (April 4–10; August 28 to September 3), in 2013 (February 13–18; June 17–23 2013), and in 2014 (May 13–17; September 9–12). In addition to these longitudinal profiles, smaller SOs were sampled during two snap-shot campaigns in 2016 (February 22 to March 10, and September 7–14) and one in 2017 (March 14–23). A total of 14 campaigns are therefore analyzed here. Sampling locations covered all important land use classes in the basin. ... 158

4.2.3. Gas analyses ... 159

4.2.4. Calculation of indirect and direct emissions ... 161

4.2.5. Statistical analyses ... 164

4.3. Results ... 164

4.3.1. Greenhouse gas concentrations in the hydrological network ... 164

4.3.2. Greenhouse gas emissions from the hydrological network ... 168

4.3.3. Emissions from agricultural and nonagricultural sectors ... 170

4.3.4. Total GHG emissions from the Seine basin ... 170

4.4. Discussion *171*
4.4.1. Limits to our calculations of the emission 171
4.4.2. Patterns of indirect CO_2, CH_4, N_2O emissions from rivers in the drainage network: differences and similarities 172
4.4.3. Direct CO_2, CH_4, N_2O emissions from the Seine basin: agricultural and nonagricultural emissions 176
4.5. Conclusion *177*
4.6. Annex *178*
4.6.1. Annex 4-1. Lithology (Albinet, 1967) and stream orders (Strahler, 1952; 1957) in the Seine basin. 178
4.6.2. Annex 4-2. Relationships between direct and indirect pCO2. 178
4.6.3. Annex 4-3 Spatial and seasonal variations in gas transfer velocities (k) of CO2, CH4 and N2O 179
4.6.4. Annex 4-4 Greenhouse gas concentrations ([GHG]) and fluxes (fGHG) with associated standard deviations and 95% confidence intervals averaged by season and by stream order. 180
4.6.5. Annex 4-5 Results of the statistical differences between mean of greenhouse gas concentrations by stream order. 181
4.6.6. Annex 4-6 Exact locations, mean and standard deviations of water quality parameters (chlorophyll a (Chl. a), total alkalinity, pH, dissolved oxygen (O2), and dissolved silica (DSi)) of the sampling stations located along the main stem of the basin. 182
5 LONG TERM CHANGES IN GREENHOUSE GAS EMISSIONS OF FRENCH AGRICULTURE AND LIVESTOCK (1852- 2014): FROM TRADITIONAL AGRICULTURE TO CONVENTIONAL INTENSIVE SYSTEMS 185
5.1. Introduction *189*
5.2. Material and methods *192*
5.2.1. Major physiographic and agricultural characteristics of France 192
5.2.2. Reconstruction of past land use and agricultural system 192
5.2.3. Reconstruction of greenhouse gas emissions 194
5.2.4. Exploring scenarios 199
5.2.1. Uncertainty analysis 200
5.3. Results *200*
5.3.1. Long-term trends of the control variables of GHG emissions 200
5.3.2. Agricultural features 203
5.3.3. Distribution of GHG emissions over the long term 205
5.3.4. Estimating GHGs under contrasted scenarios 206
5.3.5. Comparative agricultural GHG emissions in CO_2 equivalent 210
5.4. Discussion *212*
5.4.1. Controlling factors of GHG emissions 213
5.4.2. Past long-term changes in GHG emissions: practice and land use changes 216
5.4.3. Contrasted scenarios for a possible future 218
5.4.4. Weaknesses and strengths of the approach 219
5.5. Conclusions *221*

GENERAL CONCLUSION AND PERSPECTIVES 223

BIBLIOGRAPHY 231

List of figures

Fig. 0-1: CO_2 concentrations in the atmosphere from measurements in ice cores before 1958 (Etheridge et al., 1996; MacFarling Meure et al., 2006) and from the Mauna Loa observatory since 1958 (Scripps CO_2, Division Physical Sciences and NOAA Earth System Research Laboratory). 1

Fig. 0-2 Simplified schematic of the global carbon cycle retrieved from Ciais et al. (2013). Numbers represent carbon stocks in PgC (1 PgC = 10^{15} gC) and annual carbon exchange fluxes (in PgC yr^{-1}). Black numbers and arrows indicate reservoir mass and exchange fluxes estimated for the time prior to the Industrial Era, about 1750. Red arrows and numbers indicate annual 'anthropogenic' fluxes averaged over the 2000–2009 time period. These fluxes are a perturbation of the carbon cycle in the industrial era post 1750. 3

Fig. 0-3 Relative speciation (%) of carbon dioxide (CO_2), bicarbonate (HCO_3^-), and carbonate (CO_3^{2-}) in water according to pH retrieved from Pedersen et al. (2013). Speciation was computed with CurtTiPot (Gutz, 2012) using pK_1=6.532 and pK_2=10.329 at 20°C with electrical conductivity of 250µS cm^{-1} (Schwarzenbach and Meier, 1958). 4

Fig.0-4 : Change in the perception of the role of inland water according to Cole et al. 2007, from (a) a passive pipe representation, to (b) a component transporting and transforming organic and inorganic carbon from land to sea 5

Fig. 0-5 Examples of direct techniques used to measure pCO_2 a) discrete technique using syringe headspace, b) continuous technique with the equilibrator, (source: Frankignoulle et al., 2001). 10

Fig. 0-6 Sources and magnitude of net CO_2 emissions along a theoretical stream-river continuum retrieved from Hotchkiss et al. (2015) describing how the external carbon inputs (carbon from the surrounding landscape and bedrock) are greater in upstream areas than downstream, which also leads to a proportionally larger CO_2 evasion flux upstream than downstream. ER is ecosystem respiration and GPP gross primary production. 14

Fig. 0-7 Atmospheric CH_4, and N_2O concentrations before the industrial era from year 0 to the year 1750 (left) and after (right). Concentrations were determined from air enclosed in ice cores and firn air (color symbols) and from direct atmospheric measurements (blue lines, measurements from the Cape Grim observatory) (MacFarling Meure et al., 2006). Source (Ciais et al., 2013)..... 20

Fig. 0-8 Conceptual model of controls of nitrogen gas emissions from soil via nitrification and denitrification (source Davidson, 1991). Illustration of the change in perception from linear denitrification to *"leaky pipe"*. 22

Fig. 0-9 General geographical features of the Seine basin in France. a. Drainage network of the Seine River system. b. Lithological and geological structure. c. Distribution of population density in the Seine basin

(data by commune INSEE, 2015) d. Land use in the Seine basin use according to Corine Land Cover (EEA, 2012). e. Main wastewater treatment plants in the basin. 25

Fig. 0-10 Schematic representation of the RIVE model of biogeochemical processes in river systems 29

Fig. 1-1 Maps of the Seine river basin created using QGIS software(QGIS Development Team, 2016). (a) The hydrographic network with Strahler orders from 1 to 7, main urban centers (carmine red dots), small stream sampling zones (S1, S2 and S3), main stream sampling sites (orange squares along the lower Seine and the Marne rivers, the three main reservoirs (blue squares) and the main wastewater treatment plant (grey dot). (b) Wastewater treatment plants in the Seine basin mapped according to their treatment capacity (AESN 2012); (c) Land uses in the Seine basin (CLC database, IFEN 2012)(IFEN, 2012); (d) Lithology of the Seine basin (Albinet, 1967; Albinet, 1967) 41

Fig. 1-2 Measured pCO2 vs. (a) pH (NBS scale); (b) water temperature (Water temp.); (c) total alkalinity; (d) comparison of calculated pCO2 (using pH, temperature, alkalinity) and direct measurements of pCO2. Green lines represent the 95% confidence intervals. 47

Fig. 1-3 Boxplots of pCO2 assembled as function of the land uses and seasons investigated. The lower, intermediate and upper parts of the boxes represent respectively the 25th, 50th and 75th percentiles and the empty circles represent the outlier values. (a) pCO2 measured in stream waters (order 1 to 4) draining wetlands, grasslands, forests and croplands during the 2016 and 2017 field campaigns (hydro-climatic conditions are listed in Table 1-1). (b) pCO2 calculated from existing bi-monthly pH, total alkalinity and water temperature data at the outlet of the Seine River (Poses station) from 2013 to 2015 and aggregated by the four seasons of interest (see Materials and Methods, pCO2 calculations) (Data source: AESN). .. 49

Fig. 1-4 Comparison of the physical characteristics of small streams (orders 1 to 4) and of the main stream (orders 5 to 7) of the Seine River, averaged by season (excluding spring flood measurements): (a) slopes of the streams or rivers; (b) water temperatures; (c) water velocities; (d) gas transfer velocities; (a-d) Whiskers represent standard deviations; (e) boxplots of CO2 emissions assembled according to land uses. The lower, intermediate and upper parts of the boxes represent respectively the 25th, 50th and 75th percentiles and circles represent the outlier values 50

Fig. 1-5 Calculated pCO2 dynamics during bloom events (Chl. a > 50 µg l-1) since the 1990s at the outlet of the Seine River, Poses (Data source: AESN)..... 51

Fig. 1-6 Seasonal variations in calculated pCO2 at the water temperaturer (pCO2) and at 10°C (pCO2@10°C) values compared with variations in water discharge and temperature values (at Poses) for the two periods: 1989–1991 (atmospheric pCO2 = 354 ppm) and 2013–2015 (atmospheric pCO2 = 399 ppm) 52

Fig. 1-7 Spatial variations in calculated pCO2 averaged over the two periods 1989–1991 (with high organic pollution) and 2013–2015 (after wastewater treatment had been improved). Values are represented for Strahler orders superiors to 2 (Data source: AESN) 53

Fig. 1-8 (a) Long-term variations in calculated pCO2 from 1970 to 2015 at two sites on the lower Seine River: at the entrance to Paris (blue curve) and at the river outlet at Poses downstream of the main WWTP Seine-Aval (black curve), the associated shaded areas represent the 95% confidence intervals (Data source:

AESN). The red dashed curve represents the biodegradable total organic carbon fluxes (BTOC) discharged from the main SAV WWTP into the Seine River. BTOC was estimated from the relationship BTOC = 0.35 BDO (R^2 = 0.91, n = 23) established by Servais et al. (1999) which converts biological demand in oxygen (BDO, provided in Rocher and Azimi, 2017) into BTOC; (b) Relationships between calculated pCO2 at Poses and BTOC from the main SAV WWTP. 54

Fig. 1-9 Relationships between measured pCO_2 and surface water quality variables according to the different land uses sampled during the field campaigns: streams draining forests, wetlands, arable lands, grasslands, mixed in the main stream when no dominant land use could be identified, and the Marne reservoir. (a) pCO_2 vs. dissolved organic carbon (DOC); (b) pCO_2 vs. dissolved inorganic carbon (DIC); (c) pCO_2 vs. dissolved oxygen (O_2); and (d) pCO_2 vs. chlorophyll a (Chl. a) 55

Fig. 1-10 Direct pCO_2 measured during the four field campaigns vs nutrients: silica (Si), phosphate (PO_4^-), total phosphorus (Ptot), ammonium (NH_4^+), nitrite (NO_2^-), and nitrate (NO_3^-). 64

Fig. 2-1 Characteristics of the Seine basin: a) the lithology according to Albinet, (1967). b) Drainage network according to Strahler stream orders (Strahler, 1952, 1957) Monitoring stations (I. Poses, II. Poissy (Downstream Paris), III. Paris, IV. Ferté-sous-Jouarre (Upstream Paris). c) The land use according to Corine Land Cover, with 6 simplified classes (EEA, 2012). d) Wastewater treatment plants of the basin. Red dots are the WWTPs sampled in 2018. 74

Fig. 2-2 Schematic representation of the ecological RIVE (inspired from Billen et al. 1994, Garnier & Billen, 1994), with grey lines indicating the main processes simulated in the water column and at the interface with the sediment (oxygen not shown), and the implementation of the new inorganic module, based on TA (maroon) and DIC (blue) lines. 77

Fig. 2-3 Boxplots of total alkalinity (µmol L^{-1}) and dissolved inorganic carbon (DIC, mgC L^{-1}) groundwater concentrations by grouping the MESO units. The lower, intermediate and upper parts of the boxes represent respectively the 25th, 50th and 75th percentiles and the circles represent the outlier values (source: ADES). 82

Fig. 2-4 Simulated and observed carbon dioxide concentrations in the Seine waters (CO_2, mgC-CO_2 l^{-1}) as a function of the stream order averaged on the period 2010 – 2013 (whiskers indicating standard deviations). 86

Fig. 2-5 Observed (dots) and simulated (line) mean carbon dioxide concentrations (CO_2, mgC L^{-1}) along the main stem of the Marne River (km −350 to 0) and the lower Seine River (km 0–350) averaged over the period 2010-2013. The simulation envelope (grey area) represents standard deviations of CO_2 simulated. Whiskers are standard deviations between observed CO_2 concentrations. 86

Fig. 2-6 Ten-days simulated (lines) and observed (dots) water discharges on the period 2010-2013 excepted for downstream SAV where water discharges where available only for 2012 (Q, m^3 s^{-1}), concentrations of carbon dioxide (CO_2, mgC L^{-1}, and CO_2 sat, mgC L^{-1}), dissolved inorganic carbon (DIC, mgC L^{-1}), total alkalinity (TA, µmol L^{-1}), pH (-), and phytoplankton (mgC L^{-1}). Simulation envelope corresponds to standard deviations. For observed data, whiskers are standard deviations. Four monitoring stations of

interest along the main stem Marne-Poses are shown: Ferté-sous-Jouarre (upstream Paris on the Marne River), Paris (upstream at Charenton), downstream SAV WWTP, and outlet of the basin (Poses). 87

Fig. 2-7. Instream processes involved in the inorganic carbon cycle simulated by pyNuts-Riverstrahler and averaged on the period 2010-2013 for the whole Seine river network. CO_2 outgassing (A. blue - yellow, mgC m^{-2} day^{-1}), net photosynthesis (B. blue – green, mgN m^{-2} day^{-1}), benthic (C. blue - violet) and heterotrophic planktonic (D. blue - orange) respiration (mgC m^{-2} day^{-1}) are represented in the hydrographic network. 90

Fig. 2-8 Metabolism of Strahler stream orders 1, 5, and 7 of the Seine basin simulated by pyNuts-Riverstrahler and averaged over the period 2010-2013. Net primary production (NPP, mgC m^2 day^{-1}), heterotrophic respiration (Het. respiration, mgC m^2 day^{-1}), net ecosystem production (NEP, mgC m^2 day^{-1}). Only the SO 1, 5, and 7 were represented as they showed the most different behaviors. Indeed, three patterns were observed one for SO1 to SO3, another one for SO4 and SO5, and the last one for SO6 and SO7. 91

Fig. 2-9. PyNuts-Riverstrahler modeling objects. 8 “Axis” objects (main river branches, mapped with red contours) and 72 “basin” objects (upstream tributaries connected to “axis” objects). 101

Fig. 2-10 Superficial MESO (Masse d’Eau SOuterraine) water bodies of the Seine basin grouped according to the lithology and geological ages 108

Fig. 2-11. Relationships between observations averaged by decades on the period 2010-2013 of a) alkalinity (µmol L^{-1}) and water discharges (m^3 s^{-1}), and b) alkalinity (µmol L^{-1}) and phytoplankton (mgC L^{-1}) at the four stations studied: upstream Paris (upstream), Paris, downstream SAV (Down. SAV), and at the outlet (Data source: AESN). 111

Fig. 2-12. Mean CO_2 concentrations along the main stem of the Seine River depending of a) gas transfer velocities according to O’Connor and Dobbins, (1958) (neglecting the wind); Raymond et al., 2012a, equation 5 in Table 2-2); Ho et al. (2016) (neglecting the wind). Black curve is the reference of our study and grey curve is a simulation with no gas transfer velocity. b) simulations with no discharge of TA and DIC from WWTPs. 67

Fig. 3-1 Map of the Seine river network including its main tributaries. The model extends upstream of Paris to the confluence with the Marne River 118

Fig. 3-2 Width and depth profiles of the Seine estuary from its mouth to Poses. Red dots correspond to observations while black lines correspond to the values used to constrain C-GEM’s geometry 121

Fig. 3-3 Simplified conceptual scheme of the share of state variables and processes between C-GEM and Riverstrahler models. The two models simulate nutrients as N (NO_3, NH_4), P (PO_4, Total P) Si (DSi, BSi in Riverstrahler only). In the Riverstrahler, both dissolved (DOC) and particulate (POC) carbon are modelled according to 3 classes of degradability (rapid, slow and refractory); heterotrophic bacteria (BAC) are described as large and small, and the zooplankton (ZOO) includes micro-crustaceans and rotifers-cillates 125

Fig. 3-4 Simulated tidal amplitude profiles along the Seine estuary under varying discharges (Q) and tidal coefficients (C). The black lines are simulated by C-GEM while the red dots are observations from the SHOM. 129

Fig. 3-5 Salinity (left panels) and SPM profiles (rights panels) along the Seine estuary for 6 dates. Dots correspond to measurements, while grey dots correspond to simulated values over 2 tidal cycle for salinity and 20 for SPM 131

Fig. 3-6 Time series for Chl. a, NH_4, NO_3, dSi, PO_4, O_2, DIC, TAlk, pH and pCO_2 at five stations along the main axis of the Seine. Red dots correspond to measurements while black lines correspond to simulation outputs..... 135

Fig. 3-7 Longitudinal profiles along the main axis of the Seine of the different processes affecting the DIC (a, c) and TOC pools (b, d). In the top panels (a, b), the process rates are integrated over the Seine's width while they are reported per surface area in the bottom panels (c, d). Zero is the mouth of the estuary in Le Havre, vertical dashed lines, represent Poses, Paris corresponds to the km 370..... 136

Fig. 3-8 Organic (green) and inorganic carbon budget (blue) for the Seine river network. All fluxes are expressed in Gg C yr^{-1}. The surface area all the different sub-sections of the watershed are indicated in italic. 139

Fig. 4-1 Population density and main wastewater treatment plant capacities of the Seine River watershed (France) (INSEE, 2013 and the French water authorities - AESN 2005). In yellow, measurement stations located along the main stem of the Seine River (Marne River and the lower Seine) were sampled in 2010 (May 3–4; July 5–7; October 2–6 2010) in 2011 (May 17–19; August 23–28), in 2012 (April 4–10; August 28 to September 3), in 2013 (February 13–18; June 17–23 2013) and 2014 (May 13–17; September 9–12). One of the main stems of the Seine River is shown at the top of the figure with sampling stations and distance from Paris in kilometers (km=0). 158

Fig. 4-2 Greenhouse gas (CO_2, CH_4, N_2O) concentrations in water (µgC-CO_2.l^{-1}, µgC-CH_4 l^{-1} and µgN-N_2O l^{-1}) as a function of the stream order in the Seine drainage network in winter and summer averaged from the 14 campaigns conducted between 2010 and 2017. Whiskers are standard deviations between observed GHG concentrations. 165

Fig. 4-3 Greenhouse gas (CO_2, CH_4 and N_2O) and oxygen concentrations along the main stem of the Marne River (km −400 to 0) and the lower Seine River (km 40–400). Averaged concentrations for (left) nitrous oxide (N_2O), ammonium (NH_4^+) and nitrite (NO_2^-) in mgN l^{-1}; (right) carbon dioxide (CO_2) and methane (CH_4) in µgC l^{-1}, dissolved organic carbon (DOC) in mgC l^{-1}, and dissolved oxygen in mgO_2 l^{-1}. The pCO_2 values were calculated from pH, temperature and alkalinity using CO2SYS software (Pierrot et al., 2006). These data are partly described in Garnier et al. (2009 and 2013). 166

Fig. 4-4 Relationships between (a) concentrations of N_2O (µgN l^{-1}) and NO_2^- (mgN l^{-1}), (b) concentrations of N_2O (µgN l^{-1}) and NH_4^+ (mgN l^{-1}), (c) CO_2 (µgC l^{-1}) and oxygen (mgO_2 l^{-1}), and (d) CO_2 (µgC l^{-1}) and dissolved organic carbon (DOC: mgC l^{-1}). From top to bottom, example from the campaigns in May 2010, September 2012, September 2013 and September 2014. 167

Fig. 4-5 Greenhouse gas emissions (CO_2, CH_4 and N_2O) from nonagricultural sectors (Gg CO_2eq yr^{-1}) in the Seine watershed including energy transformation-manufacturing, service sector, and transport (GIS treatments applied to CITEPA data; https://www.citepa.org/fr/, 2018/01/05) 170

Fig. 4-6 Greenhouse gas emissions (CO_2, CH_4 and N_2O in Gg CO_2eq yr^{-1}) from the Seine hydrographic network and those from the watershed, divided into agricultural and nonagricultural (GIS treatments applied to CITEPA data; *https://www.citepa.org/fr/*, last accessed 2018/11/05); Data for Ile-de-France are from Wu et al. (2016) and Staufer et al. (2016). 171

Fig. 4-7 Greenhouse gas (CO_2, CH_4 and N_2O) emissions from the Seine hydrographic network (yearly average of 14 campaigns (2010–2017). The pie charts represent the proportion of GHG emissions expressed in GWP. Percentage contributions are given for small (1st to 2nd SO), intermediate (3rd to 5th SO) and large (6th to 7th SO) rivers in the Seine watershed..... 173

Fig. 4-8 Schematic representation of the sources of CO_2, CH_4 and N_2O emissions from the Seine hydrosystem. OM: organic matter; NH_4^+: ammonium 174

Fig. 4-9 Map of the lithology (Albinet, 1967) and stream orders (Strahler, 1952; 1957) in the Seine basin. 178

Fig. 4-10 Gas transfer velocity for CO2, CH4, N2O calculated according to the fifth equation in table 2 in Raymond et al. (2012) as a function of stream order (SO) in the Seine basin in winter (blue) and in summer (red). Whiskers are standard deviations between observed GHG concentrations 179

Fig.5-1. General characteristics for France of a. climate from hydroecoregion; b. agricultural patterns; c. homogenous agricultural regions (33) and perimeter of three supra-regions chosen for their identical surface area and their trend for agricultural specialisation..... 193

Fig. 5-2. Evolution of the coefficient of mechanisation from 1906 (zero mechanisation) to 1980 (100% mechanisation) as calculated from changes in the number of horses for each of the 33 regions. The coefficient is given here for France and three contrasted regions. Agriculture modernisation appeared earlier in Ile-de-France..... 198

Fig. 5-3. Long-term evolution (1850–2014) for France and the three supra-regions selected in the annual average of a. temperature; b. rainfall. Long-term evolution of major indicators of agriculture in France and the three supra-regions selected for the 22 dates analysed; c. total exogenous N inputs; d. livestock size in terms of livestock units (LU). Left axis is for the three regions of interest and right axis is for the entire France. 201

Fig. 5-4. Maps of regional distributions in France for three dates (1906, 1970, 2014) representative of major time periods: a. cereal production; b. livestock density; c. percentage of permanent grassland in total agricultural area; d. percentage of forest in rural area (i.e. cropland + grassland + forest). UAA, utilised agriculture area. 204

Fig. 5-5. Maps of regional distributions in France for three dates (1906, 1970, 2014) representative of major time periods of GHG emissions per km^2 of rural areas and per year: a. N_2O; b. CH_4; c. CO_2. See legend of Figure 4 for the names of the regions. 206

Fig. 5-6. Maps of regional distributions in France for present (2014) and for two prospective scenarios (O/S: opening and specialisation and A/R/D) of GHG emissions per km^2 and per year: a. N_2O; b. CH_4; c. CO_2. See legend of Figure 4 for the names of the regions. 207

Fig. 5-7. Long-term evolution (1852–2014) for France (a.) and the three selected supra-regions (b., c., d.) in annual average of N_2O, CH_4 and CO_2 from top to bottom. N_2O is represented for the three major land uses (forest, grassland and cropland), CH_4 for manure and enteric emissions, and CO_2 as energy for imported feed, fertiliser production and other energy, including field work, machinery and livestock breeding. Error bars provide uncertainties as calculated by the Monte Carlo analysis. 209

Fig. 5-8. Long-term evolution (1852–2014) for France (a.) and the three selected supra-regions (b., c., d.) in annual average of N_2O, CH_4 and CO_2, expressed in CO2 equivalents per year. Error bars provide uncertainties as calculated by the Monte Carlo analysis. 211

List of tables

Table 0-1 Examples of pCO_2 concentrations along different stream-river continuums in several tropical, temperate and artic regions. All values are direct pCO_2 measurements except for *Kempe et al. 1982.... 17

Table 1-1.Summary of the field data set. Median, 10th and 90th percentiles pH (measured on the NBS scale), water temperature, total alkalinity, dissolved organic carbon (DOC), dissolved inorganic carbon (DIC), total suspended solids (TSS), chlorophyll a (Chl. a), dissolved oxygen (O_2) and conductivity. Mean water discharges are showed for seasons at the outlet of the basin..... 48

Table 1-2 : Location of sampling stations used during the field campaigns in 2016-2017. Measurements undertaken: carbon dioxide partial pressure, dissolved organic carbon, particular organic carbon, dissolved organic carbon, particular inorganic carbon, dissolved oxygen, total suspended solids, water temperature, pH, total alkalinity, silica, NH_4^+, NO_3^-, NO_2^-, PO_4^-, Ptot. 63

Table 2-1 Mean characteristics of the Seine River watershed by Strahler stream order. 73

Table 2-2 Stoichiometry of the biogeochemical processes, influencing dissolved inorganic carbon and total alkalinity in freshwaters taken into account in the new inorganic carbon module..... 78

Table 2-3 Summary of the carbon related inputs of the pyNuts-Riverstrahler model..... 84

Table 2-4 Inorganic and organic carbon budget in the Seine hydrosystem (kgC km^{-2} yr^{-1}) as calculated by the pyNuts-Riverstrahler model averaged on the period 2010-2013. *Net sediment loss is the difference between the erosion and the sedimentation calculated by the model 89

Table 2-5 Parameters used in the inorganic carbon module for freshwaters..... 107

Table 2-6 Mean concentrations and standard deviations of total alkalinity (µmole L^{-1}) and dissolved inorganic carbon (mgC L^{-1}) grouped by MESO water bodies of the Seine Basin (2010-2015)..... 109

Table 2-7. Location of the sampled WWTPs. Their capacity and type of treatment are indicated. Values for TA, DIC, pH and pCO_2 are gathered..... 110

Table 3-1 State variables of C-GEM and boundary conditions..... 119

Table 3-2 Geometrical and hydrodynamic parameters in the idealized geometry of the Seine estuary. 121

Table 4-1 Parameters of the linear relationships (slope and R^2) of N_2O as a function of nitrite (NO_2^-) and ammonium (NH_4^+), and of CO_2 as a function of oxygen (O_2) and dissolved organic carbon (DOC) for each of the 11 campaigns. Corresponding values of mean discharges and temperatures (temp) for the duration of the campaign are indicated. *Slope significantly different from 0 for $R^2 > 0.16$ ($n > 20$)..... 168

Table 4-2 Comparative greenhouse gas (Gg CO_2 eq yr^{-1} of CO_2, CH_4 and N_2O) emissions from the hydrographic network (measurements made in this study), from the agricultural basin (including croplands, grasslands and forests according to Garnier et al. (2009 and 2013) and from nonagricultural sectors (data from

CITEPA 2005 and from Wu et al. (2016) for the Ile-de-France region).∑ GHG: sum of the three GHGs by compartment and by gas. 169

Table 5-1. a. Summary of the data gathered for establishing relationships between N_2O emissions and its controlling factors, *n*=394, number of data. Relationships, and associated parameter values: b. for cropland and grassland and c. for forest. NRMSE and bias are calculated for evaluation of the fitted relationships. 195

Table 5-2. Empirical relationship for calculating excretion rates (y, in kgN head^{-1} yr^{-1}) of cattle, sheep, pig and horses as a function of time (t, in year) over the period 1850-2014, and corresponding values of the parameters b, a, a', tmax and dt, calibrated against historical and current animal excretion data (from Le Noë et al., 2018)..... 197

Table 5-3. Coefficient applied for the calculations of CO_2 emissions according to major emitter sectors. N fertilisers and P fertilisers concern the production of fertilisers actually used, feed to livestock is the imported feed, machinery corresponds to the manufacture of agricultural equipment, energy for cropland, grassland and livestock, the fuel or electricity necessary for fieldwork and for livestock breeding (from Doublet et al., 2011). UAA: utilised agricultural area; LU: livestock unit. 198

Table 5-4. Total GHG emissions from agriculture in France and in the three supra-regions considered, given in CO_2 equivalent. Specific GHG emissions (tCO_2 km^{-2} yr^{-1}) are provided for comparison. Relative contributions of N_2O, CH_4 and CO_2 are also shown. 212

Introduction

Due to the carbon dioxide (CO_2) impact on the Earth's energy budget, understanding the global carbon cycle is indispensable to be able to propose alternative carbon management policies for a sustainable future (Raymond et al., 2013). The increase in atmospheric CO_2 concentration has been monitored through continuous measurements since 1958 and reconstructions of atmospheric CO_2 concentrations using ice cores (Fig. 0-1), showing that current values are also the highest in the past 1,000 years (Etheridge et al., 1996; MacFarling Meure et al., 2006).

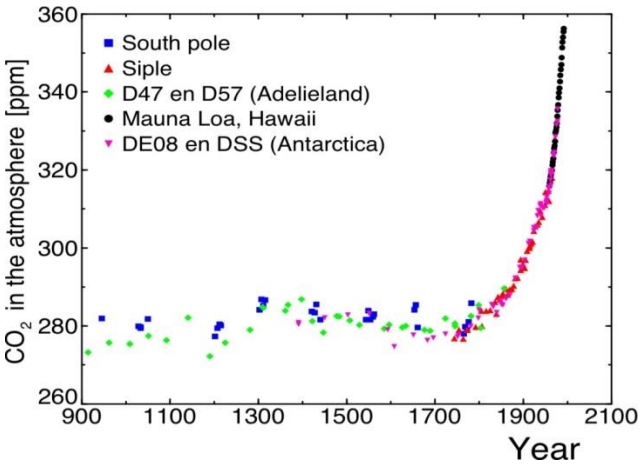

Fig. 0-1: CO_2 concentrations in the atmosphere from measurements in ice cores before 1958 (Etheridge et al., 1996; MacFarling Meure et al., 2006) and from the Mauna Loa observatory since 1958 (Scripps CO_2, Division Physical Sciences and NOAA Earth System Research Laboratory).

Further, the intergovernmental panel on climate change (IPCC) estimated that atmospheric CO_2 concentrations were the highest for the last 800,000 years (2018: 405.51 ppm, last updated 05 October 2018, Division Physical Sciences and NOAA Earth System Research Laboratory, last accessed in October 2018) leading to a stock of 829 ± 10 Pg C in the atmosphere (see Fig. 0-2, Prather et al., 2012; Joos et al., 2013). Since the pre-industrial era, a 40% increase in atmospheric CO_2 concentrations has been observed due to the use of fossil fuels and cement production (associated emission of 7.8 [7.2 to 8.4] GtC yr^{-1} averaged over 2002-2009) and changes in land use (associated emission of 1.1 [0.3 to 1.9] GtC yr^{-1} averaged over 2002-2011). This is despite an increase in terrestrial and oceanic carbon sinks of about 30% each over the period 1750-2009 to reach stocks of 4700 (3732-5720) Pg C, and 40,600± 38 Pg C, respectively (IPCC, 2013 - Ciais et al., 2013).

0.1. Overview of the global carbon cycle

The global carbon cycle can be represented as reservoirs of carbon that interact through exchange fluxes of carbon. Two main different time scales can be distinguished. The first has relatively fast reservoir turnovers (from a few years to millennia of carbon): atmosphere, ocean, surface ocean sediments, land vegetation cover, soils and freshwaters (Ciais et al., 2013). The second one is characterized by slower turnovers (10,000 years or longer) with carbon stored in rocks and sediments. These slower reservoirs can interact with fast ones through volcanic emissions of CO_2 or chemical weathering, erosion and sediment formation on the sea floor (Ciais et al., 2013). Before the industrial era, the fast turnover domain was close to steady state with small variations in atmospheric CO_2. The major human impact on the global carbon cycle was the extraction of fossil fuel from geological reservoirs and its combustion, i.e. from slow turnovers reservoir to fast ones (Ciais et al., 2013).

As represented on Fig. 0-2, terrestrial biosphere reservoir comprises organic carbon in vegetation (450-650 PgC, Fig. 0-2, Prentice et al., 2001) or in dead organic matter in litter and soils (1500 to 2400 PgC, Fig. 0-2, Batjes, 2014). Old soil carbon can also be stored in wetlands or permafrost. CO_2 is removed by plant photosynthesis (123 PgC yr^{-1},Fig. 0-2) and fixed in plant tissues, and then released in litter or soils, and can be sent back to the atmosphere mainly through respiration. These seasonal uptakes of carbon lead to seasonal variations in atmospheric CO_2 concentrations.

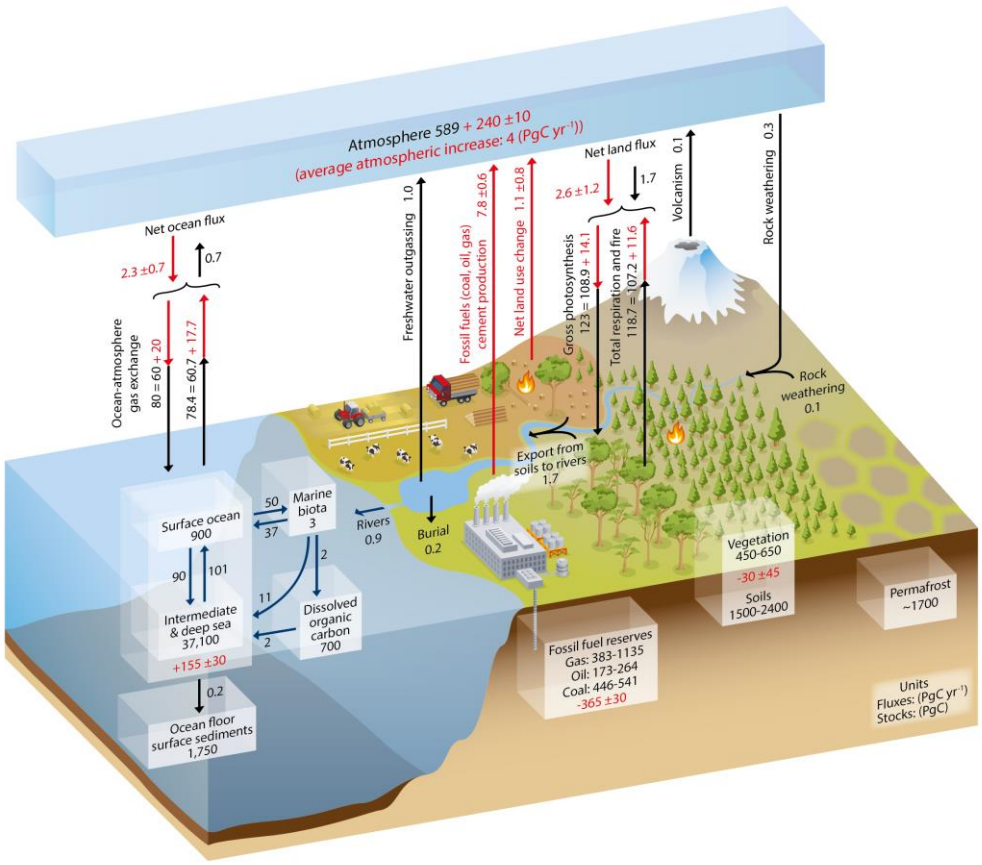

Fig. 0-2 Simplified schematic of the global carbon cycle retrieved from Ciais et al. (2013). Numbers represent carbon stocks in PgC (1 PgC = 10^{15} gC) and annual carbon exchange fluxes (in PgC yr^{-1}). Black numbers and arrows indicate reservoir mass and exchange fluxes estimated for the time prior to the Industrial Era, about 1750. Red arrows and numbers indicate annual 'anthropogenic' fluxes averaged over the 2000–2009 time period. These fluxes are a perturbation of the carbon cycle in the industrial era post 1750.

Terrestrial carbon is then transported to rivers where it can be either outgassed, buried in organic sediment or exported to coastal oceans as dissolved inorganic carbon (DIC), dissolved organic carbon (DOC) or particulate organic and inorganic carbon (POC, PIC). In general the term "dissolved" is used for compounds that pass through calcinated glass giber filters of 0.45 micrometers (µm) GFF/F filter (UNESCO, 1994), and "particulate" is used for the fraction of the sample retained on the filters. DIC is defined as the sum of bicarbonates (HCO_3^-), carbonates (CO_3^{2-}) and dissolved CO_2 (CO_2 or carbonic acid: H_2CO_3) concentrations. DOC and POC are organic carbon molecules derived from living organisms. PIC is precipitated or eroded carbonates.

Atmospheric CO_2 is exchanged with the surface ocean that contains mainly carbon in the DIC form (38,000 PgC, Fig. 0-2). These exchanges are completed through three mechanisms: the solubility, the biological (photosynthesis) pump or the marine carbonate pump (formation of

calcareous shells of some microorganisms that sink and can be re-mineralized or buried in sediments).

CO_2 equilibria in water

The three constituents of DIC (HCO_3^-, CO_3^{2-}, CO_2,) depend on ionic strength, temperature and pH (Mackereth et al., 1978) (Pedersen et al., 2013).

CO_2 reaction with water results in the following equilibrium:

$$CO_{2(aq)} + H_2O \leftrightarrow (H_2CO_3) \leftrightarrow HCO_3^- + H^+ \leftrightarrow CO_3^{2-} + 2H^+ \qquad \text{Eq. 1}$$

The pH determines the proportion between the three main carbon inorganic species (H_2CO_3, the carbonic acid which dissociates immediately) (Fig. 0-3). A pH higher than 8 will result in a low CO_2 concentration and higher CO_3^{2-} concentration while below 8, the opposite behavior is observed.

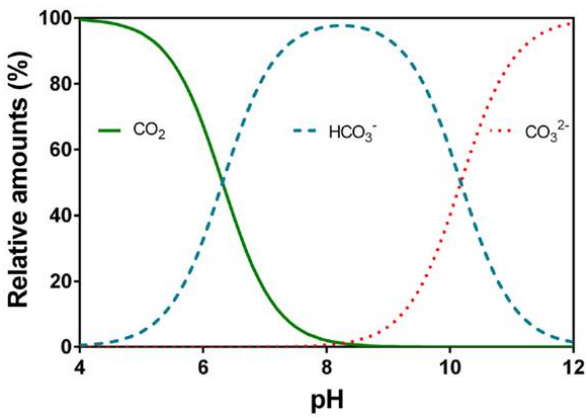

Fig. 0-3 Relative speciation (%) of carbon dioxide (CO_2), bicarbonate (HCO_3^-), and carbonate (CO_3^{2-}) in water according to pH retrieved from Pedersen et al. (2013). Speciation was computed with CurtTiPot (Gutz, 2012) using pK_1=6.532 and pK_2=10.329 at 20°C with electrical conductivity of 250µS cm^{-1} (Schwarzenbach and Meier, 1958).

Bicarbonate and carbonate are also involved in total alkalinity (TA). Alkalinity is the water's ability to neutralize strong acid and can be defined as (Michard, 2008):

$$TA = HCO_3^- + 2\,CO_3^{2-} + b \qquad \text{Eq. 2}$$

where *b* are minor species among which [H_3O^+], [OH^-] or borates. Borate concentrations are neglected in freshwater but are not negligible in sea water.

0.2. New paradigm of inland water as an active component of the carbon cycle

Despite the primary role of the carbon cycle in the Earth's climate system, lateral carbon fluxes from landscapes to surface water and associated emissions have long been underestimated. Indeed, until recently, global carbon budgets/models have (see Fig. 0-2 of IPCC 2013) represented inland waters as a passive transport pipe between land and oceans (e.g., IPCC 2007 - Denman et al., 2007). In particular, rivers were represented as having no exchanges with the atmosphere, sediments, lakes and wetlands.

However, from upland headwaters to downstream river systems, many processes (physical, chemical and biological) govern the transport and transformation of carbon along the aquatic continuum (Minshall et al., 1983). Studies focusing on ecosystems and/or processes have highlighted the importance of inland waters in the global carbon cycle. Specifically, Cole et al. (2007) illustrated this new concept by proposing a new global carbon budget that incorporates these inland waters as an active component (Fig.0-4).

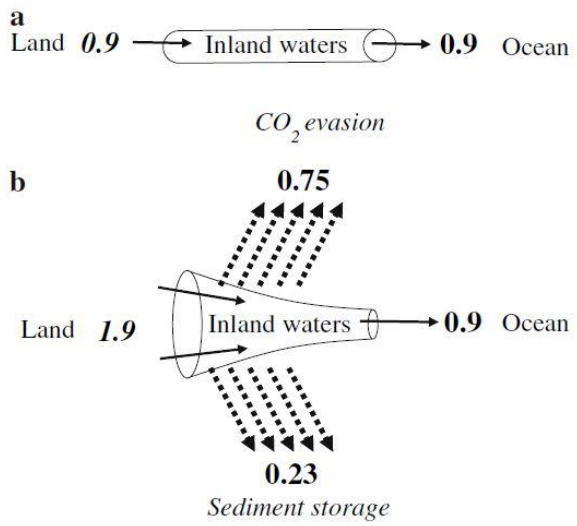

Fig.0-4 : Change in the perception of the role of inland water according to Cole et al. 2007, from (a) a passive pipe representation, to (b) a component transporting and transforming organic and inorganic carbon from land to sea

While the amount of carbon exported to the oceans can be easily estimated using measurements and/or modeling results, exports from land to aquatic systems are more difficult to quantify, and most global estimations quantify these fluxes by difference. As a result, the previous assumption that carbon is transported passively led to significant

underestimation of the amounts of carbon leaving terrestrial parts of watersheds. According to this new approach, inland waters store a significant fraction of terrestrial carbon in sediments but most terrestrial carbon is emitted to the atmosphere as CO_2 (Fig.0-4).

Recently, additional research refined global CO_2 emissions from rivers and streams, which is now estimated at between 0.23 (0.15–0.30) PgC yr^{-1} and 1.8 ± 0.25 PgC yr^{-1} (Cole et al., 2007; Battin et al., 2009b; Aufdenkampe et al., 2011; Lauerwald et al., 2015; Regnier et al., 2013; Raymond et al., 2013; Sawakuchi et al., 2017; Drake et al., 2017). Although the quantification of carbon emissions from rivers and streams (also known as carbon evasion) is still characterized by large uncertainties, the flux remains significant compared to oceanic and terrestrial carbon sinks, respectively, 2.9 ± 0.5 and 1.5 ± 0.9 PgC yr^{-1} (Le Quéré et al., 2015).

If it is now accepted that inland waters are an active component of the carbon cycle, the resulting CO_2 emissions are enhanced by (i) the amounts of inorganic and organic carbon from terrestrial landscapes (Prairie and Cole, 2009), (ii) instream biogeochemical processes that occur in the water column and in the benthic sediments and that determine instream CO_2 concentrations, and (iii) physical (hydro-climatic and morphological) characteristic of the drainage network that determine the amount of gas exchange at the air-water interface (evasion or sink).

0.3. Carbon dioxide evasion as a result of cascades of biogeochemical and physical processes

0.3.1. Carbon from terrestrial landscapes

Terrestrial delivery of carbon to inland waters was recently estimated at 5.1 Pg C yr^{-1} with an increase of around 0.3 Pg C yr^{-1} over the last decade (Drake et al., 2017). Soils are the largest pool of OC terrestrial carbon (Minshall et al., 1983) and the local canopy, which assimilates atmospheric CO_2 by photosynthesis, is the main source (Schlesinger, 1984). Litter fall, through fall, roots, microbial biomass and fungi are also main inputs (Qualls et al., 2002).

Lateral sources of organic carbon (OC)

Lateral fluxes of OC originate from plant or litter detritus, soil leaching, bank or soil erosion transported by groundwater, subsurface flows or runoff (Richey et al., 2002; Prairie and Cole, 2009; Battin et al., 2009a ; Stanley et al., 2012; Hotchkiss et al., 2015; Drake et al., 2017).

Flood events increase organic carbon delivery into rivers (Raymond and Saiers, 2010; Bianchi et al., 2013). The release of sewage (Garnier et al., 2013a) and petroleum-based household products by wastewater treatment plants (WWTPs) also supplies OC to rivers (Griffith et al., 2009). In addition, large quantities of OC can be supplied to rivers by wetlands (Mulholland and Kuenzler, 1979; Richey et al., 2002; Abril et al., 2014) or synthesized in the river itself through photosynthesis (Duarte and Prairie, 2005).

Lateral sources of inorganic carbon (IC)

Lateral fluxes of IC originate from (i) the decomposition of organic matter or root respiration in soil or (ii) the chemical weathering of silicate and carbonate minerals by carbonic acid also transported by groundwater discharge, soil leaching or erosion of carbonate rocks (Cole et al., 2007; Venkiteswaran et al. 2014; Drake et al., 2017; Marx et al., 2018). Carbonate basins are also known to deliver more CO_2 than mixed or silicate basins (Telmer and Veizer, 1999; de Montety et al., 2011 Polsenaere et al., 2013; Martin et al., 2013 ; Lauerwald et al., 2013 ; Khadka et al., 2014 ; Abril et al., 2015). In addition to being a major source of OC, WWTPs are also a source of IC for river waters (Alshboul et al., 2016). In addition to these direct IC inputs and those of the degradation of OC resulting in CO_2 production in rivers (Servais et al., 1987), other instream or benthic metabolisms can produce or consume dissolved inorganic carbon (DIC) and in turn, impact CO_2.

Instream metabolism affecting inorganic carbon (IC)

Aerobic degradation – Instream, respiration of microorganisms and photo-oxidation of OC lead to CO_2 production and in turn, increase IC (Duarte and Prairie, 2005; Drake et al., 2017).

$$\mathrm{C_{106}H_{263}O_{11}N_{16}P} + 106O_2 \rightarrow 92CO_2 + 14HCO_3^- + 16NH_4^+ + HPO_4^{2-} + 92H_2O \qquad \text{Eq. 3}$$

Nitrification – In aerobic condition, nitrification by ammonia-oxidizing bacteria (AOB) and nitrite-oxidizing bacteria (NOB) produces nitrate (Garnier et al., 2007), which, in anaerobic conditions, is denitrified into N_2 using organic matter (Laverman et al., 2010; Regnier et al., 2013a). Nitrification affects the carbonate equilibrium by producing protons, acidifying the water and transforming bicarbonate into CO_2 (Han et al., 2017).

$$NH_4^+ + 2O_2 \rightarrow 2H^+ + H_2O + NO_3^- \qquad \text{Eq. 4}$$

Denitrification – Nitrates can originate from nitrification of WWTP sewage releases, but is mostly the result of agricultural activities, leached from soil and/or transported to groundwater. Associated denitrification processes by denitrifiers instream, in riparian zones or in aquifers, generally with low concentrations in oxygen, produce CO_2 and affect DIC.

$$5CH_2O + 4NO_3^- + 4H^+ \rightarrow 5CO_2 + 2N_2 + 7H_2O \qquad \text{Eq. 5}$$

Photosynthesis – Photosynthesis depends on light to fix dissolved inorganic carbon, and on nutrient availability (NH_4^+ or NO_3^-) for phytoplankton growth and biomass development (Lancelot et al., 1991; Lower, 1999). Uptakes of NH_4^+ or NO_3^- have been shown to be significantly related to their concentrations in the water (Boyer et al., 1994). In rivers, water dilution rate and the residence time of the associated water masses strongly control phytoplankton development and lead to large quantities of biomass in larger rivers (Garnier et al., 1995). In upstream rivers, macrophytes and/or periphytons are the major primary producers.

$$106CO_2 + 16NO_3^- + H_2PO_4^- + 122H_2O + 17H^+ \rightarrow C_{106}H_{263}O_{11}N_{16}P + 138O_2 \qquad \text{Eq. 6}$$

$$106CO_2 + 16NH_4^+ + H_2PO_4^- + 106H_2O \rightarrow C_{106}H_{263}O_{11}N_{16}P + 106O_2 + 15H^+ \qquad \text{Eq. 7}$$

Weathering of carbonates/silicates: the reactions of rocks to weathering results in uptake of 1 mole of CO_2 to produce 2 moles of bicarbonates (Eq. 8 and 9). Inversely, precipitation of carbonates consumes bicarbonate and produces CO_2 (Eq. 8 from right to left).

$$CaCO_3 + CO_2 + H_2O \leftrightarrow 2\,HCO_3^- + Ca^{2+} \qquad \text{Eq. 8}$$

$$CaSiO_3 + CO_2 + H_2O \rightarrow 2\,HCO^{3-} + Ca^{2+} + SiO_2 \qquad \text{Eq. 9}$$

Additional carbon exchanges, like carbon incorporation in biomineralized structures, and sedimentation or resuspension, are generated at the water-sediment interface (Manickam et al., 1985; Butman and Raymond, 2011a, Vilmin et al., 2016).

All these mechanisms can change the concentration of DIC in the water column and, in turn, affect the pCO_2 gradient at the air-water interface. At that point, exchange by diffusion occurs

depending on the partial pressure of CO_2 (pCO_2) at the water surface with respect to atmospheric pCO_2 (Cole et al., 2007).

0.3.2. Understanding CO_2 evasion processes

Three common parameters, the gradient of CO_2 concentrations between the water and the atmosphere $[(CO_2w - CO_2atm), mol\ h^{-1}]$, mirror area of inland waters (Ω, m^2), and gas transfer velocity $(k, m\ d^{-1})$ are the keys to understanding carbon evasion $(F_{CO_2}, mol\ h^{-1})$ and need to be estimated precisely.

$$F_{CO_2} = k_{co_2}\,(CO_2w - CO_2atm)\Omega \qquad \text{Eq. 10}$$

Temperature-normalized gas transfer velocity (k_{600}) is the gas transfer velocity at a water temperature of 20 °C. Parametrization related to the gas exchange used k_{600} to compare systems excluding the physical effect of temperature.

According to Wilke and Chang (1955); Wanninkhof (1992), the gas transfer velocity k_{CO_2} (m d^{-1}) can be calculated as:

$$k_{CO_2} = k_{600} \cdot \sqrt{\frac{600}{Sc_{CO_2}(T)}} \qquad \text{Eq. 11}$$

where k_{600} is the gas transfer velocity at 20°C for a Schmidt number of 600 (m d^{-1}) and $Sc_{CO_2}(T)$ is the Schmidt number (dimensionless) calculated at water temperature T in Celsius ($°C$) calculated as:

$$Sc_{CO_2}(T) = 1911.1 - 118.11T + 3.4527T^2 - 0.04132T^3 \qquad \text{Eq. 12}$$

CO_2 concentrations in rivers

CO_2 concentrations in water can be measured directly or estimated indirectly through indirect measurements.

Direct measurements - are based on discrete samples with headspace technique (e.g., Weiss, 1981; Teodoru et al., 2009; Borges et al., 2018). For example, measurements of CO_2 can be completed with a headspace technique using four syringes with three-way valves combined with non-dispersive infrared gas analysis (IRGA) (Fig. 0-5a). This technique requires direct

filling with 30 mL of stream or river, and then 30 mL of atmospheric air. The first injection serves as a purge and the other three are used to measure pCO_2. A syringe full of air can measure pCO_2 in the air. After which, initial pCO_2 in water is computed based on the pCO_2 measured in the equilibrated air of the syringe and in the atmospheric air, and Henry's law accounting for the water temperature in the syringe and *in situ* (see Fig. 0-5 a).

CO_2 can also be measured continuously with an equilibrator (Frankignoulle et al., 2001; Frankignoulle and Borges, 2002; Abril et al., 2006). An example of equilibrator is shown in Fig. 0-5b. In this equilibrator, designed by Frankignoulle et al. (2001), the water enters the top of the equilibrator and flows through a vertical Plexiglas tube filled with marbles that increases the exchange at the water-air interface and reduces the air volume required. A membrane air pump and regulator on the top circulate equilibrated air through the IRGA (Licor ® 6262). This continuous method makes it possible to measure pCO_2 in highly turbid and dynamic environments. Note that in both techniques, gas chromatography (GC) can also be used to detect CO_2 rather than IRGA (Abril et al., 2015).

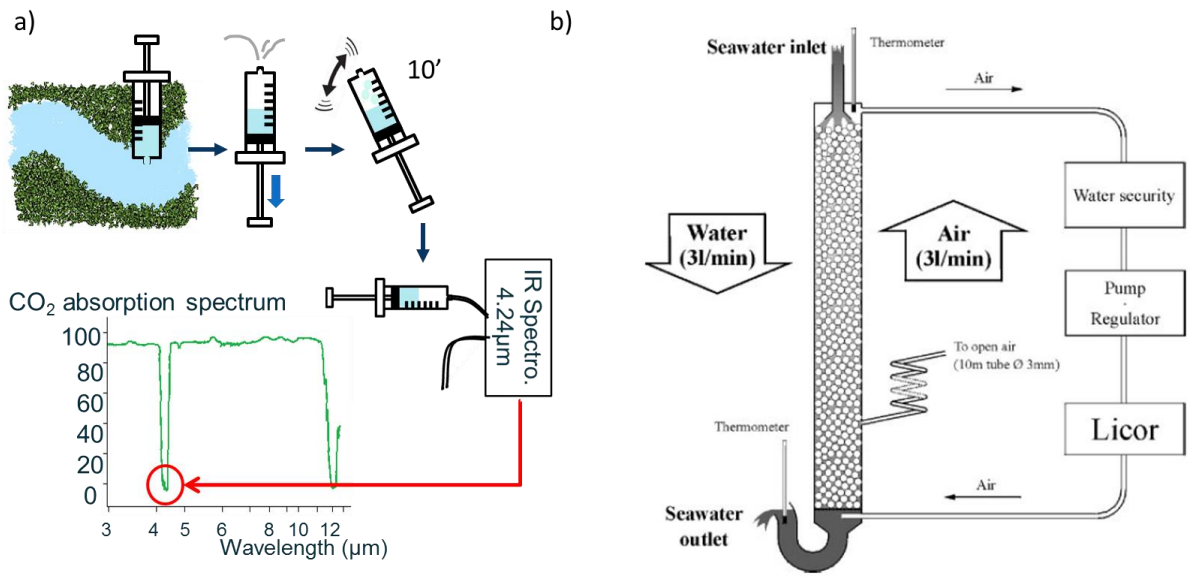

Fig. 0-5 Examples of direct techniques used to measure pCO_2 a) discrete technique using syringe headspace, b) continuous technique with the equilibrator, (source: Frankignoulle et al., 2001).

Indirect measurements - pCO_2 can be indirectly computed from the pairs of variables pH/TA, pH/DIC, DIC/TA (Park, 1969; Abril et al., 2015), and the dissociation constants of carbonic acid depending on the water temperature (Harned and Scholes, 1941; Harned et al., 1943; Millero et al., 2006). CO2sys software has been designed to estimate pCO_2 with these pairs of variables (e.g., Pierrot et al., 2006). While DIC values are scarce in national databases, pH, TA and water temperature are more common and are often used to estimate pCO_2.

Abril et al. (2015) compared these three indirect and direct methods, and reported that calculated pCO_2 was overestimated in comparison to measured pCO_2, and that no global empirical relationship can be derived to calculate pCO_2. Overestimation was related to two cumulative factors. In waters with low carbonate alkalinity and high DOC concentrations, organic acid anions can increase TA. Secondly, at low pH, in acidic and organic rich waters, the buffering capacities of the carbonate system are lower, and increase the sensitivity of calculated pCO_2 to TA. However, in freshwaters with neutral to basic pH and with TA exceeding 1,000 µmol L^{-1}, calculated pCO_2 is more robust.

Water surface exchange: mirror area

Raymond et al. (2013) highlighted the importance of surface area in estimating CO_2 emissions from inland waters. Spatial (using biomes) and temporal (clustering seasons) variations of aquatic mirror areas can be partly observed by satellite imagery at regional scale. The uncertainties concerning the extent of surface water are mainly due to their seasonal variation: partially hidden or temporarily flooded areas for example (Raymond et al., 2013). Another example is intermittent rivers and ephemeral streams (Datry et al., 2014) whose number and significance are increasing due to climate change, land use change, and water abstraction (Datry et al., 2014) and have already been recognized as playing a significant role in carbon and nutrient budgets (Looman et al., 2017; Datry et al., 2018). River dams and large reservoirs can also locally affect the estimation of mirror areas.

Gas transfer velocity

Gas transfer velocity (*k*) is estimated using many methods including floating chambers (e.g., Duchemin et al., 1995; Beaulieu et al., 2012), empirical equations (based on slope, depth, stream and wind velocity, etc., e.g. Raymond et al., 2012a), analyzing the metabolism of streams and rivers (e.g., Hall, 2016), tracer techniques (helium/sulphur hexafluoride ratio,

propane, argon, etc.: e.g., Nightingale et al. (2000)), or using the eddy covariance technique (e.g., Huotari et al., 2013).

Floating chambers have been criticized because of their inherent effects that modify water surface turbulence and natural conditions such as wind (Wallin et al., 2011; Campeau et al., 2014; Crawford et al., 2016). The eddy covariance technique cannot be used on small streams because a large open water fetch area is required (Wallin et al., 2011). Extracting *k* from metabolism of streams and rivers requires large temporal data series on oxygen (Hall, 2016). Chemical gas tracers cannot be used in large navigable rivers (Nightingale et al., 2000). Empirical model equations thus appear to be a more appropriate solution to estimate CO_2 evasion at a watershed scale of different Strahler stream orders.

In streams and in small rivers, the source of turbulence at the surface is related to bottom stress (e.g., roughness) and *k* to the stream depth, water velocity, water discharge or slope (e.g., O'Connor and Dobbins, 1958; Tsivoglou and Neal, 1976; Raymond and Cole, 2001; Wallin et al., 2011; Raymond et al., 2012a). In large rivers and estuaries, wind speed appears to be the main driver of *k* (Liss and Merlivat, 1986; Wanninkhof 1985, 1992; Crusius and Wanninkhof 2003; Borges et al., 2004; Abril et al. 2009; Alin et al., 2011; Ho et al., 2014; Roobaert et al., 2018).

Through a literature review, Alin et al. (2011) observe higher *k* with more variability in small rivers and streams (channels < 100 m, mean $k = 22.4 \pm 14.3$ cm h^{-1} [0.4 to 183.9 cm h^{-1}]) than in large rivers (channels > 100 m; mean $k = 12.8 \pm 10.7$ cm h^{-1} [1.2 to 44.5 cm h^{-1}]).

In general, the literature on the quantification of carbon sources from terrestrial landscapes and associated instream biogeochemical (metabolism) or physical (outgassing) processes, suggests that the carbon cascade is very strongly structured by an upstream-downstream gradient of biotic and abiotic factors along the aquatic continuum.

0.4. Carbon dynamics along the aquatic continuum:

The river continuum concept predicts that a continuous gradient of physical conditions occurs along the land-to-ocean continuum of a river and influences both biological characteristics and processes (Vannote et al., 1980). For example, as stream size increases, the reduction in particle size of organic material from upstream dominated by terrestrial organic inputs is related to the enhancement of autochthonous primary production, and an increase in the organic matter content resulting from instream processes (Minshall et al., 1983). The changes that take place along the river imply that what happens upstream of the river reaches has an impact on the biogeochemical functioning in downstream ecosystems, including on carbon cycling.

Carbon cycling in upstream sectors is expected to be closely linked to watershed characteristics and stream morphology, whereas downstream, instream biogeochemical processes (e.g., heterotrophic respiration) take over (Dinsmore and Billett, 2008). Indeed, small streams typically have a strong hydro-chemical connectivity with the catchment soils, enhanced by precipitation causing the mobilization and transport of DOC from soils to inland waters through runoff (Dinsmore et al., 2013). Similarly, exchanges taking place vertically via saturated interstices of hyporheic zones to aquifers (infiltration, exfiltration) play a very important role. Headwater stream flows are (in general) predominantly fed by groundwater which delivers most of the DIC (Dinsmore and Billett, 2008; Denfeld et al., 2013). These small streams often have steeper slopes and consequently, CO_2 evasion has been shown to be higher in headwater streams where high water turbulence increases the exchange with the atmosphere (Raymond et al., 2012a) (Fig. 0-6). Öquist et al. (2009) estimated that up to 90% of the DIC delivred to streams was emitted to the atmosphere within 200 meters.

Also, hydrologic residence times increase along the river leading in an increase in autochthonous production, but also an increase in photochemical degradation, flocculation and sedimentation (Guo and He, 2011; Denfeld et al., 2013). The production to respiration ratio (P/R) is expected to be higher in large river than in small streams, and decrease again in deep fluvial sectors or estuaries characterized by a turbidity maximum zone. WWTP effluents can also disturb the P/R trend in the continuum by locally decreasing the P/R ratio (Garnier et al., 1999; Garnier and Billen, 2007).

Hotchkiss et al. (2015) summarized the impact of the river continuum on the sources and evasion of CO_2 (Fig. 0-6). CO_2 evasion is higher upstream due to higher OC and CO_2 from soils and groundwater. These inputs decrease along the continuum from upstream to downstream and the proportion of CO_2 instream production due to the mineralization of terrestrial OC thus increases proportionally. Associated outgassing of CO_2 from instream production decreases slightly along the aquatic continuum, but becomes relatively greater as external carbon inputs decrease more rapidly.

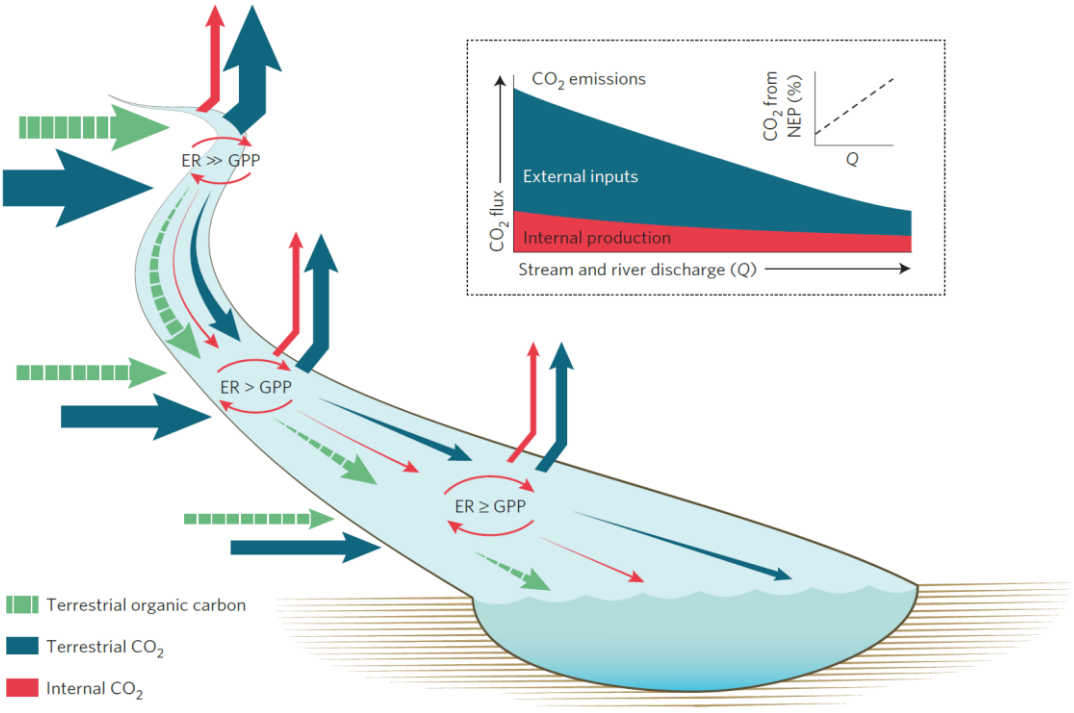

Fig. 0-6 Sources and magnitude of net CO_2 emissions along a theoretical stream-river continuum retrieved from Hotchkiss et al. (2015) describing how the external carbon inputs (carbon from the surrounding landscape and bedrock) are greater in upstream areas than downstream, which also leads to a proportionally larger CO_2 evasion flux upstream than downstream. ER is ecosystem respiration and GPP gross primary production.

In parallel with this theoretical circulation along the aquatic continuum, inputs and processes controlling the intensity of CO_2 emissions are likely to differ from one region to another according to climatic conditions, land uses or human impacts.

0.5. Lesson learned from contrasted regional climates about CO_2 evasion

The biogeochemical processes and inputs involved in the aquatic carbon cycle also depend on different temporal scales ranging from an hour and less (e.g., photosynthesis), diurnal to seasonal (e.g. temperature) or highly variable (nutrient loads), depending on their origins (Regnier et al., 2013a). Aufdenkampe et al. (2011) estimated the highest CO_2 outgassing takes place in rivers and stream in tropical regions (0.39 Pg C yr^{-1}), followed by those in temperate regions (0.013 Pg C yr^{-1}) with the lowest rates in the boreal zone and the Arctic (0.04 Pg C yr^{-1}). These differences highlight different processes according to climate and biomes, although the differences could progressively vary with climate change (Table 0-1).

0.5.1. Sub-tropical regions: a hotspot of aquatic CO_2 emission

Most CO_2 riverine emissions occur in sub-tropical or tropical regions where large rivers are often connected with wetlands (Richey et al., 2002; Abril et al., 2014; Borges et al. 2014, 2015). Richey et al. (2002) observed pronounced evasion seasonality in the Amazon with pCO_2 mirroring the hydrograph, increasing with rising water and decreasing with reduced water flow. Tropical soils are weathered and thus have lower alkalinity combined with a more dense drainage including flood plains and higher temperature than temperate rivers leading to higher CO_2 evasion rates. Abril et al. (2014) highlighted the importance of flooded land, most of which are temporary wetlands. Indeed, in the central Amazon, these authors estimated that wetlands, one of the most productive ecosystems in terms of vegetal biomass, exported half their gross primary production to river waters as dissolved CO_2 and organic carbon, whereas only a few percent came from upland non-flooded rivers. Wetland vegetation is hypothesized to support CO_2 outgassing by release into waters of labile organic carbon from litterfall or root exudations or by roots and microbial respiration in wetland soils. Moreover, extreme flood events have been shown to enhance DOC leaching and CO_2 evasion in the Amazon River (Almeida et al., 2017). Similarly, in African inland waters, Borges et al. (2015) estimated that expanding wetlands and upland riverine biomass increased CO_2 and CH_4 riverine emissions. Subtropical rivers, in Texas (USA) or in southern China, showed concentrations between those of temperate and tropical rivers (Zeng and Masiello, 2010; Yao et al., 2007)

0.5.2. Artic regions: slowly releasing CO_2 sequestered in permafrost

In the Artic with a polar climate, permafrost accounts for 22% of the land surface (Denfeld et al., 2013), and stores large quantities of long-sequestered soil carbon that is released into streams when it thaws. The peculiarity of this artic region is that permafrost minimizes the percolation of carbon into deep soils, with carbon therefore entering streams via surface or subsurface flow rather than by groundwater flow, which is much smaller in these areas (Zimov and Schuur, 2006; Frey and McClelland, 2009; Denfeld et al., 2013). In the Kolyma River (Siberia) during summer low-flow period, headwater streams were a net source of CO_2 while larger rivers contained low CO_2 and were near equilibrium with respect to atmospheric concentrations. This trend was related to higher carbon mobilized from permafrost or floodplains into small headwater streams (Denfeld et al., 2013). However, the highest pCO_2 was not linked with the highest DOC content in soils. Indeed, old DOC in permafrost soils with high molecular weight aromatic compounds was shown to be less biodegradable than young organic carbon leached by floodplains throughout the growing season from lower molecular weight and hydrophilic compounds (Wickland et al., 2007).

From these two opposite climatic regions (subtropical and artic), it appears that CO_2 evasion is mostly controlled by hydro-climatic processes and/or associated with control by land vegetation (wetlands). Additional controls may appear in temperate regions, especially where human activities greatly affect the aquatic continuum.

Table 0-1 Examples of pCO_2 concentrations along different stream-river continuums in several tropical, temperate and artic regions. All values are direct pCO_2 measurements except for *Kempe et al. 1982.

Region	Sites	pCO_2 (ppmv)	Authors
Tropical and subtropical	River and floodplain waters of the sub-Saharan Africa	4350 +- 1900 (main stem)	Richey et al., 2002
		300 - 16,942 (12 rivers)	Borges et al., 2015b
	Amazon River	1000-10,000 (River and main tributaries)	Abril et al., 2014
	Buffalo bayo, highly urbanized	3014+-603	Zeng and Masiello, 2010
	Spring Creek, undevelopped	4214+-843	Zeng and Masiello, 2010
Boreal and artic	Kolyma	3336+-2737 (streams)	Denfeld et al., 2013
		613 +- 315 (main stem)	Denfeld et al., 2013
		412+-250 (rivers)	Denfeld et al., 2013
	Boreal	1858.2 (streams)	Teodoru, 2009
		845 (intermediate)	Teodoru, 2009
		610.6 (large river)	Teodoru, 2009
Temperate	Hudson	1125+-403	Raymond et al., 1997
	York River Estuary	1070+-867	Raymond et al., 2000
	US streams	2109 (417 streams)	Jones et al., 2003
	Loir (croplands)	284	Abril et al., 2015
	Arcachon (podzolized)	1604 - 6546	Polsenaere et al., 2013
	Meuse	2292	Abril et al., 2015
	Meuse	2004+-912	Borges et al., 2018
	Loire	1240	Kempe, 1982*
	Mississippi	4752	Kempe, 1982*
	St. Lawrence	2240	Kempe, 1982*
	Seine	1982	Kempe, 1982*
	Elbe	4095	Kempe, 1982*
	Columbia	1123	Kempe, 1982*

0.6. Focus on carbon dioxide evasion control in temperate hydrosystems imprinted by human activities

0.6.1. Hydrological influence

Many natural factors controlling carbon evasion have been identified in temperate rivers. Indeed, several studies have shown that seasonal variations in pCO_2 followed the hydrological cycle with higher pCO_2 values during low water in summer (Polsenaere et al., 2013; Borges et al., 2018). In temperate rivers in the USA, pCO_2 trends were shown to follow the patterns of evapotranspiration, terrestrial leaf litter production, soil organic matter decomposition, and CO_2 evasion from soils (Jones et al., 2003). In addition, Butman and Raymond (2011b) showed that pCO_2 in streams and rivers was regionally correlated with the level of annual precipitation, and with the flushing of CO_2 from soils. Also, extreme climate events, e.g., drought that causes intermittent drying up of streams (Ylla et al., 2010, Datry et al., 2014), and floods (Almeida et al., 2017) that strongly impact carbon delivery to rivers, the hydrological regime and the hydrological connectivity (Tranvik and Jansson, 2002), finally lead to higher CO_2 emissions (Langerwisch et al., 2016). These extreme events that are expected to be more frequent with climate change (Raimonet et al., 2018) require further research.

0.6.2. Land use and impact of modern agricultural practices

Most temperate rivers are characterized by strong direct human impacts (Kempe, 1984; Davis and Koop, 2006; Garnier et al., 2007; He et al., 2011; Passy et al., 2013b; Alshboul et al., 2016; Lambert et al., 2017; Borges et al., 2018) that also disturb the carbon evasion (Regnier et al., 2013b). As shown in a recent study of the Meuse River, land uses affect pCO_2. Higher values were associated with watersheds dominated by agriculture and lower values with forested watersheds (Borges et al., 2018). One major consequence of agriculture is the alteration of soil structure and stability, resulting in soil erosion and modification of transport processes from soils to rivers, thereby increasing pCO_2 (Pimentel et al., 1995). Agricultural practices have also modified soil C content, resulting in changes in soil leaching or runoff and again modifying pCO_2 (Six et al., 2000). Land use change also affects nutrient exports into rivers possibly favoring or limiting phytoplankton growth (Billen et al., 2007), and in turn, CO_2 evasion. Liming is also known to increase CO_2 evasion (Butman and Raymond, 2011). In

the USA, a large scale decline in terrestrial CO_2 production and hence, in exports into aquatic ecosystem, was observed between 1973 and 1994 (78.4ppmv y^{-1}), that can be attributed to a decrease in riparian and wetland habitats or, to alteration of hydrologic connections between terrestrial and aquatic ecosystems (Jones et al., 2003).

0.6.3. Organic pollution from urban effluents

Carbon from WWTPs increases CO_2 emissions in inland waters (Kempe 1982, 1984; Alshboul et al. 2016). The proportion of biodegradable organic carbon in WWTP effluents is indeed about 50% (Servais et al., 1999), and is accompanied by allochthonous bacteria with high growth rates (Garnier et al., 1992a) allowing rapid mineralization in the receiving waters, and hence production of CO_2. WWTP effluents also contribute supplies of CO_2 ranging from 4.82 ± 1.7 to 8.48 ± 1.26 mgC L^{-1} in 9 WWTPs in Germany (Alshboul et al. 2016). These authors observed that CO_2 concentrations downstream from WWTPs were more than twice higher than in the upstream rivers, the latter ranging from 0.8 ± 0.2 mgC L^{-1} to 3.3 ± 0.4 mgC L^{-1}. Nutrients supplied in WWTPs effluents favor algal growth, and affect planktonic and benthic communities (Billen et al., 2001, 2007; Garnier et al., 2005; 2007), which are major actors of the carbon cycle.

0.6.4. River management

Damming is also known to induce major changes in hydrological conditions of river systems by increasing residence time and trapping particles (Vörösmarty et al., 2003), also favoring the growth of phytoplankton affecting C, N, P and Si cycling (Garnier et al., 1999b). Global carbon mineralization in reservoirs exceeds fixation (assimilation of carbon into organic compounds) leading to P/R ranging from 0.20 to 0.58 at annual scale (Maavara et al., 2017). Damming has also been shown to be a major source of methane (CH_4) due to anaerobic degradation of organic carbon (Abril et al., 2005). Carbon burial in reservoirs may be considered as an offset to carbon GHG emissions (Galy-Lacaux et al., 1997; Maeck et al., 2013; Prairie et al., 2017).

Taken together, these studies suggest that climate, natural land cover in river basins, river management (channeling, reservoir construction, etc.), intensive agriculture, population and associated wastewater releases impact carbon cycling and associated CO_2 emissions.

Similarly, they also impact nitrous oxide (N_2O) and CH_4 two other major greenhouse gases (GHGs) emitted throughout the drainage network.

0.7. Replacing CO_2 evasion as a part of regional GHG emissions

Following the Rio conference in 1992, and since then, several other protocols (Kyoto Protocol in 1997; Paris Agreement in 2015), increasing concern about GHG emissions has been taken into account in the fight against climate change. In the first step, fossil fuels and associated CO_2 emissions encouraged the scientific communities of ecologists and climatologists to include the full carbon cycle, from organic to inorganic, in global models. The two other main biogeochemical GHGs, CH_4 and N_2O were also investigated to assess budgets, understand past and future trends, and establish links between these biogeochemical cycles.

Like CO2, CH4 and N2O concentrations in the atmosphere have also increased since the industrial era (1750, Fig. 0-7).

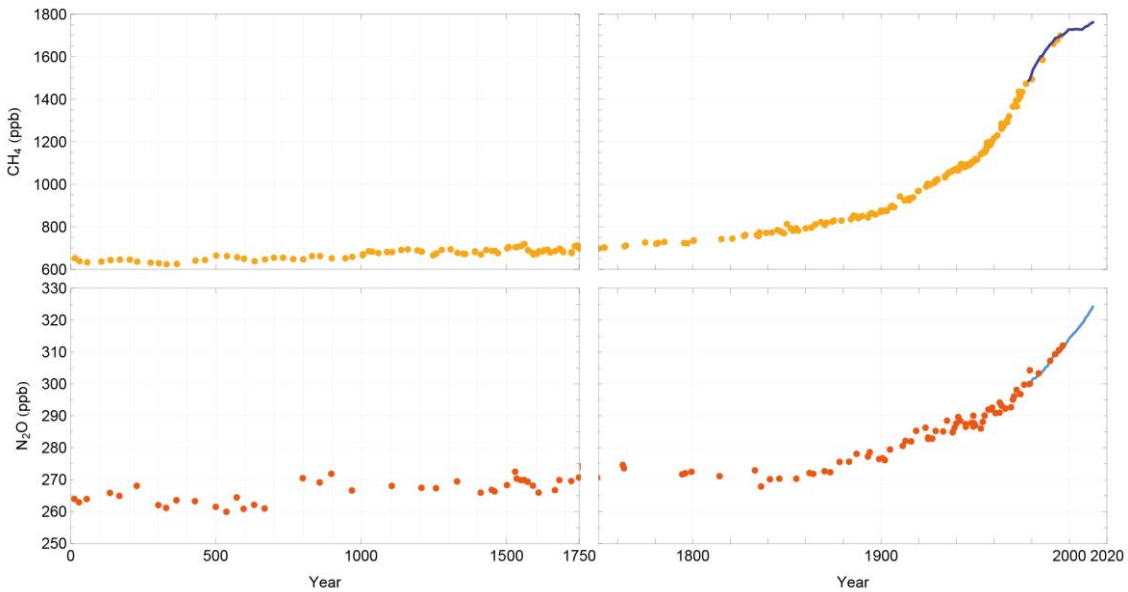

Fig. 0-7 Atmospheric CH_4, and N_2O concentrations before the industrial era from year 0 to the year 1750 (left) and after (right). Concentrations were determined from air enclosed in ice cores and firn air (color symbols) and from direct atmospheric measurements (blue lines, measurements from the Cape Grim observatory) (MacFarling Meure et al., 2006). Source (Ciais et al., 2013)

Indeed, the 150% increase in atmospheric CH_4 (from 722 ±25 ppb to 1803.2 ± 25 pbb, for 1750-2011), is related to the increase in anthropogenic emissions (agricultural production of rice, ruminants, landfills and waste, biomass burning e.g., biofuels, and fossil fuels (Dentener et al., 2005) reaching 331-335 [273-409] Tg(CH_4 yr^{-1}) for the period 2000 to 2009. Among natural sources, emissions from wetlands dominate, accounting for 218-347 [179 – 484] Tg(CH_4 yr^{-1}) (Ciais et al., 2013). Atmospheric N_2O also increased by 20% (from 270 ± 7 ppb to 324.2 ± 0.1ppb), mainly as a result of agricultural intensification (synthetic fertilizers and application of manure) that increased nitrification and denitrication resulting in N_2O production in soils and sediments and in aquatic systems (by leaching and runoff), and consequently, increased N_2O emissions. Also, atmospheric deposition of nitrogen on soils or on surface water due to fossil fuel combustion and industrial activities increased N_2O emissions. In the period 2006-2011, N_2O global anthropogenic sources amounted to 6.9 [2.7 – 11.1] Tg(N_2O yr^{-1}) while natural sources were estimated at 11.0 [5.4 – 19.6] Tg(N_2O yr^{-1}) (Seitzinger et al., 2000; Khalil et al., 2002; Ciais et al., 2013).

Recognized as responsible for climate change, atmospheric GHG concentrations depend on fluxes (biotic and abiotic processes) with the different components of the Earth's system (atmosphere, ocean, land, and lithosphere). Gradually, these interactions and stocks will have to be quantified and described to refine global budgets. CH_4 and N_2O have also been recognized as a significant efflux from freshwaters to the atmosphere (e.g., CH_4; Cole et al., 2007; Sawakuchi et al., 2014; Borges et al., 2015b; e.g., N_2O: McMahon and Dennehy, 1999; Cole and Caraco, 2001; Beaulieu et al., 2010).

0.7.1. GHG riverine emissions

In the same way as the change in perception of CO_2 transfers and transformations along the aquatic continuum (Cole et al., 2007), the "Hole-in-Pipe" model has also modified the view of linear nitrification and denitrification processes, producing intermediate N_2O under sub-optimal conditions (Davidson, 1991) (Fig. 0-8). Indeed, low ambient oxygen tension denitrification (and also, to a lesser extent, dissimilatory nitrate reduction, Tiedje, 1988) and nitrification (mainly denitrification of nitrifiers, Wrage-Mönnig et al., 2018) are known to cause N_2O emissions as an intermediate product (Cébron and Garnier, 2005; Aguilera et al., 2013).

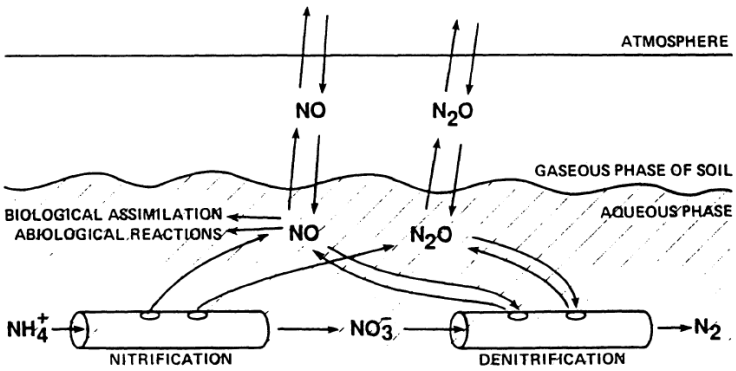

Fig. 0-8 Conceptual model of controls of nitrogen gas emissions from soil via nitrification and denitrification (source Davidson, 1991). Illustration of the change in perception from linear denitrification to *"leaky pipe"*.

For CH_4, environmental conditions favorable to methanogenesis are anoxia and depletion of alternative electron acceptors, nitrate, iron oxides, manganese oxides, and sulfate (Conrad, 1999). However, CH_4 oxidation may play a significant role in the CH_4 budget of aquatic systems, depending on several physical and environmental characteristics (Borges et al., 2015a).

While N_2O and CH_4 dynamics are mainly linked to the fate of bacteria: denitrifiers and nitrifiers for the former, and methanogens and methanotrophs for the latter, CO_2 is the result of biological metabolism of a broad spectrum of microorganisms, including production by autotrophs and degradation by heterotrophs.

In addition to CO_2 emissions from riverine continua, N_2O and CH_4 may also play a significant role due to their high global warming potential (265 and 28 times CO_2, using the 100-yr GWP, CO_2 as reference (Myhre et al., 2013)). Many regional studies on inland waters have focussed specifically on one of these three GHG concentrations, but comparisons of two or all three GHGs from streams and rivers remain scarce (e.g., Harrison et al., 2005; Hlaváčová et al., 2006; Garnier et al., 2013b; Borges et al. 2015a; 2015b; 2018; Teodoru et al., 2015 ; Schade et al., 2016).

In addition to their instream production, and like CO_2, N_2O and CH_4 may come from diffuse and point sources. Diffuse sources are directly linked to soil leaching processes, and as water infiltration is a vector of dissolved gas, they can also be supplied by groundwater. Indeed, depending on the redox condition in the aquifers, gaseous N_2O, CO_2 or CH_4 can be also produced. Whatever the sources, when subsurface runoff of groundwater reaches head surface waters, outgassing as a major process, occurs within a short distance (Garnier et al., 2009;

Öquist et al., 2009). WWTP effluents are also a direct source of N_2O and CH_4 for surface waters, but indirectly, ammonia, nitrate and organic matter contained in the wastewaters, can also be transformed in the river water column and at the sediment water interface (Garnier et al., 2009; 2013b).

Although these emissions by the aquatic continuum (also known as indirect emissions in comparison with direct emissions from the land) may not be negligible, they are rarely included in national or global inventories that mostly concern direct GHG emissions from land.

0.7.2. GHG direct emissions

The agricultural sector is known to be a significant direct emitter of N_2O and CH_4, through fertilizers and livestock, respectively. CO_2 from agricultural activities is often significantly underestimated, for example, fertilizers, manufacturing and machinery are taken into account in the industrial sector but not in the agricultural sector?

N_2O fluxes are often reported to be associated with applications of mineral fertilizer (Bouwman, 1996), particularly on wet unsaturated soils (Clayton et al., 1994), but manure and other organic fertilizers also contribute to N_2O emissions (Aguilera et al., 2013). CH_4 fluxes originate mainly from livestock (Vermorel et al., 2008), particularly ruminants, although some soils can be a CH_4 sink through CH_4 oxidation (Boeckx and Van Cleemput, 2001), while in contrast, paddy soils can be net emitters of this gas (Dentener et al., 2005). Agricultural CO_2 emissions are more due to CO_2 emitted by the use of fossil fuels for farm work, manufacture of fertilizer, of machinery, and imported animal feed Gingrich et al. (2007) than net soil CO_2 emissions resulting from the balance between the supply of humified organic matter and mineralization or leaching. However, how these different control factors combine and determine the variations in space and over time of GHG emissions by agricultural systems is still a difficult question to answer, for an interpretation that goes beyond national inventories (CITEPA, 2005).

The non-agricultural sector (transport, heating, industry, etc.) is known to be dominating in CO_2 emissions in most developed countries and to represent about 75-80% of the total emissions compared to about 15-20% linked to agriculture (Staufer et al., 2016; Wu et al., 2016; CITEPA, 2005). The Seine basin with the ¾ of its population concentrated in the Paris conurbation (12.4 M inhabitants in 2015, INSEE, 2015), and its intensive agriculture is a good

example to understand the fates and features of CO_2 in regional indirect and direct GHG emissions.

0.8. The Seine river basin: a temperate system highly impacted by humans

0.8.1. Key features of the regional Seine basin

The Seine River (776 km in length) has its spring in the Source-Seine village (Côte d'Or) and flows in a north-westerly direction into the English Channel. Geologically, the Seine basin is characterized by concentric sedimentary carbonated rocks on a basement of ancient massifs outcropping at the extreme south-east and north-east (Fig. 0-9). The medium altitude of the basin is 150 m asl. with 1% of the basin reaching more than 550 m asl. These concentric formations and low altitude gradient result in homogenous tributaries: the Oise, Marne, and Yonne and Eure Rivers (Fig. 0-9). The Seine watershed at its outlet (Poses) covers 64,870 km^2 and is the fourth biggest in France (Guerrini et al., 1998).

The stream Strahler order (SO) structure of the river network is defined as: the upper Seine River flows with a SO6, until the confluence with the Marne River (also SO6), the lower Seine River becomes SO7 until the estuary (Strahler 1957; Billen et al., 2007; Thieu et al., 2009).

The Seine basin is densely populated (nearly 230 inhabitants km^{-2}, INSEE, 2015) concentrated mainly in the Paris conurbation and in its estuary (Le Havre), and has several large WWTPs including the largest WWTP in Europe (Seine Aval, SAV WWTP) (Fig. 0-9). The middle part of the basin is one of the most intensive agricultural areas in the world, oriented toward the mass production of cereals and industrial crops (CLC database, EEA, 2012). Animal farming is highly developed and mainly concentrated in the western and eastern peripheries of the basin (Fig. 0-9).

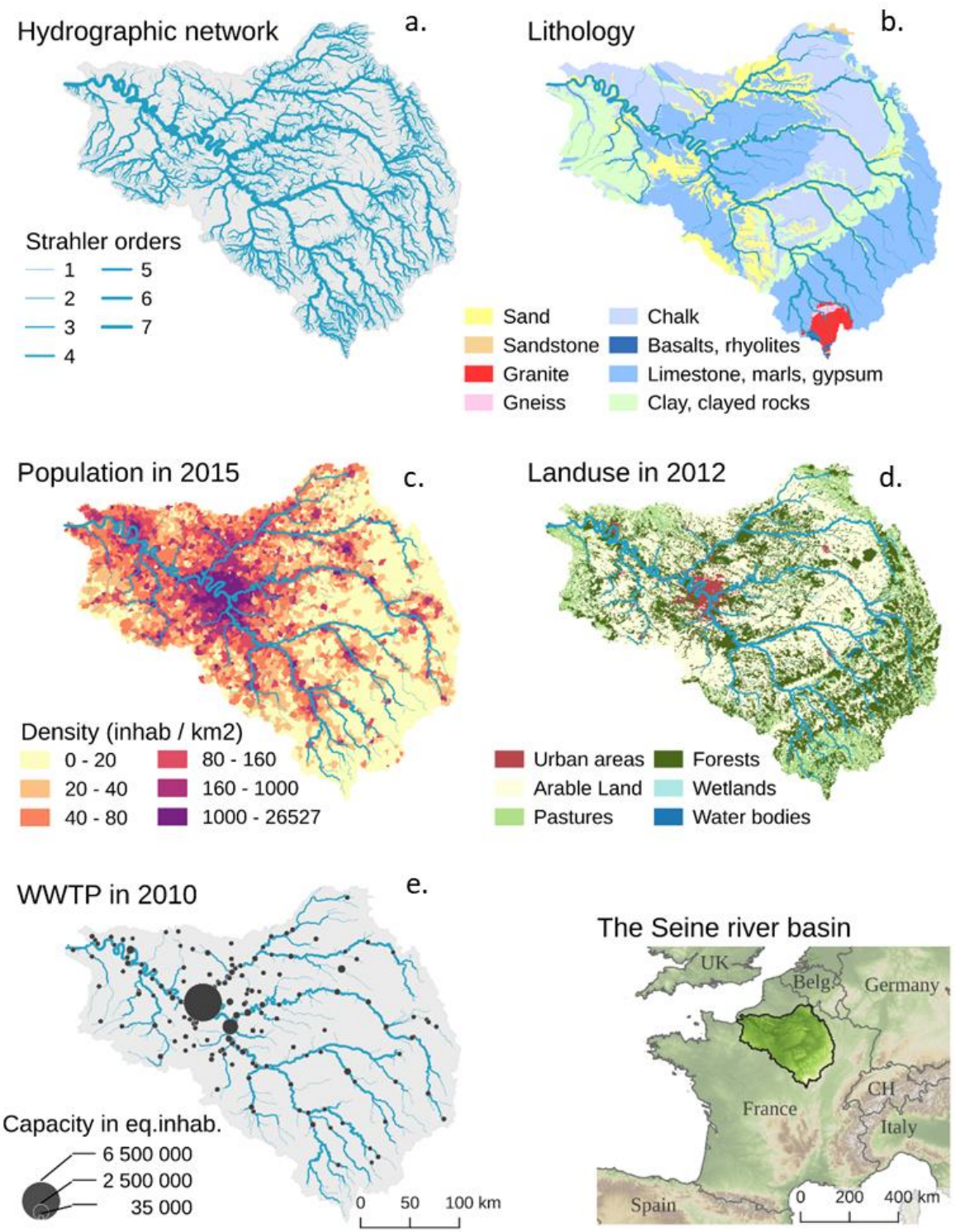

Fig. 0-9 General geographical features of the Seine basin in France. a. Drainage network of the Seine River system. b. Lithological and geological structure. c. Distribution of population density in the Seine basin (data by commune INSEE, 2015) d. Land use in the Seine basin use according to Corine Land Cover (EEA, 2012). e. Main wastewater treatment plants in the basin.

0.8.2. State of research on carbon dynamics in the Seine River

Since 1989, the PIREN-Seine programme (*Programme Interdisciplinaire de recherche sur l'environnement* – French Acronym PIREN, https://www.piren-seine.fr/en) has had a integrated vision of the functioning of the hydrographic network of the Seine as function of the human activities within its basin. The PIREN-Seine program launched by the CNRS is supported by several institutions involved in water management.

In 1989, the first questions investigated by PIREN-Seine researchers were (i) how much must organic and ammonium pollution reaching the river downstream Paris conurbation be reduced to improve oxygenation in the 30 km downstream from the effluents of the major wastewater treatment plant (Seine-Aval WWTP at Achères)? (ii) Is it possible to reduce eutrophication in the major tributaries of the Seine River (Marne, Upper Seine and Oise rivers), where river water is pumped for drinking water?

In this context, the Riverstrahler modeling tool was gradually developed. The representation of the organic carbon (OC) degradation processes by a simple first-order kinetic equation (H. W. Streeter and B. Phelps, 1925) used by sanitation engineers at that time, was replaced by an explicit representation of (i) organic matter in 6 compartments (particulate –POC- and dissolved –DOC- with 3 classes of biodegradability each, (Servais et al., 1991; Billen, 1991) and (ii) heterotrophic bacteria activities and biomasses (Garnier et al., 1992a; Garnier et al., 1992b), implemented in a module referred to as the HSB model (Billen and Servais, 1989). Because organic matter was (and still is) measured as biochemical oxygen demand (BOD) in WWTPs, several studies enabled the conversion of BOD into carbon variables for HSB (Servais et al., 1999) and to characterize and quantify heterotrophic bacterial physiological processes and biomasses not only in the river but also in the WWPT effluents (Servais et al., 1991; Servais et al., 1992; Barillier and Garnier, 1993; Servais and Garnier, 1993; Garnier et al., 1992a).

In the early 1990s, algal development up to 200 µg chl *a* l^{-1}, not only had adverse effect on drinking water production, but represented an organic load that also increased BOD, as shown by Billen et al. (1992), which led to anoxic events, fish mortality... A module of the representation of phytoplankton development was therefore linked to HSB in Riverstrahler making it possible to explore the decrease in nutrient loads needed to reduce eutrophication (Billen et al., 1994; Garnier et al., 2005, 1995).

The above studies, together with measurements of the concentrations of the differents forms of POC and DOC in the drainage network helped draw up an OC budget for the Seine River valid for the 1990s (Servais et al., 1998).

Taking into account autotrophic and heterotrophic processes in the Riverstrahler model enabled quantification of the production/respiration ratio (P/R) along the Seine aquatic continuum for the 1991-1996 period (Garnier and Billen, 2007a), revealing more complexity of P/R in the upstream-downstream pattern than that provided by the River Continuum concept (Vannote et al., 1980) due to human intervention. More recently, using a modeling approach based on the same ecological processes, Vilmin et al., 2016 assessed the organic carbon (OC) budgets downstream and upstream from the Seine-Aval WWTP with more attention paid to benthos effects on OC exports (to the estuary or to the atmosphere) and highlighted the importance of benthic respiration, which accounted for one third of the total river respiration.

Beyond these breakthroughs in the characterization of the degradation of organic matter, very little research was devoted to inorganic forms of carbon. Kempe (1984) calculated a calcite saturation index for the basin, and observed that almost the entire drainage network was supersaturated with respect to calcite. He also calculated pCO_2 indirectly at one station (Paris) in the Seine River (CO_2 mean: 1982 ppm – 1975-1979) (Kempe, 1982).

Addressing DIC or CO_2 concentrations along the Seine River was thus new. Further, taking into account the major improvements in treatment by the WWTPs since the 2000s (Aissa-Grouz et al., 2015; Aissa-Grouz et al., 2016) leading to a reduction in organic pollution and eutrophication required an update of the organic carbon budget and P/R metabolism.

0.8.3. Ecological functioning of the Seine River: the Riverstrahler model

The biogeochemical functioning of the Seine River system has been deeply modified by human activities (intensification of agricultural practices, urbanization and industrialization, etc.). The Seine river system, like many other river systems in densely populated regions of the world, is mainly controlled by anthropogenic constraints. The functioning of the Seine River mainly depends on the location of Paris Megacity, in the center of the basin, 360 km upstream from the coast. Whereas the upstream basin is influenced by terrestrial inputs from the watershed (diffuse sources of nutrients and carbon), the main branch of the Seine, from Paris to the estuary is strongly impacted by point sources of the 12 million inhabitants,

although wastewater treatments have been much improved in the last 20 years (Romero et al., 2016).

The aim of the deterministic Riverstrahler model is to represent the impact of human activities on the quality of river systems by describing the kinetics of all microscopic processes occurring within drainage networks. Accordingly, in this spatially explicit modeling approach, the drainage network is considered as a combination of basins, idealized as a regular scheme of confluent tributaries of increasing stream order (Strahler, 1957), each characterized by mean morphological properties and connected to branches represented with higher spatial resolution (1 km). The advantage of this representation of the drainage network is that the processes occurring in small first-order streams, headwater streams, and large tributaries can all be taken into account.

The model couples water flows routed through the defined structures of basins and branches with a description of the biological, microbiological, and physicochemical processes occurring within the water masses. The variables comprise nutrients, oxygen, suspended matter, dissolved and particulate non-living organic carbon, as well as algal, bacterial, and zooplankton biomasses, giving a total of 35 variables. Most of the processes that play an important role in the transformation, elimination, and/or immobilization of nutrients during their transfer through the network of rivers and streams are explicitly calculated, including algal primary production, aerobic and anaerobic organic matter degradation by planktonic and benthic bacteria, coupled with oxidant consumption and nutrient remineralization, nitrification and denitrification, phosphate reversible adsorption onto suspended matter and subsequent sedimentation.

The biogeochemical core of the Riverstrahler model (RIVE model, www.fire.upmc.fr/rive) is shown in Fig. 0-10 and a detailed description of the model parameters for benthic processes can be found in Garnier et al. (2002), and in Billen et al. (2015).

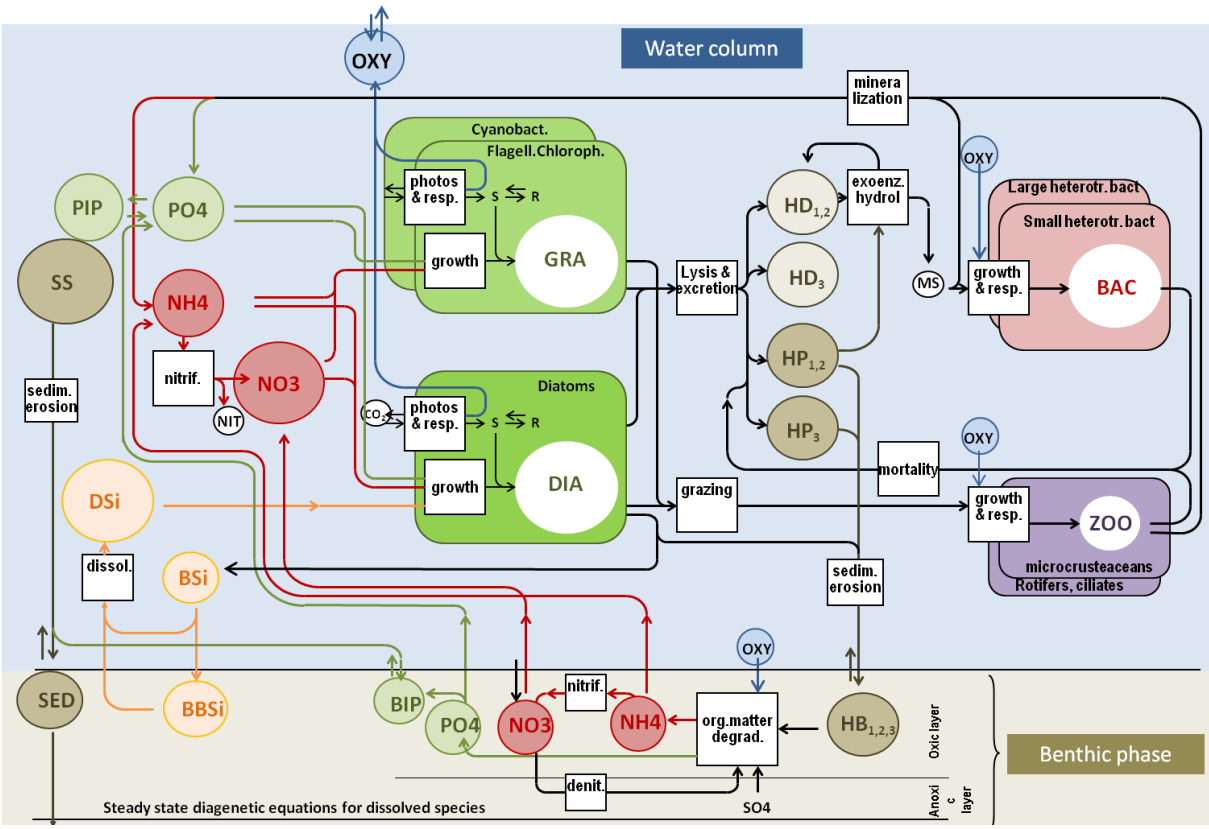

Fig. 0-10 Schematic representation of the RIVE model of biogeochemical processes in river systems

At this stage, Riverstrahler models particulate and dissolved forms of organic carbon but does not take inorganic carbon directly into account. A new inorganic module to model carbonate chemistry and the associated CO_2 fluxes along the land-to-ocean aquatic continuum (LOAC), is needed in this conceptual framework to address new scientific questions related to GHG emissions that are of great concern. Specifically, inorganic carbon modeling should make it possible to propose process based budgets to understand the role of hydrosystems in carbon cascades, and enable a better description of the biogeochemistry of the Seine River watershed under new anthropogenic or climatic constraints.

0.9. Objectives of the thesis research

A part of the C-Cascade program effort

The C-CASCADES (Carbon Cascades from Land-to-Ocean in the Anthropocene) project (2015-2018) is an innovative training network (ITN) under the Marie Skłodowska-Curie actions (http://c-cascades.ulb.ac). The aim of this project was to achieve a breakthrough in our understanding of the transfers and transformations of carbon along the Land-Ocean Aquatic Continuum (LOAC) under contrasted climate conditions. The consequences of anthropogenic perturbations for atmospheric concentrations of CO_2 and for carbon-climate system are also studied.

This thesis is part of the first work package (*WP1: Process understanding: technical development, observations and experiments*) of the C-CASCADES project that aim to study key processes involved in the LOAC including photosynthesis, microbial mineralization, erosion, etc. and the development of sensors. The results of field and lab experiments should increase the accuracy of lateral carbon fluxes (e.g., Nydahl et al., 2017).

Understanding the processes and the estimated fluxes should be included in the biogeochemical models of the WP2: Regional scale applications: benchmark studies on hot-spot areas or WP3: Global scale modeling and feedbacks on Earth system processes.

Specific research questions and organization of the manuscript

This thesis is part of a current collective effort to better understand and characterize carbon cycling along a river continuum. In this context, my Ph-D work consisted of a regional analysis of the highly human impacted Seine Basin.

The first objectif is to assess inorganic (CO_2) concentrations and emissions associated with organic carbon (DOC, POC) dynamics in the aquatic continuum of the Seine River from headwater streams to the main stem. This objective was expressed through several research questions:

What are the different sources that control inorganic and organic carbon concentrations in water and the associated CO_2 emissions to the atmosphere? This question is particularly complex because of the diversity and intensity of human pressures on the Seine watershed.

Do physical and biogeochemical processes that necessarily govern the inorganic carbon cycle from headwaters down to estuarine part of the Seine River have the same relative effects along the continuum? Addressing these challenges required a modeling approach to allow quantification of the contribution of instream processes versus lateral terrestrial sources and to establish carbon cascade budgets based on a process-based understanding of the functioning of the Seine aquatic system.

Still using the LOAC conceptual approach, the logical next step was to monitor carbon deliveries from the Seine to its estuary, raising the question of the fate of carbon riverine fluxes, and answering the question: *what is the specific role of the Seine estuary in carbon transfers and transformations?*

The second objective was to consider CO_2 emissions in parallel with emissions of two major other GHGs, N_2O and CH_4. The questions behind this objective were: *What is the share of N_2O and CH_4, emission from the hydrosystem, in the total emissions with CO_2? How important are these river emissions compared to emissions from terrestrial parts of the basin, especially agriculture, a sector known for its high N_2O and CH_4 emissions?*

According to these objectives and questions, the manuscript is composed of two parts.

The first part "*Carbon dioxide in the Seine aquatic continuum: Observations and modeling*" deals with carbon dynamics and includes Chapter 1, which is devoted to field measurements to enable quantification of carbon forms in the hydrosystem, while Chapter 2 led to the modeling of carbon dynamics and outgassing in the river continuum. Chapter 3 deals with the estuary and presents an extensive carbon budget.

The second part of the manuscript: "*Greenhouse gas (CO_2, CH_4, N_2O) emissions from the Seine basin*" and in Chapter 4, compares concentrations and emissions of CO_2 with those of CH_4 and N_2O in the hydrosystem but also in agricultural and non-agricultural areas of the Seine basin. Finally Chapter 5 targets agricultural emissions of CO_2, CH_4, N_2O over the long term and on a larger spatial scale, followed by a general conclusion and future outlook.

Part One

Carbon dioxide in the Seine aquatic continuum: observations and modeling

Chapter 1

Seasonal and spatial variability of the partial pressure of carbon dioxide in the human-impacted Seine River in France

Chapter 2

Modeling inorganic carbon dynamics in the Seine River continuum in France

Chapter 3

Carbon dynamics along the Seine River network: insight from a coupled estuarine/river modeling approach

PART ONE: SUMMARY

The first part of my Ph-D thesis was dedicated to gathering new knowledge on carbon dioxide (CO_2) concentrations and emissions from the human-impacted Seine basin, a greenhouse gas that had not yet been investigated by our research group.

A major identity of the group is to link observations on the field, and the Riverstrahler modeling approach, that is able to simulate the biogeochemical functioning of hydrosystems at the scale of their drainage network. Whereas most PhD studies deal either with field work (and/or experimental studies) or modeling activities, the first challenge of my PhD thesis was to simultaneously collect CO_2 measurements (and several other physical-chemical parameters) in the field and exploit this field knowledge to develop a module describing the cycling of inorganic carbon in the Riverstrahler model. In addition to using the data collected into a general modeling framework, major investment in data collection and processing was required not only to build the constraints required by this new model, but also to reconstruct and analyze long term trends in CO_2 concentrations based on databases from to the French Water Agency on the Seine basin (AESN). Further, the group is known for collaborating with marine teams, covering the entire land-ocean aquatic continuum, and determining the impact of river nutrient deliveries on the ecological functioning and eutrophication of the coastal zone, using the capacity of a marine model to represent the estuarine part (ECO-MARS3D: Cugier et al., 2005; Romero et al., 2018). However, this model does not include the inorganic form of carbon. Within the group, I had the luck to be able to collaborate in the new implementation of the generic estuarine model (C-GEM) on the Seine River, and in its coupling with the Riverstrahler model to track CO_2 dynamics all along the river-estuarine aquatic continuum.

In the first chapter, I identified the factors controlling the partial pressure of carbon dioxide (pCO_2), on the one hand through four field campaigns in streams and rivers draining different land uses (croplands, grasslands, forests, urban areas, wetlands), in a reservoir, and in piezometers through four contrasted hydrological time periods (in 2016: winter, spring flood, summer-autumn, and in 2017: spring). On the other hand, I analyzed long trend data series (from 1970) of pCO_2 on the main stem of the Seine River. In this way, the Seine hydrosystem was shown to be supersaturated in CO_2 with respect to atmospheric equilibrium, but this has decreased since the 1990s concomitantly with the improvement of wastewater

treatment plants. In addition to organic carbon from soil leaching, pCO_2 and CO_2 fluxes from the Seine were also shown to be clearly linked to dissolved organic carbon from wastewater effluents.

In the second chapter, I describe the new implementation of an inorganic carbon module in the biogeochemical pyNuts-Riverstrahler model. The identification of factors controlling pCO_2 (see chapter 1) helped to characterize the inputs of the carbonate system (dissolved inorganic carbon –DIC-, total alkalinity –TA-), necessary for the implementation in Riverstrahler. Therefore groundwaters, subsurface flows and wastewater treatment plants were defined in terms of DIC and TA. The module developed in chapter 2 enabled the simulation of CO_2 concentrations. Once Riverstrahler, including the CO_2 module, was validated by comparing the simulation with observations available at any location in the river drainage network, biogeochemical processes (photosynthesis, planktonic and benthic respiration, etc.) can be recovered individually and analyzed to understand and discuss both the supersaturation and heterotrophic character of the Seine hydrosystem. We also propose inorganic and organic carbon budgets for the drainage network, emphasizing the huge contribution of DIC inputs from ground- and subsurface waters.

In the third chapter, by coupling the riverine pyNuts-Riverstrahler model and the C-GEM estuarine model, we accomplished the first transient representation of biogeochemical processes involved in the concentrations and emissions of CO_2 over an entire river network. CO_2 outgassing from the riverine part of the basin was dominant (344 GgC yr^{-1}), but the estuary accounted for ~23% of the total (101 GgC yr^{-1}) over a surface area which represents 34% of the entire mirror surface of the Seine River (total: 426 km^2).

This part of the thesis led to national and international collaboration. The technique used to measure direct pCO_2 was transferred thanks to collaboration with A. V. Borges from the Chemical Oceanography Unit, University of Liège (Belgium). The basis of the inorganic carbon module was transmitted by N. Gypens (the Ecology of Aquatic System Unit, Université Libre de Bruxelles, Belgium) and A.V. Borges. Veolia Water and the *Syndicat Interdépartemental pour l'Assainissement de l'agglomération parisienne* (SIAAP) enabled measurements in WWTPs.

.

Chapter n° 1

Seasonal and spatial variability of the partial pressure of carbon dioxide in the human-impacted Seine River in France

Audrey Marescaux[1], Vincent Thieu[1], Alberto V. Borges[2], Josette Garnier[1]

[1]Sorbonne Université, CNRS, Institut Pierre Simon Laplace, UMR 7619 METIS, Paris, France
[2]Université de Liège, Unité d'Océanographie Chimique, Liège, Belgium

Article published in Scientific Reports (2018) volume 8, Article number: 13961

Abstract

Carbon evasion from rivers is an important component of the global carbon cycle. The intensification of anthropogenic pressures on hydrosystems requires studies of human-impacted rivers to identify and quantify the main drivers of carbon evasion. In 2016 and 2017, four field campaigns were conducted in the Seine River network characterized by an intensively cropped and highly populated basin. We measured partial pressures of carbon dioxide (pCO_2) in streams or rivers draining land under different uses at different seasons. We also computed pCO_2 from an existing data set (pH, water temperature and total alkalinity) going back until 1970. Here we report factors controlling pCO_2 that operate at different time and space scales.

In our study, the Seine River was shown to be supersaturated in CO_2 with respect to the atmospheric equilibrium, as well as a source of CO_2. Our results suggest an increase in pCO_2 from winter to summer in small streams draining forests (from 1670 to 2480 ppm), croplands (from 1010 to 1550 ppm), and at the outlet of the basin (from 2490 to 3630 ppm). The main driver of pCO_2 was shown to be dissolved organic carbon (DOC) concentrations ($R^2 = 0.56$, $n = 119$, $p < 0.05$) that are modulated by hydro-climatic conditions and groundwater discharges. DOC sources were linked to land use and soil, mainly leaching into small upstream streams, but also to organic pollution, mainly found downstream in larger rivers. Our long-term analysis of the main stream suggests that pCO_2 closely mirrors the pattern of urban water pollution over time.

These results suggest that factors controlling pCO_2 operate differently upstream and downstream depending on the physical characteristics of the river basin and on the intensity and location of the main anthropogenic pressures. The influence of these controlling factors may also differ over time, according to the seasons, and mirror long term changes in these anthropogenic pressures.

1.1. Introduction

Globally, streams and rivers are estimated to contribute significantly to carbon budgets, with two recent studies estimating carbon dioxide (CO_2) emissions in the order of $0.65^{+0.20}_{-0.17}$ PgC yr^{-1} and 1.80 ± 0.25 PgC yr^{-1} (Lauerwald et al., 2015; Raymond et al., 2013a). This wide range underlines continuing uncertainty, and regional studies are thus needed to provide a better description of the processes driving these carbon fluxes.

Excessive or deficient CO_2 concentration in water with respect to atmospheric equilibrium determines whether inland waters are a CO_2 source or sink. In the majority of river drainage networks, the ratio of primary production to respiration is less than 1, contributing to carbon evasion from inland waters to the atmosphere (Cole et al., 2007; Garnier and Billen, 2007; Battin et al., 2009). CO_2 supersaturation in waters with respect to the CO_2 atmospheric equilibrium can result from the bacterial mineralization of biodegradable organic material exported from soils and autochthonous production as well as inorganic carbon imports from soils (weathering of the bedrock, acidification of buffered waters, etc.) (Butman and Raymond, 2011). In rivers with extensive wetlands (flooded forests and floating macrophytes), lateral DOC enhancing mineralization in the river channel's and CO_2 transports are particularly important (Abril et al., 2014; Richey et al., 2002; Borges et al., 2015b; Borges et al., 2015a). In addition, CO_2 in rivers can be transferred from groundwaters (Venkiteswaran et al., 2014).

Under the temperate European climate, partial pressure of CO_2 (pCO_2) values in rivers display significant variability related to land use, lithology and hydrological conditions. For example, in France, pCO_2 levels of around 284 ppm were measured in the Loire (croplands) (Abril et al., 2015), from 1604 to 6546 ppm in the podzolized Arcachon catchment's streams, with higher values when discharge is low (Polsenaere et al., 2013), and 2292 ppm in the carbonate-rock-dominated Meuse watershed, which is mostly covered by forests, grasslands and croplands (Abril et al., 2015). A recent study of the Meuse River (Borges et al., 2018) revealed marked variations in pCO_2 (34 to 10,033 ppm) the higher values being associated with watersheds dominated by agriculture and lower values with forested watersheds. CO_2 undersaturation with respect to the atmospheric equilibrium has been demonstrated in the upstream part of the Danube River basin related to photosynthetic uptake in summer (Pawellek and Veizer, 1994).

In the Seine River basin, previous carbon investigations focused on organic carbon (Servais et al., 1998), methane emissions from soils, livestock and the river network (Garnier et al., 2013b) or on benthic respiration (Vilmin et al., 2016) and ecological status based on the production/respiration ratio (Garnier and Billen, 2007a). These studies did not specifically address CO_2 concentrations. Our objective here was to quantify pCO_2 in the Seine River, using both recent *in situ* measurements and calculations based on long time series of existing data, in order to evaluate the distribution of pCO_2 and CO_2 evasion in the drainage network, and to identify the major factors controlling pCO_2.

1.2. Materials and methods

1.2.1. Study site

The Seine River watershed, located in northern France, covers an area of 76,750 km^2 with a median slope of 2.2° and 89.5% of its area is less than 300 m A.S.L. It has a pluvio-oceanic regime and its annual water flow in the period 2013–2016 averaged 550 m^3 s^{-1} at the river outlet at Poses (Fig. 1-1). The Poses monitoring station, located at a navigation dam, is the most downstream station not subject to the dynamic influence of the tidal estuary. Low water flows (< 300 m^3 s^{-1}) are generally observed from March to November, while high flows (> 800 m^3 s^{-1}) occur in winter, from December to February (data provided by the HYDRO database, http://www.hydro.eaufrance.fr, 2018).

Three major diverted reservoirs (Fig. 1-1a) located in the upstream part of the basin (the Marne reservoir, the Aube reservoir and the Seine reservoir) were built to reduce high water events in winter, and to sustain the flow in late summer. They have a combined storage capacity of 800 10^6 m^3 and a surface area of 65 km² (Garnier et al., 1999).

The basin is densely populated (~ 230 inhabitants km^{-2}) mostly concentrated in the Paris conurbation (12.4 million inhabitants in 2015) in the central part of the basin. The largest wastewater treatment plant in Europe: Seine Aval, (French acronym SAV) WWTP with a dry weather capacity of 1,500,000 m^3 d^{-1}) is located 50 km downstream of the center of Paris (Fig. 1-1b). The corresponding effluents account for more than 30% of the organic carbon load of all the WWTPs in the basin (Passy et al., 2013). Major upgrading of wastewater treatments of the SAV followed the Urban Wastewater Treatment Directive (1991, 91/271/CEE) among

which the addition of flocculation (2000-2003), nitrification (2007) and denitrification (30% in 2007 and 70% in 2012) (Aissa-Grouz et al., 2015).

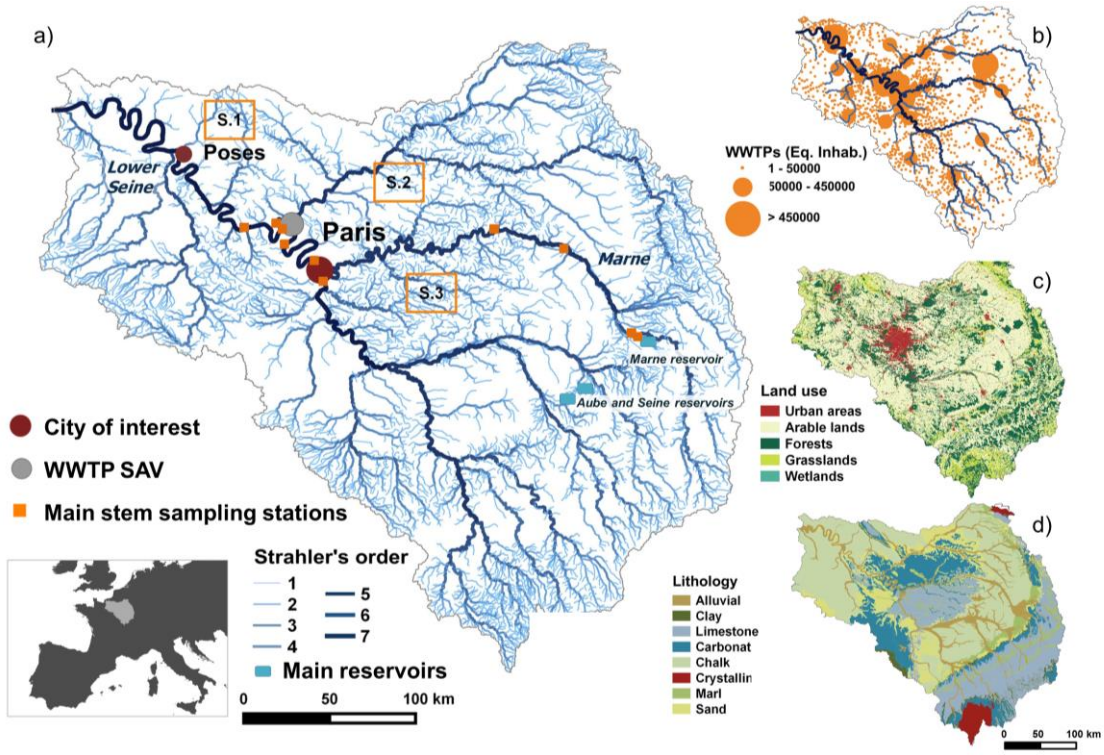

Fig. 1-1 Maps of the Seine river basin created using QGIS software(QGIS Development Team, 2016). (a) The hydrographic network with Strahler orders from 1 to 7, main urban centers (carmine red dots), small stream sampling zones (S1, S2 and S3), main stream sampling sites (orange squares along the lower Seine and the Marne rivers, the three main reservoirs (blue squares) and the main wastewater treatment plant (grey dot). (b) Wastewater treatment plants in the Seine basin mapped according to their treatment capacity (AESN 2012); (c) Land uses in the Seine basin (CLC database, IFEN 2012)(IFEN, 2012); (d) Lithology of the Seine basin (Albinet, 1967; Albinet, 1967)

The Seine counts about 1700 smaller capacity WWTPs spread throughout the basin (Fig. 1-1b). The basin comprises 56.8% arable land (mainly under intensive agriculture), 25.8% forests, 9.7% grasslands and 7.0% urban areas (CLC database, IFEN 2012, Fig. 1-1c). Wetlands have been estimated at between 10.9% and 15.6% of the surface area of the basin (Curie et al., 2007). The Strahler stream order (Strahler, 1957) of the main stream of the basin is 6th order for the Marne River and 7th order for the Seine River downstream of Paris (Fig. 1-1a). The sedimentary basin of the Seine River is characterized by geological formations with low slope gradients resulting in concentric lithology dominated by carbonate and limestone in the central part of the basin, a wide band of Cretaceous chalk and a narrow band of clay followed by Jurassic limestone at the periphery (Fig. 1-1d).

1.2.2. Sampling strategy, physical-chemical analysis and direct measurements of pCO_2

We sampled 30 sites in streams chosen because they mainly drain grasslands, forests and wetlands, croplands, and along the main streams of the Marne River (including in its reservoir) and of the lower Seine (Fig. 1-1a, exact locations in supplementary materialAnnex 1-1). Sampling campaigns were carried out in four contrasting hydro-climatological periods. Water discharges were measured at the outlet of the basin (Poses) and temperatures were measured at each sampling site in winter from February 22 to March 10, 2016, (1030 m^3 s^{-1}, 6.9 °C on average), in summer/autumn from September 7 to 14, 2016, (270 m^3 s^{-1}, 18.8 °C), spring from March 14 to 23, 2017, (580 m^3 s^{-1}, 9.9 °C) as well as during a spring flood event that was exceptional in its timing, from May 23 to June 2, 2016, (1500 m^3 s^{-1}, 13.0 °C, at sampling time with a maximum discharge reaching 2000 m^3 s^{-1} at the river outlet, at Poses). The field campaigns were assumed to be key seasonal and hydrological periods and were conducted in areas representing the main types of land use in the Seine River basin.

Direct pCO_2 measurements were based on the syringe headspace technique (Abril et al., 2015; Teodoru, 2009) combined with non-dispersive infrared gas analysis (IRGA) (Li-cor® models 820 or 840; accuracy < 3% of reading). Calibration was performed using CO_2 concentration of 799 ppm and CO_2-free dinitrogen. Four syringes coupled with three-way valves were filled directly in the stream or river, each replicate containing 30 mL of river water and 30 mL of atmospheric air. Closed syringes were continuously shaken for 10 min to equilibrate CO_2 concentrations of gas and water. The equilibrated gas was injected into the IRGA and water temperature inside the syringe was measured. The first injection served as a purge and the other three were used for pCO_2 measurements. The initial pCO_2 in water was computed based on the pCO_2 measured in the equilibrated air of the syringe and in the atmospheric air, and Henry's law accounting for the water temperature in the syringe and *in situ*.

Simultaneously, 2 L water chemistry high-density polyethylene sampling bottles were used to collect samples from bridges over the main stream, and along the banks of smaller streams. Water temperature, pH, dissolved oxygen and conductivity were measured in the field using a multi-parameter probe (YSI® 6600 V2, accuracy ± 0.2 units). Calibrations of the probe were completed with pH 7 and pH 4 buffers for pH (NBS Scale), potassium chloride (KCl) electrolyte solution for dissolved oxygen and 10 mS cm^{-1} standard for conductivity. In the laboratory, water subsamples were filtered on combusted filters for 4 h at 500 °C: GF/F 0.7

µm, 25 mm) to analyze particulate inorganic and organic carbon (PIC and POC, respectively). Filtrates enabled measurement of dissolved inorganic and organic carbon (DIC and DOC) concentrations and total alkalinity (TA). One milliliter of sulfuric acid (3 M) was added to the DOC samples to stop biological reactions. Dissolved inorganic and organic carbon were analyzed with a TOC analyzer (Aurora 1030). Nongaseous DIC analyses required acidification of the filtrated sample by adding sodium persulfate reagents (100 g L^{-1}) to dissociate the carbonates in the CO_2 that were detected by an IRGA. The inorganic free sample was used for DOC measurements. DOC was measured by wet oxidation by adding 10% phosphoric acid oxide followed by high temperature (680 °C) catalytic combustion, and then detected using an NDIR technique. TA (µmol kg^{-1}) was analyzed using an automatic titrator (TitroLine® 5000) on three 20 mL replicates of filtered water (GF/F: 0.7 µm), with hydrochloric acid (0.1 M).

Values of total suspended solids (TSS) were determined as the weight of material retained on a Whatman GF/F membrane per volume unit after drying the filter for 2 h at 120 °C. Chlorophyll *a* concentrations (Chl. a) were determined according to Lorenzen, (1967).

Aquifer waters were also sampled during the same periods. Groundwater was pumped from the piezometers using a peristaltic pump. Before the samples were collected, the piezometers were emptied by flushing to remove the standing water (5–10 L in each piezometer) (Guillaume Vilain et al., 2012). The same variables were measured or analyzed, except Chl. a.

1.2.3. pCO_2 calculations from existing data

pCO_2 were computed with the CO_2SYS software (Pierrot et al., 2006) using the water temperature and two of the three following measurements: pH, TA and DIC. In contrast to DIC, TA is often measured by the French water authorities *Agence de l'Eau Seine Normandie* (French acronym AESN, http://www.eau-seine-normandie.fr/, 2018/11/05), and thus were preferred to compute pCO_2 in combination with pH and water temperatures. The carbonate dissociation constants (K1 and K2) applied were from Millero, (1979) with zero salinity.

During our field campaigns (winter 2016, spring 2017, spring flood 2016, summer/autumn 2016, see *previous section*), we systematically combined direct measurements of pCO_2 with measurements of water temperature, pH and TA (130 samples). We found a positive relationship between the pCO_2 values directly measured during our field campaigns and those

calculated using water temperatures, pH and TA (Fig. 1-2.). This relationship was then used to correct possible bias (Abril et al., 2015) of pCO_2 values calculated with CO2SYS program.

We also used the database (42,108 data with simultaneous water temperatures, pH and TA measured between 1971 and 2015) provided by the French water authorities (AESN) to compute and analyze the pCO_2 dynamics in the Seine basin in space and over time since the 1970s. These pCO_2 data series were corrected by the relationship previously established and then averaged by months and years at each monitoring station. Within this timeframe (1970-2015), two periods of interest (ii) 1989–1991 (92 monitoring stations) and (ii) 2013–2015 (234 monitoring stations) were defined as representative of the changes that occurred recently in the Seine river basin. The former period (1989–1991) represents the period of highest organic pollution from WWTPs, only treated by activated sludge. The most recent period (2013–2015) illustrates the state after a full implementation of the Urban Wastewater Treatment Directive (1991, 91/271/CEE), including the reduction of point sources of organic carbon (industrial and domestic) discharge into the river, as well as phosphorus and nitrogen (Passy et al., 2013; Aissa-Grouz et al., 2015; 2016). In addition, we assessed the spatial variability of pCO_2 along the main stream of the Seine River, comparing the concentrations of the most important effluents up- and downstream (Paris and Poses stations, Fig. 1-1) of the SAV WWTP. We also computed pCO_2 at a constant temperature of 10°C (pCO2@10°C) downstream of the SAV WWTP to show the impact of solubility on pCO_2 (see results section: "*Long-term pCO_2 variability (1970–2015)*").

1.2.4. Determination of gas transfer velocities

Raymond et al. (2012a) pointed out that gas transfer velocity equations including slope and water velocity enable easy measurements and recommended the use of these equations at large spatial scales. We selected the equation requiring only the slope and the water velocity and that had the highest squared-R in the Raymond et al. (2012a) study (Equation 5 in Table 2 in Raymond et al. (2012a)) as we wanted to compare the variability of CO_2 evasion in the basin in space and over time. We used kinematic water viscosity coefficients and Schmidt numbers calculated according to Wanninkhof (1992).

The slopes of the streams and rivers were provided by the French water authorities (AESN). Water velocities were estimated from discharge records available at the scale of the whole drainage network for the period 2012–2014. Water temperatures were averaged by season of

interest based on our field campaigns (winter, spring and summer/autumn). The *k*-values were calculated by stream order and then aggregated by small streams (Strahler orders (SOs) 1–4) and along the main stream (SOs 5–7). Calculated *k*-values for the spring flood event were based on averaged spring water temperatures associated with measurements of high water flow collected during the exceptional spring flood (May 2016).

According to Wanninkhof (1992), Wilke and Chang, (1955) and (Raymond et al. (2012a), the gas transfer velocity k_{CO_2} (m d^{-1}) under negligible wind conditions in rivers can be calculated as:

$$k_{CO_2} = k_{600} \cdot \sqrt{\frac{600}{Sc_{CO_2}(T)}} \tag{1-1}$$

$$k_{600} = vS\ 2841 \pm 107 + \ 2.02 \pm 0.209 \tag{1-2}$$

where k_{600} is the gas transfer velocity for a Schmidt number of 600 (m d^{-1}), v is the water velocity (m s^{-1}), S the slope (-),107 et 0.209 are the standard deviations of the parameters. $Sc_{CO_2}(T)$ is the Schmidt number (dimensionless) with the water temperature T in Celsius ($°C$) calculated as :

$$Sc_{CO_2}(T) = \ 1911.1 - 118.11T \ + 3.4527T^2 - 0.04132T^3 \tag{1-3}$$

The flux (fCO_2, mgC-CO_2 m^{-2} d^{-1}) at the interface of the river and the atmosphere can be calculated as:

$$fCO_2 = k_{CO_2}\left([CO_2] - [CO_2]_{eq}\right) \tag{1-4}$$

where $[CO_2]$ is the CO_2 concentration in the water (mgC-CO_2 m^{-3}), and $[CO_2]_{eq}$ is the CO_2 concentration in equilibrium with atmospheric concentrations (mgC-CO_2 m^{-3}). Annual atmospheric pCO_2 values measured at Mauna Loa Observatory (Hawaii, U.S.A.) were provided by the NOAA/ESRL (http://www.esrl.noaa.gov/gmd/ccgg/trends/, 2018/11/05),

Scripps Institution of Oceanography (scrippsco2.ucsd.edu/, 2018/11/05). k_{CO_2} (m d^{-1}) is the gas transfer velocity (see equation 1).

1.2.5. Statistical tests

All statistical tests were performed using R software (R Core team, 2015).

Wilcoxon signed-rank tests were used to compare measured pCO_2 in the four periods, and Kruskal-Wallis tests were used to compare measured pCO_2 averages for different land uses during each period. A Shapiro-Wilk test was applied to test the normal distribution before performing the linear regression between measured pCO_2 and calculated pCO_2. Linear regressions were then performed between pCO_2 and water quality variables.

1.3. Results

1.3.1. Measured versus calculated pCO_2

The streams and rivers sampled during our field campaigns were neutral or basic and carbonate-buffered (Fig. 1-2a and 2c), excluding the overestimation of calculated pCO_2 already shown to be linked to the low buffering capacity of the carbonate system (Abril et al., 2015). A logarithmic transformation was performed on both measured and calculated pCO_2 to obtain normal distribution (Shapiro-Wilk test, $p > 0.01$)) to calculate a linear regression. A positive relationship was established ($R^2 = 0.56$, n = 130, $p < 0.01$).

$$\boldsymbol{measured\ p_{CO_2}} = \mathbf{10}^{\left(\frac{\boldsymbol{log}\left(\boldsymbol{calculated\ p_{CO_2}}\right) - \mathbf{0.51}}{\mathbf{0.85}}\right)} \text{ (p < 0.01 and degrees of freedom = 106)}$$

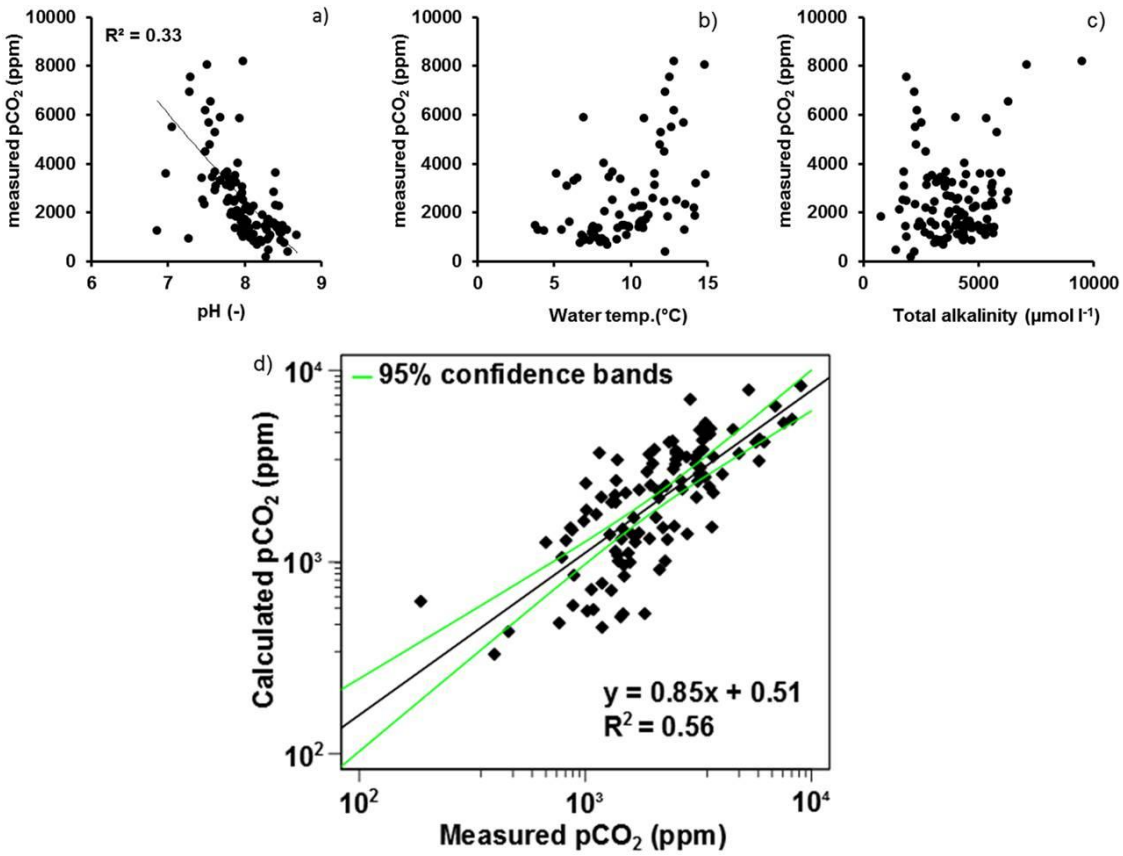

Fig. 1-2 Measured pCO2 vs. (a) pH (NBS scale); (b) water temperature (Water temp.); (c) total alkalinity; (d) comparison of calculated pCO2 (using pH, temperature, alkalinity) and direct measurements of pCO2. Green lines represent the 95% confidence intervals.

1.3.2. Field campaign dataset overview

Average water temperatures ranged between 6.9 °C and 18 °C which corresponds to the expected seasonal range for the Seine basin (Table 1-1). pH values were generally neutral to basic, with median values of pH and TA in all streams and rivers ranging respectively from 7.75 to 8.25 and from 3150 µmole l^{-1} to 4350 µmole l^{-1}(see Table 1-1). Only two acidic pH values measured during the winter in streams draining forests (data not shown). The high total alkalinity measured in all the streams and rivers (Table 1-1) indicated that waters were carbonate-buffered due to the lithology of the basin, which is dominated by carbonate rocks (Fig. 1-1d) (Meybeck, 1987). Indeed, dissolved inorganic carbon (DIC) concentrations were high (min.: 19.3 mgC l^{-1}, Table 1-1) as was conductivity (median of all campaigns: 0.554 mS cm^{-2}), suggesting that bicarbonate ions contributed most to total alkalinity. Dissolved inorganic carbon (DIC) concentrations averaged 52.55 mgC l^{-1} (median: 54.04 mgC l^{-1}). Dissolved organic (DOC) concentrations were one order of magnitude lower than those of

DIC, the highest being observed in streams draining wetlands (median: 17.25 mgC l^{-1}) while streams draining croplands had the lowest concentrations (median: 2.62 mgC l^{-1}). Total suspended solids (TSS) were highest (median 20.77 mg l^{-1}) in grasslands during the spring flood 2016 (with a median chlorophyll *a* concentration of 27.1 µg l^{-1}). Wetlands were mostly undersaturated in oxygen (median: 5.7 mgO_2 l^{-1} and min. water temperature: 6.1°C) while the rest of the data set showed oxygenated waters (median: 9.2 mgO_2 l^{-1}; min. – max.: 6.0 – 15.7 mgO_2 l^{-1}).

Table 1-1.Summary of the field data set. Median, 10th and 90th percentiles pH (measured on the NBS scale), water temperature, total alkalinity, dissolved organic carbon (DOC), dissolved inorganic carbon (DIC), total suspended solids (TSS), chlorophyll a (Chl. a), dissolved oxygen (O_2) and conductivity. Mean water discharges are showed for seasons at the outlet of the basin.

		pH (-)	Water temp. (°C)	Total alkalinity (µmole l^{-1})	DOC (mgC l^{-1})	DIC (mgC l^{-1})	TSS (mg l^{-1})	Chl. a (µg l^{-1})	O_2 (mgO_2 l^{-1})	Conductivity (mS cm^{-2})	Water flow (m^3 s^{-1})
Winter	*median*	8.05	6.9	4350	6.9	52.7	22.7	6.6	9.85	0.557	1030
2016	*10th - 90th*	7.30 - 8.50	5.0 - 8.3	2770 - 5140	2.7 - 13.8	38.1 - 64.3	10.3 - 42.7	2.4 - 9.6	5.60 - 13.37	0.327 - 0.781	
Spring	*Median*	8.25	9.9	4255	4	58.6	17	6.1	9.63	0.59	580
2017	*10th - 90th*	7.82 - 8.47	8.3 - 11.0	2375 - 5475	2.4 - 14.7	39.6 - 72.0	8.2 - 32.8	1.6 - 25.4	8.88 - 10.94	0.392 - 0.678	
Summer-autumn	*Median*	7.96	18	4037.5	3.5	53.9	7.9	2.3	8.23	0.597	270
2016	*10th - 90th*	7.83 - 8.33	15.5 - 22.6	1872.5 - 5685	2.0 - 6.6	28.2 - 73.6	4.1 - 45.3	1.1 - 10.9	9.00 - 8.23	0.373 - 0.695	
Spring flood	*Median*	7.75	13	3150	11.4	45.7	20.77	12	8.81	0.49	1500
2016	*10th - 90th*	7.29 - 7.98	11.9 - 15.5	1875 - 5800	3.4 - 20.9	26.3 - 66.9	3.2 - 214.0	2.3 - 30	5.81 - 9.58	0.311 - 0.648	

1.3.3. Variability in pCO_2

Spatial and seasonal variability of pCO_2

All samples were supersaturated in CO_2 with respect to the atmosphere, regardless of river characteristics (small stream or main stream), the associated dominant land use and the season (Fig. 1-3a). pCO_2 increased significantly i.e., by an average of 49% and 62% from winter to summer/autumn, in streams draining forests and croplands ($p < 0.05$, Wilcoxon signed-rank test, Fig. 1-3a). Values in grasslands did not typically follow this pattern ($p > 0.05$, Wilcoxon signed-rank test, Fig. 1-3a), and pCO_2 remained rather stable at 2,900 ppm, whereas pCO_2 was the highest in wetlands ($p < 0.05$, Kruskal-Wallis test), especially in spring and summer/autumn (> 4500 ppm).

For each of the four seasons monitored, pCO_2 average decreases ranked as follows: wetlands > grasslands > forests > croplands ($p < 0.05$, Kruskal-Wallis tests, Fig. 1-3a). At the outlet of the Seine River, the main stream drains composite land uses where pCO_2 averages were found to be equivalent to those measured in small streams draining grasslands (Fig. 1-3b).

In the lower Seine River, which is highly impacted by urbanization and associated treated WWTP effluents, a 69% increase in pCO_2 was observed from winter (December to February), to spring (March to June) to summer/autumn (June to November) with limited dilution by the discharge (mean discharge in winter: 1030 m^3 s^{-1}; spring: 580 m^3 s^{-1}; summer/autumn: 270 m^3 s^{-1}) (Fig. 1-3b, Table 1-1).

However, during the late spring flood (1500 m^3 s^{-1} at Poses, the Seine river outlet), pCO_2 averages increased in all the land uses (3100, 3200, 5900, 8400 ppm for croplands, forests, grasslands and wetlands, respectively) (Fig. 1-3a).

In the groundwater, pCO_2 averaged 27,000 ppm at a yearly scale, but reached up to 65,000 ppm (summer/autumn 2016), i.e., a factor of 5 to 10 compared to surface waters.

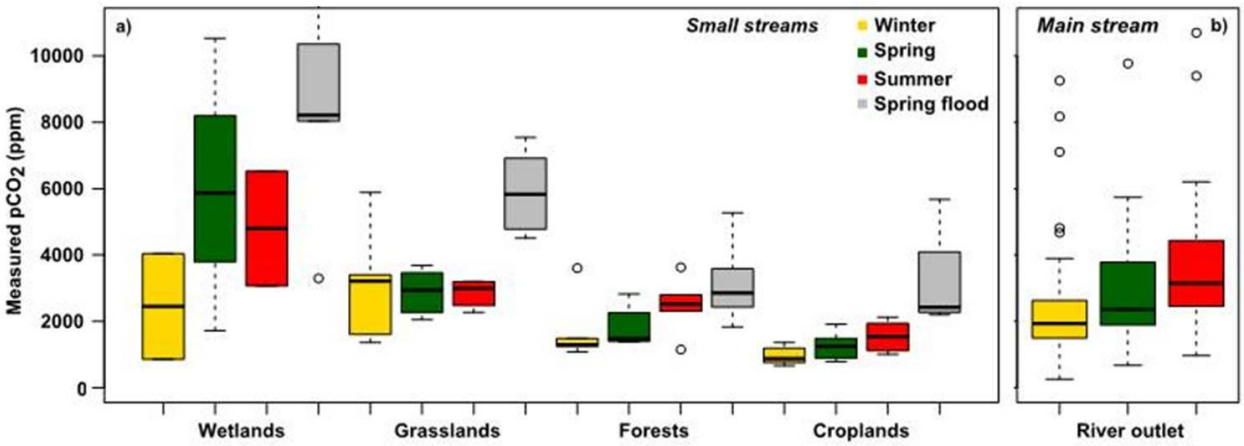

Fig. 1-3 Boxplots of pCO2 assembled as function of the land uses and seasons investigated. The lower, intermediate and upper parts of the boxes represent respectively the 25th, 50th and 75th percentiles and the empty circles represent the outlier values. (a) pCO2 measured in stream waters (order 1 to 4) draining wetlands, grasslands, forests and croplands during the 2016 and 2017 field campaigns (hydro-climatic conditions are listed in Table 1-1). (b) pCO2 calculated from existing bi-monthly pH, total alkalinity and water temperature data at the outlet of the Seine River (Poses station) from 2013 to 2015 and aggregated by the four seasons of interest (see Materials and Methods, pCO2 calculations) (Data source: AESN).

According to the k_{600} equation selected (see Materials and methods, equations 1-3), gas transfer velocity (*k*-values) was estimated from the slopes. Slope was higher for small streams (0.006 m m^{-1}) than larger rivers (0.0004 m m^{-1}) (Fig. 1-4a). Seasonal variations in water temperature increased from winter to summer/autumn (Fig. 1-4b), and velocities decreased from winter to summer/autumn (Fig. 1-4c). The resulting *k*-values ranged from 0.08 to 0.24 m h^{-1} with a decrease from small streams (*k* annual average = 0.19 m h^{-1}) to larger rivers (*k* annual average = 0.09 m h^{-1}) (Fig. 1-4d).

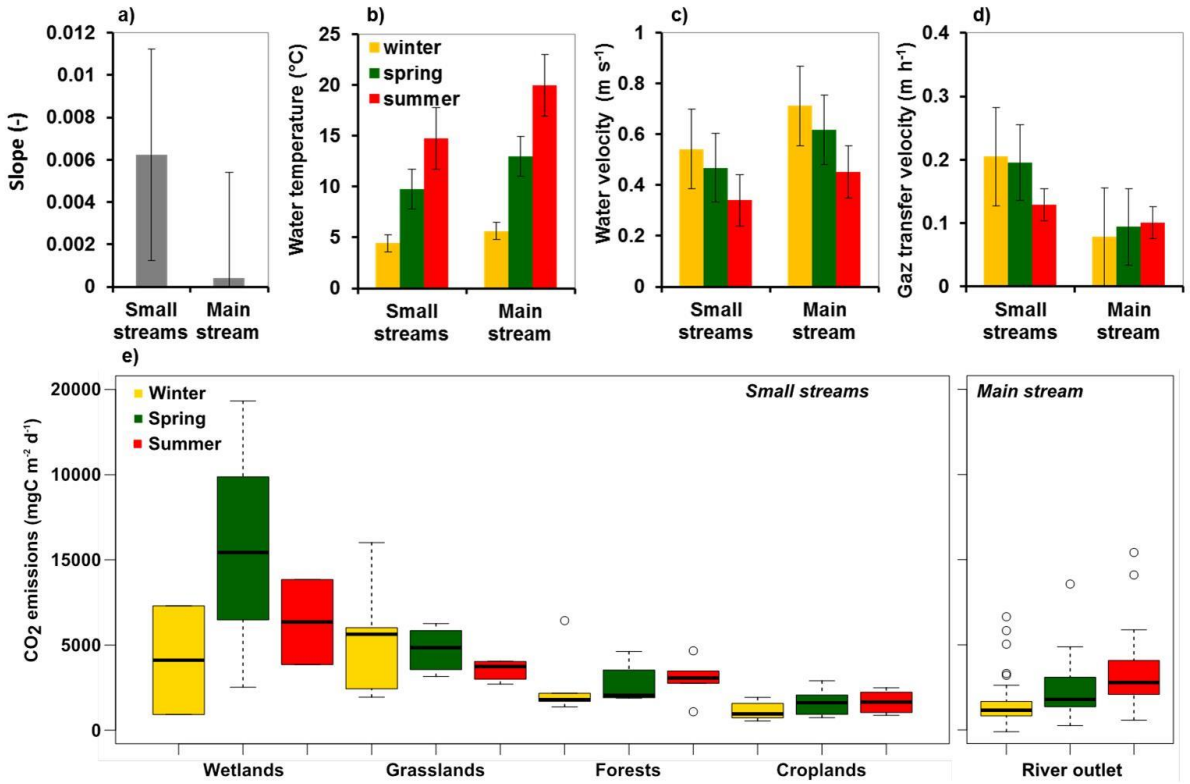

Fig. 1-4 Comparison of the physical characteristics of small streams (orders 1 to 4) and of the main stream (orders 5 to 7) of the Seine River, averaged by season (excluding spring flood measurements): (a) slopes of the streams or rivers; (b) water temperatures; (c) water velocities; (d) gas transfer velocities; (a-d) Whiskers represent standard deviations; (e) boxplots of CO2 emissions assembled according to land uses. The lower, intermediate and upper parts of the boxes represent respectively the 25th, 50th and 75th percentiles and circles represent the outlier values

Using equation (2), the higher slopes found in small streams led to higher *k*-values (Fig. 1-4a and 4d). Additionally, in the small streams in the Seine River basin, the water velocity effect prevails over the seasonal *k* dynamics, while control by water temperature is greater in higher stream orders (Fig. 1-4b, 4c and 4d). During the spring flood event, the increase in the water discharge (and velocity) led to a greater increase in *k* in small streams than in larger rivers,

respectively + 26% (spring flood: 0.24 m h^{-1}) and + 11% (spring flood: 0.10 m h^{-1}) compared to average spring *k*-values (small streams: 0.19 m h^{-1}, larger rivers: 0.09 m h^{-1}).

CO_2 fluxes at the water-atmosphere interface (Fig. 1-4e) were estimated using the pCO_2 measurements we made during our field campaigns (Fig. 1-3), CO_2 saturation values that depend on water temperatures (see Table 1-1), atmospheric pCO_2, and *k*-values estimations (Fig. 1-4d). The same seasonal pattern was observed for pCO_2 and CO_2 fluxes.

Long-term pCO_2 variability (1970–2015)

Long-term analysis of French water authority (AESN) databases showed supersaturation of CO_2 of the Seine River dating back to 1970 (98.5% data suggested supersaturation with respect to atmospheric equilibrium – pCO_2 median = 3030 ppm; mean = 4765 ppm). From that period on, the Seine River has been a source of CO_2 to the atmosphere even when frequent phytoplankton blooms occurred before wastewater treatment was improved. However, focusing on the bloom events (Chl. a > 50µg l^{-1}, Fig. 1-5), we observed the opposite pattern between Chl. a and pCO_2 dynamics, with depletion of pCO_2 concomitantly with peaks of phytoplankton. This consumption of CO_2 was not sufficient to cause undersaturation of CO_2 in the river (Fig. 1-5).

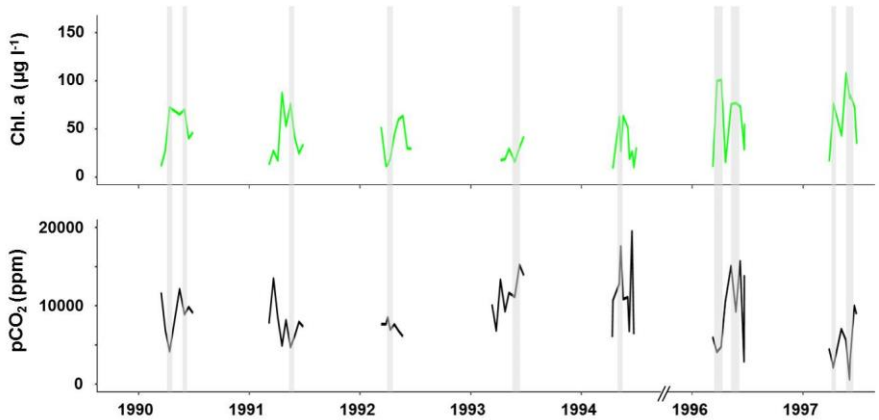

Fig. 1-5 Calculated pCO2 dynamics during bloom events (Chl. a > 50 µg l-1) since the 1990s at the outlet of the Seine River, Poses (Data source: AESN)

When we compared the two contrasted periods with respect to water sanitation and associated organic carbon releases, we found a similar range of temperature and discharge values and a seasonal pattern typical of temperate oceanic hydro-climatology regimes, i.e., high temperatures and low water in summer/autumn. The first of these two periods was however slightly drier than the second (on average 400 m3 s-1 vs. 545 m3 s-1, respectively) with no

notable change in temperature (averaging 13.9°C vs. 14.2°C, respectively. We observed that pCO2 computed at both 10°C and at water temperature were similar during winter but values at 10°C were slightly lower than at water temperature during summer (Fig. 1-6). However, general trends of pCO2 did not change.

In contrast, pCO_2 was reduced by a factor of 2.7 between the two periods (average 8,250 ppm for the period 1989–1991 versus 3020 ppm for the period 2013–2015). These weak hydro-climatologic changes cannot explain the marked decrease in pCO_2 at the river outlet between the two periods. We found no relationship between pCO_2 and discharge at this time scale, despite a clear antiparallel trend for these two variables (Fig. 1-6).

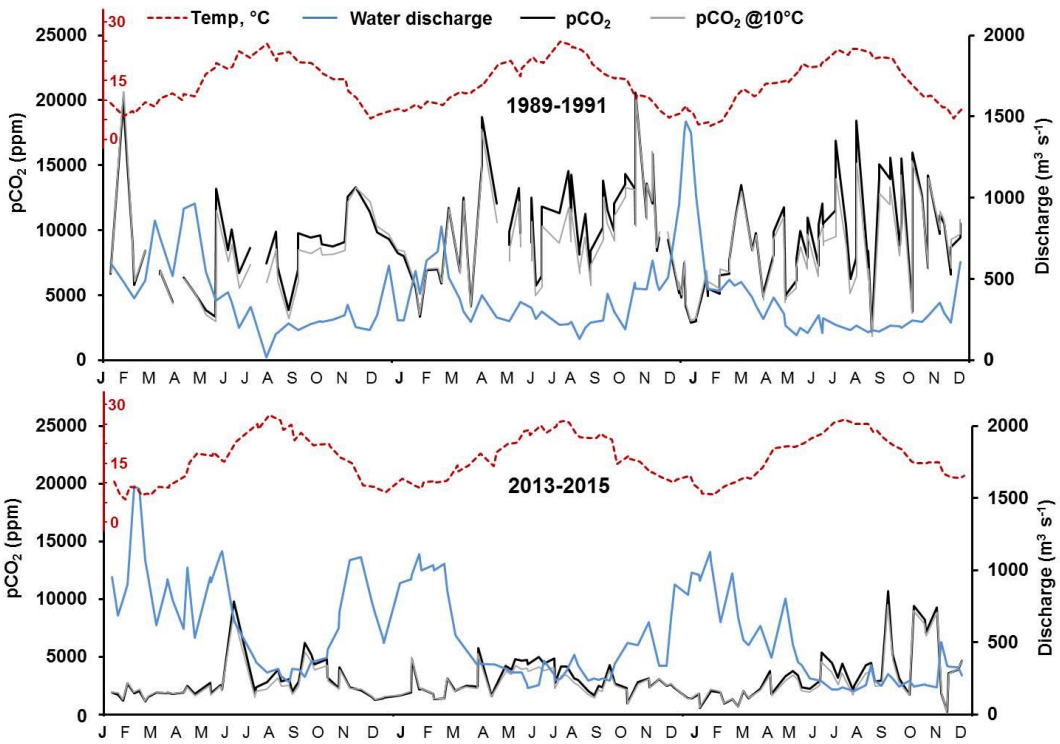

Fig. 1-6 Seasonal variations in calculated pCO2 at the water temperaturer (pCO2) and at 10°C (pCO2@10°C) values compared with variations in water discharge and temperature values (at Poses) for the two periods: 1989–1991 (atmospheric pCO2 = 354 ppm) and 2013–2015 (atmospheric pCO2 = 399 ppm)

To further explore the recent decrease in pCO_2, we assessed spatial variations in pCO_2 at the scale of the whole Seine drainage network (Fig. 1-7). Although fewer measurements were available in the earlier period (1989–1991), the decrease in pCO_2 between the two periods was obvious along the lower reach of the main stream of the Seine River, downstream of the Paris conurbation. In the recent period, the pCO_2 of both the upstream parts of the drainage

network and the main stream of the Seine River appear to be equally supersaturated ($p > 0.05$, Kruskal-Wallis tests, Fig. 1-7).

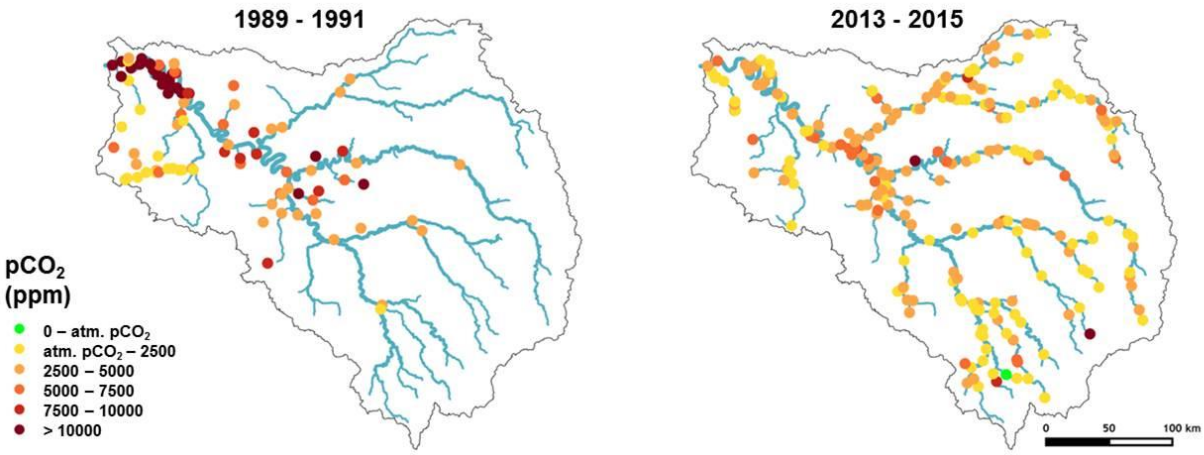

Fig. 1-7 Spatial variations in calculated pCO2 averaged over the two periods 1989–1991 (with high organic pollution) and 2013–2015 (after wastewater treatment had been improved). Values are represented for Strahler orders superiors to 2 (Data source: AESN)

Since the 1970s, upstream of the discharge of treated effluent from the SAV WWTP, the long-term trend of pCO_2 values in Paris has varied around 5000 ppm (Fig. 1-8a). A few kilometers downstream, at the outlet of the Seine River at Poses (strongly influenced by Parisian wastewater discharges) pCO_2 progressively increased to reach a maximum of 12,000 ppm in the 1990s, and then slowly decreased to present values of 3000–4000 ppm (Fig. 1-8a). This decrease in pCO2 was concomitant with changes in the fluxes of biodegradable total organic carbon (BTOC) discharged by the WWTPs of the Parisian conurbation managed and operated by the Greater Paris sanitation authority (French acronym SIAAP) after treatment (Fig. 1-8a). From the 1990s to 2015, the BTOC load decreased by 80% (from 13.8 to 2.8 kt BTOC yr-1) following the construction (on the SAV WWTP site) of a new WWTP in 1991 and of three new waste water treatment plants between 2005 and 2008, conjointly with improvement in treatment at existing plants. A positive linear relationship ($R2 = 0.52$, $n = 29$, $p < 0.05$) was found between annual pCO2 at the outlet of the Seine River (Poses) and BTOC fluxes from the SAV WWTP (Fig. 1-8b).

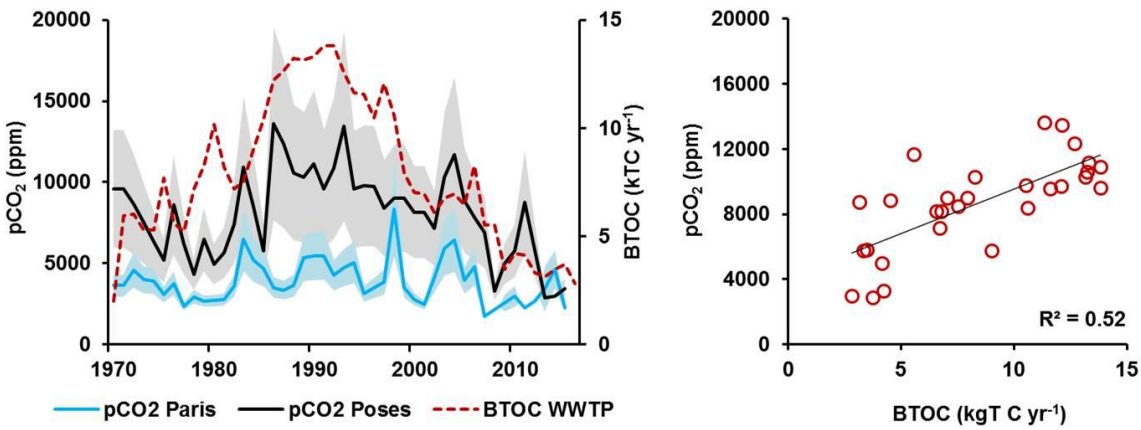

Fig. 1-8 (a) Long-term variations in calculated pCO2 from 1970 to 2015 at two sites on the lower Seine River: at the entrance to Paris (blue curve) and at the river outlet at Poses downstream of the main WWTP Seine-Aval (black curve), the associated shaded areas represent the 95% confidence intervals (Data source: AESN). The red dashed curve represents the biodegradable total organic carbon fluxes (BTOC) discharged from the main SAV WWTP into the Seine River. BTOC was estimated from the relationship BTOC = 0.35 BDO (R^2 = 0.91, n = 23) established by Servais et al. (1999) which converts biological demand in oxygen (BDO, provided in Rocher and Azimi, 2017) into BTOC; (b) Relationships between calculated pCO2 at Poses and BTOC from the main SAV WWTP.

1.3.4. pCO_2 environmental controls

We found a positive linear relationship between pCO_2 and DOC (R^2 = 0.56, n = 119) (Fig. 1-9a). DOC measured in grasslands (DOC average: 10.3 mg L^{-1}; SD: 5.8 mg L^{-1}) and wetlands (DOC average: 21.0 mg L^{-1}; SD: 14.6 mg L^{-1}) showed wider and higher ranges of concentration compared to arable lands (DOC average: 3.8 mg L^{-1}; SD: 2.7 mg L^{-1}) (Fig. 1-9a). Generally, the ranges of DOC and pCO_2 were lower in winter and higher in summer/autumn and during the spring flood. No relationship was found between pCO_2 and DIC or nutrients (Fig. 1-9b, see supplementary materialAnnex 1-2Annex 1-2). The highest pCO_2 and the lowest oxygen concentrations were measured in anoxic wetlands, whereas the opposite was found in the Marne River reservoir, and overall, a negative relationship between pCO_2 and dissolved oxygen was observed for all land uses (R^2 = 0.22, n = 120, $p < 0.05$, Fig. 1-9c). We also found a positive relationship between pCO_2 concentrations and Chl. a concentrations (R^2 = 0.26, n = 113, $p < 0.05$, Fig. 1-9d).

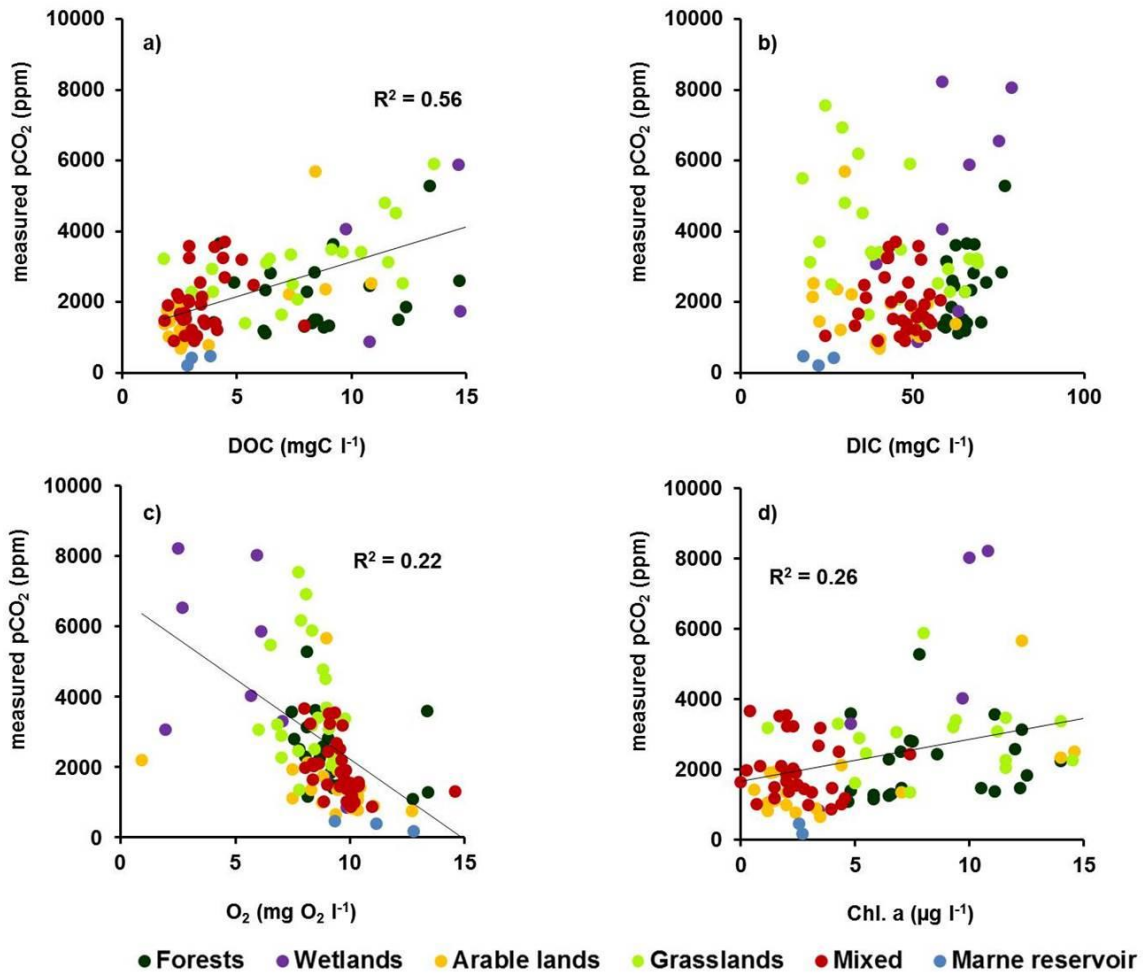

Fig. 1-9 Relationships between measured pCO_2 and surface water quality variables according to the different land uses sampled during the field campaigns: streams draining forests, wetlands, arable lands, grasslands, mixed in the main stream when no dominant land use could be identified, and the Marne reservoir. (a) pCO_2 vs. dissolved organic carbon (DOC); (b) pCO_2 vs. dissolved inorganic carbon (DIC); (c) pCO_2 vs. dissolved oxygen (O_2); and (d) pCO_2 vs. chlorophyll a (Chl. a)

Interestingly, pCO_2 values measured during the field campaigns in the Marne reservoir showed CO_2 undersaturation with respect to the atmospheric equilibrium, averaging 360 ppm in the reservoir and 413 ppm in the air; slight supersaturation (457 ppm (reservoir) and 402 ppm (air)) was only observed in the late summer/autumn samples. Chl. a concentrations in the reservoir were low (mean: 2.6 µg l^{-1}) and DOC level was around 3.2 mgC l^{-1}, i.e., with no sign of eutrophication (Fig. 1-9a and 9d).

1.4. Discussion

1.4.1. pCO_2 supersaturation of the Seine hydrosystem

Since the 1970s, the whole drainage network of the Seine basin has been supersaturated in pCO_2 with respect to the atmospheric equilibrium. Supersaturation was observed for 98.5% of computed pCO_2 as well as for the direct field measurements. These results are in agreement with those obtained in the lower reaches of other temperate rivers. In comparison to the mean of 3000 ppm at the outlet of the Seine basin, average pCO_2 in the Meuse River (Belgium) on the period 2011-2014 was found equaling 2004±912 ppm and all samples were also supersaturated in CO_2 (min. 971 ppm) (Borges et al., 2018). Such variations can be found within the Scheldt River estuary (Belgium) and measurements in five of its tributaries (Dender: 8300 ppm, Zenne: 5700 ppm, Dijle: 7252 ppm and Nete River: 6700 ppm, and an average of 9500 ppm for the lower Scheldt) (Abril et al., 2000). Other Rivers as the Leyre (France) showed the same range of values (average: 4429 ppm, min.: 901 ppm max.: 23,047 ppm) (Abril et al., 2015). At the global scale, pCO_2 in streams and rivers have been averaged at 1600 ppm in a range of 132 to 11,770 ppm (Raymond et al., 2013a). The wide range of pCO_2 values in rivers were already mentioned with variations from 10 to 100 times the saturation value (Neal et al., 1998).

Conversely, we measured undersaturation in the Marne reservoir with pCO_2 below or near atmospheric equilibrium, in agreement with the results reported by Crawford et al.(Crawford et al., 2016) for river basins containing dam reservoirs. Riverine reservoirs have a higher residence time than the river itself, leading to particle sedimentation and a decrease in turbidity, conditions that favor primary production, i.e., consumption of CO_2 and production of oxygen. During our field campaigns, we did not observe eutrophication conditions (Fig. 1-9) or relationships between pCO_2 and nutrients (see supplementary material Annex 1-2). Without eutrophication of the reservoir, the biomass produced does not form an organic load that would – paradoxically – consume O_2 and release CO_2 (Garnier et al., 2000).

pCO_2 is known to be affected by metabolic processes related to nutrient availability(Halbedel and Koschorreck, 2013). In the Seine River, we could have expected a relationship with ammonium (NH_4^+) as activated sludge treatment releases dissolved organic carbon and high ammonium load (Aissa-Grouz et al., 2015). However, no direct relationship was found with

NH_4 or other nutrients, which shows the complexity of the controls on pCO_2 mentioned below.

Because the main stream of the Seine River was known for its phytoplankton blooms before domestic wastewater was efficiently treated (Aissa-Grouz et al., 2015, 2016), we analyzed bloom events (Fig. 1-5) to try and identify possible short periods of undersaturation. Despite the fact we found evidence for the opposite pattern between phytoplankton (Chl. a) and pCO_2 for phytoplankton blooms above 50 µg Chl. a l^{-1}, the Seine River waters remained supersaturated.

This result supports the assumption that other environmental variables actively control pCO_2 in the Seine River.

1.4.2. Hydro-climatic controls on pCO_2

As shown in Fig. 1-6, seasonal pCO_2 concentrations (in the long term) varied in parallel with temperature (i.e., with the highest values in summer/autumn) and opposite to hydrology. Such dynamics are typical for the temperate oceanic regime of the Seine River, with high discharge in winter and low discharge in summer/autumn (Ducharne, 2008).

Hydro-climatic effects resulted from a combination of water temperature and hydrology leading to a seasonal increase in pCO_2 and CO_2 evasion fluxes (fCO_2) from winter to summer/autumn (Borges et al., 2018; Butman and Raymond, 2011). Indeed, the hypothesis of control by water temperature is strengthened by the results of the field campaigns for different land uses with increasing pCO_2 according to the season (pCO2 in winter < spring < summer/autumn), which can be interpreted as an enhancement of DOC mineralization whatever the land use. However calculating pCO_2 at 10°C, revealed that temperature effect on solubility is rather low. In addition, long term seasonal variations in pCO_2 suggest possible control by hydrological regimes (high pCO_2 in low flow periods). In fact, both water temperature and hydrological regimes (water velocity) contributed to the variations in the gas transfer velocity (*k*-values), and the associated fCO_2. Moreover, for both *k*-values and fCO_2 we demonstrated opposite seasonal patterns in the upstream and downstream parts of the Seine River system, differences that could be more attributed to water velocities in small streams and water temperatures in higher stream orders (see equation 4, Fig. 1-4b, 4c, and 4d). Higher k-*values* upstream, caused by higher turbulence, logically led to important CO_2 outgassing compared to the lower k-values of the lower Seine River, down to its outlet.

The highest pCO_2 values were measured during the exceptional flood when groundwater overflows may have reinforced pCO_2 in the surface water. These high in-stream pCO_2 levels were found concomitantly with high *k*-values (10–55% higher than levels measured in small streams in the other seasons) and would be expected to enhance CO_2 evasion from rivers to the atmosphere. Similar effects of hydro-climatic conditions have also been observed in the tropics, e.g., in a large Amazonian river with a 20% higher outgassing of CO_2 during extreme flood years than in other years (Almeida et al., 2017), and in the Zambezi River, with pCO_2 up to twofold higher during the wet season (Teodoru et al., 2015). Polsenaere and Abril, (2012) compared two French streams and one river and observed that the stream with the highest concentration of CO_2 also had the highest CO_2 degassing flux.

Several authors have already suggested that climate change may alter the frequency and amplitude of flood events in the Seine River basin, with more extreme hydrological conditions (Raimonet et al., 2018; Ducharne and Ledoux, 2003; Habets et al., 2013), so that pCO_2 and CO_2 evasion could increase in the future.

1.4.3. Control of pCO_2 by the soil organic carbon stock

Analyzing in-stream pCO_2 measured in the various upstream land uses as a function of DOC underlined the importance of soil organic carbon stocks as a controlling factor. pCO_2 and DOC were higher in streams draining wetlands and grasslands compared to those draining forests and croplands (Fig. 1-3 and Fig. 1-9a). According to Arrouays et al. (2001), the organic carbon stocks in croplands are less than 4.5 kg C m^{-2}, but reach nearly 7.0 kgC m^{-2} in grasslands and forests and around 9.0 kgC m^{-2} in wetlands. These values are consistent with the higher carbon sequestration rate of grasslands and wetlands: 104 ± 73 gC m^2 $year^{-1}$ on average in Europe (Soussana et al., 2007). Thus, differences in pCO_2 according to land use here can be explained by the drainage of different organic soils and subsequent POC and DOC mineralization depending on water circulation and temperature. This result is clearly illustrated by the flood event flushes during the growing season when DOC (spring flood DOC median: 11.44 mgC l^{-1}) and pCO_2 (spring flood median: 3297 ppm) reached their highest values.

In addition to the carbon leached from riparian zones and sediments, organic carbon can be leached from soils where spring biological activity had already built up a large quantity of biomass that is potentially subject to mineralization.

Organic carbon quality has also been shown to influence pCO_2 in streams in the North Central European plains in Germany and Poland (Bodmer et al., 2016), and Belgium (Borges et al., 2018; Lambert et al., 2017). The biodegradable fraction of DOC is usually around 25% in upstream waters but may decrease to 5% in winter, and may be 50% in treated effluents (Servais et al., 1998; Garnier et al., unpublished data). This supports lower observed pCO_2 in winter and higher values linked to WWTP effluents. Increasing biological mineralization of land-based organic matter (OM) in response to a rise in temperature (Ducharne et al., 2007) during the growing season, or increasing biodegradable DOC exports during high water or flood events (Huntington et al., 2016) appear to be two major driving factors of pCO_2.

DOC and pCO_2 inputs originating from land runoff and/or aquifer base flow (i.e., diffuse sources), are added to inputs from wastewater effluents (i.e., point sources, as wastewaters treated in specific plants are well localized).

1.4.4. Control of pCO_2 by urban effluents: long term evidence

Whereas hydro-climatic conditions and diffuse pCO_2 and DOC inputs appeared to determine the seasonal variations in pCO_2, long term changes in pCO_2 observed over 1970–2015 suggested control by point sources, which are known to dominate observed changes in the Seine River (Passy et al., 2013; Aissa-Grouz et al., 2016; Aissa-Grouz et al., 2015; Romero et al., 2016). Indeed, the long-term annual pCO_2 values in the urbanized main stream of the Seine River strictly mirror variations in releases of urban OM by the largest WWTP of the Paris conurbation. Until 1990, the wastewater collection rate was intensified but wastewater treatment was not improved (Billen et al., 2001; Barles, 2007). Later on, the OM from discharged effluent decreased, with a stepwise increase in the number of WWTPs within the Parisian conurbation (Billen et al., 2001b) and improved treatment processes, in response to both the Urban Wastewater Directive (1991/271/EC) and the Water Framework Directive (WFD, 2000/60/EC). In 2012, the technique changed from activated sludge to fully operational tertiary treatment (nitrification in 2007 followed by 70% denitrification in 2012)[21], and improved water quality in terms of organic pollution and nutrients. Subsequently, that helped in reducing pCO_2 concentrations and enabled to recover acceptable levels of dissolved oxygen (Romero et al., 2016) downstream of major urban releases in the lower Seine an estuary. Because CO_2 evasion pattern is likely to follow the pattern of pCO_2 (see Fig. 1-3 and Fig. 1-4), our results would support those reported by Prasad et al. (2013). Indeed, they compared the urbanized Anacostia waters to the lower Potomac waters flowing into the

Chesapeake Bay (U.S.A.), and showed similar effect of organic matter and nutrients from urbanized landscapes on CO_2 evasion.

Whatever the period studied during the last 45 years, point source organic pollution appeared to be the main determinant of pCO_2 downstream of the treated effluents discharged into the lower Seine River. However, hydro-climatic conditions also influence pCO_2. For example, with no significant seasonal variations in OM fluxes discharged as point sources, higher pCO_2 concentrations in summer are explained by a low OM dilution rate during low waters and high temperatures.

1.4.5. Limits of the approach

The measurements we took in 2016 and 2017 showed neutral or basic carbonate buffered waters and DOC average seasonal concentrations of 3.5 to 11.4 mgC l^{-1}, excluding overestimation of calculated pCO_2 linked to the contribution of organic acids to TA (Abril et al., 2015). Abril et al. (2015) also emphasized the importance of accurate pH measurements. We think that the variability we found when establishing the relationship between measured pCO_2 and computed pCO_2 (Fig. 1-2) could be linked to the accuracy of pH measurements. As a result, the long-term pCO_2 analyses were subject to similar variability (see the 95% confidence intervals in Fig. 1-8a). Nevertheless, the amplitude of pCO_2 variations over the 45 years period enabled a robust analysis.

The choice of computing *k* using one of the equations provided by Raymond et al. (2012a) could lead to bias. Indeed the equation was proposed based on measurements made on small streams (median depth, 0.28 m) and during low flow (median discharge, 0.54 m^3 s^{-1}). We took into account slope, water velocity -*discharge divided by the wetted cross section*- and water temperature, but not other physical or environmental factors causing turbulence in streams, e.g., water turbidity, bed frictions, the direction and the intensity of wind, and chemical or bio-films (Raymond et al., 2012a; Polsenaere and Abril, 2012). Although there is need for direct measurements of *k* in higher stream orders to reduce uncertainties in flux calculations, *k*-values calculated for the Seine River range between 0.08 m h^{-1} (in winter for the main stem) and 0.21 m h^{-1} (in winter for streams). *k*-values and patterns found for the Seine River are in agreement with *k*-values estimated for other large rivers (e.g., in New England, on the Upper Mississippi and the Upper Colorado Rivers, Raymond et al. (2012). Raymond et al. (2013a) who averaged the *k* of the entire drainage network (mixing large rivers and streams) by

coastal segmentation and related catchment regions (COSCAT) (Meybeck et al., 2006) provided an annual *k*-value of 0.22 m h^{-1} for the region including the Seine River (COSCAT 401), close to the ones we used for streams. As small streams (SOs 1-4) represent 91% of the surface area of the Seine drainage network (French water authorities, AESN), our *k*-values seem reasonable. In addition, main stems *k*-values calculated for the Seine basin are in the range of global estimations found by Raymond et al. (2013a) (median: 0.22 m h^{-1}, min.: 0.07 m h^{-1}, max: 1.43 m h^{-1}).

At this stage, it is not possible to quantify the apportionment of pCO_2 originating from carbonated groundwater from that resulting from carbon mineralization or WWTP inputs. The modelling approach in progress should provide quantitative insights and δ^{13}C-DOC/POC analysis could also be useful to identify the different sources of pCO_2 (Polsenaere and Abril, 2012).

1.5. Conclusions

This study showed that since 1970, both small-order streams and urbanized downstream rivers in the Seine River basin have been supersaturated in CO_2 and a source of CO_2 to the atmosphere. CO_2 supersaturation with respect to the atmospheric equilibrium appeared to be controlled differently in space (depending on land uses or on the location of the main WWTP effluent discharge) and over time (seasonal or interannual). CO_2 supersaturation depended on complex interactions between land based and groundwater discharges (upstream diffuse sources), and urban pressures (downstream point sources) modulated by hydro-climatic factors.

In the small streams of the drainage network, in sparsely populated zones, the highest pCO_2 in summer was shown to originate from mineralization (increasing with water temperatures) of organic carbon from diffuse sources including in-stream bottom sediments, riparian and/or terrestrial soils varying according to land uses. Hydro-climatic variations, especially water velocity in small streams greatly affected gas transfer velocity, and helped determine in-stream pCO_2 (and evasion). During the exceptional flood event, high water discharges following a period of growth probably increased the DOC flushed from soils, leading to higher pCO_2, especially in streams draining wetlands and grasslands. High pCO_2 in streams may be also linked to high pCO_2 of groundwaters that feed the surface water during low flow, and to the overflow of aquifers during floods, with particularly high pCO_2.

Based on the 1970–2015 time series, point source organic pollution appeared to be the main driver of pCO_2 in the lower Seine River, downstream of the main outlet of WWTP effluents, and whatever the period studied. pCO_2 was highest in summer during low waters and high temperatures, and lower in winter when the discharged effluents were diluted. Despite the notable decrease in organic pollution following improvements in WWTPs since the 1990s, pCO_2 has remained higher than atmospheric values, strongly suggesting the influence of carbonated groundwater.

In the next step, a CO_2 budget of the Seine drainage network will help (i) quantify the role played by temperate human-impacted rivers in the global carbon budget, and (ii) estimate the amount of pCO_2 point sources vs. diffuse sources. The present study also points to the need for high frequency and more spatially resolved pCO_2 values and direct measurements of *k*. In addition, to anticipate the impact of climate change with the expected extreme hydrological conditions, further research is needed to understand the interactions between the terrestrial (soils and their land-use), and aquatic (hydrosystems) (Rasilo et al., 2017), groundwater discharges) compartments of watersheds.

1.6. Annex

1.6.1. Annex 1-1: Location of sampling stations used during the field campaigns in 2016-2017

Table 1-2 : Location of sampling stations used during the field campaigns in 2016-2017. Measurements undertaken: carbon dioxide partial pressure, dissolved organic carbon, particular organic carbon, dissolved organic carbon, particular inorganic carbon, dissolved oxygen, total suspended solids, water temperature, pH, total alkalinity, silica, NH_4^+, NO_3^-, NO_2^-, PO_4^-, Ptot.

Sampling stations	Latitude (WGS 84)	Longitude (WGS 84)	Land uses	Winter	Spring flood	Summer/ Automn	Spring
Melarchez	N 48°52'05.5''	E 003°11'38.4"	Agriculture	22/02/16	30/05/16	08/09/16	14/03/17
Theil	N 48°48'58.2''	E 003°06'43.3"	Agriculture	22/02/16	30/05/16	08/09/16	14/03/17
Avenelles	N 48°49'44.5''	E 003°07'03.4"	Agriculture	22/02/16	30/05/16	08/09/16	14/03/17
Tresmes	N 48°48'45.5''	E 002°59'31.3"	Agriculture	22/02/16	30/05/16	08/09/16	14/03/17
Ru Bourgogne	N 48°50'13.26	E 003°06'35.84	Agriculture	08/03/16	31/05/2016	14/09/16	15/03/17
Avenelles	N 48°50'23.40	E 003°08'22.27	Agriculture	08/03/16	30/05/2016	14/09/16	15/03/17
Forests 6	N 49°20'55.8"	E 002°54'08.6"	Forests	25/02/16	25/05/16	06/09/16	21/03/17
Forests 5	N 49°21'37.8"	E 002°52'52.6"	Forests	25/02/16	25/05/16	06/09/16	21/03/17
Forests 3	N 49°22'26.3"	E 002°48'67.9"	Forests	25/02/16	25/05/16	06/09/16	21/03/17
Forests 2	N 49°22'33.4"	E 002°48'40.9"	Forests	25/02/16	25/05/16	06/09/16	21/03/17
Forests 4	N 49°21'82.7"	E 002°48'32.5"	Forests	25/02/16	25/05/16	06/09/16	21/03/17
Forests 1	N 49°22'26.7"	E 002°47'41.0"	Forests	25/02/16	25/05/16	06/09/16	21/03/17
Grasslands 4	N 49°29'27.5"	E 001°38'96.1"	Grasslands	24/02/16	23/05/16	07/09/16	23/03/17
Grasslands 2	N 49°32'10.6"	E 001°34'54.4"	Grasslands	24/02/16	23/05/16	07/09/16	23/03/17
Grasslands 3	N 49°32'11.0"	E 001°34'55.0"	Grasslands	24/02/16	23/05/16	07/09/16	23/03/17
Grasslands 6	N 49°30'31.3"	E 001°40'14.0"	Grasslands	24/02/16	23/05/16	07/09/16	23/03/17
Grasslands 5	N 49°30'56.7"	E 001°39'18.1"	Grasslands	24/02/16	23/05/16	07/09/16	23/03/17
Grasslands 1	N 49°32'10.4"	E 001°34'40.3"	Grasslands	24/02/16	23/05/16	07/09/16	23/03/17
Der lake	N 48°36'15.1"	E 004°43'04.8"	Lake	NA	24/05/16	12/09/16	16/03/17
St Maurice	N 48°48'58.16"	E 002°25'27.35"	Mixed	22/02/16	30/05/16	12/09/16	14/03/17
Choisy	N 48°46'20.52	E 002°24'38.58"	Mixed	22/02/16	30/05/16	08/09/16	14/03/17
Bougival	N 48°52'53.85"	E 002°06'53.99"	Mixed	23/02/16	26/05/16	13/09/16	22/03/17
Conflans S.	N 48°59'22.49"	E 002°04'59.13"	Mixed	23/02/16	26/05/16	13/09/16	22/03/17
Porcheville	N 48°58'26.12"	E 001°48'19.15"	Mixed	23/02/16	26/05/16	13/09/16	22/03/17
Conflans O.	N 48°59'53.14"	E 002°04'17.64"	Mixed	23/02/16	26/05/16	13/09/16	22/03/17
Matougues	N 48°59'49.1"	E 004°14'29.8"	Mixed	NA	24/05/16	12/09/16	16/03/17
Dormans	N 49°04'31.3"	E 003°38'10.3"	Mixed	NA	24/05/16	12/09/16	16/03/17
St Maurice	N 48°48'58.16"	E 002°25'27.35"	Mixed	NA	24/05/16	12/09/16	16/03/17
Arrigny	N 48°37'19.6"	E 004°42'03.5"	Mixed	NA	24/05/16	12/09/16	16/03/17
Wetlands 1	N 49°22'27.7"	E 002°47'430"	Wetlands	10/03/16	25/05/16	06/09/16	21/03/17
Wetlands 2	N 49°22'21.0"	E 002°47'550"	Wetlands	10/03/16	25/05/16	06/09/16	21/03/17
Wetlands 5	N 49°21'44.6"	E 002°49'742"	Wetlands	10/03/16	25/05/16	06/09/16	21/03/17
Wetlands 3	N 49°22'22.7"	E 002°48'565"	Wetlands	10/03/16	25/05/16	06/09/16	21/03/17
Wetlands 4	N 49°21'12.9"	E 002°48'742"	Wetlands	10/03/16	25/05/16	06/09/16	21/03/17
G.Piezo 1	N 48°50'25.60"	E 003°06'14.76"	Groundwater	08/03/2016	31/05/2016	14/09/2016	15/03/2017
G.Piezo 2	N 48°50'20.60"	E 003°06'22.75"	Groundwater	08/03/2016	31/05/2016	14/09/2016	15/03/2017
G.Piezo 4	N 48°50'12.12"	E 003°06'32.58"	Groundwater	08/03/2016	31/05/2016	14/09/2016	15/03/2017
Ave. PZ1	N 48°50'23.48"	E 003°08'22.23"	Groundwater	08/03/2016	30/05/2016	14/09/2016	15/03/2017
Ave. PZ2	N 48°50'08.01"	E 003°08'43.03"	Groundwater	08/03/2016	30/05/2016	14/09/2016	15/03/2017
Ave. PZ3	N 48°49'47.38"	E 003°09'25.15"	Groundwater	08/03/2016	30/05/2016	14/09/2016	15/03/2017

1.6.2. Annex 1-2 : Direct pCO2 measured during the four field campaigns vs nutrients

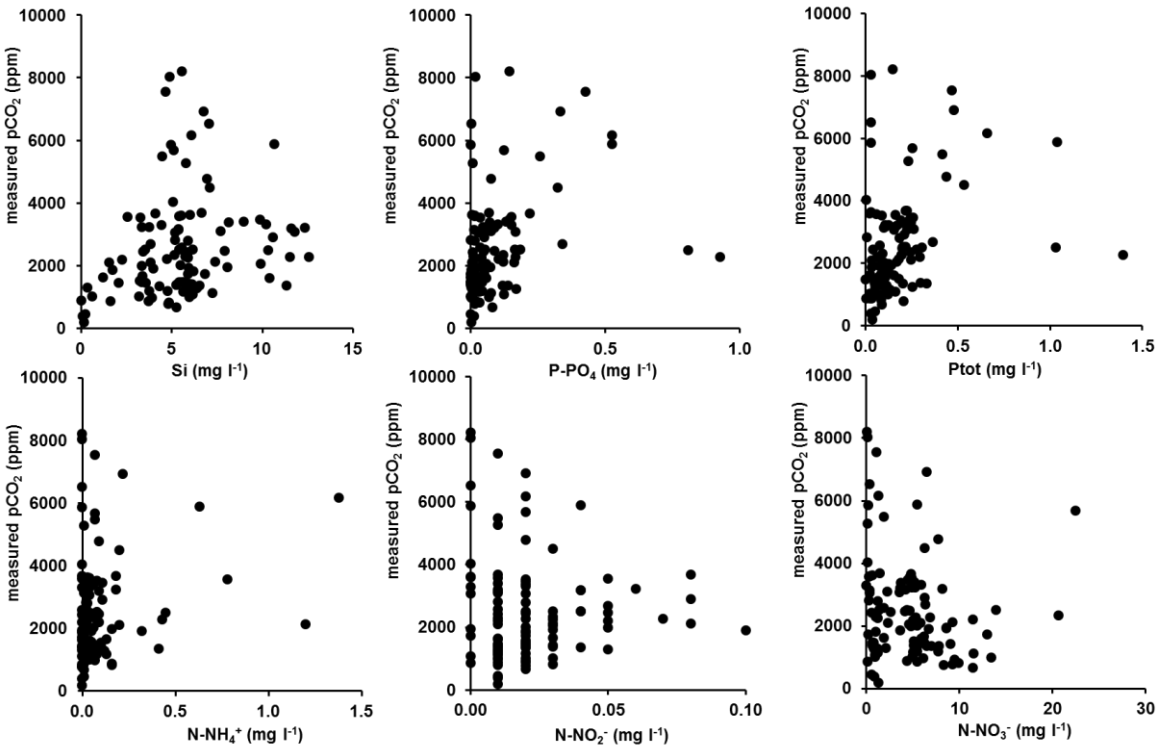

Fig. 1-10 Direct pCO_2 measured during the four field campaigns vs nutrients: silica (Si), phosphate (PO_4^-), total phosphorus (Ptot), ammonium (NH_4^+), nitrite (NO_2^-), and nitrate (NO_3^-).

Acknowledgements

The project including this study received funding from the European Union's Horizon 2020 research and innovation program under the Marie Sklodowska-Curie grant agreement No. 643052. Audrey Marescaux received a PhD grant. Many thanks to Abdelkader Azougui, Anunciacion Martinez Serrano, Benjamin Mercier and Sébastien Bosc for their participation in the fieldwork and for their help with chemical analyses in the lab.

Vincent Thieu (assistant professor at Sorbonne University Paris) and Josette Garnier (Research Director at the *Centre National de la Recherche Scientifique*, France) are co-supervisors of Audrey Marescaux's PhD. Alberto Vieira Borges is a senior research associate at the Fonds National de la Recherche Scientifique (Belgium). We are pleased to thank three anonymous reviewers for their constructive comments on the manuscript.

The data used in the study are available to readers upon request.

Chapter n° 2

Modeling inorganic carbon dynamics in the Seine River continuum in France

Audrey Marescaux[1], Vincent Thieu[1], Nathalie Gypens[2], Marie Silvestre[3], Josette Garnier[1]

[1]Sorbonne Université, CNRS, Institut Pierre Simon Laplace, UMR 7619 METIS, Paris, France
[2]Université Libre de Bruxelles, Ecologie des Systèmes Aquatiques, Bruxelles, Belgium
[3]Sorbonne Université, CNRS, FIRE FR3020, Paris, France

Article to be submitted to Water Research

Abstract

Inland waters have been recognized as an active component of carbon cycle where transformations and transports are associated to carbon dioxide outgassing. We propose a modeling approach by formalizing an inorganic carbon module integrated in the biogeochemical model, pyNuts-Riverstrahler, to estimate the carbon fate in the aquatic continuum. Our approach was implemented on the human impacted Seine River (France), the diffuse and point sources constraints to the model being characterized by field measurements in groundwater and in wastewater treatment plants. Simulated carbon dioxide emissions from the hydrosystem were estimated at 362 Gg C yr^{-1}. Simulations of dissolved inorganic carbon, total alkalinity, pH, and carbon dioxide (CO_2) concentrations according to Strahler stream orders showed a good agreement with observations and seasonal variability could be captured. Metabolism in the Seine hydrographic network highlighted the importance of benthic activities in small head streams while planktonic activities were mainly observed downstream in larger rivers. The net ecosystem productivity remained negative throughout all the years and at any place within the river network, highlighting the heterotrophy of the basin. In parallel, CO_2 supersaturation with respect to atmospheric concentrations of the basin was shown. The outgassing was the most important in small streams while CO_2 concentrations peaks were simulated downstream the major wastewater treatment effluent.

Highlights:

- A module of inorganic carbon was added in the PyNut-Riverstrahler model
- CO_2 riverine concentrations are modulated by groundwater discharge and instream metabolism
- CO_2 emissions account for 30% of inorganic carbon exports, the rest being exported as DIC

2.1. Introduction

Rivers have been demonstrated to be active pipes for transports, transformations, storage and outgassing of inorganic and organic carbon (Cole et al., 2007). Although there are large uncertainties on fluxes quantification from inland waters, carbon dioxide (CO_2) outgassing has been estimated as a significant efflux to the atmosphere, subjected to regional variabilities (Cole et al., 2007; Battin et al., 2009b; Aufdenkampe et al., 2011; Lauerwald et al., 2015; Regnier et al., 2013; Raymond et al., 2013a ; Sawakuchi et al., 2017; Drake et al., 2017). These variabilities are controlled by regional climate, watersheds characteristics and are related with terrestrial carbon exports under different forms, from organic to inorganic, and dissolved to particulate. Organic carbon entering rivers can originate from terrestrial ecosystems as plant detritus, soil-leaching or soil-erosion and groundwater supply, but it can also be synthesized instream by photosynthesis or brought by dust particles (Prairie and Cole, 2009; Drake et al., 2017). Inorganic carbon sources originate from groundwater, soil leaching and exchange by diffusion at the air-water interface, depending on partial pressure of CO_2 (pCO_2) at water surface with respect to atmospheric pCO_2 (Cole et al., 2007; Drake et al., 2017; Marx et al., 2018). Additional carbon exchanges, e.g., incorporation into biomineralized structures or resuspension, occur at the water-sediment interface and can be buried. Biogeochemical processes involved in the aquatic carbon cycle also depend on different temporal scales ranging from hours (e.g, photosynthesis), seasons (e.g. temperature) or be highly variable (nutrients loads) (Regnier et al., 2013a). As a whole, oligo and mesotrophic hydrosystems generally act as a source of carbon while surface of eutrophic systems can be undersaturated with respect to atmospheric pCO_2 (Prairie and Cole, 2009).

Direct measurements of pCO_2 along the drainage network are still too scares to accurately support temporal and spatial analyses of CO_2 variability. While calculations from pH, temperature and alkalinity may help to reconstruct spatio-temporal patterns of CO_2 dynamics (Marescaux et al., 2018a) only modeling tools can predict the fate of carbon in whole aquatic systems. Indeed, modeling approaches have allowed to simulate and quantify carbon fluxes between different reservoirs: atmosphere, biosphere, hydrosphere and lithosphere (e.g., Bern-SAR, Joos et al., 1996; ACC2, Tanaka et al., 2007; TOTEM, Mackenzie et al., 2011; MAGICC6, Meehl et al., 2007). In addition to these box-approaches, some more comprehensive mechanistic models, describing biogeochemical processes involved in carbon cycling and CO_2 evasion, have been set up for oceans (e.g., Doney et al., 2004; Aumont et al.,

2015), coastal waters (e.g., Borges et al., 2006; Gypens et al., 2004; 2009, 2011), and estuaries (e.g., Cai and Wang, 1998; Volta et al., 2014). In the inland waters, the NICE-BGC model (Nakayama, 2016) represents well CO_2 evasion at the global scale based on CO2SYS software (Pierrot et al., 2006). However, to our knowledge, whereas several river models describe the carbon cycle through organic matter input and degradation by aquatic microorganisms (e.g., PEGASE: Smitz et al., 1997; ProSe: Vilmin et al., 2018, QUAL2Kw: Pelletier et al., 2006; QUAL-NET: Minaudo et al., 2018, QUASAR: Whitehead et al., 1997, and RiverStrahler: Garnier et al., 2018), none of them describe the inorganic carbon cycle including carbon dioxide outgassing.

The biogeochemical model, Riverstrahler (Billen et al., 1994; Garnier et al., 1995) is a generic model of water quality and biogeochemical functioning of large river systems, taking into account dissolved and particulate organic carbon (DOC and POC), each form of carbon being separated into 3 classes of degradability: refractory, slowly or rapidly biodegradable (Servais et al. 1995, Garnier et al., 2008a). The purpose of our study is the implementation of a generic module of inorganic carbon into the newly developed pyNuts modeling environment for the Riverstraher model that enables to couple watershed characteristics and the river network (pyNuts-Riverstrahler: Thieu et al., 2015; Raimonet et al., 2018; Desmit et al., 2018) in order to quantify the sources, transformations, sinks and gaseous emissions of carbon.

The Seine River (north-west of France) has been studied for long using the Riverstrahler model. For example, the model has allowed to quantify deliveries to the coastal zone and understand eutrophication phenomena (Billen and Garnier, 2000; Billen et al., 2001; Passy et al., 2016), nitrogen transformation and N_2O emissions (Garnier et al., 2007; Garnier et al., 2009; Vilain et al., 2012) as well as retention (Billen and Garnier, 2000; Billen et al., 2018), and organic carbon metabolism (Garnier and Billen, 2007; Vilmin et al., 2016).

It is only recently that we investigated pCO_2 and emphasized the factors controlling pCO_2 dynamics in the Seine River (Marescaux et al., 2018a). A further aim in newly implementing this CO_2 module in the pyNuts-Riverstrahler model on the Seine River was to quantify and discuss autotrophy versus heterotrophy patterns in regard to CO_2 concentrations and supersaturation in the drainage network. Therefore, we built a representation of ecological processes involved in the inorganic carbon cycle.

2.2. Material and methods

2.2.1. Description of the Seine basin

Situated in the North-West of France within 0° 07' – 4° 00' E and 46° 57' - 50° 01' N, the Seine basin (~76 285 km²) has a temperate climate and a pluvio-oceanic hydrologic regime. The medium altitude of the basin is 150 m above sea level (ASL) with 1% of the basin reaching more than 550 m ASL in the Morvan (Guerrini et al., 1998). The annual water flow at Poses (stream order 7, basin area 64867 km²), the most downstream monitoring station free from tide influence, averaged 490 m^3 s^{-1} in the period 2010–2013 (data provided by the HYDRO database, http://www.hydro.eaufrance.fr, last accessed 2018/11/05). The major tributaries include the Marne and upper Seine rivers upstream from Paris, and the Oise River downstream Paris Fig. 2-1c. Maximum of water discharge of these tributaries occurs during winter with the lowest temperature and rate of evapotranspiration; the opposite behavior is observed during summer (Guerrini et al., 1998). Three main reservoirs, storing water during winter and sustaining low-flow during summer, are located upstream on the Marne River and the upstream Seine and its Aube tributary. The total storage capacity of these reservoirs is 800 10^6 m^3 (Garnier et al., 1999).

Lithological and hydrogeological context

Excepted the crystalline rocks in the North and from the highland of the Morvan (South), the Seine basin is in majority located in the lowland Parisian basin with sedimentary rocks (Mégnien, 1980, Pomerol and Feugueur, 1986; Guerrini et al., 1998). It is characterized by concentric sedimentary structure dominated, from external to internal circular arcs, successively by limestone and marl from Jurassic, chalk from Cretaceous, and at the periphery of the basin, carbonates, Tertiary limestone and sand (Fig. 2-1a). The main tributaries flow across these concentric structures resulting in relatively homogeneous lithology within the main sub-basins.

Concerning the hydrogeology, the most important aquifers are in carbonate rocks (limestone, chalk…) or detrital (sand and sandstone) material separated by impermeable or less permeable layers. In the literature, ten simple or multilayer aquifers were described for the Seine basin. The most superficial unconfined aquifer (from soil to tens of meters deep) feeds

the river during summer and the opposite behavior is observed during winter (AESN, 1978). Riverine alluvium (sand, gravels, clay) from Quaternary constitutes an eleventh aquifer. Although thin (less than 10 m), its connectivity with the river and superficial aquifer makes it a very productive aquifer. In the Parisian basin, complex unconfined aquifers are mainly from Quaternary alluvium, from Tertiary Beauce limestone and Fontainebleau sand, as well as Jurassic chalk or karstic limestone outcrops (Guerrini et al., 1998; Flipo et al., 2016)

Morphology by Strahler stream order

The homogeneity in hydrology and lithology described above made the Strahler stream order (SO) approach (Strahler, 1957) interesting for describing the main morphological characteristics of the Seine basin, a basic concept adopted in the Riverstrahler modeling approach (Billen et al., 1994). The smaller perennial streams are order 1. Only confluences between two river stretches having the same SO produce an increase in Strahler ordination (SO+1) (Fig. 2-1c). Mean hydro-physical characteristics of the Seine River are aggregated by stream orders in Table 2-1. The hydrographic network and the slopes (S, m m^{-1}) were provided by the Agence de l'Eau Seine Normandie (French acronym AESN, http://www.eau-seine-normandie.fr/, last accessed 2018/11/05); water discharges by the national Banque Hydro database (http://www.hydro.eaufrance.fr/, last accessed 2018/11/05); mean width (W, m) is assumed to follow empirical relationship with upstream watershed area (WSA, km^2) (see Eq. 1; Billen et al., 1994):

$$W = 0.8\,WSA^{\frac{1}{2}} \qquad \text{Eq. 1}$$

mean depth (D, m) is related to the slope (S, m m^{-1}) and water flow (Q, m^3 s^{-1}) by the relationship derived from Manning's formula:. (see Eq. (2), Billen et al., 1994):

$$D = [0.045Q(W(S^{1/2}))^{-1}]^{3/5} \qquad \text{Eq. 2}$$

The width, depth, water flow, and water velocity increase by order while the draining surface area, the cumulated length of the stream/river (cum. length), and the slopes decrease with the order (Table 2-1).

Table 2-1 Mean characteristics of the Seine River watershed by Strahler stream order.

SO	number streams	draining area	cum. length	Width	depth	Slope	water flow	water velocity
		km^2	*km*	*m*	*m*	*m m*$^{-1}$	*m*^{3} *s*$^{-1}$	*m s*$^{-1}$
1	2643	30,097	10,688	2.42	0.14	0.00952	0.15	0.34
2	603	10,635	4488	5.12	0.29	0.00345	0.67	0.36
3	148	7798	2936	8.30	0.44	0.00224	2.04	0.46
4	47	6690	1792	22.15	0.79	0.00177	6.13	0.32
5	13	8627	1044	45.01	1.10	0.00103	24.89	0.45
6	4	7864	636	77.69	2.51	0.00100	82.22	0.42
7	1	4573	467	186.18	2.61	0.00101	416.20	0.81

Landuse

The land use is closely related to the lithology and the morphology of the Seine River basin. Indeed, in the crystalline Morvan, forest and grassland are dominant while open-fields on chalk have allowed intensive agriculture (more than 50% of the basin, CLC - EEA, 2012) (Fig. 2-1b). In the east limestone area, grassland and forest prevail. Finally urban areas have grown along the lower Seine River and mainly downstream from the confluence with the Marne River, that enabled the water supply of the Parisian population and trade exchanges by navigation (Guerrini et al., 1998).

Population and wastewater treatment plants

The Seine basin is densely populated (~ 230 inhabitants km^{-2}). Population is mostly concentrated in the Paris conurbation (12.4 million inhab. in 2015) (INSEE, 2015) (Fig. 2-1d). As a result of this high population density, 1900 wastewater treatment plans (WWTPs) are spread throughout the basin; among those 20 have a treatment capacity above 100,000 Eq. Inhab (AESN). Located 70 km downstream Paris, the largest wastewater treatment plan in Europe (Seine Aval, SAV WWTP) can treat up to 6 10^6 inhabitant equivalents par day, releasing 15.4 m^3 s^{-1} in the lower Seine River (Syndicat interdépartemental pour l'assainissement de l'agglomération parisienne - French acronym SIAAP, http://www.siaap.fr/, last accessed 2018/11/05).

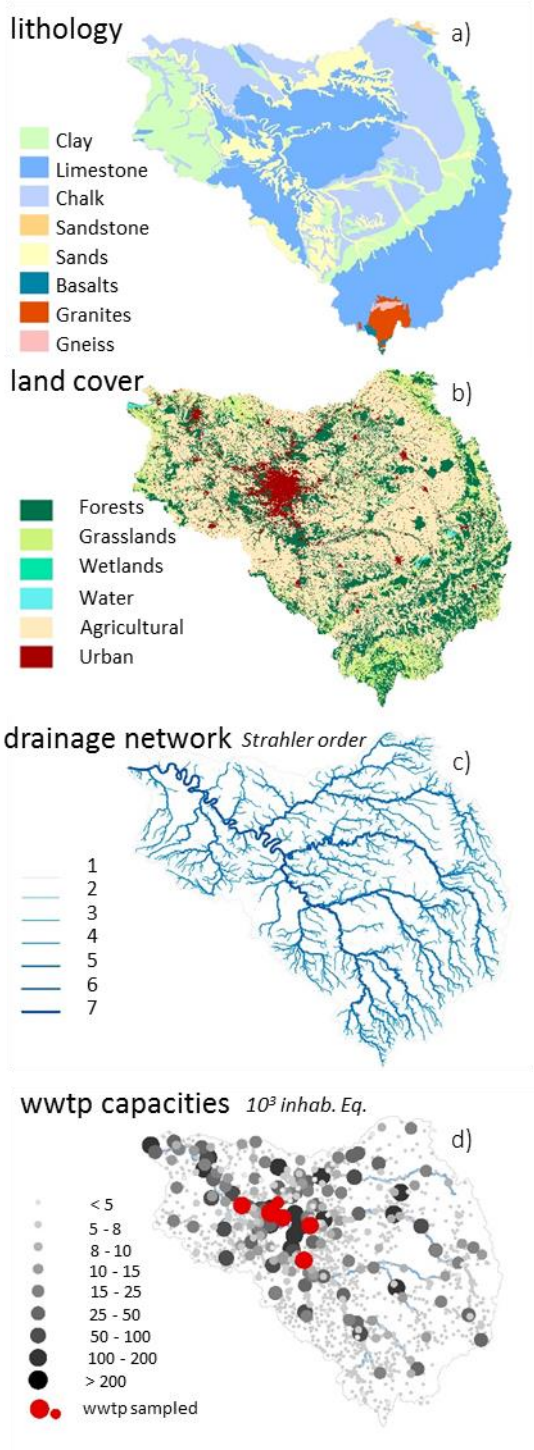

Fig. 2-1 Characteristics of the Seine basin: a) the lithology according to Albinet, (1967). b) Drainage network according to Strahler stream orders (Strahler, 1952, 1957) Monitoring stations (I. Poses, II. Poissy (Downstream Paris), III. Paris, IV. Ferté-sous-Jouarre (Upstream Paris). c) The land use according to Corine Land Cover, with 6 simplified classes (EEA, 2012). d) Wastewater treatment plants of the basin. Red dots are the WWTPs sampled in 2018.

2.2.2. The pyNuts-Riverstrahler model and its biogeochemical model, RIVE

The core of the biogeochemical calculation of the pyNuts-Riverstrahler model (described here after) is formed by the RIVE model (among many others: Billen et al. 1994, Garnier et al. 1995, Garnier et al., 2002; Servais et al., 2007) (https://www.fire.upmc.fr/rive/) which aims at simulating concentrations of oxygen, nutrients cycling (nitrogen (N), phosphorus (P), and silica (Si)), particulate suspended matter, dissolved and particulate organic carbon (three classes of biodegradability). Biological compartments are represented by 3 taxonomic classes of phytoplankton (diatoms, Chlorophyceae, and cyanobacteria), 2 types of zooplankton (rotifers with short generation time and microcrustaceans with long generation time), 2 types of heterotrophic bacteria (small autochthonous and large allochthonous) as well as nitrifying bacteria (ammonium oxidizing bacteria and nitrite oxidizing bacteria).

The model also describes processes (erosion, organic matter degradation, denitrification etc.) occurring at the interface with the benthic sediment, this later having its own variables state variables (benthic organic matter, inorganic particulate P, benthic biogenic Si). A detailed list of the state variables of the RIVE model is provided in annex 1. Most of the kinetic parameters involved in this description have been determined through field or laboratory experiments under controlled conditions and are fixed *a priori*, needing calibration procedures within the range of their determination (see the detail of the kinetics and parameters in Annex 2-2). Up to now, there was no explicit representation of inorganic carbon in the RIVE model.

PyNuts is a modeling environment which enable to calculate the constraints (diffuse and point sources) to Riverstrahler at a multi-watersheds scale (Thieu et al., 2015; Raimonet et al., 2018; Desmit et al., 2018). PyNuts-Rivertrahler is thus a generic model of water quality and biogeochemical functioning of large drainage networks, that simulates water quality with RIVE within entire drainage networks.

In PyNuts-Riverstrahler, modeling units can be described as a set of river axis with a spatial resolution of 1 km (axis-object), or they can be aggregated to form upstream basins that are idealized as a regular scheme of tributary confluences where each stream order is described by mean characteristics (stream-order-object). Here, the Seine basin was decomposed into 80 modeling units, including 8 axis (axis-object) and 72 upstream basins (stream-order-object) (Annex 2-3). Thus, the new implementation of the inorganic carbon module required to define

diffuse source of total alkalinity and disssolved inorganic carbon (see part: *Documenting input constraints* of the pyNuts-Riverstrahler model).

Runoffs were calculated over the whole Seine basin using water discharges measurements at 48 gauged stations (source: Banque Hydro). Surface and base flow contributions were estimated applying BFLOW automatic hydrograph separation method (Arnold and Allen, 1999) over the recent time series of water discharges (2010-2017). For the study period (2010-2013), mean base flow index (BFI = 0.71) of the Seine Basin indicates the importance of groundwater contribution to river discharge, with spatial heterogeneity following the main lithological structures, but not significant differences when summarizing the BFI criteria by strahler order.

2.2.3. Development of an inorganic carbon module

A module on the carbonate system and CO_2 flux was newly implemented into the biogeochemical RIVE model. This inorganic carbon module was based on the module described by N. Gypens and A.V. Borges (2006, personal communication), modified from the one used in the MIRO biogeochemical model for coastal waters of the Southern Bight of the North Sea (Hannon et al., 2001, Gypens et al., 2004). It calculates pCO_2 concentrations in the water and the flux of CO_2 exchange between the river network and the atmosphere. It also interacts with other biogeochemical processes (e.g., respiration, denitrification, nitrification) and groups (e.g., bacteria, zooplankton, phytoplankton) described in the RIVE model.

Introducing the carbonate system

This module represented in Fig. 2-2, aims at computing the speciation of the carbonate system which introduces two new state variables: dissolved inorganic carbon (DIC), total alkalinity (TA), and a third variable derived from them: carbon dioxide (CO_2). The module implies four equations (see Annex 2-4 - Eq. 1, 2, 3) that also enable to calculate bicarbonate ($HCO3^-$), carbonate (CO_3^{2-}), hydronium (H_3O^+). Indeed, two variables of the carbonate system have to be known, in order to calculate all other components (Zeebe and Wolf-Gladrow, 2001). In our case, it appears that the quality of the pH ($-\log_{10}[H_3O^+]$) measurements is highly dependent on the equipment and to avoid this bias, that may overestimate CO_2 (Abril et al., 2015), we calculated pH as a function of total alkalinity and dissolved inorganic carbon using the Culberson's equation (Culberson, 1980).

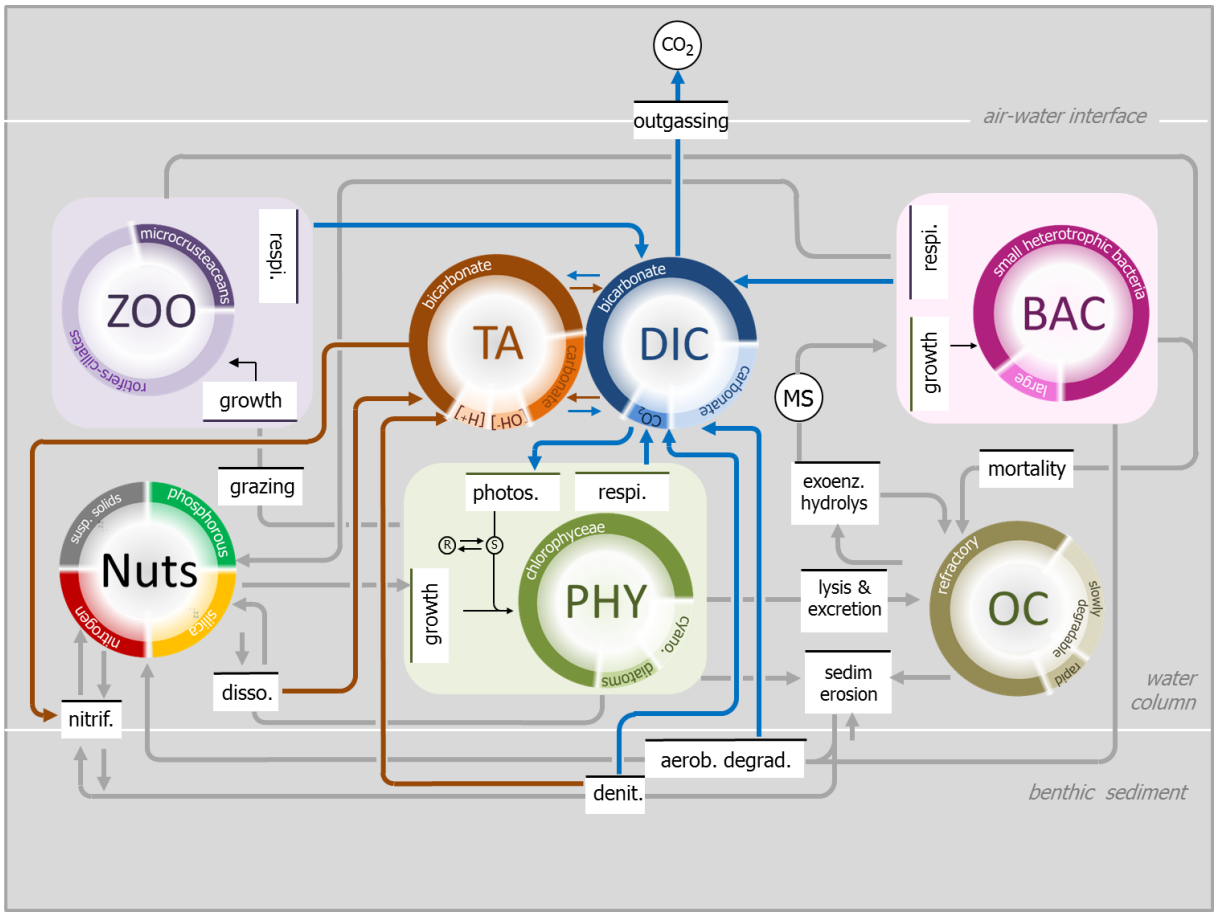

Fig. 2-2 Schematic representation of the ecological RIVE (inspired from Billen et al. 1994, Garnier & Billen, 1994), with grey lines indicating the main processes simulated in the water column and at the interface with the sediment (oxygen not shown), and the implementation of the new inorganic module, based on TA (maroon) and DIC (blue) lines.

Aquatic processes affecting TA and DIC

Dissolved or particulate organic matters are mostly degraded by microbial activities (more or less quickly according to their biodegradability), resulting in CO_2 production (Servais et al. 1995), and thus inducing a change in DIC concentrations in the water column (see Fig. 2-2). The exchange of CO_2 between the water surface and the atmosphere increase or decrease DIC, depending on the gas transfer velocity (*k*-value) and CO_2 gradient concentrations at the water surface – atmosphere interface (Table 2-2, Annex 2-4.5). Photosynthesis and denitrification processes affect DIC and TA (Table 2-2), while instream nitrification only influences TA (Fig. 2-2).

Table 2-2 Stoichiometry of the biogeochemical processes, influencing dissolved inorganic carbon and total alkalinity in freshwaters taken into account in the new inorganic carbon module.

Process	Equation	DIC	TA	Eq.
FCO_2	$CO_2(aq) \leftrightarrow CO_2(g)$	±1	0	3
Aerobic degradation	$C_{106}H_{263}O_{11}N_{16}P + 106O_2 \rightarrow 92CO_2 + 14HCO_3^- + 16NH_4^+ + HPO_4^{2-} + 92H_2O$	+1	0	4
Photosynthesis (NO_3^- uptake)	$106CO_2 + 16NO_3^- + H_2PO_4^- + 122H_2O + 17H^+ \rightarrow C_{106}H_{263}O_{11}N_{16}P + 138O_2$	-1	+17/106	5
Photosynthesis (NH_4^+ uptake)	$106CO_2 + 16NH_4^+ + H_2PO_4^- + 106H_2O \rightarrow C_{106}H_{263}O_{11}N_{16}P + 106O_2 + 15H^+$	-1	-15/106	6
Denitrification	$5CH_2O + 4NO_3^- + 4H^+ \rightarrow 5CO_2 + 2N_2 + 7H_2O$	+1	+1	7
Nitrification	$NH_4^+ + 2 \rightarrow 2H^+ + H_2O + NO_3^-$	0	-2	8

State equations and parameters of the inorganic carbon module

These processes affecting TA and DIC result in equations governing inorganic carbon dynamic as:

$$TA = TA_{t-1} + dt.\ \frac{dTA}{dt} + \mathrm{TA_{inputs}} \qquad [9]$$

and,

$$\frac{dTA}{dt} = ((Denit - 2.nitr[\text{'}AOB\text{'}]).\ M(N)^{-1} + (\frac{17}{106}\frac{uptPhyNO_3^-}{uptPhyN} - \frac{15}{106}\frac{uptPhyNH_4^+}{uptPhyN}).phot\ .M(O_2)^{-1})1000 \qquad [10]$$

where,

TA_{t-1} is the value of total alkalinity (µmol L^{-1}) at the previous time step (t-1). $Denit$ and $nitr[\text{'}AOB\text{'}]$ are respectively the denitrification, and nitrification by ammonia-oxidizing

bacteria (AOB) processes as implemented in the RIVE model (mgN L^{-1} h^{-1}); $M(N)$ is the molar mass of the nitrogen (14 g mol^{-1}); $M(O_2)$ is the molar mass of the dioxygen (32 g mol^{-1}). TA_{inputs} is TA (µmol L^{-1}) sources entering in the water column by diffuse sources (groundwater and subsurface discharges) and point sources (WTTPs).

$$DIC = DIC_{t-1} + dt.\ \frac{dDIC}{dt} + \mathrm{DIC}_{\mathrm{inputs}} \qquad [11]$$

and,

$$\frac{dDIC}{dt} = (respbact + respZoo + respBent) + denit\ .M(C).M(N)^{-1} + phot.M(C).M(O_2)^{-1} + \frac{F_{CO_2}}{depth} \qquad [12]$$

where,

DIC_{t-1} is the value of dissolved inorganic carbon (mgC L^{-1}) at the previous time step (t-1). "$respbact$", "$respZoo$", *"respBent"* are respectively the heterotrophic planktonic respiration of bacteria, zooplankton and benthic bacteria already implemented in RIVE (mgC L^{-1} h^{-1}). " $phot$" is the net photosynthesis (mgO_2 L^{-1} h^{-1}) with differentiated nitrogen uptake (uptPhyN, mgN L^{-1} h^{-1}) for nitrate (uptPhyNO_3^-, mgC L^{-1} h^{-1}), and ammonium (uptPhyNH_4^+, mgC L^{-1} h^{-1}); F_{CO2} is the CO_2 flux at the interface water-atmosphere in mgC m^{-2} h^{-1} described in Annex 2-4.5; depth is the water depth (m); $M(C)$ and $M(O_2)$ are the molar masses of the carbon and oxygen (12 and 32 g mol^{-1}, respectively).

Because, the RIVE model is based on assumption of a perfect homogeneity of the water column and then, the flux of carbon at the water-atmosphere interface F_{CO2} impacts the water column in its entire depth.

The full inorganic carbon module is described in Annex 2-4, and the different constants and parameters used in the inorganic carbon module are introduced in Annex 2-4.6.

2.2.4. Documenting input constraints of the pyNuts-Riverstrahler model

Diffuse sources from soil and groundwater

Diffuse sources are taken into account by assigning a yearly mean concentration of carbon and nutrients respectively to subsurface and groundwater flow components. These concentrations are then combined with a 10 days' time step description of surface and base flows to simulate the seasonal contribution of diffuse emissions to the river system. For nutrient, several application of the Riverstrahler on the Seine river basin allowed to refine the quantification of diffuse sources, among other: Billen and Garnier, (2000), and Billen et al. (2018) for nitrogen; Aissa-Grouz et al. (2016) for phosphorous; Billen et al. (2007), Sferratore et al. (2008), and Thieu et al. (2009) for N, P and Si. In this study we revised our estimates for diffuse organic carbon sources and propose values of TA and DIC for the Seine basin. Summary of all carbon related inputs of the model are showed in Table 2-3.

Dissolved organic carbon (DOC) input concentrations were extracted from the AESN database (http://www.eau-seine-normandie.fr/, last accessed 2018/11/05) and averaged by land use for subsurface sources (mean: 3.13 mgC L^{-1}; sd: 4.56 mgC L^{-1}; 3225 data for 2010-2013). For groundwater source, concentrations were extracted from the ADES database (www.ades.eaufrance.fr, last accessed 2018/11/05) and averaged by MESO water bodies (French acronym: Masse d'Eau SOuterraine, see Annex 2-5; mean: 0.91 mgC L^{-1}; sd: 0.8 mgC L^{-1}; 16,000 data for 2010-2013). These concentrations were similarly separated into 3 pools of different biodegradability, with 7.5% rapidly, 17.5% slowly biodegradable and 75% of refractory DOC for subsurface sources and, 100% of refractory DOC for groundwater flow (Garnier, unpublished).

Total POC inputs were calculated based on estimated total suspended solids (TSS) fluxes, associated with a soil organic carbon (SOC) content provided by the LUCAS Project (samples from agricultural soil), the BioSoil Project (samples from European forest soil), and the "Soil Transformations in European Catchments" (SoilTrEC) Project (samples from local soil data coming from five different critical zone observatories (CZOs) in Europe) (Aksoy et al., 2016). TSS concentrations were calculated using fluxes of TSS provided by WaTEM-SEDEM (Borrelli et al., 2018) and runoffs averaged over the periode1970-2000 (SAFRAN-ISBA-MODCOU, SIM, Habets et al., 2008). The POC mean was 8.2 mgC L^{-1}, sd: 10.4 mgC L^{-1} in

subsurface runoff, and 0.8 mgC L^{-1}, sd: 1.0 mgC L^{-} in groundwater discharge. The same ratio of DOC reactivity was applied for three classes of degradability of POC.

DIC and TA are brought by subsurface and groundwater discharges (Venkiteswaran et al., 2014). DIC is defined by the sum of bicarbonates (HCO_3^-), carbonates (CO_3^-) and CO_2. Unlike HCO_3^- and CO_3^- measured in groundwater on a regular basis by French authorities (ADES, www.ades.eaufrance.fr, last accessed 2018/11/05), CO_2 concentrations were not measured in their survey. TA values are also provided in ADES data base.

For calculating DIC concentrations in groundwaters, we therefore used our own CO_2, measurements, equaling on average 15.92 mgC-CO_2 L^{-1}, sd: 7.12 mgC-CO_2 L^{-1} (55 measurements in 6 pizeometers in the Brie aquifer in 2016-2017) (see methodology in Marescaux et al., 2018a). DIC and TA were averaged for the 48 unconfined hydrogeological MESO units of the basin (see concentrations in Annex 2-5) on the recent period (2010-2015), including the period of simulations. In Fig. 2-3, a summary of TA and DIC inputs by MESO units is shown by grouping MESO units according to the lithology and geological ages. Interestingly, DIC and TA values extracted from the ADES database for the MESO unit number 3103 corresponding to those of the Brie aquifer (DIC mean: 76 mgC l^{-1}, sd: 11 mgC l^{-1}, TA mean: 5553 µmol l^{-1}, and sd: 988 µmol l^{-1}) compare well with our field measurements (annual mean concentrations of 72 mgC l^{-1} (DIC), and 4700 µmol l^{-1} (TA) (Annex 5)).

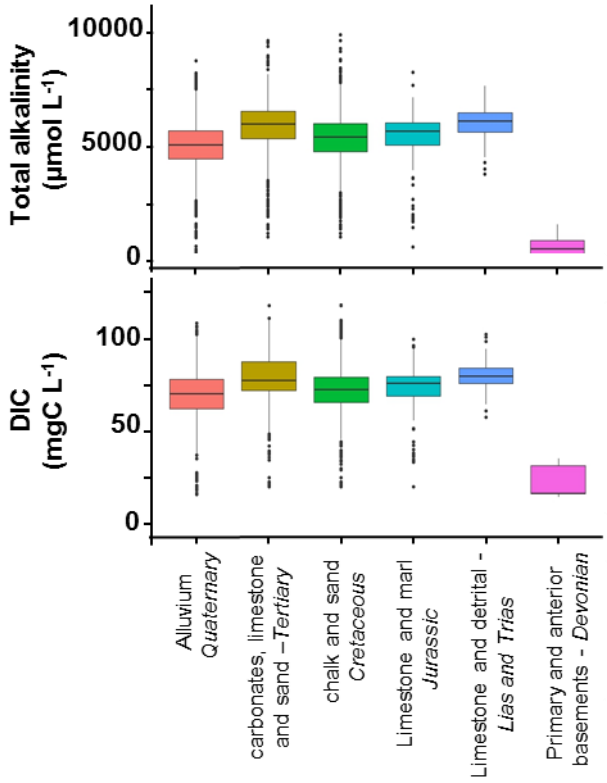

Fig. 2-3 Boxplots of total alkalinity (µmol L^{-1}) and dissolved inorganic carbon (DIC, mgC L^{-1}) groundwater concentrations by grouping the MESO units. The lower, intermediate and upper parts of the boxes represent respectively the 25th, 50th and 75th percentiles and the circles represent the outlier values (source: ADES).

Documenting TA and DIC diffuse sources based on MESO units ensures a good representation of their spatial heterogeneity in the Seine river basin. Indeed carbonates shows higher TA and DIC mean concentrations while crystalline waters had the lowest mean concentrations in TA and DIC (Primary and anterior basements from Devonian, Fig. 2-3). Aquifers from Tertiary and alluvium of Quaternary showed more heterogeneous distribution of concentrations (Fig. 2-3). TA and DIC by MESO units are then spatially averaged at the scale of each modeling unit of the pyNuts-Riverstrahler model (80 modeling objects, subdivided according to Strahler ordination, Annex 2-3), thus forming a semi distributed estimate of groundwater concentrations.

Estimates of TA and DIC subsurface concentrations (also required as inputs by the pyNuts-Riverstrahler model) are not routinely obtained during field surveys, unlike for groundwater. Moreover, measurements in small streams cannot be considered as representative of subsurface concentrations because they are expected to strongly degas within 200 m as showed for N_2O in Garnier et al. (2009), and CO_2 in Öquist et al. (2009). For these reasons we have thus considered similar concentrations and spatial distribution for subsurface

components that those obtained for groundwater (from 25 to 92 mgC L^{-1} of DIC, and from 663 to 5580µmol L^{-1} of TA, Fig. 2-3).

Point sources from WWTP effluents

The pyNuts-Rivestrahler model integrates carbon and nutrients raw emissions from local population starting from the collection of households emissions into sewage network until their release with or without treatment in WWTPs. In the Seine river basin, most of these releases are adequately treated before being discharged to the drainage network. DOC discharge from WWTP have been described according to treatments type and ranged from 2.9 to 9.4 gC $inhab^{-1}$ day^{-1} while POC discharge ranged from 0.9 to 24 gC $inhab^{-1}$ day^{-1} based on sample of water purification treatment observed in the Seine basin (Garnier et al. 2006; Servais et al. 1999).

Measurement of TA and DIC were performed on 8 WWTPs selected to reflect various treatments capacities (from 6 10^3 inhab. Eq to 6 10^6 inhab.) and different treatments types (activated, sludge, Biostyr® Biological Aerated Filter) in the Seine river basin. Sampling and analysis protocols are provided in Annex 6. Unfortunately, this sampling did not allow to highlight differences in per capita emission of TA and DIC. Consequently, we used a fixed value of 3993 µmol L^{-1} for TA and 70 mgC L^{-1} for DIC, which correspond to the weighted mean by WWTP capacity of our measurements, and are in agreement with values from Alshboul et al. (2016b) found in the literature.

Table 2-3 Summary of the carbon related inputs of the pyNuts-Riverstrahler model

Input variables	Flow	database	averaged	values	source
DOC	subsurface	AESN	land use	mean: 3.13 mgC L^{-1}; sd: 4.56 mgC L^{-1};	http://www.eau-seine-normandie.fr/
	groundwater	ADES	MESO units	mean: 0.91 mgC L^{-1}; sd: 0.8 mgC L^{-1}	www.ades.eaufrance.fr
POC	subsurface	LUCAS, BioSoil and SoilTrEC Projects	based on estimated total suspended solids (TSS) fluxes, associated with a soil organic carbon (SOC) content	mean: 8.2 mgC L^{-1}, sd: 10.4 mgC L^{-1}	(Aksoy et al., 2016)
	groundwater			mean: 0.8 mgC L^{-1}, sd: 1.0 mgC L^{-1}	
DIC	subsurface	ADES	MESO units	from 25 to 92 mgC L^{-1}	www.ades.eaufrance.fr
	groundwater			from 25 to 92 mgC L^{-1}	
TA	subsurface	ADES	MESO units	from 663 to 5580µmol L^{-1}	www.ades.eaufrance.fr
	groundwater			from 663 to 5580µmol L^{-1}	
DOC	Point sources	Measurments	According to WWTP treatment and capacity	2.9 to 9.4 gC $inhab^{-1}$ day^{-1}	(Garnier et al. 2006; Servais et al. 1999)
POC	Point sources	Measurments		0.9 to 24 gC $inhab^{-1}$ day^{-1}	
DIC	Point sources	Measurments	weighted mean by WWTP capacity	70 mgC L^{-1}	This study
TA	Point sources	Measurments	weighted mean by WWTP capacity	3993 µmol L^{-1}	This study

2.2.5. Observations data

We selected the timeframe of 2010-2013 for setting up and validating the new inorganic module. This period includes the year 2011 which has been particularly dry (annual average water discharge at Poses averaged: 366 m^3 s^{-1}) and 2013 wet (annual average water discharge at Poses: 717 m^3 s^{-1}) while 2010 and 2012 showed intermediate hydrological conditions (annual average water discharges at Poses: 418 m^3 s^{-1}; 458, m^3 s^{-1}, respectively) (data source: Banque Hydro).

pCO_2 values (ppmv) were calculated using CO2SYS software algorithms (version 25b06, Pierrot et al., 2006) according to existing datasets of pH, total alkalinity and water temperature measurements for the chosen period 2010–2013 (8693 records of these three variables, i.e., around 1209 stations distributed throughout the Seine basin) collected by the AESN. The carbonate dissociation constants (K1 and K2) applied were calculated from (Millero, 1979) with zero salinity and depending of the water temperature. pCO_2 calculations from pH and TA can lead to overestimation of pCO_2 (Abril et al., 2015). The pCO_2 calculated data were corrected by a relationsip established for the Seine basin and based on pCO_2 field measurements (Marescaux et al., 2018a). For computing interannual average over the 2010-2013 time period, data were averaged monthly, then annually at each measurement stations, and then spatially averaged (e.g., by Strahler orders).

Four stations offering sufficient data, over the 2010-2013 time period, have been selected for appraising seasonal patterns. They are located along the main stem of the Marne-Lower Seine River and chosen for their interests: Poses (the outlet), Poissy (downstream SAV WWTP), Paris and Ferté-sous-Jouarre (upstream Paris) (Fig. 2-1).

All data were processed using R (R Core team, 2015) and QGIS (QGIS Development Team, 2016). Kruskal-Wallis tests were used to compare simulated and measured pCO_2 averages.

2.3. Results

2.3.1. Validation of spatial and seasonal variations of pCO_2

CO_2 from small streams to larger section of the Seine River

Simulations of CO_2 concentrations averaged for 2010-2013 by Strahler orders showed that pyNuts-Riverstrahler succeeds in reproducing the general trends of CO_2 observations (7565 data) (Fig. 2-4). Although not significant, CO_2 concentration means tend to decrease in small streams (width < 100 m) from SO1 to SO4, and to finally increase in larger stream (width > 100 m) from SO5 to SO7), downstream the Paris conurbation. Some discrepancy appears for orders 1, with simulations higher than observations while, for orders 2 to 7, simulations were conversely lower than observations. The corresponding *k*-values calculated for the Seine ranged between 0.04 and 0.23 m h^{-1} with higher values in first streams and lower values in larger rivers (not shown), CO_2 outgassing being positively related to *k-value* (Annex 2-4.5 eq. [25]). If *k-value* increases with a negative CO_2 concentrations gradient from the water column to the atmosphere, CO_2 concentrations will decrease (eq. [4]) and reduce the inorganic carbon stock of the water column.

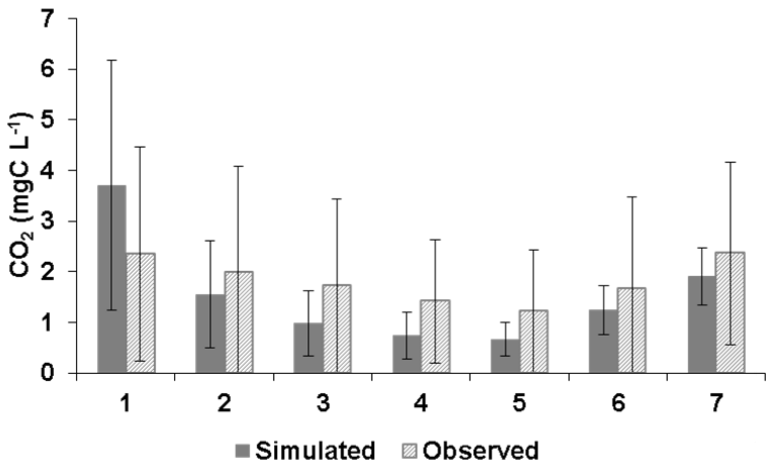

Fig. 2-4 Simulated and observed carbon dioxide concentrations in the Seine waters (CO_2, mgC-CO_2 l^{-1}) as a function of the stream order averaged on the period 2010 – 2013 (whiskers indicating standard deviations).

Profiles of the main stem Marne - Poses

On the same period, a focus on the main stem from the Marne river (SO6) until the outlet of the Seine River (Poses, SO7) showed that longitudinal variations are well represented by the model, with higher concentrations of CO_2 downstream Paris, and a peak of CO_2 concentrations immediately downstream the SAV WWTP, followed by a progressive decrease until the estuary (Fig. 2-5).

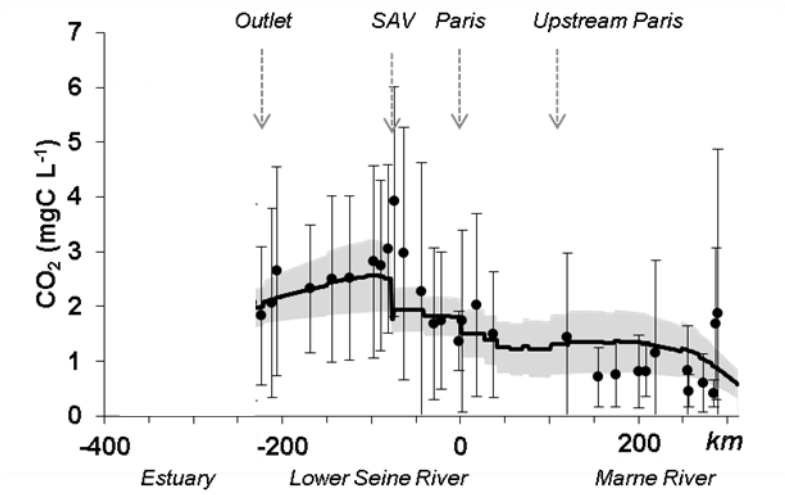

Fig. 2-5 Observed (dots) and simulated (line) mean carbon dioxide concentrations (CO_2, mgC L^{-1}) along the main stem of the Marne River (km −350 to 0) and the lower Seine River (km 0–350) averaged over the period 2010-2013. The simulation envelope (grey area) represents standard deviations of CO_2 simulated. Whiskers are standard deviations between observed CO_2 concentrations.

Seasonal variations

Upstream, within Paris, and downstream of Paris, simulations provide the right levels of CO_2, DIC, TA and pH (Fig. 2-6). In addition to a good range of values, DIC and TA simulations show the observed seasonal patterns with the depletion observed in summer-autumn related to low-flow support by reservoirs. Downstream of Paris (Fig. 2-6, left), CO_2 concentrations reflect the opposite pattern of water discharge with a decrease in CO_2 in May-June when the water flow increases.

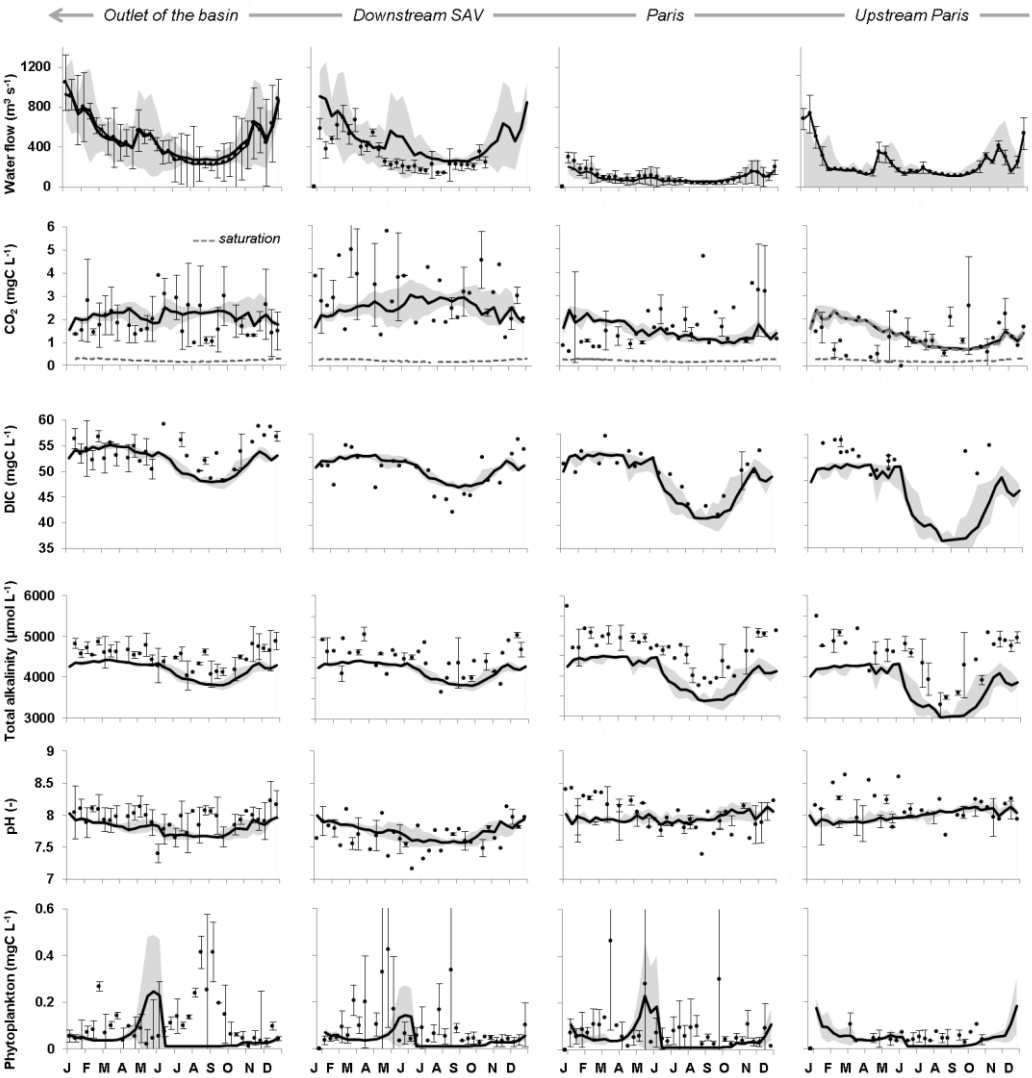

Fig. 2-6 Ten-days simulated (lines) and observed (dots) water discharges on the period 2010-2013 excepted for downstream SAV where water discharges where available only for 2012 (Q, m^3 s^{-1}), concentrations of carbon dioxide (CO_2, mgC L^{-1}, and CO_2 sat, mgC L^{-1}), dissolved inorganic carbon (DIC, mgC L^{-1}), total alkalinity (TA, µmol L^{-1}), pH (-), and phytoplankton (mgC L^{-1}). Simulation envelope corresponds to standard deviations. For observed data, whiskers are standard deviations. Four monitoring stations of interest along the main stem Marne-Poses are shown: Ferté-sous-Jouarre (upstream Paris on the Marne River), Paris (upstream at Charenton), downstream SAV WWTP, and outlet of the basin (Poses).

The model does not reproduce the summer blooms, whereas there is a lag in the simulated spring bloom emergence, compared to the observations (Fig. 2-6, bottom). Relationships between observed values of alkalinity and water discharges and between alkalinity and phytoplankton are not straightforward, alkalinity increasing with increasing discharge (see in Annex 2-7).

2.3.2. Inorganic and organic carbon budgets

Taking into account the rather good simulation levels, we established an average inorganic and organic budget for the studied period (2010-2013) (Table 2-4). The budget of inorganic and organic carbon (IC and OC) shows the high contribution of external inputs (sum of point and diffuse sources represent 92% and 68% of IC and OC inputs) and riverine exports (69% and 65% respectively of IC and OC outputs). These exports are at least one order of magnitude higher for IC budget (Table 2-4). The important contribution of the Seine aquifer induced the IC flux brought by groundwater to be dominant over those from subsurface (respectively 57% vs 34 % of total IC inputs), while for OC, the sub-surface contributions are higher than groundwater ones (54% vs 14% of the total OC fluxes). This is due to high OC concentrations in top soil.

Interestingly, relative contributions of point sources to OC inputs are higher than for IC (23% and 6.5% of the OC and IC inputs, respectively) (Table 2-4).

Heterotrophic respiration by microorganism represents only 1.6% of the IC inputs. Similarly, IC losses by net primary production also account for a small proportion, i.e. 0.5 % of the IC inputs. For the OC budget, despite a contribution of autochthonous inputs from instream biological metabolisms (NPP and nitrification, 8% of inputs, and heterotrophic respiration, 6.5%) relatively high compared to their proportion in IC fluxes (2.3%), allochthonous terrestrial inputs still dominate the OC budget (Table 2-4).

The Seine River exports at the outlet 69% of the IC entering or produced in the drainage network, and 54% of OC brought to the river (including both particulate and dissolved forms) (Table 2-4). Instream OC losses are related to the heterotrophic respiration (6.5%) and while a net transfer to benthic sediment is estimated (28.5% of losses) including sedimentation and erosion processes. In the IC budget, ventilation of CO_2 is an important physical process (30% of the overall losses) (Table 2-4).

Table 2-4 Inorganic and organic carbon budget in the Seine hydrosystem (kgC km^{-2} yr^{-1}) as calculated by the pyNuts-Riverstrahler model averaged on the period 2010-2013. *Net sediment loss is the difference between the erosion and the sedimentation calculated by the model

2010-2013	**Processes involved in inorg C budget**	kgC km^{-2} yr^{-1}	%
Input to river	Diffuse sources from subroot	5963	*34.4*
	Diffuse sources from groundwater	9968	*57.5*
	Urban point sources	1135	*6.5*
	Heterotrophic respiration	270	*1.6*
	Denitrification	0	*0*
Output from river	Delivery to the outlet	12482.5	*68.9*
	Ventilation	5512.5	*30.4*
	Nitrification	37.3	*0.2*
	NPP	95.1	*0.5*
2010-2013	**Processes involved in org C budget**	kgC km^{-2} yr^{-1}	%
Input to river	Diffuse sources from subroot	870	*54.2*
	Diffuse sources from groundwater	227	*14.2*
	Urban point sources	375	*23.4*
	Nitrification	37.3	*2.3*
	NPP	95.1	*5.9*
Output from river	Delivery to the outlet	1081	*65*
	Heterotrophic respiration	107.8	*6.5*
	Net sedimentation	473	*28.5*

2.3.3. Carbon aquatic processes

Whereas IC and OC budgets of the Seine hydrosystem are clearly dominated by external terrestrial inputs and outputs through deliveries at the coast, we focus here on processes involved in the IC and OC cycles (Fig. 2-7Fig. 2-8).

Average spatial distribution of IC processes, as calculated by the model, is mapped for the 2010-2013 period (Fig. 2-7). Benthic activities are the most important in smaller streams. Differently, net primary production and heterotrophic planktonic respiration, which both follow a similar spatial pattern, increase with Strahler order, reaching their higher values in the lower Seine River. All these biological processes involved in the IC cycle are therefore highly active in the main stem of the river, while on the opposite CO_2 outgassing mainly occurs in small head water streams of the basin, with a hotspot in the part of the basin with higher slopes (a limited area in the south) (Fig. 2-8).

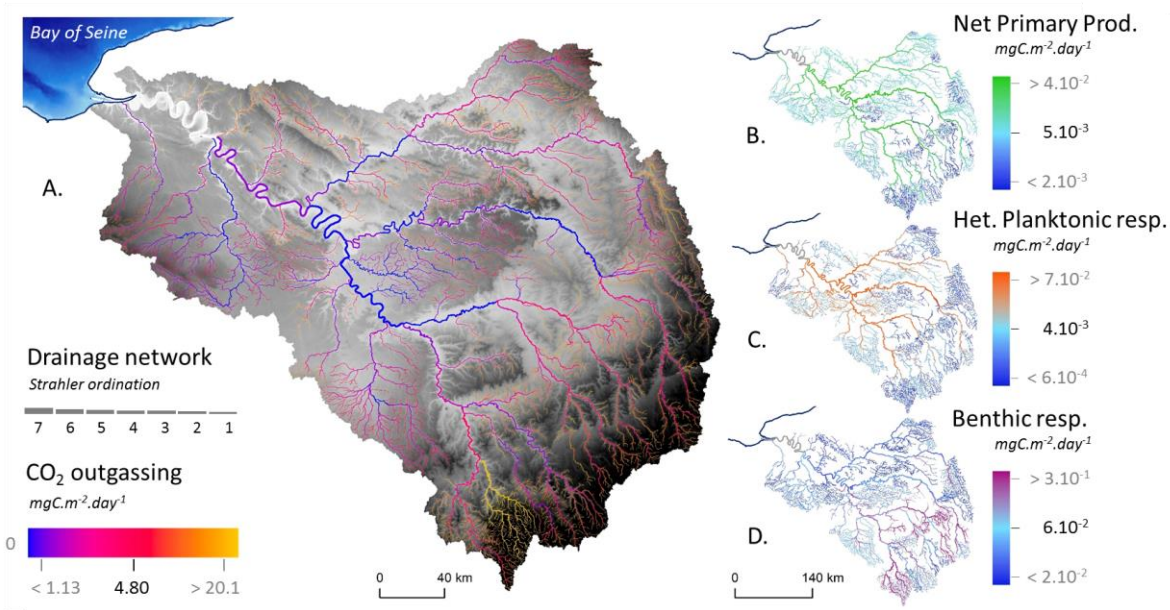

Fig. 2-7. Instream processes involved in the inorganic carbon cycle simulated by pyNuts-Riverstrahler and averaged on the period 2010-2013 for the whole Seine river network. CO_2 outgassing (A. blue - yellow, mgC m^{-2} day^{-1}), net photosynthesis (B. blue – green, mgN m^{-2} day^{-1}), benthic (C. blue - violet) and heterotrophic planktonic (D. blue - orange) respiration (mgC m^{-2} day^{-1}) are represented in the hydrographic network.

Regarding the OC processes, mostly linked to biological activity, they are analyzed in terms of ecosystem metabolism (Fig. 2-8).The net ecosystem production (NEP, mgC m^{-2} day^{-1}) is defined as:

$$NEP = NPP - Het.\ Respiration$$

Where: NPP is the net primary production (mgC m^{-2} day^{-1}) depending on the growth of phytoplankton. This NPP is bio-accumulated by phytoplankton or assimilated by zooplankton and/or benthos that return organic carbon by respiration (Het. respiration, mgC m^{-2} day^{-1}) to CO_2 emissions.

Simulations show that NEP remains negative in the entire drainage network (Fig. 2-8). In SO1, this negative NEP is associated to almost no NPP, and heterotrophic respiration is dominated by benthic activities (see Fig. 2-7). In SO5, NEP is less negative than in SO1 (Fig. 2-8), heterotrophic respiration is lower than in SO1 while NPP is higher. In the lower Seine River (SO7), NPP increases as well as heterotrophic respiration, which reaches its highest value in this downstream stretch receiving treated effluents from WWTPs. Therefore, the increase in NPP does not result in positive NEP. The entire drainage network is thus

supersaturated in CO_2 with respect to atmospheric concentrations, and constitutes a source of CO_2. This supersaturation is the highest in smaller orders, lower in intermediate ones and increases again in the lower Seine River (Fig. 2-8b, see also Fig. 2-4).

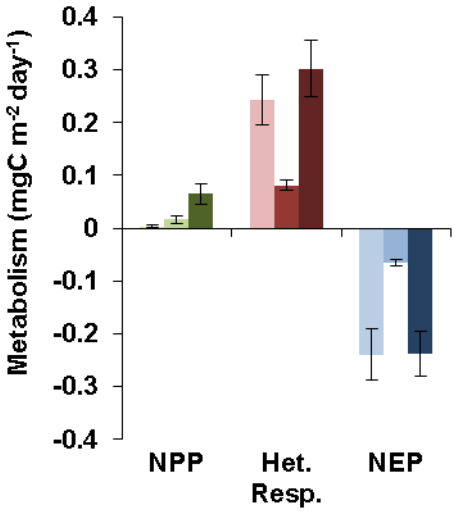

Fig. 2-8 Metabolism of Strahler stream orders 1, 5, and 7 of the Seine basin simulated by pyNuts-Riverstrahler and averaged over the period 2010-2013. Net primary production (NPP, mgC m^2 day^{-1}), heterotrophic respiration (Het. respiration, mgC m^2 day^{-1}), net ecosystem production (NEP, mgC m^2 day^{-1}). Only the SO 1, 5, and 7 were represented as they showed the most different behaviors. Indeed, three patterns were observed one for SO1 to SO3, another one for SO4 and SO5, and the last one for SO6 and SO7.

2.4. Discussion

2.4.1. Validation of the model

Simulated CO_2 concentrations tend to be higher than observed for SO-1. These differences may be related to the high variability of CO_2 in SO1, and the scarcity of measurements in springs. However, Öquist et al. (2009) estimated that up to 90% of daily soil DIC import into streams was emitted to the atmosphere within 200 meters. Soil emissions being highly difficult to capture, we have considered that concentrations in groundwater (DIC and TA) closely reflect the composition of diffuse sources and then, soils composition. Such assumption probably underestimates the DIC/TA ratio brought to the river in small stream. Simulated concentrations in SO-2 to 7 are lower than observed values (Fig. 2-4). For SOs 6 and 7, the way of taking into account gas transfer velocity in the modeling approach could explain these discrepancies (see Annex 2-8). Indeed, the gas transfer velocity value reported by Alin et al. (2011) was used for streams and rivers up to 100 m width, as they recommended. Whereas these *k*-values provided adequate simulations in the river up to 100 m width, for river widths superior to 100 m, *k*-value was calculated according to the equation of O'Connor and Dobbins (1958) modified by Ho et al. (2016) which was probably too high for larger rivers with no tidal influence (Annex 2-8). An equation for large river with no tidal influence using wind speed could be more appropriated (Alin et al., 2011). However, Riverstrahler model does not consider the wind as an input, which would have required a much higher spatio-temporal resolution to reflect it heterogeneity in the Seine basin (from 0 to 5-6 m s^{-1}) with diurnal cycle affected by phenomena as breeze (Quintana-Seguí et al., 2008). Future work of direct *k* measurements and/or a new representation of *k*-values in the model could help to improve outgassing simulations with pyNuts-Riverstrahler.

Regarding seasonal patterns, dissolved inorganic carbon and alkalinity amplitudes are well captured and the level of values is correct. DIC and TA observations show a strong decrease from June/July to November (maximal amplitude decrease of 10 mgC L^{-1} and 1000 µmol L^{-1}) that the model represent. For the Seine River, the water flow decrease in summer is mainly related to the decrease of runoff water, meaning that groundwater contribution is comparatively higher at this time. According to our measurements, these groundwaters are more concentrated in TA, DIC and CO_2 than runoff water. However, in addition to groundwater contributions, reservoirs support low-flow and are characterized by lower TA,

DIC and CO_2 concentrations. Then, the decrease observed is related to the contribution of reservoirs. In addition, phytoplankton blooms especially occurring at low water consume DIC.

2.4.2. Export fluxes

The new implementation of an inorganic carbon module in pyNuts-Rivesterahler enables to estimate the CO_2 outgassing of the Seine River at 362 GgC yr^{-1}. This is lower than in our previous estimate of 590 GgC yr^{-1} using CO_2 measurements only (Marescaux et al., 2018b). An underestimation by the model could be due to lower *k*-values used here. The outgassing by surface area of river of 1293 gC m^{-2} yr^{-1} is in the higher range of estimates from other studies (ranging from 70 to 4008 gC m^{-2} yr^{-1} ; Li et al., 2013 and references herein, e.g. Butman and Raymond, 2011). More precisely, a focus on temperate river outgassing's estimates for the St Lawrence River (Yang et al., 1996), Ottawa River (Telmer and Veizer, 1999), Hudson River (Raymond et al., 1997), and the Mississippi River (Dubois et al., 2010) shows lower rates (from 70 to 1284 gC m^{-2} yr^{-1}) than in the Seine River. This high variability for these temperate rivers is highly dependent on the consideration or not, of the first orders streams in the outgassing. Similarly to our study, Butman and Raymond (2011), take into accounts small streams and rivers while lower estimates correspond to study for large rivers, excluding small streams. Indeed, CO_2 concentrations (see Fig. 2-2) and outgassing are often more important in headwater streams than in large rivers due to higher CO_2 concentrations and gas transfer velocities (Marx et al., 2017; Raymond et al., 2012a). The mapping of CO_2 outgassing in the Seine basin clearly shows that small streams release more CO_2 than median and larger rivers (see Fig. 2-7).

Regarding organic carbon, Meybeck (1993) estimated the DOC export to the ocean for temperate climate at 1.5 gC m^{-2} yr^{-1}, a value that is higher than our OC estimate of 1.0 gC m^{-2} yr^{-1} for the Seine River Basin, before entering the estuarine section. This might be explained by the low altitude of the Seine River, limiting erosion, and by the change in the trophic state of rivers after the implementation of water directives in the late 1990s (Guerrini et al., 1998; Rocher and Azimi, 2017; Romero et al., 2016). In addition, the CO_2/OC ratio of export to estuary of the Seine hydrosystem is 5.1, which is higher from the one of the Mississippi River (4.1; Dubois et al., 2010b; Li et al., 2013) and may be related to important outgassing from headwater streams in our study. However, integrated over their whole basin, the Mississipi, with its surface area > 40 times higher than the Seine, exports 2435 GgC yr^{-1} of OC (Dubois et

al., 2010) while the small Seine River only 71 ± 12 GgC yr^{-1}. Note that, such a Seine River export is three time less than the one calculated in 1979 (250 Gg C yr^{-1} , Kempe, 1984). This difference must be related to improvements in water treatments in the basin decreasing DOC concentrations in the Seine River, precisely of 2.8 times since the 1990's (Rocher and Azimi, 2017) and phytoplankton blooms near disappearance (Aissa Grouz et al., 2016).

We estimate DIC export of the Seine River at 820 ± 201 GgC yr^{-1}, a value higher than basin of the same size or even higher (e.g., Ottawa River, drainge area of 149,000 km2, 520 GgC yr^{-1} , Telmer and Veizer, (1999); Li et al. (2013)). The high concentrations of HCO_3^- in the Seine basin already documented and related to the lithology of the Seine basin (limestone and gypsum beds from Cretaceous and Tertiary) (Kempe, 1982; 1984) may explain this high export to outlet of the river. With both high CO_2 and DIC exports, the ratio of CO_2/DIC exports from the Seine River is close to the global one (0.44 vs 0.5, Li et al., 2013).

2.4.3. Metabolism

Model simulations with the new inorganic carbon module enable to analyze spatial variations of CO_2 regard to metabolism activities (heterotrophic respiration, NPP and NEP).

Mean NEP remained negative in the entire basin resulting from heterotrophic conditions producing CO_2 (Fig. 2-7 and Fig. 2-8). In small streams, NPP and heterotrophic respiration are lower than in higher SOs due to shorter water residence times. However, benthic respiration (Fig. 2-8) makes NEP of small streams as important as NEP of highest SOs impacted by wastewater effluents, and small SOs are the most concentrated in CO_2, brought by groundwaters. Intermediate Strahler streams showed smallest CO_2, respirations or NPP with NEP less than 0.1 mgC m^{-2} day^{-1}. In higher stream orders both respiration and net photosynthesis are the highest (Fig. 2-7 and Fig. 2-8) and metabolisms (photosynthesis) have an impact on CO_2 concentrations (Fig. 2-6). However, SO7 remains mostly heterotroph, with NEP being as negative as in small orders (Fig. 2-8).

The model never calculates positive NEP related to an increase of NPP, a situation generally observed in the past (Garnier and Billen, 2007; Aissa-Grouz et al., 2016). Despite phytoplankton biomass being underestimated by the model, by a factor of about two the Seine hydrosystem does not show any more episodes of autotrophy as it used to be (Garnier and Billen, 2007).

The model highlights the importance of benthic activities in headwater streams (Fig. 2-7) that decrease downstream as heterotrophic planktonic activities increase in larger rivers, a typical pattern described by the river continuum concept (RCC, Vannote et al., 1980) and quantified for the Seine River (Billen et al., 1994; Garnier et al., 1995; Garnier and Billen, 2007). These results are also in agreement with those by Hotchkiss et al. (2015) that suggested that the percentage of CO_2 emissions from metabolism increases with stream size while CO_2 emissions of small streams were derived from allochtonous terrestrial CO_2. Benthic respiration represented 34% of respiration in the main stem, supporting the findings by Vilmin et al. (2016) showing that benthic respiration represented 1/3 of the respiration of the main stem. Regarding headwaters streams, Battin et al. (2009a) described benthic activities as the highest (as also observed in our study, Fig. 2-7) where microbial biomass is associated to streambeds where exchanges with subsurface flow bring nutrients, oxygen and increases mineralization.

On the recent period 2010-2013 studied here, and in all SOs, the NPP never exceeds heterotrophic respiration (ratio NPP –P– to heterotrophic respiration –R– greater than 1) (Fig. 2-8). Whereas in the past, eutrophication of the Seine River led to a P:R ratio above 1 in large rivers at least during spring blooms, with P and R values increasing up to 2.5 mgC m^{-2} day^{-1} (Garnier and Billen, 2007), P:R ratio is now systematically below 1, with P and R values being one order of magnitude lower (compared to the factor of two of underestimation of algal biomass). These changes, linked to an overall decrease in biological metabolism are explained by the improvements of treatment in WWTPs decreasing the organic carbon load into rivers and associated pollution and hence, decreasing CO_2 concentration along the main stem of the Seine River (Marescaux et al., 2018a). Improvement of treatments in wastewater especially reduced nutrient inputs to the river, especially phosphates, nowadays a limiting nutrient to algal development in the SOs 5 and 6, reducing algal peaks from 150 µgChla l^{-1} in the 1990 to hardly 50 µgChla l^{-1} presently (Romero et al., 2016; Aissa-Grouz et al., 2016).

2.5. Conclusion

The first simulations with the river biogeochemical pyNuts-Riverstrahler model including the processes involved in the inorganic carbon cycle represent rather well the CO_2 concentrations and outgassing along the hydrosystem.

This modeling approach highlighted the need for measurements of gas transfer velocities in the Seine River to enable to choose the best model equation or to propose a new one. Such direct measurements of this gas transfer velocity should be completed spatially and seasonally.

CO_2 concentrations appear differently controlled along the Seine hydrosystem. In small orders, concentrations are mainly driven by groundwater discharges. In larger rivers, in addition to the influence of groundwater, concentrations show pattern linked to hydrosystem metabolisms. Indeed, blooms tend to decrease CO_2 concentrations, increasing the NEP although the hydrosystem remains heterotrophic and supersaturated with respect to the atmospheric CO_2 concentrations. Heterotrophic respiration increases CO_2 concentrations with peaks downstream WWTP effluents enriched in organic carbon.

Around 30% of the DIC inputs widely dominated by soils, groundwater or WWTP effluents are outgassed while 69% are exported to the estuary.

Acknowledgements

The project leading to this application received funding from the European Union's Horizon 2020 research and innovation program under the Marie Sklodowska-Curie grant agreement No. 643052. A PhD grant is attributed to Audrey Marescaux. Many thanks are due Sébastien Bosc, Anunciacion Martinez Serrano, and Benjamin Mercier for their kind participation in the fieldwork and for their assistance with chemical analyses in the lab. We thank Muriel Chagniot (Veolia Water – France), and the operators of the WWTPs of Veolia for their precious help in organizing the field campaigns. The SIAAP (Vincent Rocher) are also sincerely acknowledged for their contribution is sampling the largest WWTP of the Paris conurbation and the long term view on treatments in the SIAAP WWTPs provided by their recent book (Rocher and Azimi, 2017). Vincent Thieu (assistant-professor at the University Pierre and Marie Curie, Paris) and Josette Garnier (Research Director at the Centre National de la Recherche Scientifique, France) are co-supervisors of the PhD. Nathalie Gypens is professor at the Université Libre de Bruxelles (Belgium).

2.6. Annex

2.6.1. Annex 2-1 : List of state variables of the Rive model

GROUP *	VARIABLE	DESCRIPTION
	Q	mean discharge during the 10 day period in m3/s
PHY	DIA	diatom biomass in mgC/l
	GRA	green algae (chlorophyceae) biomass in mgC/l
	CYA	cyanobacteria biomass in mgC/l
	MES	mineral suspended solid in mg/l
NUTS	NO3	nitrates in µmol/l:
	NH4	ammonium in µmol/l
	PO4	phosphates in µmol/l
	PIT	total inorganic phosphorus in µmolP/l [**]
	SIO	dissolved silica in µmol/l
	OXY	dissolved oxygen in µmol/l
ZOO	ZOR	rotiferan-like zooplankton in mgC/l
	ZOC	cladoceran-like zooplankton in mgC/l
BACT	BAG	heterotrophic bacteria > 1µ in mgC/l
	BAP	heterotrophic bacteria <1µ in mgC/l
	NIT	ammonium oxidizing nitrifying bacteria in mgC/l
	NAT	nitrite oxidizing nitrifying bacteria in mgC/l
OC	DOC1	rapidly biodegradable dissolved organic matter in mgC/l
	DOC2	slowly biodegradable dissolved organic matter in mgC/l
	DOC3	refractory dissolved organic matter in mgC/l
	POC1	rapidly biodegradable particulate organic matter in mgC/l
	POC 2	slowly biodegradable particulate organic matter in mgC/l
	POC 3	refractory particulate organic matter in mgC/l
	DSS	low molecular weight directly assimilable organic substrates in mgC/l
Benthic	SIB	biogenic non-living particulate (amorphous) silica in µmol/l
	BOC1	benthic (deposited) rapidly biodegradable organic matter in gC/m²
	BOC2	benthic (deposited) slowly biodegradable organic matter in gC/m²
	BOC3	benthic (deposited) refractory organic matter in gC/m²
	BPI	benthic (deposited) inorganic phosphorus in mmolP/m²
	BBS	benthic (deposited) biogenic silica in mmol/m²
	BFE	benthic (deposited) faecal bacteria in 1000/m²l
	SED	deposited inorganic material in g/m²
	FEL	free living faecal bacteria in nb/l
	FEA	attached faecal bacteria in nb/l
	N2O	nitrous oxide in µmol/l
	NO2	nitrite in µmol/l
	CH4	methane in µmol/l
IC	CO2 (***)	Carbon dioxide in mgC/l
	TA (***)	Total alkalinity in µmol/l
	DIC (***)	Dissolved inorganic carbon in mgC/l

(*) “Group” refer to generic group name provided in Fig. 2-2 in this paper
(**) An instantaneous equilibrium is considered for adsorption of ortho-phosphate on MES, so that PIT is the only primary state variable to be considered.
(***) New state variable added in the RIVE model
All biomasses (DIA, GRA, CYA, BAG, BAP, NIT, NAT, ZOR, ZOC) as well as organic matter pools (DOC 1-2-3, POC 1-2-3, BOC 1-2-3) are considered to have constant C:N:P ratios, namely C/N=7

2.6.2. Annex 2-2: Kinetics and parameters of the Rive model (updated from Garnier et al., 2002).

Process	kinetic expression	Parameters				
phytoplankton dynamics			**Meaning**	**Diatoms**	**Chloro-phyc.**	**Units**
Photosynthesis (phot)	kmax (1-exp-(α I/kmax)) PHY	kmax*	maximal rate of photosynth.	0.2	0.25	h^{-1}
		α	initial slope of P/I curve	0.0012	0.0012	h^{-1} $(\mu E.m^{-2} s^{-1})^{-1}$
reserves synthesis	srmax *M*(S/PHY,Ks) PHY	srmax*	max. rate of reserve synthesis	0.1	0.25	h^{-1}
		Ks	1/2 saturation cst	0.06	0.06	
reserves catabolism	kcr R	kcr.*	rate of R catabolism	0.2	0.2	h^{-1}
growth (phygrwth)	mufmax *M*(S/PHY,Ks) lf PHY	mufmax	max. growth rate*	0.05	0.05	h^{-1}
nutrient limitation factor	with lf = *M*(PO_4,Kpp) or *M*(NO_3 +NH_4, Kpn) *or M*($Si0_2$, KpSi)	Kpp Kpn KpSi	1/2 sat. cst for P uptake 1/2 sat. cst for N uptake 1/2 sat. cst for Si uptake	15 14 0.53	62 14 -	µg P l^{-1} µg N l^{-1} mgSiO_2 l^{-1}
respiration	maint PHY +ecbs phygrwth	maint* ecbs	maintenance coefficient. energetic cost of biosynthesis	0.002 0.5	0.002 0.5	h^{-1} -
excretion (phyex)	exp phot.+ exb PHY	exp exb	"income tax" excretion "property tax" excretion	0.0006 0.001	0.0006 0.001	h^{-1} h^{-1}
lysis (phylys)	kdf + kdf (1+ vf)	kdf* vf +	mortality rate parasitic lysis factor	0.032 0 / 20	0.064 0 / 20	h^{-1} -
phyto sedimentation	(vsphy/depth).PHY	vsphy	sinking rate	.006	.001	m h^{-1}
NH_4 uptake	phygrwth /cn NH_4/(NH_4+NO_3)	cn	algal C:N ratio	7	7	g C(g N)$^{-1}$
NO_3 uptake	phygrwth /cn NO_3/(NH_4+NO_3)					
PO_4 uptake	phygrwth /cp	cp	algal C:P ratio	40	40	g C(g P)$^{-1}$
SiO_2 uptake	phygrwth /cSi	cSi	algal C:Si ratio	2	-	g C(g SiO_2)$^{-1}$
temperature dependency	p(T) = p(Topt).exp(-(T-Topt)² / dti²)	Topt dti	optimal temperature range of temperature	21 13	37 15	°C °C
zooplankton dynamics				**Total zooplankton.**		
ZOO growth (zoogwth)	µzox.*M*(PHY-PHYo),KPHY*)*.ZOO	µzox KPHY PHYo	max. growth rate 1/2 sat cst to PHY threshold phyto conc.	0.025* 0.4 0.025		h^{-1} mgC l^{-1} mgC l^{-1}
ZOO grazing	grmx.*M(*(PHY-PHYo) KPHY*)*.ZOO	grmx	max grazing rate	0.1*		h^{-1}
ZOO mortality	kdz.ZOO	kdz	mortality rate	0.05*		h^{-1}
temperature dependency	p(T) = p(Topt).exp(-(T-Topt)² / dti²)	Topt dti	optimal temperature range of temperature	25 10		°C °C
Lamellibranchs				**Dreissena.**		
Filtration rate		fmax	max filtration rate	0.01*		m^3 $gDW^{-1}h^{-1}$
temperature dependency	p(T) = p(Topt).exp(-(T-Topt)² / dti²)	Topt dti	optimal temperature range of temperature	25 8		°C °C
bacterioplankton dynamics				**small bac**	**large bac**	
POCi production by lysis	εpi . (phylys+bactlys+zoomort)	εp1 εp2 εp3	POC1 fraction in lysis pducts POC2 fraction in lysis pdcts POC3 fraction in lysis pdcts	0.2 0.2 0.1		- -
enzym. POCi hydrolysis	kib.POCi	k1b k2b	POC1 lysis rate POC2 lysis rate	0.005 0.00025		h^{-1} h^{-1}
POCi sedimentation	(vsm/depth).Hip	Vs	Hip sinking rate	0.05		m h^{-1}
Hid production by lysis	δe . (phylys+bactlys+zoomort)	εd1 εd2 εd3	DOC1 fraction in lysis pdcts DOC2 fraction in lysis pdcts DOC3 fraction in lysis pdcts	0.2 0.2 0.1		- - -
enzym. DOCi hydrolysis	eimax. *M(*DOCi,KHi*)*.BAC	e1max e2max KH1 KH2	max. rate of DOC1 hydrolysis max. rate of DOC2 hydrolysis 1/2 sat cst for DOC1 hydrol. 1/2 sat cst for DOC1 hydrol.	0.75 0.25 0.25 2.5	0.75 0.25 0.25 2.5	h^{-1} h^{-1} mgC l^{-1} mgC l^{-1}
direct substr. Uptake	bmax. *M(*S,Ks*)*.BAC	bmax Ks	max. S uptake rate 1/2 sat cst for S uptake	0.16 0.1	0.6 0.1	h^{-1} mgC l^{-1}
bact. growth (bgwth)	Y. bmax. *M(*S,Ks*)*.BAC	Y	growth yield	0.25	0.25	-
bact. mortality (bactlys)	kdb.BAC	kdb	bact. lysis rate	0.02	0.05	h^{-1}
bact. sedimentation	(vsb/depth).BAC	vsb	bacteria sinking rate	0	0.02	m h^{-1}
Ammonification	(1-Y)/Y.bgwth/cn	cn	bact. C:N ratio	7		gC (gN)$^{-1}$
PO4 production	(1-Y)/Y.bgwth/cp	cp	bact. C:P ratio	40		gC (gP)$^{-1}$
temperature dependency	p(T) = p(Topt).exp(-(T-Topt)² / dti²)	Topt dti	optimal temperature range of temperature	20 17	22 12	°C °C

Process	kinetic expression	Parameters				
nitrification and phosphorus dynamics			**Meaning**	**nitrifying bacteria**		**Units**
NIT growth (nitgwth)	nix.*M*(NH_4,KNH_4).*M*(O_2,KO_2). NIT	µnix* KNH4 KO2	max growth rate of NIT 1/2 sat cst for NH4 1/2 sat cst for O2	0.046 1.12 0.6		h^{-1} mgN l^{-1} mgO_2 l^{-1}
NH4 oxidation	nitgwth/rdtnit	rdtnit	NIT growth yield NIT	0.1		mgC (mg NH_4)$^{-1}$
NIT mortality	kdnit.NIT	kdnit*	NIT mortality rate	0.01		h^{-1}
PO4 adsorpt/desorpt. (planktonic phase)	Langmuir isotherm	Pac KPads	SM max. adsorpt. capacity 1/2 saturation ads. cst.	0.0056 0.67		mgP (mgMES)$^{-1}$ mgP l^{-1}
temperature dependency	p(T) = p(Topt).exp(-(T-Topt)² / dti²)	Topt dti	optimal temperature range of temperature	23 15		°C °C
benthos recycling						
susp. matter sedim.	(vsm/depth)*MES	vsm	sinking rate			m^{-1}
Diffusion (interstitial ph.)	Fick law	Di	app. diffusion coefficient	8 10^{-5}		cm² s^{-1}
Mixing (solid phase)	Fick law	Ds	mixing coefficient	2 10^{-5}		cm² s^{-1}
orgN mineralis. (maorg)	kib.POCi/cn					
orgP mineralis.	kip.POCi/cp	k1p* k2p*	orgP hydrolysis rate of POC1 orgP hydrolysis rate of POC2	0.05* 0.0025*		h^{-1} h^{-1}
benth. nitrification	kNi*NH4 *(in oxic layer)*	kNi	1st order nitrification cst	0.1		h^{-1}
NH_4 adsorpt/desorpt.	1st order equilibrium	Kam	1st order adsorpt. cst for NH4	9		-
PO_4 adsorpt/desorpt. (in benthos)	1st order equilibrium	Kpa Kpe	PO4 adsorpt. (oxic layer) PO4 adsorpt. (anoxic layer)	100 0		- -
SiO_2 redissolution	kdbSi.SIB	kdbSi	silica redissolution rate	0.0001		h^{-1}
temperature dependency	p(T) = p(Topt).exp(-(T-Topt)² / dti²)	Topt dti	optimal temperature range of temperature	30 15		°C °C

*These parameters depend on temperature according to the relation mentioned.

+*M*(C,Kc) = C/(C+Kc) : hyperbolic Michaelis-Menten function .

+vf: parasitic lysis amplification function. It is maintained at zero while algal density of each group remains lower than a threshold value of 65 µg Chl a l^{-1} and temperature is below 15°C.

2.6.3. Annex 2-3: Modeling objects of the Seine basin

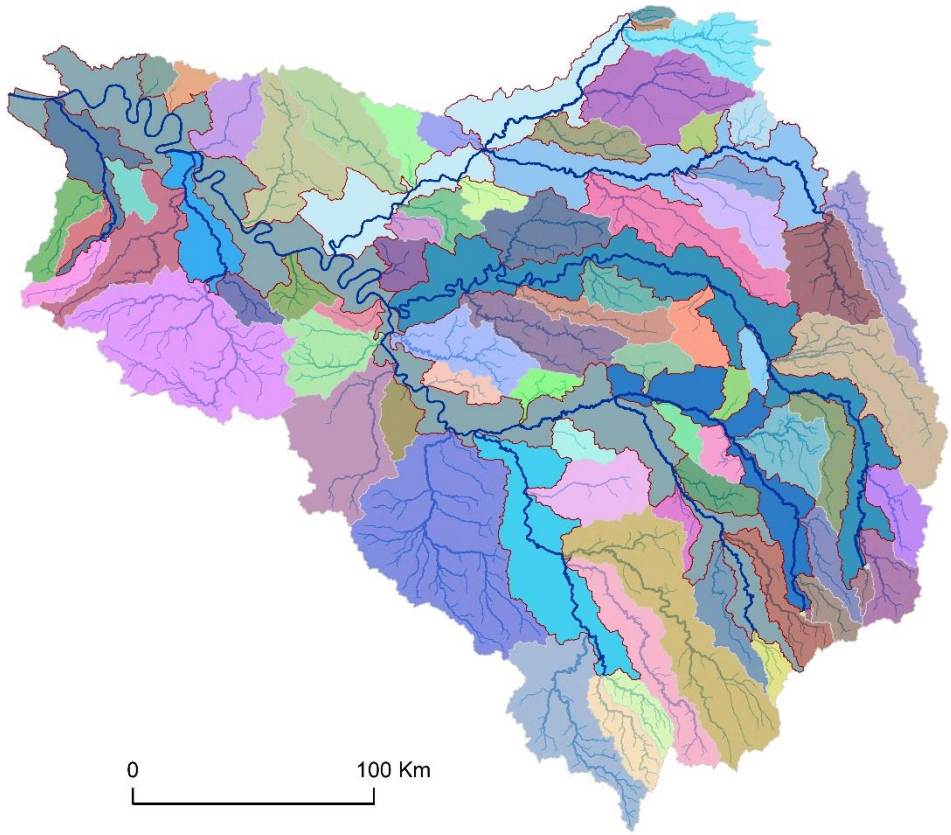

Fig. 2-9. PyNuts-Riverstrahler modeling objects. 8 “Axis” objects (main river branches, mapped with red contours) and 72 “basin” objects (upstream tributaries connected to “axis” objects).

2.6.4. Annex 2-4: Description of the inorganic carbon module implemented in pyNuts-Riverstrahler

The carbonate systems

The major dissolved forms of the carbonate system are CO_2 (aq) aqueous carbon dioxide, H_2CO_3 (aq) carbonic acid, HCO_3^- (aq) bicarbonate ion, CO_3^{2-} (aq) carbonate ion.

$$CO_2(g) \rightleftharpoons CO_2(aq) \quad [1]$$

$$CO_2(aq) + H_2O\ (aq) \rightleftharpoons H_2CO_3\ (aq) \rightleftharpoons HCO_3^-(aq) + H^+(aq) \quad [2]$$

$$HCO_3^-(aq) \rightleftharpoons CO_3^{2-}(aq) + H^+(aq) \quad [3]$$

The acid dissolution constants from the second and the third equations are respectively:

$$K_1 = \frac{[H^+][HCO_3^-]}{[CO_2]} \quad [4]$$

$$K_2 = \frac{[H^+][CO_3^{2-}]}{[HCO_3^-]} \quad [5]$$

$$with\ pK = -logK \quad [6]$$

Carbonates system as a function of DIC

Carbonates dissociation can be determined by total inorganic carbon.

$$DIC = [CO_2] + [HCO_3^-] + [CO_3^{2-}] \quad [7]$$

With the insertion of [4] and [5] in [7], DIC becomes:

$$DIC = \frac{[H^+][HCO_3^-]}{K_1} + [HCO^{3-}] + \frac{[HCO_3^-]K_2}{[H^+]} \quad [8]$$

$$\leftrightarrow\ [HCO_3^-] = \frac{DIC}{\frac{[H^+]}{K_1} + \frac{K_2}{[H^+]} + 1} \qquad [9]$$

And with $[HCO_3^-]$, we can calculate $[CO_3^{2-}]$ and $[CO_2]$ with [8] and [9].

$$[CO_2] = \frac{[H^+]}{K_1}\frac{DIC}{\frac{[H^+]}{K_1} + \frac{K_2}{[H^+]} + 1} \qquad [10]$$

$$[CO_3^{2-}] = \frac{K_2 C}{[H^+]}\frac{DIC}{\frac{[H^+]}{K_1} + \frac{K_2}{[H^+]} + 1} \qquad [11]$$

The dissociation constants of carbonic acid

According to Millero et al. (2006), Harned and Scholes (1941), Harned et al. (1943) the dissociation constants of carbonic acid (molar concentration unit) are calculated as:

$$pK_1 = -126.34048 + \frac{6320.813}{T_K} + 19.568224 * ln(T_K) \qquad [12]$$

$$pK_2 = -90.18333 + \frac{5143.692}{T_K} + 14.613358 * \ln(T_K) \qquad [13]$$

Where T_k is the water temperature in Kelvin (°K).

And,

$$K_1 = 10^{-pK_1} \qquad [14]$$

$$K_2 = 10^{-pK_2} \qquad [15]$$

pH calculation

In the pyNuts-Riverstrahler model, pH was not yet calculated. In the inorganic carbon module, we added the calculation of H_3O^+ concentrations and pH derived from Culberson (1980) to enable to calculate the speciation of carbonates (equations 9-11).

$$DIC_{conv} = \frac{DIC}{12\,rho}\,10^6 \qquad [16]$$

(conversion from mgC L^{-1} to µmol kg^{-1}, where rho (kg m^{-3}) is the water density from Millero and Poisson, 1981),

$$Xdiss = \left(1 - \frac{Bor0}{CA}\right).K_b + \left(1 - \frac{DIC_{conv}}{CA}\right).K_1 \qquad [17]$$

$$Ydiss = \left(1 - \frac{Bor0 + DIC_{conv}}{CA}\right).K_1.K_b + \left(1 - 2.\frac{DIC_{conv}}{CA}\right).K_1.K_2 \qquad [18]$$

$$Zdiss = \left(1 - \frac{Bor0 + 2.DIC_{conv}}{CA}\right).K_1.K_2.K_b \qquad [19]$$

$$aCulb = \frac{(Xdiss^2 - 3.Ydiss)}{9} \qquad [20]$$

$$bCulb = \frac{-(2Xdiss^3 - 9.Xdiss.Ydiss + 27.Zdiss)}{54} \qquad [21]$$

$$phyCulb = cos(\frac{bCulb}{(aCulb^3)^{0.5}}) \qquad [22]$$

$$[H_3O^+] = 2.aCulb^{0.5}.cos\left(\frac{phyCulb}{3}\right) - \frac{Xdiss}{3} \qquad [23]$$

$$pH = -\log_{10}[H_3O^+] \qquad [24]$$

Where Bor0 is the total dissolved boron concentration that can genereally be neglected in freshwaters (Emiroglu et al., 2010).

CO_2 flux calculation

The carbonate speciation function enables to calculate the concentration in aqueous carbon dioxide (CO_2) (eq. 10).

The flux (gC m^{-2} h^{-1}) of CO_2 at the interface of the river and the atmosphere is calculated as:

$$F_{CO_2} = \frac{k}{24}\,(CO_2 - CO_2atm).rho.10^{-3} \qquad [25]$$

Monthly atmospheric CO_2 (CO_2atm, mgC L^{-1}) were measured at Mauna Loa Observatory (Hawaii, U.S.A.) and provided by the NOAA/ESRL: (http://www.esrl.noaa.gov/gmd/ccgg/trends/, last accessed 2018/11/05), Scripps Institution of Oceanography (scrippsco2.ucsd.edu/, last accessed 2018/11/05). Concentration in ppm from Mauna Loa Observatory were converted in mgC L^{-1} using the solubility according to Weiss, (1974). CO_2 concentration in the water (CO_2) (mgC L^{-1}) was calculated according to the section "

Carbonates system as a function of DIC". rho ($kg\ m^{-3}$) is the water density calculated by the International One Atmosphere Equation (Millero and Poisson, 1981).

The flux of CO_2 is depending on the gas transfer velocity (k) that can be determined from the temperature-normalized gas transfer velocity (k_{600}). k_{600} is the gas transfer velocity at a water temperature of 20°C. Parametrization related to the gas exchange used k_{600} to compare systems excluding temperature physical effect. According to Wilke and Chang (1955); Wanninkhof (1992), the gas transfer velocity k(m d^{-1}) can be calculated as:

$$k = k_{600} \cdot \sqrt{\frac{600}{Sc_{CO_2}(T)}} \qquad [26]$$

k_{600} is the gas transfer velocity for a Schmidt number of 600 (m d^{-1}), and $Sc_{CO_2}(T)$ is the Schmidt number (dimensionless) calculated with the water temperature (T) in Celsius ($°C$) calculated as :

$$Sc_{CO_2}(T) = 1911.1 - 118.11T + 3.4527T^2 - 0.04132T^3 \qquad [27]$$

For rivers of widths inferior to 100 m (SO 1-5), k_{600} equation used was retrieved from Alin et al. (2011):

$$k_{600} = \frac{13.82 + 0.35v * 100}{100} \qquad [28]$$

where k_{600} (m d^{-1}) depends on v, the water velocity (m s^{-1}).

In general, k_{600} equations for rivers of widths superior to 100 m require wind velocity (e.g., Chu and Jirka, 2003; Alin et al., 2011; Raymond et al., 2012a). At this stage the pyNuts Riverstrahler model does not consider the wind as an input, which would have required a much higher spatio-temporal resolution to reflect it heterogeneity in the Seine basin (from 0 to 5-6 m s^{-1}) with diurnal cycle affected by phenomena as breeze (Quintana-Seguí et al., 2008). Thus, for river width superior to 100 m, the k_{600} equation from O'Connor and Dobbins, (1958) and Ho et al. (2016), neglecting the term related to the wind, was selected (see Annex 2-8):

$$k_{600} = \frac{a\sqrt{\frac{v}{depth}}}{100} \qquad [29]$$

where k_{600} (m d^{-1}) depends on v, the water velocity (m s^{-1}) and the river depth (m) and the coefficient "a". The coefficient was test from 0 to 2 for SO6 and SO7. We found that SO6 showed a behavior near the original coefficient of 1.539 from O'Connor and Dobbins, (1958) with 1.55, and the SO7 a behavior near the one of 0.77 proposed by and Ho et al. (2016) with 0.55.

Parameters, constants and equations used in the inorganic carbon module.

Table 2-5 Parameters used in the inorganic carbon module for freshwaters

Parameters	Acronym	Units	Sources
Dissociation constants of carbonic acid	K_1, K_2	µmol l^{-1}	Harned and Scholes (1941), Harned et al. (1943), and, Millero et al. (2006)
Solubility	k0	mol kg^{-1} atm^{-1}	Weiss (1974)
gas transfer velocity	*k-value*	m h^{-1}	Wanninkhof (1992), Wilke and Chang (1955) Alin et al. (2011, eq. for river width inferior to 100m) and O'Connor and Dobbins (1958) updated in Ho et al. (2016), for river width superior to 100m.
water density	Rho	kg m^{-3}	Millero and Poisson (1981)
pH	pH	-	Culberson (1980)
Apparent ionization constant of boric acid	Kb	hPa	Schubert (2011)

2.6.5. Annex 2-5 Representation of superficial MESO water bodies

Groundwaters are under strong anthropogenic pressures due to water capture for drinking water production or pollution by agriculture. The European directive (Water Framework Directive - 2000/60/CE) aims to reach the good environmental status of surface and groundwaters and introduced the notion of groundwater bodies (French acronym: Masse d'Eau SOuterraine - MESO) (Fig. 2-10). These MESO units are defined by hydrogeological criteria (e.g., extent and characteristics of the geological layers, feeding area, hydraulic connection between geological layers, interaction with surface waters and associated terrestrial ecosystems…) and non-hydrogeological criteria (capture or the possibility of capture; impact of pressures, potential pollution, administrative boundaries…). The status and upward trends in the concentrations of any pollutant in groundwaters are followed at the MESO scale. The Seine basin includes 48 unconfined (fully or partially) MESO units (see map), they were regrouped according to the lithology and geological ages (colors) to simplify the representation.

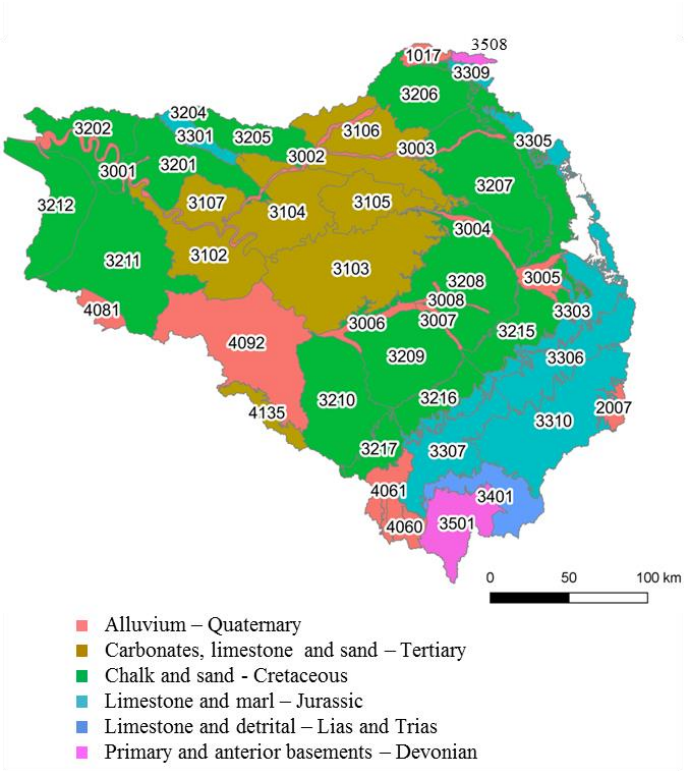

Fig. 2-10 Superficial MESO (Masse d'Eau SOuterraine) water bodies of the Seine basin grouped according to the lithology and geological ages

Table 2-6 Mean concentrations and standard deviations of total alkalinity (µmole L^{-1}) and dissolved inorganic carbon (mgC L^{-1}) grouped by MESO water bodies of the Seine Basin (2010-2015).

MESO code	**Dominant lithology and geological age**	**TA (µmole L^{-1})**		**DIC (mgC L^{-1})**	
		mean	*sd*	*mean*	*sd*
1017	Alluvium - Quaternary	5113	388	79	3
2007		4454	671	75	7
3001		4030	1018	71	12
3002		5058	677	85	6
3003		5288	1025	90	11
3004		4532	992	72	10
3005		4624	487	79	8
3006		3960	493	69	7
3007		4254	382	67	7
3008		4274	832	70	10
4060		4701	291	74	2
4061		4701	291	74	2
4081		1568	1462	35	16
4092		4245	785	72	10
3102	carbonates, limestone and sand – Tertiary	4719	878	81	15
3103		5453	988	76	11
3104		5580	673	92	10
3105		5387	768	91	7
3106		5321	360	89	10
3107		5264	488	86	5
4135		3774	1011	64	11
3201	chalk and sand - Cretaceous	5264	488	83	4
3202		4574	546	76	6
3204		4831	389	81	1
3205		5192	470	83	5
3206		5134	576	83	7
3207		4268	941	70	11
3208		3911	866	64	10
3209		4169	680	69	8
3210		4669	590	75	6
3211		4173	801	67	10
3212		4713	401	77	4
3214		5172	941	87	12
3215		4394	1202	73	13
3216		4732	1011	77	11
3217		5002	481	77	4
3218		4590	995	75	12
3301	Limestone and marl - Jurassic	1660	346	41	5
3303		5120	467	82	6
3304		4939	265	78	4
3305		5236	971	88	12
3306		4629	754	77	8
3307		4907	585	80	6
3309		4938	365	81	4
3310		4454	671	75	7
3401	Limestone and detrital – Lias and Trias	5053	699	82	8
3501	Primary and anterior basements - Devonian	765	228	25	4
3508		663	683	27	9

2.6.6. Annex 2-6: Sampling strategies and protocol for the sampling of wastewater treatment plants sampled in the Seine Basin

Table 2-7. Location of the sampled WWTPs. Their capacity and type of treatment are indicated. Values for TA, DIC, pH and pCO_2 are gathered.

WWTPs	Location	Capacity (Inhab. Eq.)	Water treatment	TA (µmole L^{-1})	DIC (mgC L^{-1})	pH	pCO_2 (ppmv)
Butry	49°04’60N, 2°12’00E	6105	Low load actived sludge	5885	76.27	7.3	31723
Auvers	49°04’00N, 2°10’00E	34,300	Biostyr NDN and PDN	3700	53.39	7.26	28723
Dammarie	48°30'57"N, 2°36'43"E	80,000	Biostyr	4800	68.55	7.45	17268
Rosny	49°0'7"N, 1°39'11"E	120,000	Biological active sludge	4500	55.50	7.4	18651
Troyes	48°20'5"N, 4°2'37"E	300,000	P, biostyr, Ni-denit + post denit	#N/A	86.31	7.4	29930
Seine Centre	48°55'58"N, 2°14'43"E	800,000	P, biostyr, Ni-denit + post denit	3590	47.44	8.17	#N/A
St-Thibault-des-Vignes	48°52'20"N, 2°40'27"E	400,000	P, biostyr, Ni-denit + post denit	5660	73.55	7.40	15732
SAV	48°58′25″ N, 2°09'56"E	6,000,000	P, biostyr, Nit-denit + post denit	2915	#N/A	7.91	#N/A
Inputs of the model (weighted average per capacity):				3993	69.75		

Water samples were filtrated on combusted filters (4h at 500°C: GF/F 0.7 µm, 25mm), and filtrates enabled measurement of DIC and TA concentrations. Dissolved inorganic carbon was analyzed with a TOC analyzer (Aurora 1030). Nongaseous DIC analyses required acidification of the filtrated sample by adding sodium persulfate reagents (100 g L^{-1}) to dissociate the carbonates in the CO_2 that were detected with non-dispersive infrared gas analysis (IRGA). TA (µmol kg-1) was analyzed using an automatic titrator (TitroLine® 5000) on three 20 mL replicates of filtered water (GF/F: 0.7 µm), with hydrochloric acid (0.1 M).

2.6.7. Annex 2-7: Relationships between alkalinity and water discharges or phytoplankton

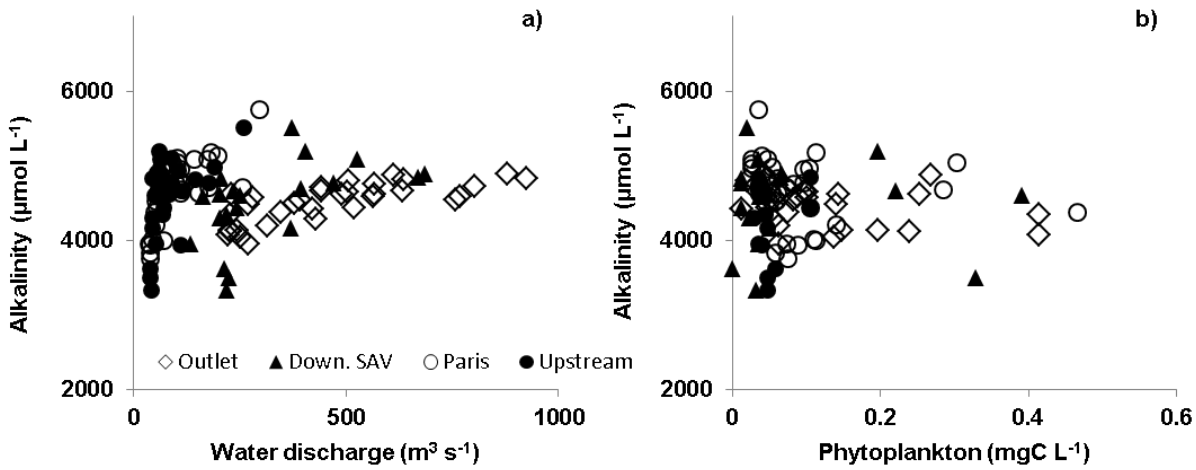

Fig. 2-11. Relationships between observations averaged by decades on the period 2010-2013 of a) alkalinity (µmol L^{-1}) and water discharges (m^3 s^{-1}), and b) alkalinity (µmol L^{-1}) and phytoplankton (mgC L^{-1}) at the four stations studied: upstream Paris (upstream), Paris, downstream SAV (Down. SAV), and at the outlet (Data source: AESN).

2.6.8. Annex 2-8: Impact of the choice of the gas transfer velocity formalisms and the water effluent discharges on the main stem CO2 concentrations.

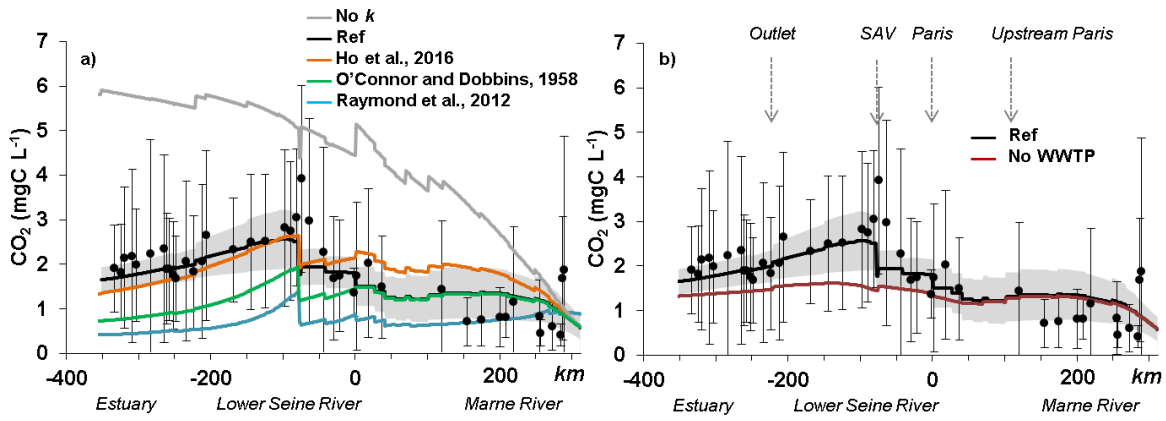

Fig. 2-12. Mean CO_2 concentrations along the main stem of the Seine River depending of a) gas transfer velocities according to O'Connor and Dobbins, (1958) (neglecting the wind); Raymond et al., 2012a, equation 5 in Table 2-2); Ho et al. (2016) (neglecting the wind). Black curve is the reference of our study and grey curve is a simulation with no gas transfer velocity. b) simulations with no discharge of TA and DIC from WWTPs.

Chapter n°3

Carbon dynamics along the Seine River network: insight from a coupled estuarine/river modeling approach

Goulven G. Laruelle[1,2]*, Audrey Marescaux[1,2], Romain Le Gendre[3], Josette Garnier[1,4], Christophe Rabouille[5], Vincent Thieu[1]

[1]Sorbonne Université, CNRS, Institut Pierre Simon Laplace, UMR 7619 METIS, Paris, France

[2] IFREMER LEAD NC, New Caledonia

[3] FR636 IPSL, Sorbonne Université, CNRS, Paris, France

[4] FR3020 FIRE, Sorbonne Université, CNRS, Paris, France

[5] CEA-CNRS-UVSQ, Sorbonne Université, UMR 8212 LSCE, Gif-sur-Yvette, France

Article submitted to Frontiers (December 2018)

Abstract

Largest river flowing into the English Channel, the Seine discharges over 700 Gg of carbon (C) every year into the sea mostly under the form of Dissolved Inorganic Carbon (DIC) and emits 445 Gg under the form of carbon dioxide (CO_2) to the atmosphere over its entire river network. The latter, which drains 76,000 km^2, is heavily populated with 18 106 inhabitants and is thus submitted to large anthropic pressure. The offline coupling of two Reactive Transport Models is used to understand the complex spatial and temporal dynamics of carbon, oxygen and nutrients and quantify the CO_2 exchange at the air-water interface along the main axis of the river. The estuarine section of the Seine is simulated by the generic estuarine model C-GEM (for Carbon Generic Estuarine Model), while the upstream part of the network, devoid of tidal influence is simulated by the pyNuts-Riverstrahler modeling platform which also includes an explicit representation of the drainage network ecological functioning. Our simulations provide a process-based approach to assess nutrients, oxygen, total organic carbon (TOC) and the carbonate system (DIC and alkalinity) over the entire year 2010. Our coupled modelling chain allows quantifying the respective contributions of the estuarine and freshwater sections of the system in the removal of carbon as well as following the fate of TOC and DIC along the river network. Our results also allow calculating an integrated carbon budget of the Seine river network for year 2010.

Keywords: Dissolved Inorganic and organic Carbon, Carbon dioxide, Reactive-transport model, Seine River and Estuary, Biogeochemical budget.

3.1. Introduction

At the interface between the oceanic and terrestrial realms, rivers and estuaries transport ~0.9 Pg C (organic and inorganic) every year into coastal seas (Regnier et al., 2013; Resplandy et al., 2018). Generally oversaturated in carbon dioxide (CO_2) with respect to the atmosphere, these systems collectively further emit between 0.8 and 2.0 Pg C every year into the air under the form of CO_2 (Cai, 2011; Regnier et al., 2013; Laruelle et al., 2013; Raymond et al., 2013a; Lauerwald et al., 2015). Because of this significant role as carbon filters, rivers and estuaries are critical components of the Land-Ocean Aquatic Continuum (LOAC) and have been under growing scrutiny over the past decade (Cole et al., 2007; Battin et al., 2009; Bauer et al., 2013; Regnier et al., 2013). However, large uncertainties are still currently associated to the quantification of global CO_2 fluxes at the air-water interface in these systems, partly due to the scarcity of data available to constrain such global budgets and also due to the difficulty to derive reliable annual estimates of the CO_2 exchange with the atmosphere at the system scale (Regnier et al., 2013a). For instance, the global outgassing of CO_2 taking place in rivers have been estimated at 0.6 and 1.8 Pg C yr^{-1} only two years apart by Lauerwald et al. (2015) and Raymond et al. (2013a), respectively, and the global outgassing of CO_2 from estuaries has been successfully revised downward from 0.4 - 0.6 Pg C yr^{-1} (Abril and Borges, 2004; Borges, 2005; Borges et al., 2005; Chen and Borges, 2009) to 0.1 – 0.15 Pg C yr^{-1} over the past decade (Laruelle et al., 2013; Chen et al., 2013). Even at the scale of a single system, short scale spatial and temporal gradients (of the order of kilometers and days) cannot be captured by a realistic monitoring network. Moreover, the origin of the carbon outgassed (i.e. oversaturated waters in DIC *versus* degradation of organic carbon) is also largely unknown in most systems. Spatially and temporally resolved numerical models are necessary to capture the CO_2 dynamics at the air-water interface, both in time and space (Regnier et al., 2013a). In this context, Reactive Transport Models (RTM) allow reproducing the changes in chemical species concentrations due to both transport and biogeochemical transformations, thus providing a mechanistic insight into the fate of chemical species of interest in riverine and

estuarine environments (Volta et al., 2014, 2016a&b; Romero et al., 2018; Marescaux et al., in prep).

Here, the application to the Seine estuary-river system of the generic transport reactive model C-GEM (for Carbon Generic Estuarine Model, Volta et al., 2014) combined with pyNuts-Riverstrahler (Thieu et al., 2015; Raimonet et al., 2018) allows understanding the carbonate system dynamics in a well monitored and intensively studied system. Fully transient simulations over the entire year 2010 are performed to quantify the annually integrated CO_2 exchange at the air-water interface and better understand the evolution over the year and along the estuarine-river continuum of the CO_2 exchange with the atmosphere and organic carbon degradation as well as the longitudinal variations of inorganic to organic carbon ratio in response to anthropic pressures. While Riverstrahler, and its simplistic derived application to the estuary, has been thoroughly validated for the Seine River over the years (Garnier et al., 2008, 2010), this integrated study is the first application of C-GEM to the Seine estuary. Moreover, the version of Riverstrahler used in our simulations includes a new biogeochemical module which explicitly resolves the complex carbonate system dynamics (Marescaux, 2018). The first part of the results section thus consists of a validation of the hydrology of C-GEM in the estuarine section of the river domain. Then, the ability of both models to capture carbon, oxygen and nutrients dynamics is assessed over the year 2010. These simulations allow better understanding the fate of organic and inorganic carbon throughout the river network and the respective contributions of the different sections of this river network to the conversion of organic carbon into DIC and the outgassing of CO_2 into the atmosphere. A comprehensive carbon budget is then assembled which allows quantifying the organic to inorganic carbon ratio in the different section of the Seine river network (i.e. the estuary, between Poses and Paris and upstream of Paris).

3.2. Methods

3.2.1. Study area

Largest river to flow into the English Channel both in terms of nutrients, carbon loads and fresh water discharge, the Seine River hosts in its central part a large urban area (the Paris conurbation: 12.4 M inhab), a very dense industrial network (40% of French industries) and the biggest wastewater treatment plant in Europe (The Seine Aval WWTP: 1.5 Mm^3 d^{-1}). Further downstream, the Rouen conurbation (0.4 M inhab) appears nowadays as a new pole of economic development, thus forming the "Grand Paris" (Attali, 2010) which steer urban sprawling along the Seine axis from Paris to the sea shore at Le Havre (Fig. 3-1). The Seine watershed also supports intensive cropping activities with 57 % of land devoted to intensive agriculture.

The Seine estuary is characterized by tidal amplitudes comprised between 3 and 8 m at its mouth in Le Havre and a tidal penetration of 168 km up to a dam located at Poses (upstream area : 64,860 km² which corresponds to 85% of the Seine watershed, Fig. 3-1). At the estuarine mouth, the water discharge ranges from less than 200 m^3 s^{-1} in summer to over 1500 m^3 s^{-1} under high water conditions in winter with an average of 490 m^3 s^{-1} over the 2010-2013 period (Marescaux et al., 2018). Our simulation domain includes the entire river network which is subdivided into three main areas: the estuary, simulated by C-GEM between Le Havre and Poses, the mid-section of the Seine between Poses and Paris and, finally all tributaries located upstream of Paris (Fig. 3-1). Over this domain, the main axis of the Seine is fed by 3 major tributaries. The Eure (6000 km²) and the Risle (2300 km²) are both located within the extension of the tidal influence (16 and 152 kilometers from the mouth of the estuary, respectively) while the Oise (17,000 km²) joins the main river 70 km downstream of Paris and delivers 20 % of the freshwater of the entire system. In addition, a large WWTP located in Rouen (kilometer 116) discharges 76,000 m^3 d^{-1} of treated effluents and significantly affects the biogeochemistry of the system.

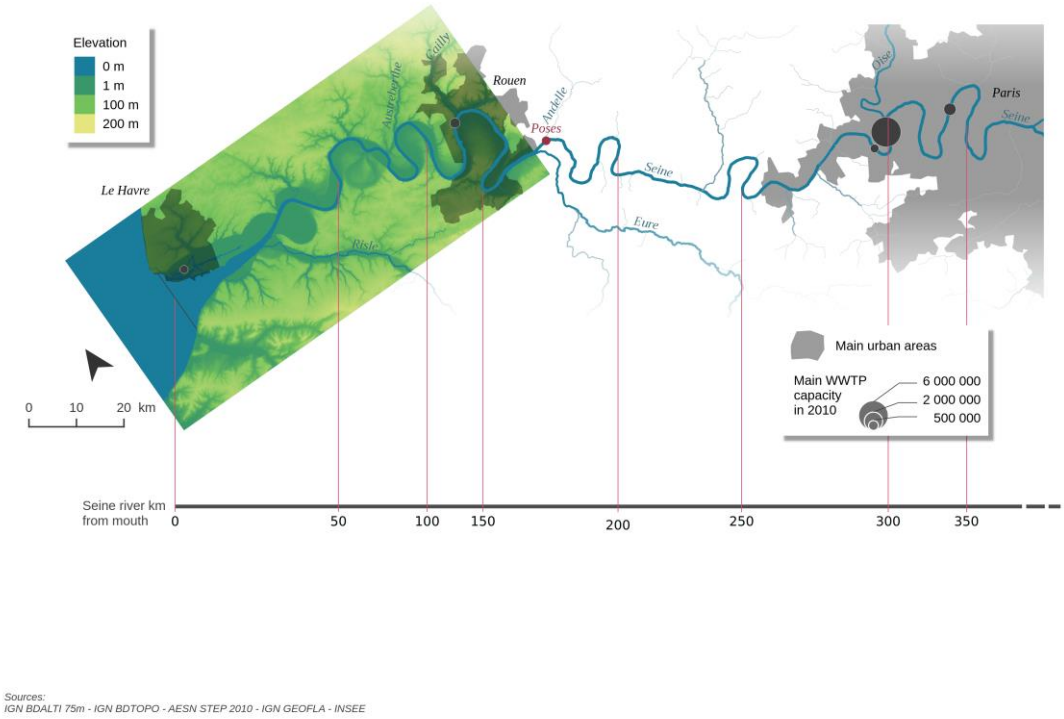

Fig. 3-1 Map of the Seine river network including its main tributaries. The model extends upstream of Paris to the confluence with the Marne River

3.2.2. Modeling strategy

Our study relies on the off-line coupling of two transient, spatially discrete models: C-GEM and pyNuts-Riverstrahler. C-GEM is a recently developed generic estuarine model (Volta et al., 2014, 2016b) which has already been applied to several estuaries distributed along the coast of the North Atlantic Ocean (Volta et al., 2016b; Laruelle et al., 2017a) while the pyNuts-Riverstrahler platform is a well-established model coupling watersheds and river network (Garnier and Billen, 1994; Billen et al., 1994; Thieu et al., 2015). Simulations similar to those described in Marescaux (2018) are first performed with pyNuts-Riverstrahler for year 2010 over the entire Seine watershed. Then, the estuarine section of the main axis of the Seine River located between Poses (kilometer 168) and Le Havre (estuarine mouth, kilometer 0) is modeled by C-GEM using the outputs simulated by pyNuts-Riverstrhaler at Poses as upstream boundary conditions (Table 3-1). In addition, the several tributaries located downstream of Poses, which are also explicitly simulated by Riverstrahler are accounted for

as point sources into C-GEM (the Risle, Austerberthe, Cailly, Andelle and Eure Rivers, Fig. 3-1). Downstream, C-GEM is constrained by modeling results from the ECO-MARS3D model at Le Havre (Romero et al., 2018b) (Table 3-1). Both C-GEM and Riverstrahler include an explicit description of suspended particulate matter (SPM) which accounts for erosion and deposition processes as a function of the flow velocity. The explicit description of the SPM modules for C-GEM and Riverstrahler are described in Volta et al. (2014) and Billen et al. (2015, 2018) respectively.The equations should be inserted in editable format from the equation editor.

Table 3-1 State variables of C-GEM and boundary conditions.

State variables		**Marine Boundary condition**	**Riverine Boundary condition**
Name, Symbol	**Unit**		
Salinity, S	-	MARS3D (hourly)	Assumed to be null
Phytoplankton, PHY	µM C	MARS3D (hourly)	Riverstrahler (10 days)
Oxygen, O_2	µM O_2	WOA (monthly)	Riverstrahler (10 days)
Dissolved silica, DSi	µM Si	MARS3D (hourly)	Riverstrahler (10 days)
Total organic carbon, TOC	µM C	MARS3D (hourly)	Riverstrahler (10 days)
Ammonium, NH_4	µM N	MARS3D (hourly)	Riverstrahler (10 days)
Nitrate, NO_3	µM N	MARS3D (hourly)	Riverstrahler (10 days)
Phosphate, PO_4	µM P	MARS3D (hourly)	Riverstrahler (10 days)
Dissolved inorganic carbon, DIC	µM C	Calculated from TAlk and pCO_2 (monthly)	Riverstrahler (10 days)
Total alkalinity, TAlk	µM C	Broullón (monthly)	Riverstrahler (10 days)
Suspended particulate matter, SPM	g l^{-1}	MARS3D (hourly)	Riverstrahler (10 days)

3.2.3. Modeling chain description

C-GEM

C-GEM is a generic depth-averaged one-dimensional reactive transport model designed to simulate estuarine hydrodynamics, transport and pelagic biogeochemistry of alluvial estuaries with relatively little data and computation demand. The hydrological module of C-GEM and underlying hypothesis are extensively described in Volta et al. (2014) and the biogeochemical reaction network used in the present study is presented as in Volta et al. (2016b). The model combines a set of algorithms for advection and dispersive transport of solids and solutes and mixes multi-component biogeochemical reactions with a 1-D hydrodynamic description. The C-GEM hydrodynamic module requires specification of the river discharge and the tidal amplitude at the estuarine mouth, and is supported by a simplified representation of the estuarine geometry. This geometry is adequate to describe the shape of tidal estuaries (Savenije, 1992, 2012; Volta et al., 2014) and only requires the implementation of a limited number of geometrical parameters (Table 3-2), such as the estuarine length and depth, as well as the channel width (B0) at both marine and land limits. In the particular case of the Seine estuary, two convergence lengths (CL) were used to best represent the observed width profile of the system (Fig. 3-2a). Over the first 32 kilometers of the estuary, B0=10,000 m and CL= 10,700 m. From this point forward and until Poses, the width was calculated using B0=480m and CL= 105,500m. The depth profile was approximated by a regular increase from 4.8m at the mouth to 6.8m 152 kilometers upstream (i.e. Caudebec) followed by a linear decrease to 2.3m at the end of the tidal influence at kilometer 168 (Fig. 3-2b). The use of relatively simple representations of the depth profile was proven sufficient to reproduce the hydrodynamics and transport of several tidal estuaries with C-GEM in previous studies (Scheldt and Elbe Estuaries in Volta et al., 2016b and Delaware Bay in Laruelle et al., 2017b for instance).

Table 3-2 Geometrical and hydrodynamic parameters in the idealized geometry of the Seine estuary.

Name	Description	Value
EL	Estuarine length [km]	168
H_0	Depth at the estuarine mouth [m]	4.8
B_0	Width at the estuarine mouth [m]	10,000
B_2	Width at the inflection point [m]	480
B_x	Width at the estuarine upper limit [m]	30
A_0	Cross-sectional area at the estuarine mouth [m²]	48,000
CL	Convergence length in the lower estuary [m]	10,700
CL2	Convergence length in the upper estuary [m]	105,500
T	Tidal period [s]	45720

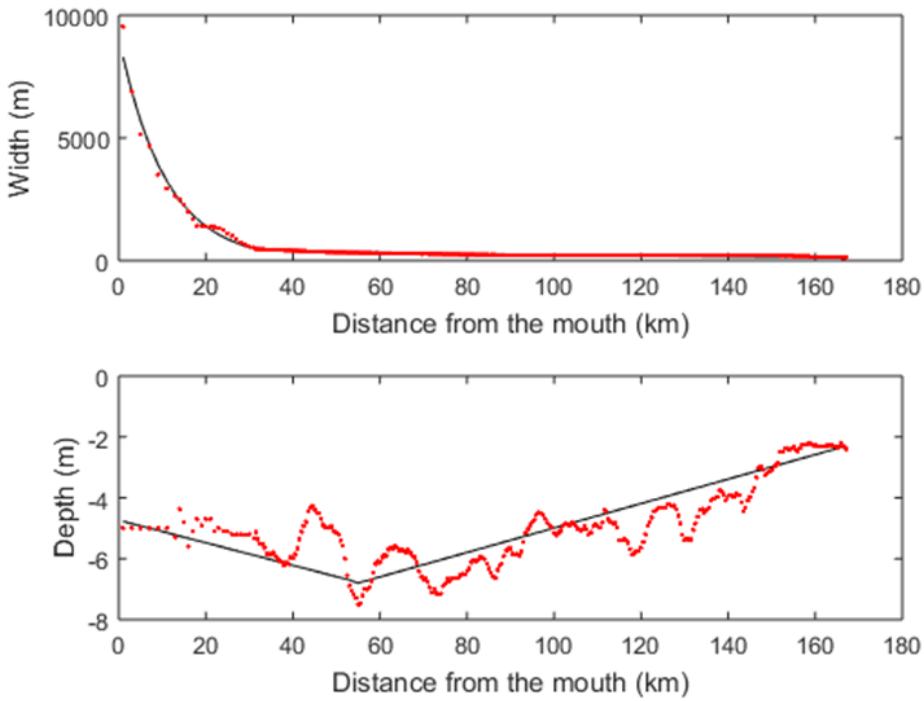

Fig. 3-2 Width and depth profiles of the Seine estuary from its mouth to Poses. Red dots correspond to observations while black lines correspond to the values used to constrain C-GEM's geometry

pyNuts-Riverstrahler

pyNuts-Riverstrahler is a modelling environment written in python (the “py” prefix), setting up the Riverstrahler generic model of water quality for describing the cycling of carbon and nutrients (“Nuts” suffix) in large river systems (Billen et al., 2015, 2018; Raimonet et al., 2018). Biogeochemical processes are simulated within the water column (assumed perfectly mixed), at the water-atmosphere interface (for gaseous variables), at the interface with benthic sediments (see Billen et al., 2015), and at the interface with terrestrial part of the watershed, namely the riparian zone (see Billen et al., 2018).

It allows simulating seasonal (with a 10 days period resolution) and spatial (with a kilometric resolution) variations in the drainage network from small perennial streams to larger stem. The pyNuts-Riverstrahler covers the entire drainage network, and requires as inputs a spatially explicit knowledge of agricultural diffuse sources and urban point sources, as far as constraints imposed by the morphology of the rivers, weather and climate, thus forming the upstream limit conditions of the river model.

The genericity of the Riverstrahler model has been demonstrated throughout successful applications to contrasted fluvial basins, from temperate climate including (among other) the Mosel (Garnier et al., 2000), the Danube (Garnier et al., 2002), the Scheldt (Thieu et al., 2009) among other, sub-tropical climate as the Red River (Le et al., 2014) or the Nam Kan river (Causse et al., 2015) and under nordic climate, such as the Kalix and Lule rivers (Sferratore et al., 2008). The Riverstrahler model has also been chained with the coastal marine model (Eco-Mars 3D, Cugier et al., 2005), extended to the estuarine part in terms of hydrosedimentary representation (Passy et al., 2016), and with nutrient description (Romero et al., 2018b). The development of the pyNuts modeling environment has made it possible, with the same intention, to develop continental applications of the Riverstrahler to multiple hydrosystems on an entire marine façade in Western Europe (Desmit et al., 2018).

Biogeochemical description

The biogeochemical modules of C-GEM and pyNuts-Riverstrahler include similar key state variables and processes in spite of a greater level of complexity of Riverstrahler's reaction network (Fig. 3-3). Both models include an explicit description of all nutrients (nitrate, ammonium, phosphates and dissolved silica), dissolved oxygen, phytoplankton and a representation of the carbonate system. C-GEM only simulates diatoms and non-diatoms, while pyNuts-Rivestrahler described biogeochemical cycles including their interactions with biological compartments, including three functional phytoplankton groups (diatoms, Chlorophyceae, and Cyanobacteria), zooplankton (rotifers and microcrustaceans) and heterotrophic bacteria (small autochthonous and large allochthonous) as well as nitrifying bacteria. The most significant difference between both models regards the benthic compartment which is ignored in the current version of C-GEM while pyNuts-Riverstrahler explicitly takes into account a benthic module (recently updated: Billen et al., 2015) simulating exchanges with the water column for several variables (benthic organic matter, inorganic particulate phosphorus, benthic biogenic silica). The lack of benthos in C-GEM is implicitly compensated by the assumption that, in the estuary, denitrification especially occurs in the turbidity maximum zone within the water column. Both models use invariant parameterization within their respective simulation domain thus assuming homogeneity of the physiological properties of organisms along the river network (Garnier et al., 2002) but use different parametrizations between the riverine and estuarine sections of the Seine. pyNuts-Riverstrahler have been extensively validated for the Seine River and the set-up used for the current study is identical to that described *in extenso* in Marescaux (2018). C-GEM relies on a generic parametrization derived from a large collection of modeling studies performed on temperate estuaries (Volta et al., 2016a). Several modifications to this generic estuarine parameterization were implemented during the calibration stage (namely, the rate of aerobic degradation of organic matter which was increased from 6.08 10^{-4} µMC s^{-1} to 1.2 10^{-3} µMC s^{-1}, the half-saturation constant for TOC degradation which was decreased from 183 µMC to 100 µMC and the nitrification rate which was increased from 2.73 10^{-5} to 5 10^{-4} µMN s^{-1}) but

these calibration values all fall with ranges reported by the literature survey of Volta et al. (2016a).

Finally, both models include similar inorganic carbon module, which allows quantifying the estuarine inorganic carbon dynamics. The latter is a recent development of pyNuts-Riverstrahler described *in extenso* in Marescaux (2018) while its implementation in C-GEM is described in Volta et al. (2014) and derived from Arndt et al. (2011). In both models pH is the main variable controlling the estimation of dissolution and hydration of CO_2. Its computation follows numerical schemes provided by Culberson (1980, for pyNuts-Riverstrahler) and Follows et al. (2006, for C-GEM) using iterative procedures, which accounts for total (TAlk) and carbonate alkalinities. While the model accounts for borate species, contributions from ammonium, fluorine, phosphate, silicate, sulfide and other minor species are neglected because their concentrations are much lower than those of carbonate species (Vanderborght et al., 2002). In the estuarine model (C-GEM), the apparent equilibrium constants for CO_2 solubility and dissociation of water (H_2O), carbonic acid (HCO^{-}_{3}), bicarbonate (CO^{2-}_{3}), and boric acid ($B(OH)^{-}_{4}$) are functions of temperature and salinity following equations described in Cai and Wang (1998) and Dickson et al. (1992). In the riverine model, the influence of boric acid is not taken into account as it can generally be neglected in freshwaters (Emiroglu et al., 2010).

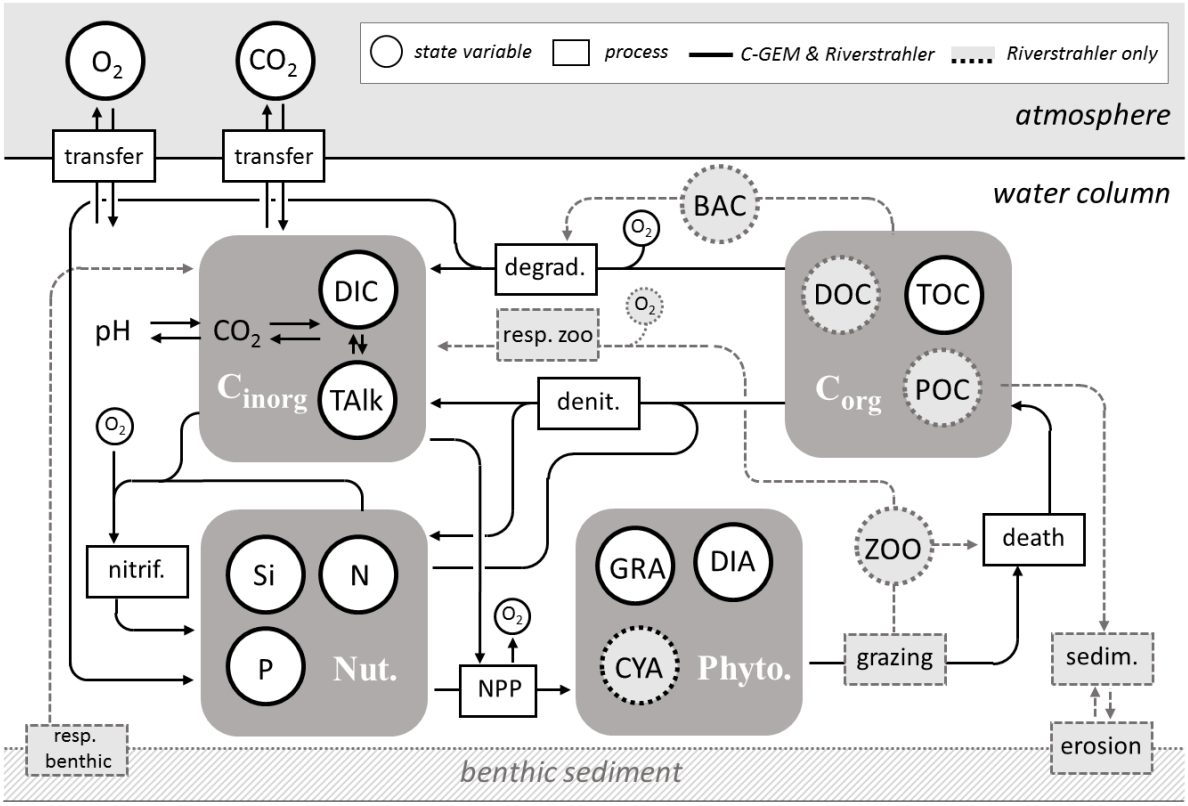

Fig. 3-3 Simplified conceptual scheme of the share of state variables and processes between C-GEM and Riverstrahler models. The two models simulate nutrients as N (NO_3, NH_4), P (PO_4, Total P) Si (DSi, BSi in Riverstrahler only). In the Riverstrahler, both dissolved (DOC) and particulate (POC) carbon are modelled according to 3 classes of degradability (rapid, slow and refractory); heterotrophic bacteria (BAC) are described as large and small, and the zooplankton (ZOO) includes micro-crustaceans and rotifers-cillates

3.2.4. Simulations Set-up

2.4.1. Numerical schemes

C-GEM calculations for transport and reaction are solved in sequence by applying an operator splitting approach (Regnier et al., 1998; Regnier and Steefel, 1999) and a finite difference scheme of a regular grid (Δx=2000m) with a time step Δt=150s. The reaction network is formulated and numerically resolved as described in Volta et al. (2014). Each simulation begins with a spin-up period of 2 months using the boundary conditions and forcing of the first tidal cycle, which ensures that the system reaches steady-state conditions.

pyNuts-Riverstrahler calculations are based on a Lagrangian description of carbon and nutrient transformation along the drainage network (idealized as a regular scheme of confluences) taking into account sources and/or dilution by lateral water from direct watersheds and assuming permanent hydrological conditions every 10 days-period. Biogeochemical processes simulated are incremented according to the residence time of the water masses with a 6 minutes time step. Climatic constraints such as light and temperature are described with daily variations, while both point and diffuse sources concentrations are averaged over the simulated year.

C-GEM uses the outputs of Riverstrahler as upstream boundary conditions for phytoplankton concentrations, nutrients, organic and inorganic carbon, SPM, as well as water discharge. The following section describes the specifics of the coupling between both models for each state variable and described the other forcing required to perform the simulations.

2.4.2. Model coupling and boundary conditions

C-GEM requires to be forced with a set of boundary conditions upstream and downstream. These include concentrations for all state-variables of the model and time series for water elevation at the marine boundary as well as fresh water discharge at the riverine boundary. Most of these data are provided by outputs of the ECO-MARS3D model (Romero et al., 2018b) at the downstream boundary and by Riverstrahler at the upstream boundary.

Downstream, all required inputs were available at a 1 hour temporal resolution, which allows capturing the tidal cycle. For each state variable, the concentration used as boundary condition was calculated by averaging in width and depth the concentrations extracted from ECO-MARS3D along a North-South transect interception the estuarine mouth at the longitude of 0.1°E. The only state variables not provided by ECO-MARS3D were DIC and TAlk. The latter was thus extracted from a recent global monthly climatology for oceanic alkalinity (Broullón et al., 2018). Monthly values for DIC were then calculated, using CO2SYS (van Heuven et al., 2011) from these TAlk values and monthly pCO_2 estimates extracted from the global coastal pCO_2 climatology of Laruelle et al. (2017a).

At the upstream boundary condition, all state variables required to run C-GEM were provided by the outputs of Riverstrahler at Poses (kilometer 168) at a temporal resolution of 10 days except for salinity which was assumed to be null. Linear interpolations were performed to generate continuous values for each calculation time-step in C-GEM. Five tributaries connecting the main axis of the Seine River downstream of Poses were also taken into account as point sources following the procedure described in Volta et al. (2014, 2016b): the Risle, the Austreberthe, the Cailly, the Eure and the Andelle are respectively injected at 16, 88, 124, 152 and 166 kilometers away from the estuarine mouth, and the effluents of the Rouen conurbation injected at kilometer 111 (Fig. 3-1).

3.3. Results

3.3.1. Model validation

Hydrodynamics and transport

The performance of the hydrodynamics module was first evaluated through a series of steady state simulations under varying discharge and tidal conditions (Fig. 3-4). A set of six increasing tidal amplitudes from 3.1m to 7.7m were applied at the marine boundary. The selected range of tidal amplitudes at the mouth corresponds to six tidal coefficients (C35, C45, C65, C80, C95 and C115) on a scale ranging from 20 to 120. The smallest (C35) and largest tidal coefficients (C115) represent extreme spring and neap tides, respectively. Two values of fresh water discharges were applied at the riverine boundary condition. The lowest value (250 m^3 s^{-1}) is roughly equivalent to summer moderate regime conditions while the highest value (800 m^3 s^{-1}) is equivalent to a moderately high water regime at Poses (based on long term discharge chronicle available in the BanqueHydro database, http://hydro.eaufrance.fr/, last accessed November 2018). The longitudinal profile of the tidal amplitude under the 12 possible combinations of the tidal amplitude and water discharge was compared to average profiles derived, for similar conditions, from observations collected by 18 tidal gauging stations located along the estuarine length provided by the 'Grand Port Maritime de Rouen' (Fig. 3-4). The match between both models is very good under all conditions with average RMSE < 30cm over the entire profile and in particularly good agreement under average conditions (i.e. tidal amplitudes at the mouth comprised between 4 and 7m, Fig. 3-4, panels c to h).

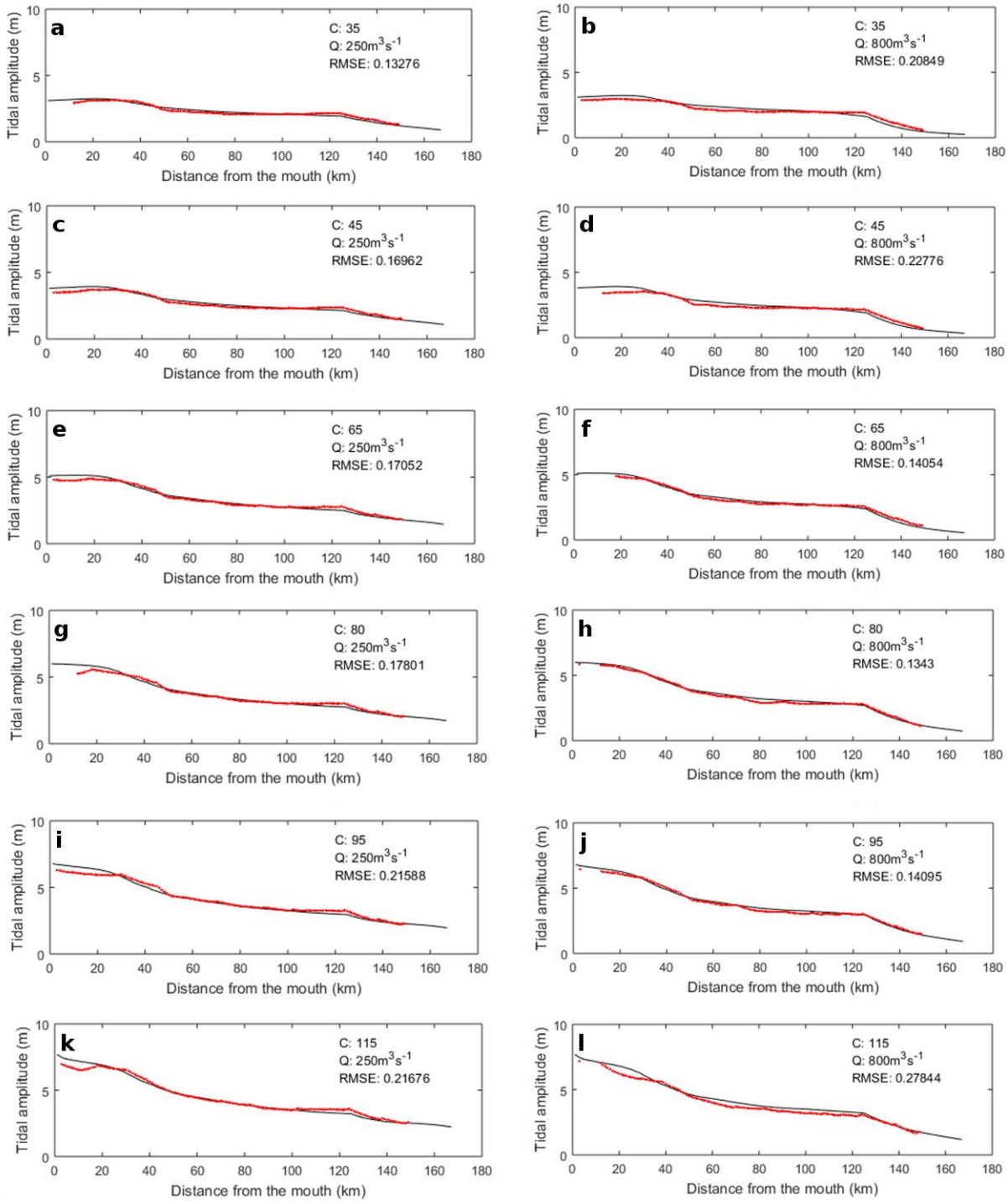

Fig. 3-4 Simulated tidal amplitude profiles along the Seine estuary under varying discharges (Q) and tidal coefficients (C). The black lines are simulated by C-GEM while the red dots are observations from the SHOM.

The propagation of the tidal amplitude along the estuary is characterized by a gradual decrease of the tidal amplitude throughout the first 50 kilometers of the estuary followed by a 70 kilometers long section within which the tidal amplitude decreases at a slower rate. For any given tidal amplitude at the mouth, profiles under high and low water discharges are relatively similar until kilometer 120. After this point, the tidal amplitude decreases sharply in all simulations, as water depth reaches 4 meters, to only about 1 meter by kilometer 150 under high discharge and 2 meters under low water discharge. The tidal propagation is stopped by a dam at Poses and the river is devoid of tidal influence upstream of this limit. Note that, because of the significant fluvial traffic in the Seine, the water discharge is regulated at Poses thus preventing extreme fresh water flows that could significantly modify the salt water and tidal intrusion in the estuary.

A transient simulation was performed with the full hydrodynamics and transport modules over the entire year 2010. Because of its relatively short convergence length compared to its width at the mouth, the Seine estuary is marine-dominated, which translates into a relatively short saline intrusion (Savenije, 2012). In our simulations, salinity never exceeds 1 further than 30 kilometer upstream. A limited number of measurements in the downstream portion of the estuary at stations Honfleur (kilometer 16) and Tancarville (kilometer 32) only allows assessing performances of the model against field data under the form of longitudinal salinity profile. Fig. 3-5 (left panels) presents six such longitudinal profiles reconstructed for the year 2010. These profiles reveal that observations always fall within the range reported by the model over a full tidal cycle but also that the magnitude of the salinity change between kilometers 10 and 20 is usually quite large. Also, our simulations reveal that the extension of the salinity intrusion is always comprised between 20 and 30 kilometers from the estuarine mouth regardless of the tidal or freshwater discharge conditions, which is consistent with observations (Morelle et al., 2018) and previous modeling studies (Grasso et al., 2018).

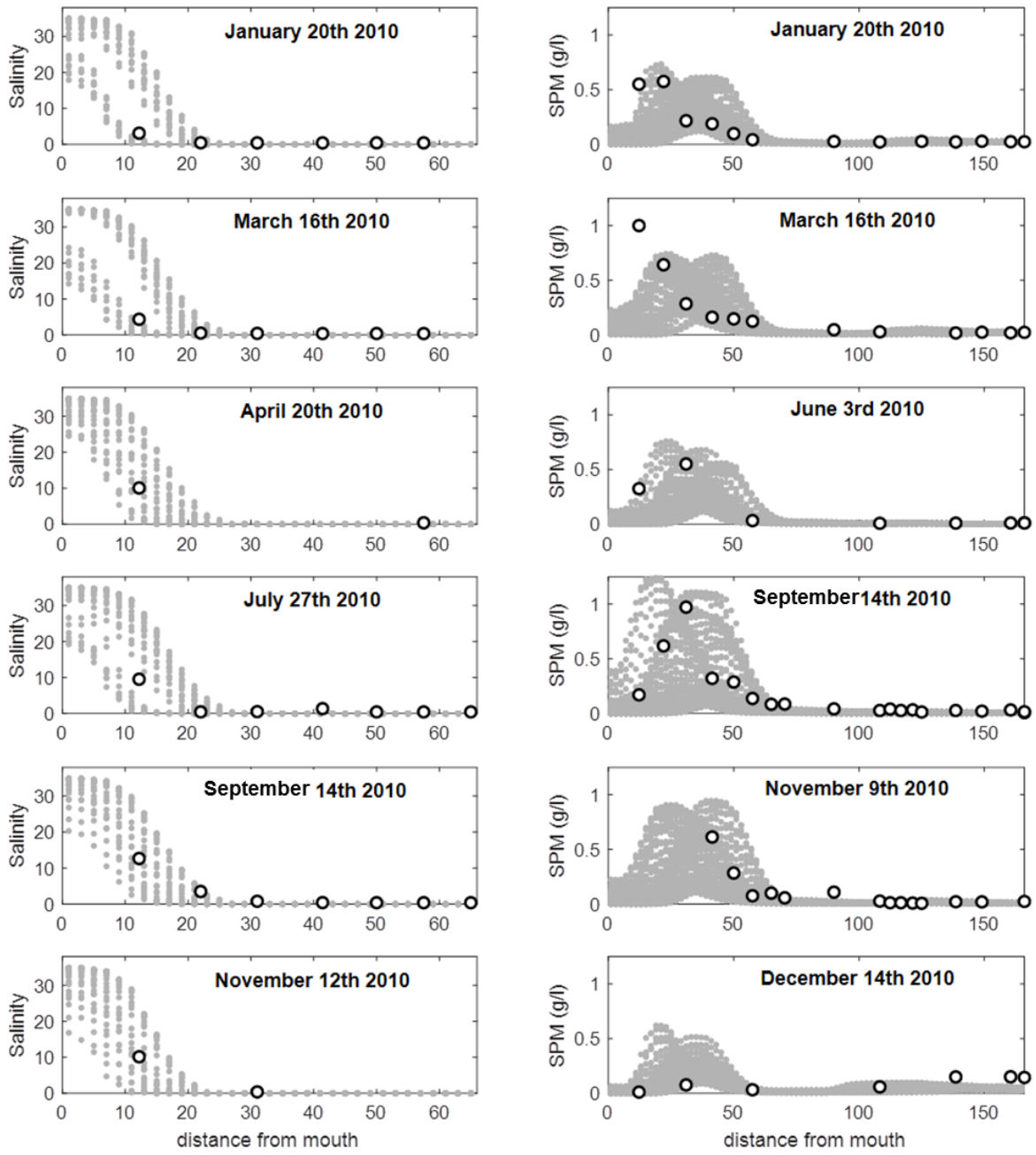

Fig. 3-5 Salinity (left panels) and SPM profiles (rights panels) along the Seine estuary for 6 dates. Dots correspond to measurements, while grey dots correspond to simulated values over 2 tidal cycle for salinity and 20 for SPM

Longitudinal profiles of SPM were also analyzed and compared with observations (Fig. 3-5, right panels). Overall, the model properly captures the characteristic maximum of SPM around kilometer 20-30 which varies in intensity between 0.4 and 1.2 g l^{-1} depending on the tidal amplitude, the water discharge and its SPM charge. The comparison between model and

observation reveals a good match and is consistent with previous modeling studies (Grasso et al., 2018). Overall, the range of SPM concentrations predicted over 20 tidal cycles encompasses 88% of the observations and the location of the turbidity maximum is usually captured accurately by the model. The results reported compile values over a 10 days period in order to match the time step of the upstream boundary condition of the estuarine model for SPM concentrations and water discharge provided by pyNuts-Riverstrahler at Poses.

Biogeochemistry

Fig. 3-6 displays the temporal evolution of concentrations for chlorophyll a, ammonium (NH_4), nitrate (NO_3), phosphate (PO_4), dissolved silica (DSi), dissolved oxygen (O_2), TOC and the carbonate system (i.e., DIC, TAlk, pH and pCO_2) at five locations which combines outputs of both C-GEM and pyNuts-Riverstrahler along the main axis of the Seine. For each variable and location, time series are provided and compared with field measurements. The five locations correspond to the upstream end of the turbidity maximum zone (TMZ, 55 kilometers from the estuarine mouth), 115 kilometers upstream of, where the tidal amplitude is about half of that at the marine boundary, in Poses (kilometer 168) where both models are connected, and at kilometers 208 (upstream of Poses) and 300 (1 km before the Oise confluence), within the domain simulated by pyNuts-Riverstrahler.

In our simulation, phytoplankton concentrations (represented by Chl. a, calculated as the sum of all phytoplankton species and converted from µmol C l^{-1} into mg Chl. a m^{-3}) are characterized by a maximum in late Spring. This phytoplankton bloom is delayed by about a month compared to the observations and displays relatively constant values throughout the entire system until Honfleur. At this point, because of the combined effects of dilution and light attenuation generated by SPM preventing primary production, phytoplankton concentrations slightly decrease and never exceed 20 mg Chl.a m^{-3} at the marine boundary condition. The phytoplankton maximum is concomitant with the seasonal consumption of nutrients, particularly noticeable for DSi and NH_4. The latter is also characterized by a decrease along the upstream-downstream axis, in spite of several punctual injections

corresponding to the discharge of the different tributaries as well as the waste water treatment plant located in Rouen. NO_3 display relatively constant concentrations (~500 µmol l^{-1}) along the river/estuarine gradient until the strong marine dilution taking place from kilometer 20 until the estuarine mouth after Honfleur where the width of the estuary increases exponentially because of the change in convergence length (Fig. 3-2b). Data reveal a summer maximum in PO_4 throughout the entire system, which is captured by the model, although over-estimated in the estuarine section. Overall, there is nonetheless a relatively good match between modelled and observed nutrient levels in spite of a slight over-estimation of NO_3 and PO_4 during the warmest month of the year in the estuarine domain and an over estimation of the DSi consumption in late spring generated by the delayed phytoplanktonic bloom in the simulations. Dissolved oxygen also displays seasonal variations with maximum values >400 µmol O_2 l^{-1} in winter and a drop below 300 µmol O_2 l^{-1} in the heat of summer. O_2 is the variable which displays the best match between model outputs and observations at all locations.

Time series for TOC, DIC and TAlk also reveal a relatively good fit with observations. TOC, which displays little seasonal variability and a progressive consumption from Paris to the estuarine mouth, is slightly over estimated by the model, particularly towards the end of the year. At kilometer 58, 111 and 308, the fit between modeled and observed TOC is very good until day 250. DIC and TAlk are both comprise between 3500 and 4500 µmol C l^{-1} in all locations throughout the year and display lower values between days 200 and 300. These seasonal variations are well captured by the model which predicts DIC with accuracy while slightly underestimating TAlk. pH and pCO_2 predicted by both models are relatively close to observations in terms of seasonal average but also struggle to capture the seasonal signal observed in the data. Together, both models are able to simulate the progressive increase in pH from 7.8 in Paris to 8.1 at the estuarine mouth but the seasonal dip taking place in summer is only adequately reproduced by pyNuts-Riverstrahler at kilometer 208. Downstream, a pH maximum develops around day 150, as a consequence of the late phytoplankton bloom simulated by the model while observations report an annual minimum. The opposite seasonal

trend is observed for pCO_2 which is characterized by baseline values mostly comprised between 2000 and 3500 ppm in winter but exhibits a maximum in summer with values in excess of 10,000 ppm in Poses, which are not captured by the models, especially in the estuarine section. In our simulations, pCO_2 does not exhibit any seasonal variations downstream of Poses and remains essentially bounded between 2500 and 4000 ppm over the entire estuarine section. The propagation of this seasonal mismatch at the boundary condition between both models (Poses) results in an underestimation of pCO_2 in the estuarine section between days 120 and 180.

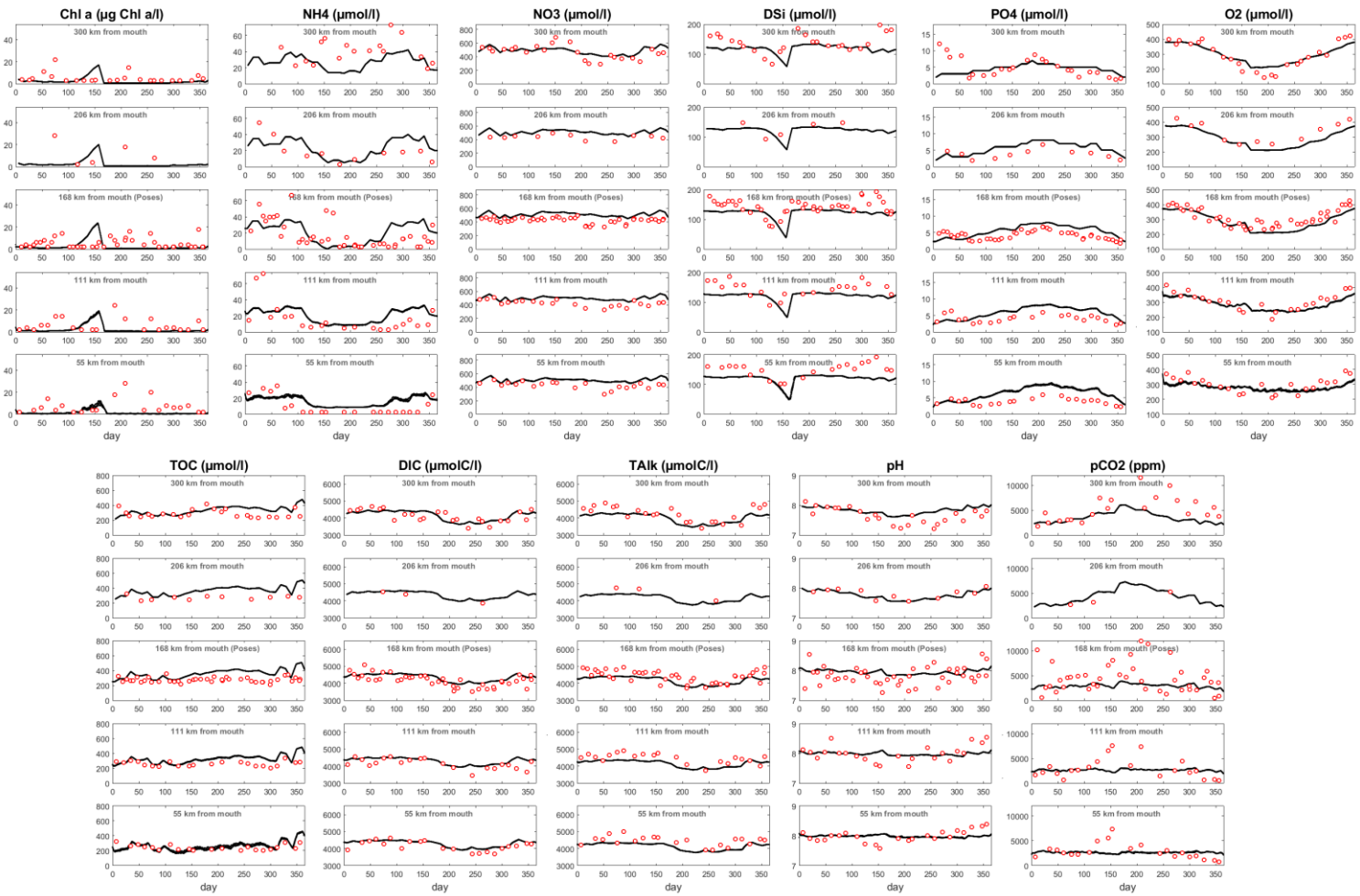

Fig. 3-6 Time series for Chl. a, NH_4, NO_3, dSi, PO_4, O_2, DIC, TAlk, pH and pCO_2 at five stations along the main axis of the Seine. Red dots correspond to measurements while black lines correspond to simulation outputs

3.3.2. Carbon dynamics

Processes controlling the carbon dynamics along the Seine River and estuary

A mechanistic understanding of the carbon dynamics along the main axis of the Seine can be provided by the analysis of the respective contributions of aerobic degradation (Respiration), denitrification, Net Primary Production (NPP) and CO_2 outgassing to the change in DIC and TOC concentrations along the main axis of the Seine between Le Havre and Paris (Fig. 3-7). The use of width-integrated yearly averaged rates allows analyzing the CO_2 dynamics per unit length of estuarine segment and identifying variations all along the domain that would otherwise be difficult to compare by using volume/surface-integrated estimates (Fig. 3-7a,b). In parallel, Fig. 3-7c,d also reports those rates per unit surface area which provides insight regarding the intensity of the biogeochemical processes controlling the fate of carbon.

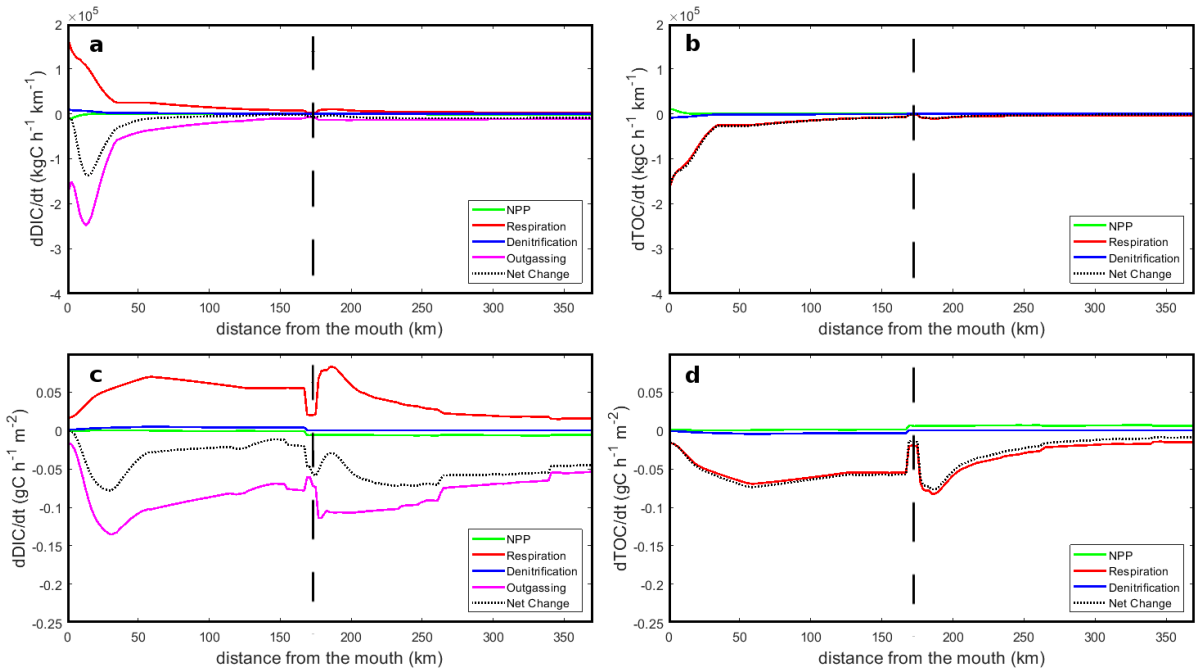

Fig. 3-7 Longitudinal profiles along the main axis of the Seine of the different processes affecting the DIC (a, c) and TOC pools (b, d). In the top panels (a, b), the process rates are integrated over the Seine's width while they are reported per surface area in the bottom panels (c, d). Zero is the mouth of the estuary in Le Havre, vertical dashed lines, represent Poses, Paris corresponds to the km 370.

The main process responsible for changes in DIC along the river-estuarine gradient is CO_2 outgassing (a loss represented negatively), which goes increasing from Paris until Poses and reduces DIC concentrations in water (Fig. 3-7a). In terms of outgassing intensity per surface area, however, the rates simulated in the estuarine and riverine sections of the model are comparable (Fig. 3-7c). In the estuary (km 0 to 168), the outgassing of CO_2 increases from 0.2 gC d^{-1} m^{-2} to 3 gC d^{-1} m^{-2} between Poses to 30 kilometers upstream of Le Havre and drops sharply towards the estuarine mouth. The width integrated fluxes reveal that, in spite of lower emission rates, the 50 most downstream kilometers of the system account more than half of the total CO_2 flux towards the atmosphere (51%) as a consequence of the exponential widening of Seine towards the sea (Fig. 3-2a). The dominant instream biogeochemical source of DIC for the system is the aerobic degradation of organic matter, which displays a progressive increase from Paris (0.04 gC d^{-1} m^{-2}) to Poses (2 gC d^{-1} m^{-2}) and sustains a rate comprised between 0.8 and 1.2 gC d^{-1} m^{-2} in most of the estuarine section, except for the 20 most downstream kilometers. Primary production and denitrification only contribute marginally to the DIC balance of the system and the net change in DIC is negative all along the simulated river-estuarine continuum.

Along its journey through the main axis of the Seine from Paris to the estuarine mouth, organic matter is mostly converted into DIC with a negative net change comprised between -0.1 and -2 gC d^{-1} m^{-2}. This consumption is almost exclusively driven by aerobic degradation and denitrification is almost negligible. The latter is nonetheless slightly more intense in the estuarine section of the Seine but remains two orders of magnitudes less intense than respiration. The source terms for organic carbon (i.e. NPP) never exceed 0.1 gC d^{-1} m^{-2} and reaches 100 kgC d^{-1} km^{-1} at the estuarine mouth. Overall, these profiles reveal that the main axis of the Seine barely produces organic matter instream and is essentially sustained by tributaries and lateral inputs while converting a large proportion of the organic carbon produced upstream into DIC.

Integrated budget of the Seine estuarine/river network

Every year, 1204 Gg C are injected into the Seine river network, including 101 Gg C yr^{-1} under the form of organic carbon as diffuse and point sources (Marescaux et al., 2018) providing a ratio of OC/IC of around 0.1. This organic to inorganic carbon ratio drops below 4% at the estuarine mouth where 716 Gg C yr^{-1} and 29 Gg C yr^{-1} of DIC and TOC are exported to the sea, respectively. The overall CO_2 outgassing of the entire Seine and estuarine system reaches 445 Gg C yr^{-1} in 2010 (Fig. 3-8). 44% of this CO_2 release takes place upstream of Paris (196 Gg C yr^{-1}), mostly in the large upstream Seine River network (137 Gg C yr^{-1}) compared to the smaller Marne one (59 Gg C yr^{-1}). Downstream of Paris, however, the main axis only contributes 21 Gg C yr^{-1} between Paris and Poses while the estuary and the various tributaries emit 101 and 127 Gg C yr^{-1}, respectively. Looking at the inputs, 465 Gg C y^{-1} reach Paris, mostly under the form of DIC (92%). Another 319 Gg C yr^{-1} are introduced into the main axis of the Seine between Poses and Paris. 71% of those come from tributaries, which mostly contribute to the DIC pool (216 Gg C yr^{-1}) while the 91 Gg C y^{-1} provided by urban releases and point sources exhibit a much high proportion of OC (18%). 31% of the OC reaching the main axis of the Seine between Paris and Poses is thus delivered by urban releases and point sources. Within this section of the network, a significant DIC removal takes place in the various tributaries of the Seine, most notably the Oise for which the total outgassing amounts to 98 GgC yr^{-1}. Downstream of Poses, in the section of the main axis simulated by C-GEM, most of the carbon processing takes place in the estuary where 46 Gg C y^{-1} are converted from organic matter into DIC (71% of the entire river network) and 101 Gg C yr^{-1} are emitted as CO_2 into the atmosphere. The estuarine net primary production, however remains relatively low with 3.6 Gg C yr^{-1} but still represents 32% of the production occurring in the upstream fluvial part. As illustrated by Fig. 3-7, the large contribution of the estuarine section of the Seine to NPP and respiration can be partly attributed to its relatively large water surface area.

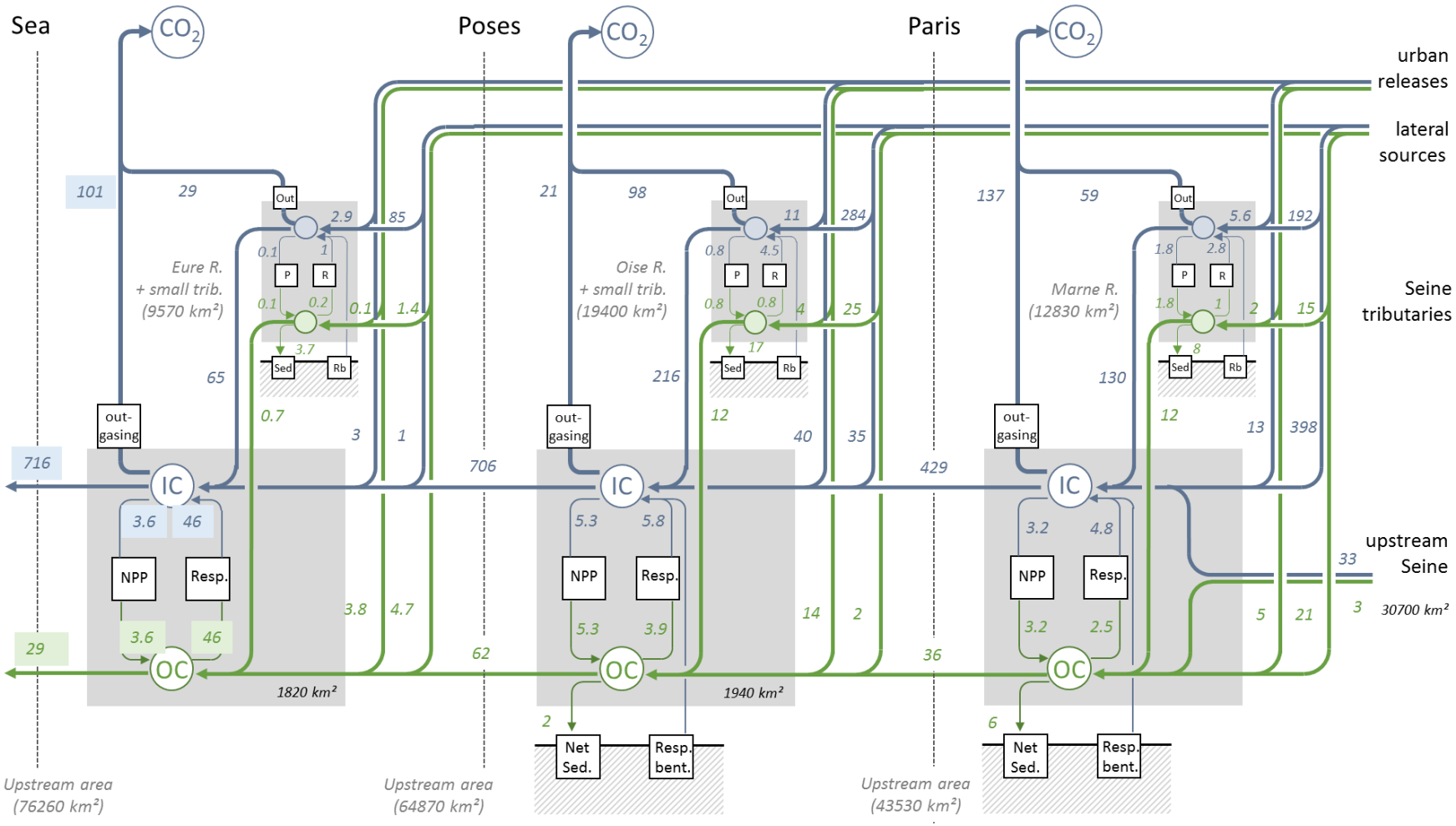

Fig. 3-8 Organic (green) and inorganic carbon budget (blue) for the Seine river network. All fluxes are expressed in Gg C yr^{-1}. The surface area all the different sub-sections of the watershed are indicated in italic.

3.4. Discussion

3.4.1. Interests and weaknesses of the approach

The simulations presented in this study are, to our knowledge, the first transient representation of the inorganic carbon biogeochemical processing of an entire river network resulting from the full coupling of a riverine and estuarine RTMs. Such an off-line coupling was recently published using Rivertrahler and ECO-MARS3D for nutrients biogeochemical processing only (Romero et al., 2018b). The relatively good performances, at least in terms of level of water quality variables, of both C-GEM and Riverstrahler for chlorophyll, nutrients, oxygen as well as organic and inorganic carbon dynamics proves that our approach is able to capture the main biogeochemical dynamics of the Seine River network all along its main axis and provide a realistic representation of the main biogeochemical processing taking place in the different tributaries (i.e., nutrient consumption, organic matter degradation etc..). All variables simulated fall within the range of the values observed on the field and most seasonal patterns such as nutrient consumption are reproduced. Our simulations describe a heterotrophic system characterized by a moderate biogeochemical processing and relatively little production in the estuarine section as suggested by previous studies (Garnier et al., 2001). One of the main controls of the biogeochemical dynamics of the Seine river network is the significant anthropic pressure which translates into large nutrients and organic matter point sources, in particular in Achères downstream the WWTP SAV and Rouen as was evidenced by (Servais et al., 1991; Romero et al., 2016; Marescaux et al., 2018). Although the timing of the simulated phytoplankton bloom is late by a few weeks, the amplitude of the nutrient consumption is similar to observation and the decrease in dissolved silica confirms the domination of diatoms within phytoplankton biomass (Garnier unpublished; Morelle et al., 2018).

Because of the advective nature of the riverine environment, a proper simulation of the seasonality of the carbonate cycle in a riverine environment puts a lot of pressure on the accuracy of the most upstream concentrations. It is thus a testament to the robustness of the hydrological modules of both models that proper seasonal signals in most chemical species can be adequately transferred along the riverine gradient and from Riverstrahler to C-GEM in spite of significantly different temporal resolution. While several RTMs including biogeochemical modules have been developed and successfully applied to several rivers and

estuaries over the past decades (Regnier et al., 1997; 1999; 2002; Laruelle et al., 2009; Arndt 2007; 2009; 2011; Romero et al., 2018), it should be noted that both C-GEM and pyNuts-Riverstrahler are designed to be generic tools relying on parameterizations elaborated with the intend of an ease of deployment to any temperate system (Volta et al., 2014; 2016a&b; Laruelle et al., 2017; Desmit et al., 2018). Thus, this successful local application opens the door to simulation of entire stretches of coastline of this estuarine/riverine modeling chain following the recent independent regional application of both C-GEM (Laruelle et al., 2017) and Riverstrahler (Desmit et al., 2018).

3.4.2. A carbonate module in the land-ocean aquatic continuum.

One of the main features of the biogeochemical modules used in this study is the explicit resolution of the carbonate cycle, which is seldom included in riverine and estuarine RTMs. As for nutrients, the values simulated by both models for DIC, TAlk, pH and pCO_2 fall well within the average values observed on the field for these variables throughout the entire length of the system and the seasonality of DIC and TAlk are properly captured. This is also demonstrated for the riverine section of the Seine in Marescaux (2018). However, the complex seasonal dynamics of the carbonate system was not fully captured for pH and pCO_2. These variables are very sensitive to minor changes in DIC and TAlk and are thus particularly difficult to simulate with accuracy. Nonetheless, the baseline pH and pCO_2 values simulated by C-GEM in the estuarine section of the Seine match observations for most of the year. The discrepancy with observations corresponds to the propagation at the connection between both models of the late phytoplankton bloom, which prevents the model to reproduce a drop in pH observed in the field around day 150. It should also be noted that previous modeling attempts at simulating the carbonate cycle in estuarine environments however did not involve a spatial component and only reproduced annually or seasonally averaged conditions (Volta et al., 2016a&b). Overall, our longitudinal profiles for DIC, TAlk, pH and pCO_2 do match average observations.

This is illustrated by the large changes in pCO_2 and pH observed at any given station along the Seine and particularly clear in Poses (Fig. 3-6). Nonetheless, because of the largely oversaturated nature of the Seine in pCO_2 throughout the year and the fact that baseline pCO_2 values simulated by both C-GEM and Riverstrahler, we are confident that our integrated yearly budget for the CO_2 emissions from the river network of the Seine is relatively realistic. Considering that the pCO_2 values simulated by our estuarine model match the yearly baseline

values, our estimate should be regarded as a lower end estimate. Based on the most downstream pCO_2 time series, assuming that the gradient of pCO_2 at the air-water interface is underestimated by the estuarine model by a factor of 2 between days 120 and 180, the resulting CO_2 emissions would only increase by ~15%. One of the striking features of these calculations is that with a conservative estimate of outgassing of 101 Gg C yr^{-1} over the 168 most downstream kilometers of the Estuary (and 51 Gg C yr^{-1} in the 50 most downstream kilometer), the estuary contributes at least 23% to the global emission of CO_2 from the entire river network of the Seine which amounts to 445 Gg C yr^{-1}. This exercise reveals the importance of the latter because, in part, of the large increase in available surface area. This was already evidenced by Volta et al. (2016a; b) for the Scheldt and the Elbe. This evidences the importance of including an explicit description of the morphology of estuaries when performing an integrated analysis.

3.4.3. Features and fates of Carbon in LOAC at regional scale

Interestingly, the contribution of the estuary to the Seine's river network matches that derived for the global scale (23%) by comparing the estuarine outgassing of 0.15 Pg C yr^{-1} calculated by Laruelle et al. (2013) to the riverine outgassing of 0.65 Pg C yr^{-1} calculated by Lauerwald et al. (2015). Such local and global results further highlight the importance of integrating estuaries into calculations of the carbon removal by the LOAC either at local scale (i.e., such as in this study), regional scale (Laruelle et al., 2015) or global scale (Regnier et al., 2013b). In addition, the outgassing of 101 GgC yr^{-1} reported to the surface area of the Seine's estuary (146 km^2) yields an average emission rate per surface area of 58 mol C m^{-2} yr^{-1}. While this value sits at the high end of the range of emissions reported for tidal estuaries (estimated at 18.2 mol C m^{-2} yr^{-1} by Laruelle et al. (2013)), European estuaries under heavy anthropic pressures tend to display higher emission rates ranging from 30 to 70 mol C m^{-2} yr^{-1} (Frankignoulle et al., 1998).

Throughout its journey along the Seine's LOAC, the fraction of organic carbon remains below 10% in all sections of the network and goes increasing from below 5% in the tributaries upstream of Paris to ~10% at the confluence of the Seine and the Oise and decrease again to 4% at the mouth of the estuary. This decreasing trend in the estuarine domain is consistent with that suggested by the global synthesis of Bauer et al. (2013) although that study implies a larger fraction of organic carbon in global riverine waters suggesting that the natural organic load of the Seine is relatively low. The significant increase in the mid-section of the main axis

of the river is a direct consequence of the strong anthropogenic pressures existing on the Seine river-network. For instance, large punctual inputs indeed take place, in particular between Paris and Poses where the organic to inorganic carbon ratio exceeds 0.1 as a consequence of the discharge of a large amount of the treated effluents of the 12.5 million inhabitants of the Parisian conurbation on the lower Seine River. Noteworthy, the contribution of the organic load in this Paris-Poses stretch has been much higher in the period 1980-1990 before efficient treatments, especially in the huge SAV WWTP as shown in terms of BOD load in Rocher and Azimi (2017) and oxygenation of the river (Romero et al., 2016). Overall, the organic carbon retention (calculated as 1 minus the ratio of organic carbon exported to the organic carbon inputs) for the entire river network amounts to 54% for the estuarine section.

Although significant, this number is slightly lower than the range of organic retentions calculated for six European estuaries surrounding the North Sea by Volta et al. (2016a). These systems, which include the Scheldt, the Thames, and the Oder were shown to all convert over half of the organic carbon passing through them (76 ± 20%). However, the total carbon retention (i.e., taking into account both DIC and TOC) of the Seine estuary amounts to 9%, which is comparable to the Scheldt (10%), the Elbe (11%) and the Weser (12%) and falls at the low end of the range of 15 ± 7% reported by Volta et al. (2016a).

3.5. Conclusions

This study presents an integrated modeling investigation of the carbon and nutrient dynamics along the LOAC of the Seine river network. Our approach relies on the coupling of two transient, spatially resolved models for the estuary (C-GEM) and the river network (pyNuts-Riverstrahler) able to simulate Chl. a, nutrients, oxygen and the carbonate cycle. Our simulations performed over year 2010 properly capture the longitudinal profiles and seasonal variations of all variables and reveal a system under strong anthropic pressure with large nutrients and organic matter inputs. Our study thus allows calculating an integrated carbon budget of the Seine river network which evidences the large contribution of the estuary to both CO_2 outgassing and TOC degradation. While the spring maximum in pCO_2 observed on the field is not reproduced by our models, the baseline pCO_2 simulated by the model allows estimating a conservative outgassing of the estuarine section to be 101 Gg C yr^{-1}, which amounts to 23% of the entire river network. The estuary also transforms 65% of the TOC into DIC between Poses and Le Havre, lowering the OC to IC ratio from 0.1 upstream of Poses to 0.04 at the estuarine mouth. Because of the generic nature of both C-GEM and pyNuts-

Riverstrahler, similar applications to other river networks or entire stretches of coastline can be ambitioned in the future.

Authors contribution

GGL designed most of the set-up for the simulations of the estuarine model and drafted the first version of the manuscript. The riverine model simulations were carried out by AM with the help of VT. GGL, AM, JG and VT contributed to early drafts of the manuscript and helped structuring it. In addition, VT performed the calculations necessary to the riverine carbon budget, RL provided marine boundary conditions to the estuarine model and CR provided insight for the discussion. All co-authors commented and reviewed the latest versions of the manuscript.

Conflict of Interest

The authors declare that the research was conducted in the absence of any commercial or financial relationships that could be construed as a potential conflict of interest.

Funding

GL was supported by Labex L-IPSL LP3, which is funded by ANR (grant #ANR-10-LABX-0018). AM was supported by the C-CASCADES (https://c-cascades.ulb.ac.be/) project of which this study was a part, received funding from the European Union's Horizon 2020 research and innovation programme under the Marie Sklodowska-Curie grant agreement No. 643052.

Part Two

Greenhouse gas (CO_2, CH_4, N_2O) emissions from the Seine basin

Chapter 4

Carbon dioxide, methane and nitrous oxide emissions from the human-impacted Seine watershed in France

Chapter 5

Long term changes in greenhouse gas emissions of French agriculture and livestock (1852-2014): from traditional agriculture to conventional intensive systems

PART TWO: SUMMARY

While nitrous oxide (N_2O) and methane (CH_4) emissions from the Seine drainage system and the agricultural basin were published separately in 2009 and 2013, respectively, (Garnier et al., 2009; Garnier et al., 2013); the CO_2 study (see Part 1, chapters 1 and 2) allowed the joint (and updated) analysis of these three greenhouse gases. Thanks to field studies in 2016 and 2017, new N_2O and CH_4 samples were analyzed and combined with other data from campaigns (2010 to 2014) undertaken prior to my Ph-D thesis.

Therefore, in the fourth chapter, CO_2, CH_4 and N_2O concentrations were compared and analyzed according to seasonal variations (summer and winter) and along the drainage network of the Seine hydrosystem based on Strahler ordination. While CO_2 and N_2O concentrations with higher values in headwaters tended to decrease in medium orders, they increased again in the lower Seine; CH_4 concentrations can be interpreted as an upstream- downstream increase with higher concentrations in summer than in winter. Concentrations of the three GHGs were clearly strongly impacted by wastewater effluents, with peaks in the lower Seine River downstream from the outlet of the main WWTP treating the Parisian conurbation (12.6 M inhabitants).

Drainage network emissions were calculated and compared with those of the agricultural basin (quantified on the same basis as in previous work by our research group (Garnier et al., 2009; Garnier et al., 2013), to which non-agricultural emissions (e. g. urban and transport) reported in national inventories (CITEPA) were added. Among the 61,300 Gg CO_2 equivalents (eq.) of emitted GHGs (CO_2, N_2O, CH_4), 3.7% originate from the drainage system, of which 95% is CO_2-related. Agricultural emissions represented 23 % of total GHGs emissions of the Seine River basin. Agricultural and urban emissions are thus largely dominant.

In the fifth and final chapter, we concentrated our effort on agricultural GHGs, but extended the scope of the study to the whole of France and three regions of interest:

- the Seine Basin, with its temperate climate and intensive cereal cropping agriculture,
- the Great West (including the Brittany region), with the oceanic-temperate climate and intensive livestock farming,
- the Great South West (including the Garonne and the Lot departments), with a temperate warm climate, particularly favorable for maize cultivation.

We found a total of 114,000 Gg CO_2 eq. yr^{-1} (for 2010-2014) of agricultural emissions for the whole of France distributed respectively as 29%, 49%, and 22% of N_2O, CH_4 and CO_2.

These emissions were reconstructed for the past (estimated at about half the present values in 1955, and a quarter in 1852) and finally, put in perspective view with two future scenarios: one scenario following the current trend of the agro-food system with specialization and intensification associated with international trade (bringing these emissions to 165,000 Gg CO_2 eq. yr^{-1} in 2040), and another one with a structural change in agro-food system oriented towards agro-ecology and organic farming, enabling the reduction of agricultural GHG emissions to a value close to that of 1955 (57,000 Gg CO_2 eq. yr^{-1} in 2040).

These two chapters provide quantitative figures on past, present and future emissions of N_2O, CH_4 and CO_2, placing emissions from the Seine basin in a national framework and highlighting possible levers for reducing GHG emissions.

Chapter n°4

Carbon dioxide, methane and nitrous oxide emissions from the human-impacted Seine watershed in France

Audrey Marescaux[1], Vincent Thieu[1], Josette Garnier[1]

[1]Sorbonne Université, CNRS, Institut Pierre Simon Laplace, UMR 7619 METIS, Paris, France

Article published in Science of the Total Environment 643 (2018) 247-259

Graphical abstract

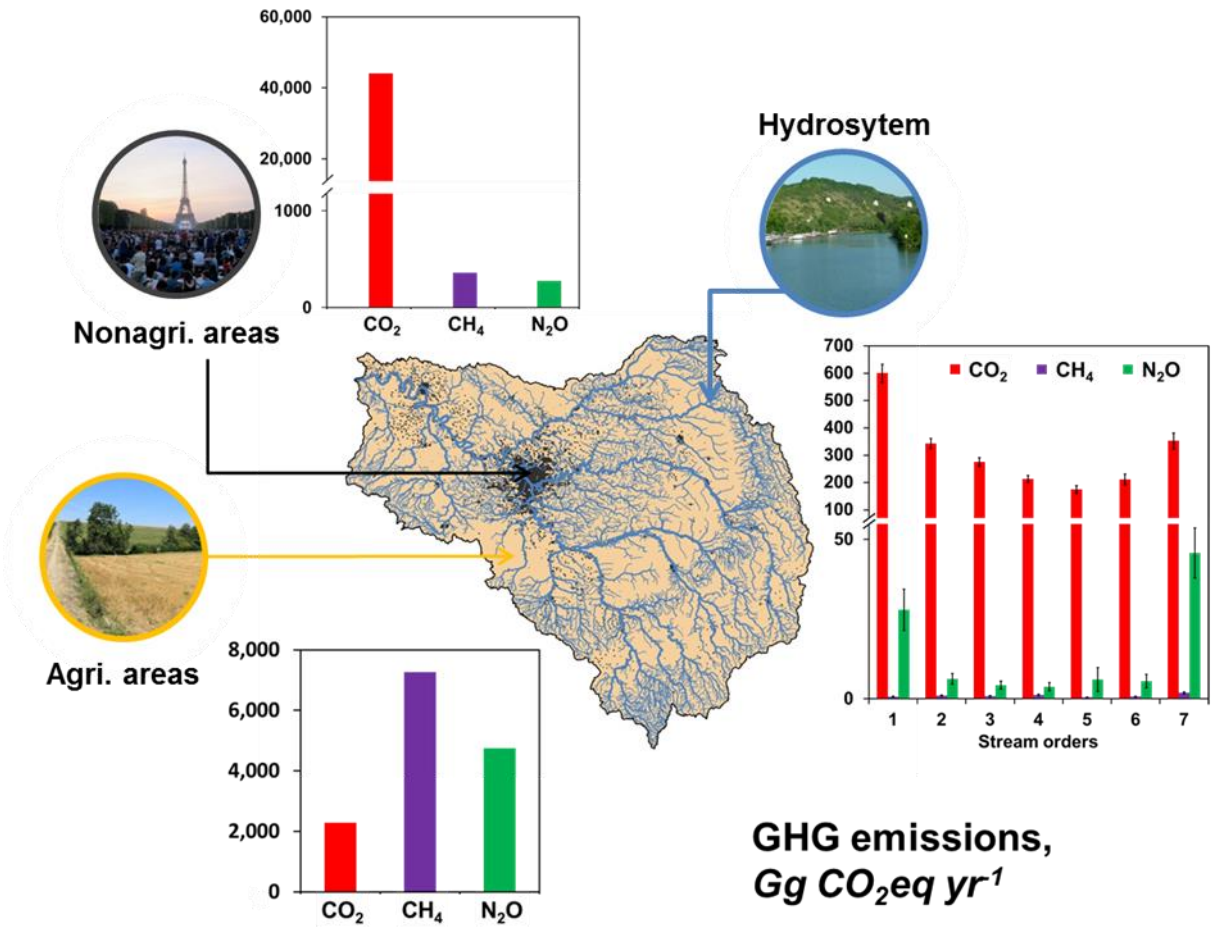

Abstract

Greenhouse gas (GHG) emissions from rivers and lakes have been shown to contribute significantly to global carbon and nitrogen cycling. In temperate and human-impacted regions, simultaneous carbon dioxide, methane and nitrous oxide emissions from aquatic systems are poorly documented. We estimated carbon dioxide (CO_2) concentrations in the Seine hydrosystem (71,730 km^2, France) using direct measurements in 14 field campaigns conducted between 2010 and 2017, and calculations of CO_2 partial pressures compared with methane (CH_4) and nitrous oxide (N_2O) concentrations.

In the main stem of the Seine River, CO_2 showed the same spatial gradient as N_2O and CH_4 with peaks in concentration downstream from the arrival of effluents from wastewater treatment plants enriched in organic matter, thus favoring mineralization. It is likely that high CO_2 concentrations upstream were due to organic carbon inputs from soils and enriched CO_2 groundwater discharges, whereas high N_2O and CH_4 upstream values were likely due to denitrification in riparian wet areas and anoxic decomposition of organic matter-rich wetlands, respectively. In addition, seasonal variations in all three GHGs were observed with higher concentrations in summer when higher temperatures promote mineralization and low water reduces the dilution of organic matter mainly originating from WWTP effluents.

GHG emissions were calculated and compared with agricultural and nonagricultural (urban, transport) fluxes in the basin. In the Seine River network, CO_2 emissions dominated riverine GHG emissions, reaching 95.3%, while N_2O and CH_4 emissions accounted for 4.4% and 0.3%, respectively. These indirect emissions from the hydrosystem were estimated to account for 3.7% of the total GHG emissions from the basin that amounted to 61,284 Gg CO_2eq yr^{-1}. Comparatively, direct agricultural and nonagricultural GHG emissions were estimated at 23.3% and 73.0%., respectively.

Keywords: Seine Basin; CO2; CH4; N2O; direct/indirect emissions; human impacts

4.1. Introduction

Carbon dioxide (CO_2), methane (CH_4) and nitrous oxide (N_2O) have been shown to dominate the well-mixed greenhouse gases (GHGs), contributing 80% of the positive radiative forcing driving climate change (Myhre et al., 2013). Between 1750, the beginning of the Western industrial revolution, and 2011, atmospheric concentrations of CO_2, CH_4 and N_2O increased by 40%, 150% and 20%, respectively, reaching values of 390.5 ppm (± 0.2 ppm), 1803.2 ppm (± 0.2 ppm) and 324.2 ppb (± 0.2 ppb) (Hartmann et al., 2013).

For the 1750–2011 period, anthropogenic CO_2 emissions at the global scale reached 555,000 ± 85 teragrams of carbon (TgC). Fossil fuel combustion and cement production were responsible for 67.5% of it while land use change accounted for 32.4% (Almajhdi et al., 2013). For the 2000–2009 period, anthropogenic CH_4 global emissions were estimated at 248 (228–276368) TgC-CH_4 yr^{-1} (bottom-up approach) (Almajhdi et al., 2013). The Intergovernmental Panel on Climate Change (IPCC) report (2013), attributed 60.4% of CH_4 sources to agriculture and waste, 10.6% to biomass and biofuel burning and 29% to fossil fuel combustion. N_2O atmospheric concentrations have also increased considerably since the preindustrial era, due to intensification of agriculture and the use of synthetic nitrogen (N) fertilizers and manure applications that increased the production of N_2O in soils, sediments and aquatic ecosystems. In addition to fertilization, industrial processes (e.g., manufacture of nylon), effluents from wastewater treatment, cattle feedlots and excrement, biomass burning and land emissions due to atmospheric nitrogen deposition (from agriculture, fossil fuel combustion, burning biomass and industrial activities) also contributed to an increase in N_2O emissions of 6.9 (2.7–11.1) TgN (N_2O) yr^{-1} over the last two decades (Seitzinger et al. 2000; Khalil et al. 2002; Ciais et al., 2013).

Global emissions of these three GHGs from streams and rivers have been reported in the literature as important fluxes in the continental GHG budgets. CO_2 emissions from rivers and streams have been quantified at between 230 (150-300) TgC yr^{-1} and 1,800 ± 250 TgC yr^{-1} or 840–6,600 Tg CO_2equivalent yr^{-1} (Tg CO_2eq), (Cole et al., 2007; Battin et al., 2009b; Aufdenkampe et al., 2011; Lauerwald et al., 2015; Regnier et al., 2013; Raymond et al., 2013a ; Sawakuchi et al., 2017; Drake et al., 2017). CH_4 global inland water emissions have been estimated at 1.5–26.8 Tg CH_4 yr^{-1} or 42.0–750.4 Tg CO_2eq (Bastviken et al., 2011; Sawakuchi et al. 2014; Borges et al. 2015; Stanley et al. 2016) while N_2O riverine emissions have been reported to range between 50.6 (46.5-55.5) Gg N_2O yr^{-1} and 1,980 Gg N_2O yr^{-1} or

13.4 Tg CO_2eq and 524.7 Tg CO_2eq (Kroeze et al., 2010; Beaulieu et al., 2011; Hu et al., 2016). In CO_2eq, global CO_2 emissions are about ten times higher than CH_4 and N_2O emissions. Many regional studies on inland waters have proposed a specific focus on CO_2 emissions (Butman and Raymond 2011; Denfeld et al. 2013; Abril et al. 2014; Ran et al., 2017, van Geldern et al., 2015, among others), CH_4 emissions (e.g., Bastviken et al. 2004; Garnier et al., 2013; Sawakuchi et al., 2014; Spawn et al. 2015; McGinnis et al. 2016) or N_2O emissions (e.g., Seitzinger et al. 2000; Garnier et al., 2009; Yu et al., 2013; Turner et al., 2015). However, only a few studies have assessed the three GHG concentrations together or emissions from lentic ecosystems (reservoirs and lakes) (e.g., Huttunen et al., 2003; Zhao et al., 2013; Miettinen et al., 2015; Huang et al. 2015; Wang et al. 2017) or from streams and rivers (e.g., Harrison et al., 2005; Hlaváčová et al., 2006; Borges et al., 2015; Teodoru et al., 2015; Schade et al., 2016; Borges et al., 2018).

Anthropogenic activities are known to have marked impacts on biogeochemical cycles and on CO_2, CH_4 and N_2O emissions (e.g., Kempe, 1982 and 1984; Seitzinger et al., 2000; Garnier et al., 2007; Rajkumar et al., 2008; Barros et al., 2011; Baulch et al., 2011; Regnier et al., 2013; Alshboul et al., 2016b; Deemer et al., 2016; Martinez-Cruz et al., 2017; Prairie et al., 2017). N_2O emissions from the highly urbanized Seine drainage network have been estimated at 0.10–0.20 gigagrams (Gg) N-N_2O yr^{-1} or 42–83 Gg CO_2eq yr^{-1} (Garnier et al. 2009), while CH_4 emissions have been estimated at 0.30 GgC-CH4 yr^{-1} or 11.2 Gg CO_2eq yr^{-1} (Garnier et al., 2013b). CO_2 emissions from the Seine basin have not yet been investigated, apart from occasional values of pCO_2 calculated in the Seine at Paris (annual mean for 1975–1979: 1997 ppmv; Kempe, 1982). Nevertheless, comparison of the three GHG budgets at the global scale (with a factor of 10 between CO_2 and N_2O or CH_4 emissions expressed in CO_2 eq), supports the hypothesis that CO_2 emissions could also account for a large proportion of the GHG emissions at the regional scale of a single watershed.

This paper compares GHG behaviors (CO_2, CH_4, N_2O) in the Seine River, a temperate hydrosystem subjected to strong anthropogenic pressures and quantifies the emissions from the drainage network. Earlier papers by our team already examined water concentrations and emissions of N_2O (Garnier et al., 2009) and CH_4 (Garnier et al., 2013). Here we report on new field investigations to examine pCO_2 and CO_2 emissions together with CH_4 and N_2O. Space-time analyses at the scale of the Seine River basin using this unique GHG data set were expected to provide new insights into GHG riverine emissions, particularly the impact of wastewater effluents from the Parisian conurbation (12 M inhabitants). The second aim of this

study was to compare the indirect emissions from the drainage network with estimated direct emissions from land under different uses (croplands, grasslands and forests, and livestock farming) and due to other activities (energy transformation, industry, residential and tertiary sectors, as well as transport) using existing data, in order to identify the main sources of emissions.

4.2. Material and methods

4.2.1. Study site

The Seine River is located in the north of France with a catchment of approximately 71,730 km^2 at Poses, where a weir separates the river from its estuary, and flows into the English Channel. Its average annual discharge over the past 10 years at the outlet is 500 m^3 s^{-1} (French water authorities *Agence de l'Eau Seine Normandie* - French acronym AESN, http://www.eau-seine-normandie.fr/, last accessed 2018/11/05). The Seine basin is densely populated (> 200 inhabitants (inhab.) km^{-2} for the basin as a whole but reaching more than 20,000 inhab. km^{-2} in inner Paris and around 5,000–7,000 inhab. km^{-2} in the Paris conurbation) (Fig. 4-1) (INSEE 2013). Heavily urbanized and industrialized in its downstream sector, the upstream basin is dominated by croplands.

The Seine River watershed can be represented by the Strahler stream order (SOs) (Strahler, 1952; 1957) a concept describing any hydrological network from its source (SO 1) to its estuary by a regular pattern of confluence of tributaries with increasing stream order. The Seine hydrological network is represented by more than 3,000 first SOs to one SO 7 (the lower Seine river) (Annex 4-1). The main stem studied here is the downstream Marne River (SO 6) and the lower Seine (SO 7). The Marne River basin is intensively cropped and densely populated in its downstream sector and used to be one of the most eutrophic rivers of the drainage network (Garnier et al., 2005) (Fig. 4-1). The Marne joins the Seine River at the entrance of Paris. Downstream from Paris, the Seine River receives the treated effluents of 12 million inhabitants, strongly impacting the lower Seine River, downstream from the confluence with the Oise River (SO 6). The main land use classes in the basin are croplands (56.8% of the basin), forests (25.8%) and grasslands (9.7%), urbanized areas represent 7.0% (CLC database, IFEN, 2006) and wetlands (between 10.9%-15.6%; Curie et al., 2007). The lithology of the sedimentary basin of the Seine River is dominated by chalk, limestone and carbonates (Annex 4-1).

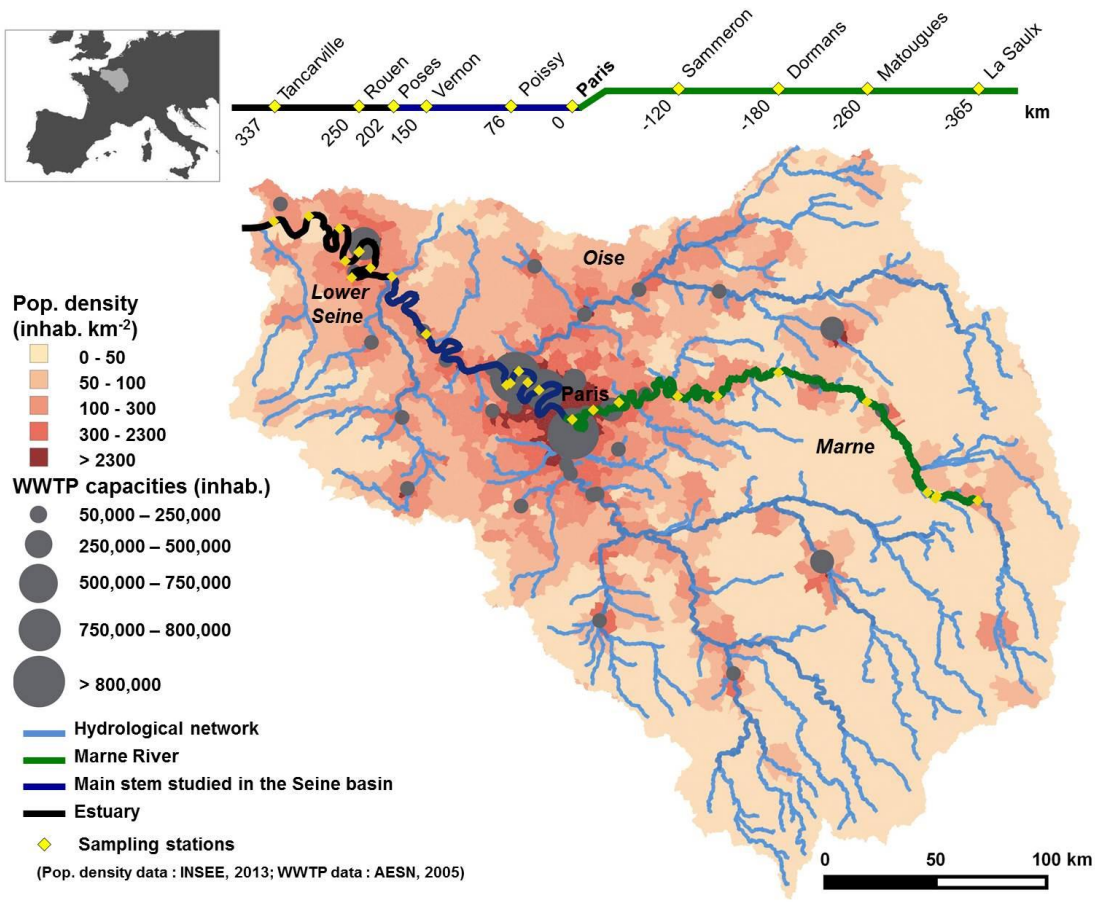

Fig. 4-1 Population density and main wastewater treatment plant capacities of the Seine River watershed (France) (INSEE, 2013 and the French water authorities - AESN 2005). In yellow, measurement stations located along the main stem of the Seine River (Marne River and the lower Seine) were sampled in 2010 (May 3–4; July 5–7; October 2–6 2010) in 2011 (May 17–19; August 23–28), in 2012 (April 4–10; August 28 to September 3), in 2013 (February 13–18; June 17–23 2013) and 2014 (May 13–17; September 9–12). One of the main stems of the Seine River is shown at the top of the figure with sampling stations and distance from Paris in kilometers (km=0).

4.2.2. Sampling strategies

Eleven field campaigns were conducted at 23 sampling locations over a distance of 700 km (exact locations in Annex 1-6). Sampling sites were selected to account for the spatial variability of the upstream basin along the Marne River, upstream and downstream from the main WWTPs, including Paris, and along the lower Seine. The 11 field campaigns at low water were conducted in 2010 (May 3–4 May; July 5–7; October 2–6 2010), in 2011 (May 17–19; August 23–28), in 2012 (April 4–10; August 28 to September 3), in 2013 (February 13–18; June 17–23 2013), and in 2014 (May 13–17; September 9–12). In addition to these

longitudinal profiles, smaller SOs were sampled during two snap-shot campaigns in 2016 (February 22 to March 10, and September 7–14) and one in 2017 (March 14–23). A total of 14 campaigns are therefore analyzed here. Sampling locations covered all important land use classes in the basin.

In the field, 100 ml borosilicate serum bottles were filled with water without air to determine N_2O and CH_4 levels. To stop biological processes and gas exchange, 50 µl of $HgCl_2$ (2%) was added to the bottles that were then sealed with a rubber septum. In addition, 2-l water chemistry sampling bottles (high-density polyethylene) were filled and pH (NBS scale), water temperature, turbidity, dissolved oxygen and conductivity variables were measured using a multiparameter instrument (YSI® 6600 V2). Buffers (pH 4 and 7) were used for pH calibration, potassium chloride electrolyte solution for dissolved oxygen, and 10 mS cm^{-1} standard for conductivity.

In the laboratory, total alkalinity (TA) (µmol kg^{-1}) was analyzed using three replicates of 20 ml of filtered water (GF/F: 0.7 µm) with an automatic titrator (TitroLine® 5000) and HCl 0.1M. Dissolved nitrate and ammonium were determined on filtered water (GF/F, 0.7 µm) with an automated analyzer (Gallery™ Automated Photometric Analyzer) according to Jones (1984) and Slawyk and MacIsaac (1972), respectively.

For dissolved organic carbon (DOC), analyses were collected in glass flasks after filtration on GF/F Whatman grilled filters (GF/F, 0.7 µm porosity, at 500°C for 4 h) and acidified (0.1 ml H_2SO_4 4 M in 30 ml of water). DOC was analyzed with a TOC analyzer (Aurora 1030 TOC Analyzer, O–I-Analytical).

4.2.3. Gas analyses

Dissolved carbon dioxide.

Partial pressure of CO_2 (pCO_2) (ppmv) was measured in small SOs (1–3) and along the main stem (SOs 6-7), using a syringe headspace technique coupled with a non-dispersive infrared (NDIR) gas analyzer (Licor LI-820 or LI-840, USA) (Abril et al., 2015). In four syringes, 30 ml of stream water and 30ml of air were equilibrated in CO_2 by shaking them continuously for 10 minutes. The first syringe was used to purge the system and measurements were made using the other three. Dry pCO_2 was converted into CO_2 water concentrations (µgC l^{-1}) (Weiss, 1974; Weiss and Price, 1980).

We completed our data set of field measurements with existing datasets of pH, total alkalinity and water temperature measurements from which we calculated pCO_2 values (ppmv) with CO2SYS software algorithms (Pierrot et al., 2006) using water temperature, alkalinity and pH measurements for the period 2007 –2017 (22,142 of these three variables, i.e., around 1,400 stations distributed throughout the Seine Basin at a monthly to bimonthly frequency) collected by the French water authorities – AESN). The carbonate dissociation constants (K1 and K2) applied were from (Millero, 1979) with zero salinity. CO_2 solubility was from Weiss (1974). The pCO_2 were corrected by the relationships established between direct and indirect pCO_2 measurements for the Seine River basin (Marescaux et al., 2018; see Annex 4-2) to reduce pCO_2 indirect calculation bias (see Abril et al., 2015).

Annual means of atmospheric wet pCO_2 values were provided by the NOAA/ESRL (http://www.esrl.noaa.gov/gmd/ccgg/trends/, Scripps Institution of Oceanography scrippsco2.ucsd.edu/, 2018/01/05) and averaged over the period 2007 –2017. Atmospheric wet pCO_2 values were converted into dry values according to Weiss and Price (1980) using a relationship between the air and water temperatures for the Seine basin (Ducharne, 2008). Atmospheric wet pCO_2 and pCO_2 was used to calculate CO_2 concentrations (µgC l^{-1}) at equilibrium in the water with CO_2 solubility (Weiss, 1974).

Dissolved nitrous oxide (N2O) and methane (CH4).

N_2O concentrations were determined with a gas chromatograph (Perichrom ST 200) combined[2] with an electron capture detector (GC-ECD) (Garnier et al. 2007 and 2009). CH_4 concentrations were also measured using a gas chromatograph coupled to a flame ionization detector (GC-FID) (Garnier et al., 2013). Only the three 2010 campaigns were already included in Garnier et al. (2013) for CH_4. For N_2O and CH_4 determination, we used the same sampling and laboratory procedures as in the studies cited just above.

4.2.4. Calculation of indirect and direct emissions

Calculation of indirect emissions from hydrosystems

The diffuse flux (*f*(GHG), mgC-CO_2, mgC-CH_4 or mgN-N_2O m^{-2} day^{-1}) of GHG at the interface of the river and the atmosphere can be calculated as:

$$f(GHG) = k_{GHG}\left([GHG] - [GHG]_{eq}\right) \qquad \text{Eq. 1}$$

where $[GHG]$ is the concentration of greenhouse gases in the water (mgC-CO_2 m^{-3}, mgC-CH_4 m^{-3}, mgN-N_2O m^{-3}), and $[GHG]_{eq}$ is the concentration of greenhouse gas at equilibrium with respect to atmospheric concentrations (mgC-CO_2 m^{-3}, mgC-CH_4 m^{-3}, mgN-N_2O m^{-3}).

According to Wanninkhof (1992), Wilke and Chang (1955) and Raymond et al. (2012a), the gas transfer velocity k_{GHG} (m day^{-1}) under negligible wind conditions in rivers can be calculated as:

$$k_{GHG} = k_{600} \cdot \sqrt{\frac{600}{Sc_{GHG}(T)}} \qquad \text{Eq. 2}$$

The k_{600} (Eq. 3) in Raymond et al. (2012a) was selected as being appropriate to compare GHG emissions at large spatial scales, and for analyses of bulk biogeochemical budgets (Raymond et al., 2012a).

$$k_{600} = v.S.2841 \pm a + 2.02 \pm b \qquad \text{Eq. 3}$$

where v is the water velocity (m s^{-1}) and S the slope (-); k_{600} is the gas transfer velocity for a Schmidt number of 600 (m day^{-1}). Coefficients a and b are standard deviations of 107 and 0.209, respectively. The French water authority database - AESN, enabled estimation of the water velocity from water discharge records in the basin for the period 2012–2014, and also provided measured slopes. Slopes and water velocity were then averaged by SO and by season.

Schmidt numbers ($Sc_{GHG}(T)$, dimensionless) of the calculated GHG (-) depend on water temperature T in degree Celsius (°C) as described in Wanninkhof (1992)

$$Sc_{CO_2}(T) = 1911.1 - 118.11T + 3.4527T^2 - 0.041320T^3 \quad \text{Eq. 4}$$

$$Sc_{CH_4}(T) = 1897.8 + 114.28T + 3.2902T^2 - 0.039061T^3 \quad \text{Eq. 5}$$

$$Sc_{N_2O}(T) = 2055.6 - 137.11T + 4.3173T^2 - 0.054350T^3 \quad \text{Eq. 6}$$

Each flux was calculated for each SO and day. The total emission of the hydrosystem (E) (mgC-CO_2 day^{-1}, mgC-CH_4 day^{-1} or mgN-N_2O day^{-1}) corresponds (see Eq.7) to the sum of GHG fluxes calculated for each SO (F_{SO}) multiplied by the number of rivers per SO (n_{SO}) and the average water surface of these SOs (A_{SO}, m^2). The number of rivers per SO (n_{SO}) and the water surface (A_{SO}) were extracted from the drainage network based on the topological records of the French water authorities - AESN.

$$E = \sum_{SO=1}^{8} \mathrm{F_{SO}\ n_{SO}\ A_{SO}} \quad \text{Eq. 7}$$

These values were averaged per period (summer –*April to October*- and winter –*November to March*-) and per SO (1–7). Finally, the annual estimate was assumed to have the combination of values calculated using average summer and winter characteristics (see Garnier et al., 2009 and 2013).

While humans have increased direct emissions through agricultural and industrial activities, emissions have also increased indirectly in aquatic and semi-aquatic (lake, river, riparian zone) and terrestrial (e.g., forest) ecosystems (Jurado et al., 2017).

Direct greenhouse gas emissions from agricultural and nonagricultural activities in the Seine basin

We used the estimations of N_2O and CH_4 emissions caused by agricultural activities in the Seine basin reported in previous studies (Garnier et al., 2009 and 2013).

N_2O agricultural emissions were calculated from a review of emission coefficients for the major land use classes (croplands, grasslands and forests). An ongoing study aiming at refining N_2O emissions by accounting for a relation between N_2O emissions and mineral nitrogen fertilizers applied under different classes of rainfall would approximately amount 9

GgN-N_2O yr^{-1} close to the 11.4 GgN-N_2O yr^{-1} previously reported in Garnier et al. (2009), established from a different approach, and used here.

The total amount of CH_4 emitted from agricultural sources, i.e., essentially by livestock (enteric fermentation and manure degradation) was calculated based on the number of animals per species and per age in the Seine Basin, and the specific emission factors for each species (kg-CH_4 $head^{-1}$ $year^{-1}$) (Garnier et al., 2013). Again, according to Garnier et al. (2013), we estimated CO_2 emissions from agricultural sources considering the use of 180 kgN ha^{-1} yr^{-1} nitrogen fertilizers on agricultural land and the emission of 0.52 tC-CO_2 per ton of N fertilizers produced. We also assumed that 100 l ha^{-1} yr^{-1} of fossil energy is required for farm work. Taking into account the cropped area, these emissions amounted to 622 Gg C-CO_2 yr^{-1} (Garnier et al., 2013). As a first approximation, we disregarded the effect of possible sequestration by soils and emissions linked to changes in land use.

We estimated nonagricultural GHG emissions based on data in Wu et al. (2016) and Staufer et al. (2016) for the Ile-de-France Region, while data at the scale of the French administrative Departments were used for the rest of the Seine basin, excluding Ile-de-France (available at https://www.citepa.org/fr/, 2018/01/05, from_CITEPA, French Interprofessional Technical Center for Studies on Air Pollution, last accessed 2018/11/05). CITEPA provides accurate census data on urban GHG emissions including energy transformation, manufacturing, the service sector and transport using the CORe Inventory AIR emissions methodology (CORINAIR, https://www.eea.europa.eu/publications/EMEPCORINAIR, last accessed 2018/11/05) from the European Environment Agency with a NUTS 3 resolution (French Departments). To analyze the nonagricultural emissions separately, we grouped the different sectors in three major classes:

(i) energy transformation + manufacturing,
(ii) residential + tertiary sectors,
(iii) transport

All nonagricultural GHG emissions were collected with spatially explicit references and processed using GIS technology (QGIS Development Team, 2016) to be scaled to the limits of the Seine River basin. Total GHG emissions were estimated by summing riverine, agricultural and nonagricultural GHG emissions.

4.2.5. Statistical analyses

The GHG concentrations and associated water temperatures were bootstrapped with 10,000 iterations, using the R package "boot.ci" (R Core team, 2015) in order to obtain mean, standard deviation and 95% confident intervals for each season and each SO. This procedure allows estimating the distribution of a sample from a limited dataset. For each bootstrap, the consistency between the generated mean value and that of the original dataset was checked. The uncertainty of the GHG flux (expressed as 95% confidence interval) was quantified with Monte Carlo simulations using equation (1) consisting of 10,000 runs (Beck, 1987). The required distributions of the input parameters were either provided by the bootstrapping (for GHG concentrations and water temperatures) or equation (3) for the gas exchange velocities assuming a Gaussian distribution of coefficient *a* and *b*. For these calculations, we also assume that each of these parameters varies independently from one another.

The variability of GHG concentrations and gas transfer velocity between orders and seasons was tested using Kruskal-Wallis and Wilcoxon signed-rank tests, respectively. Coefficients of determination (R^2) were used to check for correlations between GHG concentrations, nutrients and environmental parameters. Significant correlations are designated by an asterisk, taking into account the number of data.

4.3. Results

4.3.1. Greenhouse gas concentrations in the hydrological network

The annual mean CO_2 concentrations in the water were spatially significantly higher for the first and last SOs (> 2,000 µgC-CO_2 l^{-1}), similar to N_2O (> 1 µgN-N_2O l^{-1}). The annual mean CH_4, concentrations were only significantly higher in the 7th SO, especially in summer (> 3 µgC-CH_4 l^{-1}) (Fig. 4-2) (Annex 4-5). The mean annual concentrations in medium river SOs (3–5) were generally lower(< 2000 µgC l^{-1} for CO_2, < 1.5 µgC l^{-1} for CH_4, and ~ 0.6 µgN l^{-1} for N_2O). No significant differences in N_2O concentrations were found in any of the SOs in the two seasons selected (winter and summer). CO_2 concentrations were only significantly higher in summer than in winter in the 1st SO whereas summer CH_4 concentrations were higher in the majority of SOs (Fig. 4-2, Table Annex 4-4).

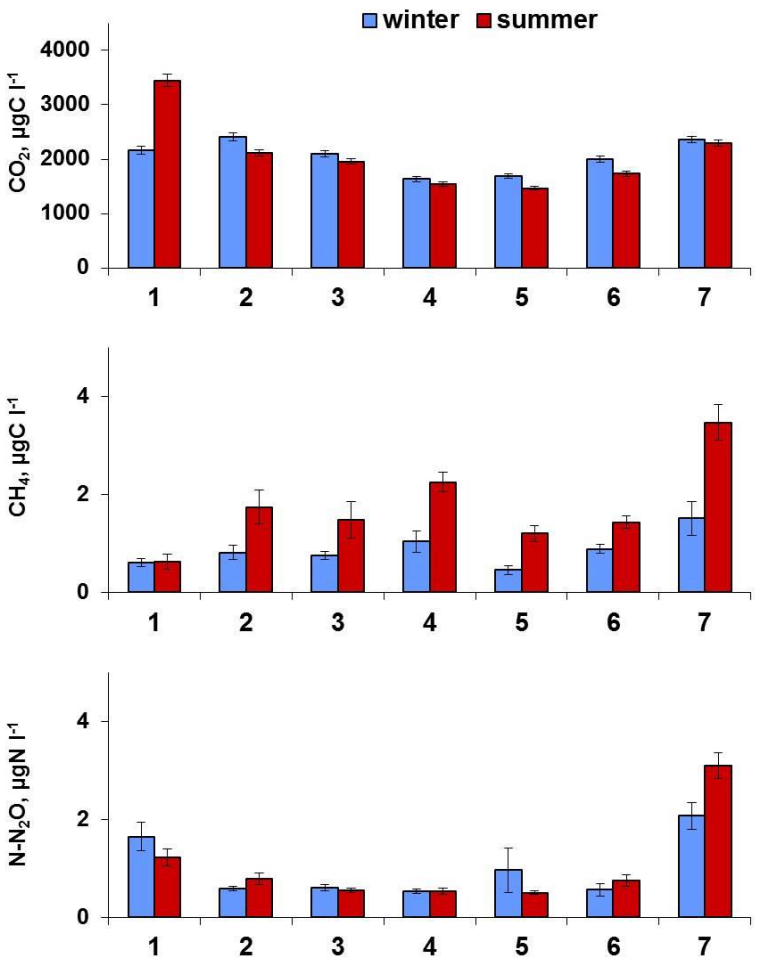

Fig. 4-2 Greenhouse gas (CO_2, CH_4, N_2O) concentrations in water (µgC-CO_2.l^{-1}, µgC-CH_4 l^{-1} and µgN-N_2O l^{-1}) as a function of the stream order in the Seine drainage network in winter and summer averaged from the 14 campaigns conducted between 2010 and 2017. Whiskers are standard deviations between observed GHG concentrations.

Atmospheric annual mean dry pCO_2 concentrations were around 398±0.12 ppmv on average for the 2010–2017 period (Division Physical Sciences and NOAA Earth System Research Laboratory), which gave an average concentration at equilibrium of 213 µgC l^{-1} with a range of 151–331 µgC l^{-1} for all the campaigns. Aquatic CO_2 concentrations in winter and in summer were always supersaturated with respect to atmospheric concentrations. Similarly, N_2O and CH_4 concentrations in the range of µg, were systematically above the saturation level of the water (mean N_2O saturation value: 275 ngN l^{-1} with a range of 115–490 ngN l^{-1}; mean CH_4 saturation value: 43 ngC l^{-1} with a range of 27–61 ngC l^{-1}).

Our data set enabled us to focus on the three GHG concentrations along the main streams of the Marne River (Fig. 4-3, from −365 to 0 km, SO 6) and the lower Seine River (Fig. 4-3, km

from 0 to ± 350 km, SO 7) where the concentrations were the highest (Fig. 4-3; see also Fig. 2).

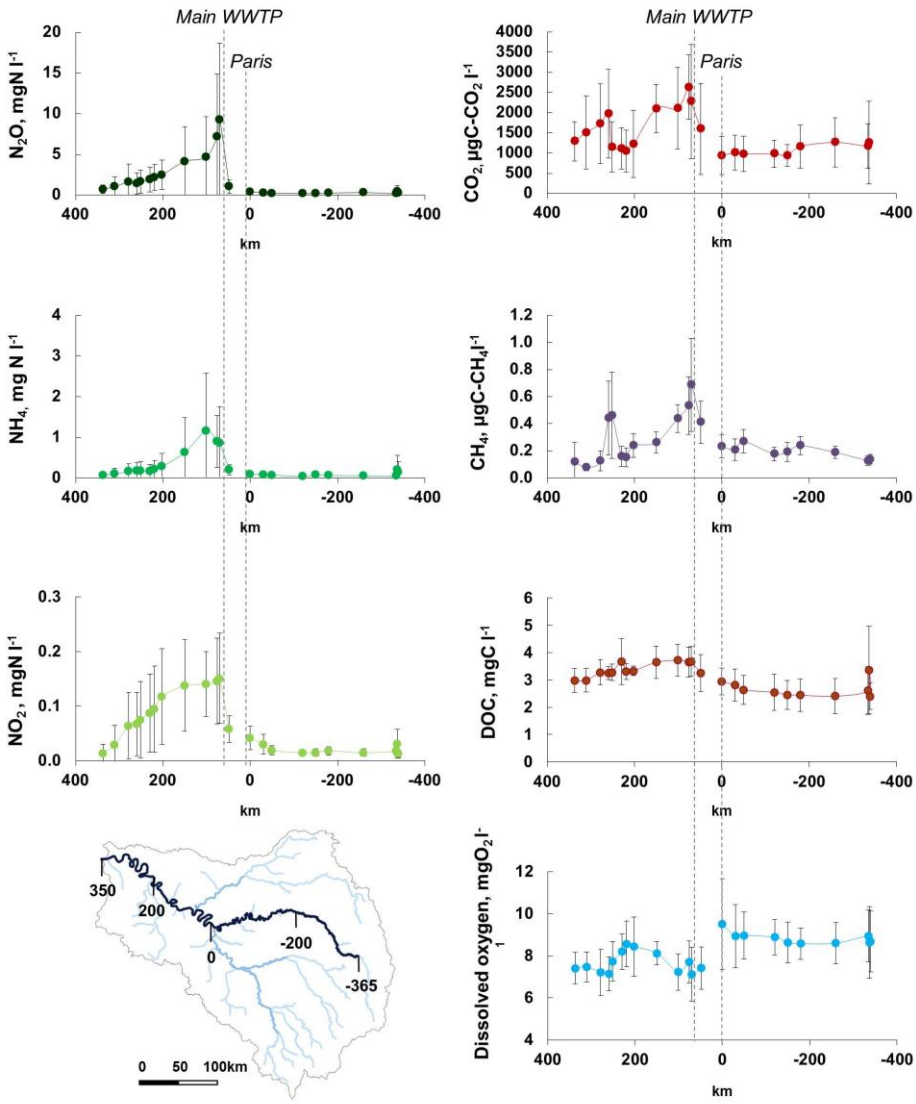

Fig. 4-3 Greenhouse gas (CO_2, CH_4 and N_2O) and oxygen concentrations along the main stem of the Marne River (km −400 to 0) and the lower Seine River (km 40–400). Averaged concentrations for (left) nitrous oxide (N_2O), ammonium (NH_4^+) and nitrite (NO_2^-) in mgN l^{-1}; (right) carbon dioxide (CO_2) and methane (CH_4) in µgC l^{-1}, dissolved organic carbon (DOC) in mgC l^{-1}, and dissolved oxygen in mgO_2 l^{-1}. The pCO_2 values were calculated from pH, temperature and alkalinity using CO2SYS software (Pierrot et al., 2006). These data are partly described in Garnier et al. (2009 and 2013).

The 11 longitudinal profile campaigns (from April to October i.e., in the summer period) were averaged for each GHG concentration for 2010–2014, and for each station (10 on the Marne branch and 13 on the lower Seine, Fig. 4-3). Despite wide variability, the longitudinal profiles of three GHG gases (CO_2, CH_4, N_2O) shared similar spatial trends of their concentrations (Fig. 4-3). Indeed, the concentrations were highest downstream from the effluent outlets in the Paris conurbation and from the city of Rouen. These patterns mirrored NO_2^-, NH_4^+ and DOC concentrations that are typically high in wastewater effluents. As nitrification and organic matter degradation consume oxygen, the opposite trend was observed for oxygen concentrations (Fig. 4-3).

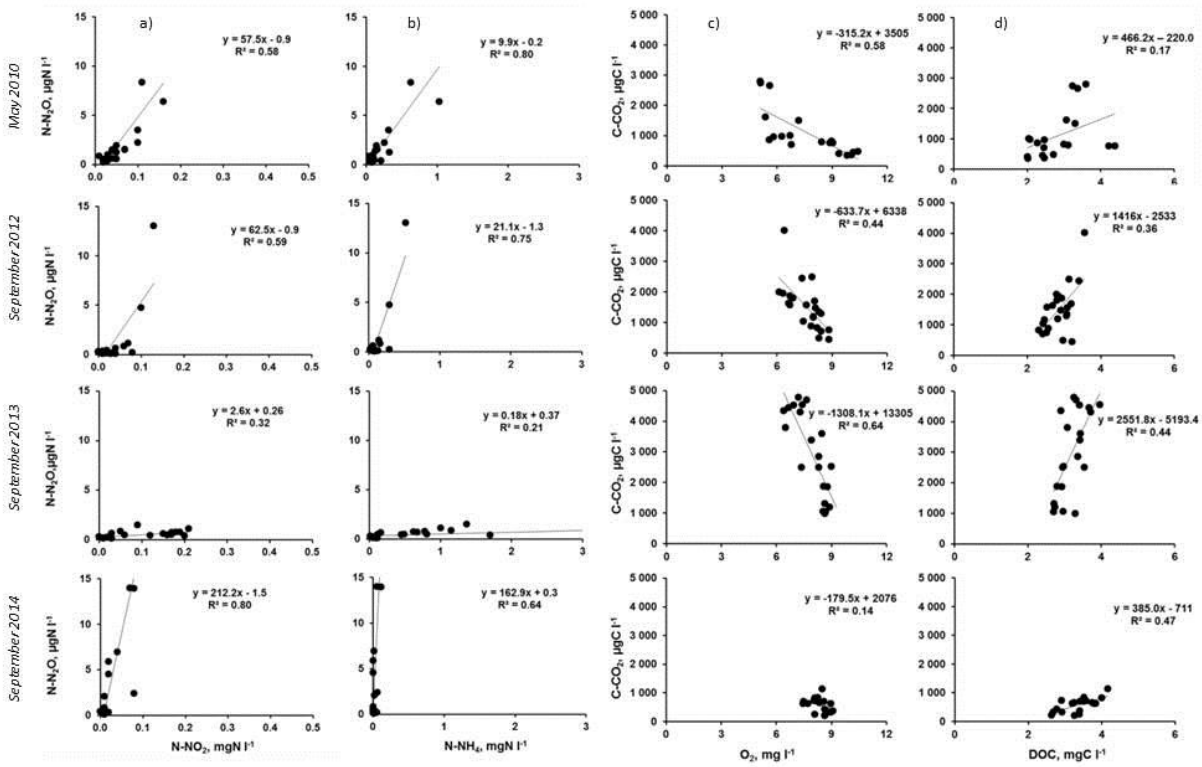

Fig. 4-4 Relationships between (a) concentrations of N_2O (µgN l^{-1}) and NO_2^- (mgN l^{-1}), (b) concentrations of N_2O (µgN l^{-1}) and NH_4^+ (mgN l^{-1}), (c) CO_2 (µgC l^{-1}) and oxygen (mgO_2 l^{-1}), and (d) CO_2 (µgC l^{-1}) and dissolved organic carbon (DOC: mgC l^{-1}). From top to bottom, example from the campaigns in May 2010, September 2012, September 2013 and September 2014.

Of these 11 campaigns, eight showed a positive significant relationship ($R^2 > 0.55$; $n = 23$) between N_2O and NO_2^- concentrations, and in six, N_2O was also correlated with NH_4^+ ($R^2 > 0.40$; $n = 23$) (Fig. 4-4, Table 4-1).

No relationship was found between N_2O and NO_3^-. CO_2 was positively and significantly correlated with DOC (six out of 11 campaigns, $R^2 > 0.27$; $n = 23$) and negatively correlated with oxygen (five out of 11 campaigns, $R^2 > 0.35$), but no correlation was found between CH_4 concentrations and other variables of interest (e.g., O_2, dissolved organic carbon). The slopes of the relationships varied greatly (by a factor of 100), depending on the discharge and the temperature during the campaigns (Fig. 4-4; Table 4-1).

Table 4-1 Parameters of the linear relationships (slope and R^2) of N_2O as a function of nitrite (NO_2^-) and ammonium (NH_4^+), and of CO_2 as a function of oxygen (O_2) and dissolved organic carbon (DOC) for each of the 11 campaigns. Corresponding values of mean discharges and temperatures (temp) for the duration of the campaign are indicated. *Slope significantly different from 0 for $R^2 > 0.16$ ($n > 20$).

Dates	Discharge	temp	N_2O vs. NO_2	R^2	N_2O vs. NH_4	R^2	CO_2 vs. O_2	R^2	CO_2 vs. DOC	R^2
	$m^3 s^{-1}$	°C	µgN l^{-1} mgN l^{-1}		µgN l^{-1} mgN l^{-1}		µgC l^{-1} mgC l^{-1}		µgC l^{-1} mgC l^{-1}	
3-5 May 2010	282.3	14.8	57.5	0.58*	9.9	0.80*	-315.2	0.58*	466.2	0.17*
5-7 July 2010	161.0	16.1	39.8	0.78*	12.7	0.61*	-30.2	0.01	183.9	0.06
2, 4-7 October 2010	347.3	16.1	85.3	0.73*	21.7	0.81*	-290.4	0.14	398.0	0.36*
17-19 May 2011	184.3	18.4	1.4	0.29*	0.1	0.17*	-143.6	0.36*	307.0	0.27*
23-25, 27-28 August 2011	229.7	22.0	15.5	0.57*	2.5	0.17*	-34.8	0.12	57.2	0.12
4-10 April 2012	289.0	12.8	33.5	0.77*	7.9	0.42*	-60.7	NA	177.4	0.01
29 Sept-3 August 2012	169.3	21.0	62.5	0.59*	21.1	0.75*	-633.7	0.44*	1416.0	0.36*
17-20, 22-23 June 2013	659.7	18.8	18.1	0.67*	3.7	0.25*	-306.7	0.23*	275.2	0.21*
16, 18-19, 21-22 Sept. 2013	353.6	16.9	2.6	0.32*	0.2	0.21*	-1308.1	0.64*	2551.8	0.44*
13-17 May 2014	327.6	15.3	8.1	0.28*	0.7	0.12	-554.5	0.37*	526.6	0.65*
9-11 Sept 2014	252.0	19.6	212.2	0.80*	162.9	0.64*	-179.5	0.14	385.0	0.47*

4.3.2. Greenhouse gas emissions from the hydrological network

The difference in GHG concentrations between the atmosphere and the surfaces of the water, and gas transfer velocities, control emissions of GHGs. Gas transfer velocity depended on k_{600} (Eq. 3) and on the Schmidt number (Eq. 4-6). k_{600} decreased with SOs due to the decreasing slope, and increased with water velocity as a result of turbulence. Schmidt numbers depend on temperature sensitivities of the specific solubility of the different gases, resulting in different k patterns (Annex 4-3).

Greenhouse gas emission fluxes showed that the Seine hydrological network is a source of three gases (CO_2, CH_4 and N_2O) to the atmosphere. In particular, budgets showed that CO_2 summer emissions (1,440 10^3 kgC-CO_2 day^{-1}) were lower than winter emissions (1,800 10^3 kgC-CO_2 day^{-1}) (annual amount 592 GgC-CO_2 yr^{-1} on average, Fig. 4-7). Seasonal CH_4 emissions were 554 kgC-CH_4 day^{-1} and 433 kgC-CH_4 day^{-1} in summer and winter, respectively (i.e., an average annual diffusive emission of 0.180 GgC-CH_4 yr^{-1}). N_2O emissions amounted to 708 kgN-N_2O day^{-1} in summer and 601 kgN-N_2O day^{-1} in winter (i.e., an annual average of 0.240 GgN-N_2O yr^{-1}) (Fig. 4-7). In addition, the annual budget shows that 44% of the CO_2 emissions were emitted from the first and second SOs of the Seine basin, while the 6th and 7th SOs contributed the most nitrous oxide, more than 50% of the emissions. CH_4 emissions were more evenly distributed among upstream (SOs 1, 2), intermediate (SOs 3, 4, 5) and downstream reaches (SOs 6, 7).

Considering global warming potential (GWP) for the last 100 years, i.e. 28 for CH_4 and 265 for N_2O, the hydrosystem's annual N_2O budget (99 Gg CO_2eq yr^{-1}) was 14 times higher than CH_4 diffusive emissions (7 Gg CO_2eq yr^{-1}), an N_2O budget that itself was around 22 times lower than the CO_2 budget (2,170 Gg CO_2eq yr^{-1}) (Fig. 4-7, Table 4-2).

Table 4-2 Comparative greenhouse gas (Gg CO_2 eq yr^{-1} of CO_2, CH_4 and N_2O) emissions from the hydrographic network (measurements made in this study), from the agricultural basin (including croplands, grasslands and forests according to Garnier et al. (2009 and 2013) and from nonagricultural sectors (data from CITEPA 2005 and from Wu et al. (2016) for the Ile-de-France region).∑ GHG: sum of the three GHGs by compartment and by gas.

	Hydrosystem	Agri. areas	Nonagri.	∑ GHG
	Gg CO_2eq yr^{-1}			**Gg CO_2eq yr^{-1}**
CO_2	2,170	2,281	44,077	48,528
CH_4	7	7,267	360	7,634
N_2O	99	4,747	276	5,122
∑ GHG	2,276	14,295	44,713	61,284

Interestingly, CO_2 emissions accounted for 95.3% of the three GHG emissions from the hydrosystem (indirect emissions), while N_2O and CH_4 emissions accounted for 4.4% and 0.3%, respectively.

4.3.3. Emissions from agricultural and nonagricultural sectors

Total GHG emissions from the agricultural basin were estimated at 14,295 Gg CO_2eq yr^{-1}. CH_4, N_2O and CO_2 emissions contributed 51%, 33% and 16% of agricultural emissions, respectively (Table 4-2).

Total direct GHG emissions from the nonagricultural basin were estimated at 44,713 Gg CO_2eq yr^{-1}, the majority from the Ile-de-France region (92%). Nonagricultural emissions of CO_2 were more than 100 times higher than those of CH_4 and N_2O (Table 4-2). Whereas CO_2 emissions were rather well distributed among the categories, CH_4 and N_2O emissions occurred mainly in the energy & manufacturing sector. These emissions were approximately three times higher than the sum of those from the residential & tertiary and transport sectors (Fig. 4-5).

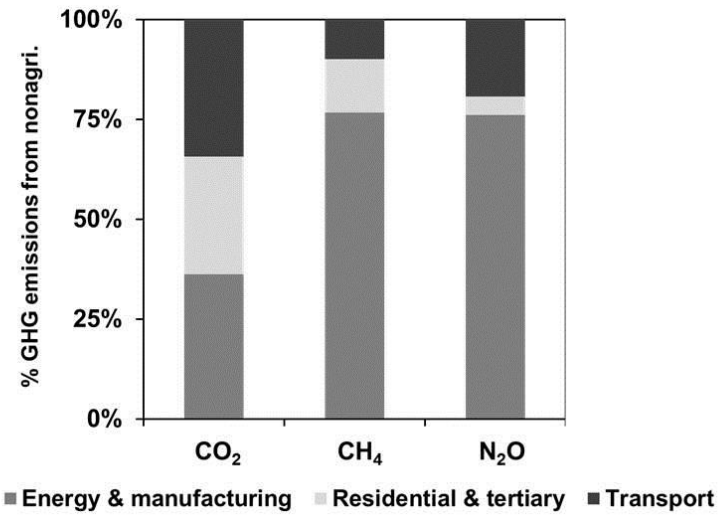

Fig. 4-5 Greenhouse gas emissions (CO_2, CH_4 and N_2O) from nonagricultural sectors (Gg CO_2eq yr^{-1}) in the Seine watershed including energy transformation-manufacturing, service sector, and transport (GIS treatments applied to CITEPA data; https://www.citepa.org/fr/, 2018/01/05)

4.3.4. Total GHG emissions from the Seine basin

Total GHG emissions from the basin were estimated at 61,284 Gg CO_2eq yr^{-1}. When both direct emissions (including agricultural and nonagricultural activities) and indirect emissions (from the hydrosystem) were summed, the value was much higher for CO_2 (48,528 Gg CO_2eq yr^{-1}), while CH_4 and N_2O were estimated at 7,634 Gg CO2eq yr^{-1} and 5,122 Gg CO_2eq yr^{-1}, respectively (Fig. 4-6). While agricultural activities were responsible for a quarter of the total GHG emissions in the Seine basin (14,295 vs. 61,284 Gg CO_2eq yr^{-1}, Table 4-2), the

hydrosystem only accounted for a small proportion of the total emissions of each of the three gases 4.5% for CO_2, 0.1% for CH_4, and 1.9% for N_2O (Fig. 4-6, Table 4-2).

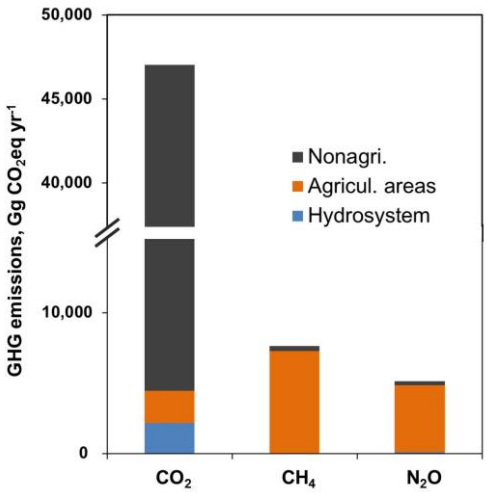

Fig. 4-6 Greenhouse gas emissions (CO_2, CH_4 and N_2O in Gg CO_2eq yr^{-1}) from the Seine hydrographic network and those from the watershed, divided into agricultural and nonagricultural (GIS treatments applied to CITEPA data; *https://www.citepa.org/fr/*, last accessed 2018/11/05); Data for Ile-de-France are from Wu et al. (2016) and Staufer et al. (2016).

4.4. Discussion

4.4.1. Limits to our calculations of the emission

To calculate gas emissions from the drainage network, *k* was computed according to Raymond et al. (2012), which validated the equation on small streams. The equation selected for *k* is linearly dependent on the slope and the water velocity averaged per SO and per season. Although the Seine catchment is relatively flat as the Seine source is located around 500 m asl. (French water authorities – AESN), the importance of the slope in *k* can lead to under- or overestimation of GHG fluxes. Similarly, exceptional flood events resulting in high turbulence (and water velocity) were not taken into account in this study, which could bias our estimations. However, comparing our results with those previously published for N_2O and CH_4 using a different equation (Garnier et al., 2009 and 2013), did not change the numbers much. We thus consider that our results provide robust estimates, although there is a need for *k* measurements in the Seine hydrosystem, which could increase the accuracy of GHG emissions. Although uncertainties persist in the estimates of GHG direct emissions in the Ile-

de-France region and the rest of the basin, we believe that the order of magnitude is also correct.

4.4.2. Patterns of indirect CO_2, CH_4, N_2O emissions from rivers in the drainage network: differences and similarities

Surprisingly, 95.3% of the indirect GHG emissions of the Seine drainage network were mainly linked to CO_2, compared to CH_4 (0.3%) and N_2O (4.4%) emissions. Considering the higher stream orders (SOs) of the Seine River as productive systems (Garnier et al., 2005, 2007) and despite the recent decrease in algal bloom (Aissa-Grouz et al., 2016), we had expected uptakes of CO_2 in the river network. Studying pCO_2 at the scale of the whole Seine drainage network revealed oversaturation in CO_2 at all locations and in both seasons, which we interpreted as being caused by soil leaching as well as inputs from aquifers where concentrations were up to ten times higher than those in the surface water (20,000–60,000 ppm in the Brie aquifer, data not shown), and releases of effluents from WWTPs.

Oversaturation of the GHGs with respect to atmospheric concentrations was not only observed in the Seine River (see also Garnier et al., 2009 and 2013), but also in the other temperate river, the Meuse (Borges et al., 2018), where groundwater has also been reported to be a source of CO_2 oversaturation. Contributions from groundwaters, quickly degassed at the head of the basin, were experimentally demonstrated by Garnier et al. (2009) for N_2O. Further, the higher GHG emissions in small SOs can be linked not only with higher concentrations but also with higher gas exchange rates (k and k_{600}) (see Eq. 2, 3), k being linked with the slope of the basin, on average higher for lower SOs.

In headwaters, allochthonous organic matter inputs and nitrate fertilizer leaching are also possible sources of GHG emissions from mineralization of organic carbon in the soil and groundwaters, along with denitrification in riparian zones (see Fig. 4-8; and Richey et al., 2002; Venkiteswaran et al., 2014). Denitrification in soils or sediments (i.e., nitrate reduction) is known to produce more N_2O in anoxic or suboxic conditions (Garnier et al., 2010; Vilain et al., 2014; Benoit et al., 2015) than nitrification. Regarding CH_4, anoxic organic-enriched locations of the river banks or in-stream sediment may enhance methanogenesis. While high CO_2 and CH_4 concentrations have been reported to be related to the extent and connectivity with wetlands in a tropical river system (Borges et al., 2015a; Teodoru et al., 2015), the (intensively cropped) Seine River basin only contains a small proportion of wetlands. We

identified CO_2 emissions from headwaters (1st and 2nd SOs) dominating the GHG source of the hydrosystem at 44%, like Marx et al. (2017), who estimated that 36% of CO_2 global riverine emissions originate from headwaters. In comparison to CO_2 emissions for the Seine basin, N_2O emissions from headwaters represented 34% and CH_4 emissions only 25% of their respective total emissions (see Fig. 4-7). However in three US headwater streams draining land under mixed uses, Schade et al. (2016) found lower CO_2 emissions in these mainly sandy streambeds, than in the carbonated streambeds in the Seine River, but potentially high CH_4 and N_2O emissions, probably due to organic-enriched streams where these authors reported a close relationship between total GHG emissions and concentrations of dissolved organic carbon (DOC).

In medium sectors of the Seine River, the decreasing contribution of groundwater as well as a decreasing ratio of terrestrial and riparian surface areas compared to the water volume could explain the lower emissions (Fig. 4-8).

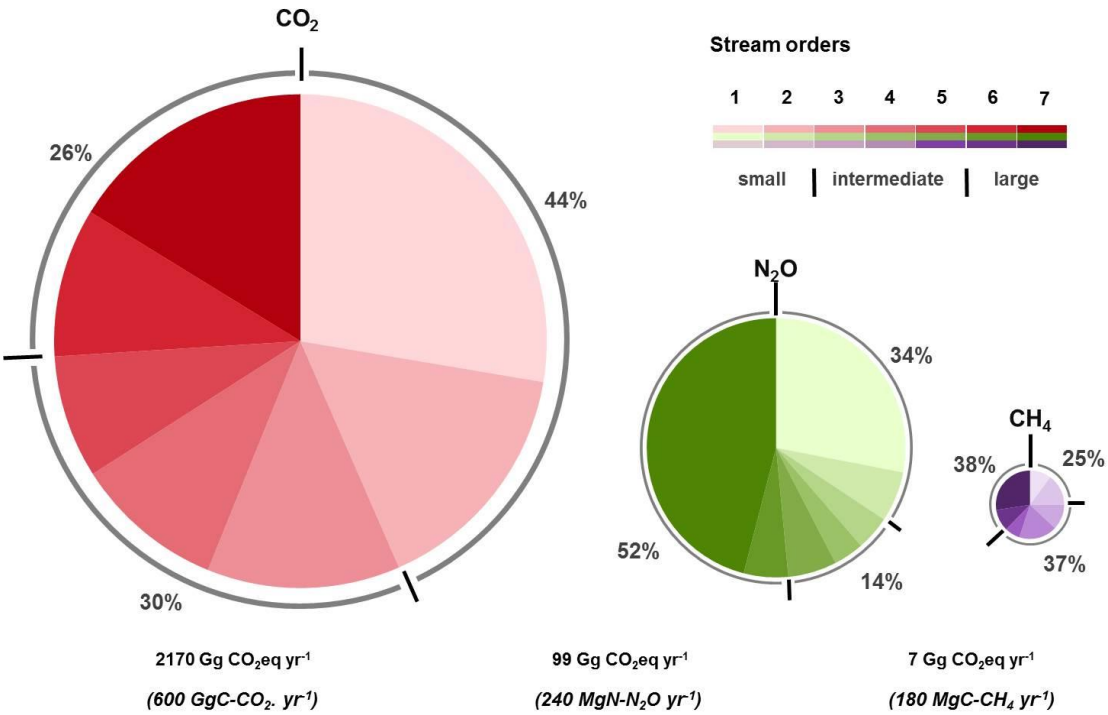

Fig. 4-7 Greenhouse gas (CO_2, CH_4 and N_2O) emissions from the Seine hydrographic network (yearly average of 14 campaigns (2010–2017). The pie charts represent the proportion of GHG emissions expressed in GWP. Percentage contributions are given for small (1st to 2nd SO), intermediate (3rd to 5th SO) and large (6th to 7th SO) rivers in the Seine watershed.

Higher emissions of the three GHGs in the higher SOs (6–7) can be interpreted as a response to WWTP effluents discharged downstream from the Paris conurbation (Fig. 4-8). As the water column was not fully anoxic even in the sector of effluent outlet, CH_4 may be linked to methanogenesis in the sediment that is rich in settled organic matter, while CO_2 is expected to result from organic matter respiration in both the water column and sediment (Battin et al. 2009; Vilmin et al. 2015; Garnier et al., 2009 and 2013). For N_2O emissions, in addition to denitrification in suboxic zones (at the scale of the bottom sediment-water interface, but also at the particle level (Garnier et al., 2007, 2009; Jia et al., 2016; Xia et al., 2017), nitrification of the ammonium massively supplied by effluents was also a source of N_2O emissions (Garnier et al., 2007, 2009; Burgos et al., 2017). With lower gaseous exchange rates calculated in these higher SOs, the emissions of the three GHGs accounted for 26%, 52% and 38% of the total drainage network flux for CO_2, CH_4 and N_2O, respectively in the 6th and 7th SOs (see Fig. 4-7).

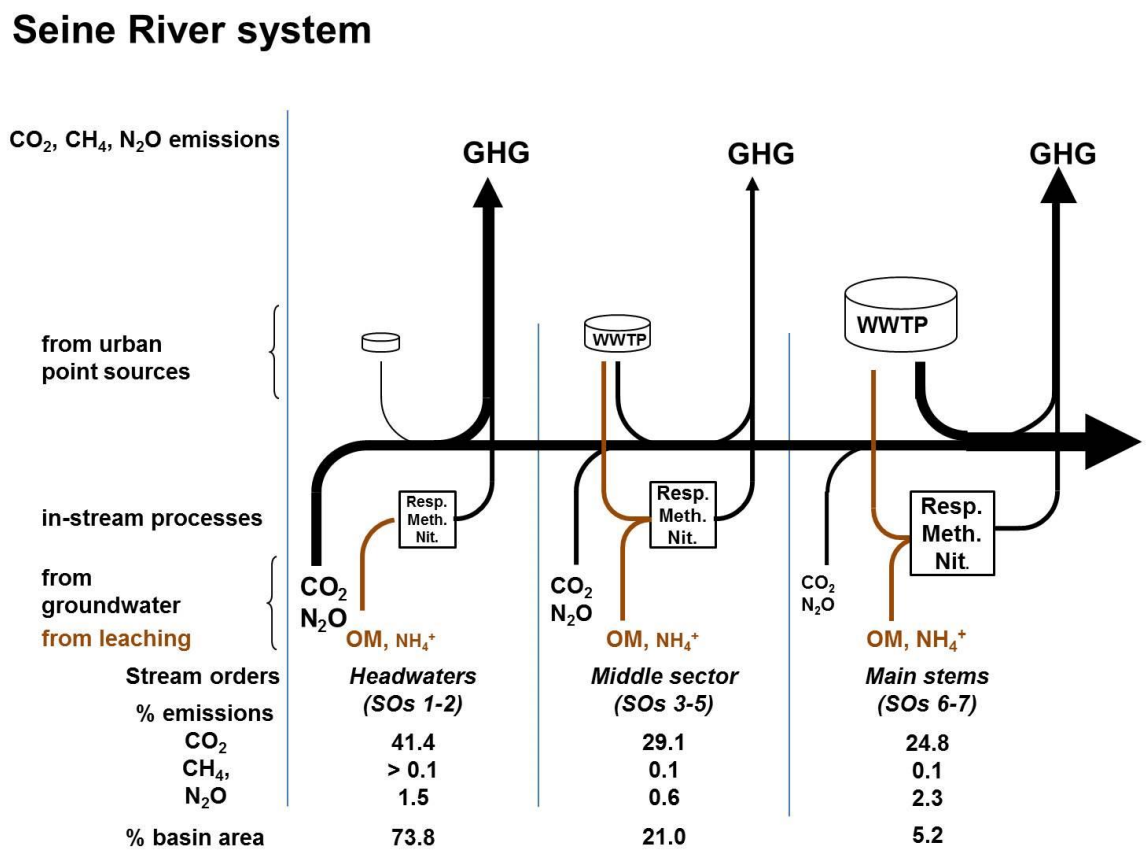

Fig. 4-8 Schematic representation of the sources of CO_2, CH_4 and N_2O emissions from the Seine hydrosystem. OM: organic matter; NH_4^+: ammonium

Physiological processes enhanced by higher temperature did not systematically lead to higher GHG emissions in the summer, pointing to complex interactions between in-stream microbial processes (mineralization) and the contribution of groundwater (diffuse sources) and discharge of effluents (point sources). Upstream-downstream patterns of the three GHG concentrations, which were further detailed in 11 longitudinal profiles along the main stem of the Marne River and the lower Seine stem, showed "background" concentrations along the main stem of the Marne compared to the peaks observed downstream. The impact of the Parisian WWTPs was quite clear immediately downstream from their outlets and decreased within the 30 km downstream, partly due to dilution by the Oise River and in-stream processes. Farther downstream, GHG concentrations again increased, reflecting the major impact of the treated effluent from the Rouen conurbation. Although the number of inhabitant equivalents treated is 12 times higher in the Paris WWTPs than in Rouen's, the carbon load was only six times higher (i.e., a lower carbon abatement in the Rouen WWTP, with its smaller capacity), explaining the high impact. Such an impact of point source pollution, i.e., a discharge of labile organic matter into rivers, has already been reported to increase pCO_2 (Kempe, 1984). The significant relationships between (i) N_2O, NH_4^+ and NO_2^- and (ii) CO_2, oxygen and DOC we found in our study corroborated the importance of in-stream processes that are mainly supported by anthropogenic inputs via urban effluents (i.e., mineralization of organic matter, denitrification, nitrification and lower oxygen concentration in the lower Seine River). In African rivers, Borges et al. (2015b) reported similar net heterotrophic dynamics for these aquatic ecosystems based on the relationships between pCO_2, CH_4 and dissolved oxygen (O_2), despite lower domestic wastewater inputs in tropical systems, but with forested riparian zones and wetlands that also enriched the river in organic matter.

It is worth mentioning that only diffusive emissions of CH4 were taken into account, although 40% ebullition of indirect emissions could be added (Garnier et al., 2013). However taking the high contribution of CO_2 emissions in the drainage network into account would not affect the overall results.

4.4.3. Direct CO_2, CH_4, N_2O emissions from the Seine basin: agricultural and nonagricultural emissions

Indirect GHG emissions from the hydrographic network accounted for 3.7% of the total emissions, 23.3% being linked to agricultural activities and land use, 73.0% to nonagricultural uses (dominated by the urban sources in the Ile-de-France region).

Such a high proportion of nonagricultural GHG (heating, transport, energy and industry) from a very highly populated area (Ile-de-France with 12 M inhab. vs. 16 M inhab. for the entire Seine basin) is not surprising, and is in line with results reported for other large cities (Pataki et al., 2006). Although human respiration, which accounts for 10% of the total (1 kg CO_2 $inhab^{-1}$ yr^{-1}, Prairie and Duarte, 2007), was included in the estimates as the measurements came from tower fluxes and atmospheric inversion (Breón et al., 2015; Wu et al., 2016), we did not subtract this flux. Urban agriculture and many other small sectors (Wu et al., 2016), reported to account for 2.7%, were not taken into account either. On the whole, according to Bréon et al. (2015), we can consider that in megacities such as Paris and it conurbation, net CO_2 fluxes are dominated by fossil fuel emissions. These Ile-de-France fuel emissions are hypothesized to account for 12% of those from France as a whole (Boden et al., 2013).

Among the 23.3% of agricultural emissions, the highest proportion (51%) was related to CH_4 although since the late 1970s, livestock has been confined to the periphery of the Seine basin (Mignolet et al., 2007). N_2O emissions accounted for 33% and CO_2 for 16% of agricultural emissions. Whereas intensive cereal cropping contributed to N_2O direct emissions though fertilization (Bouwman, 1996; Cayuela et al., 2017), it also contributes to CO_2 emissions linked to the manufacture of fertilizers and direct fuel consumption for the cultivation of the 35,000 km^2 basin (Garnier et al., 2013).

Finally, for a highly human-populated basin such as the Seine, the riverine emissions accounted for only a small fraction (3.7%) of total emissions. However, cities have mitigation options, such as green technologies, and changes in lifestyle (drastic reduction in fossil energy consumption for individual vehicles, better insulation of buildings, etc.) as well as structural changes in agricultural production (e.g., more organic agriculture without mineral fertilizers, carbon storage) that may alter the proportions of emissions currently estimated to be dominated by CO_2 emissions.

4.5. Conclusion

In this study, we estimated emissions of greenhouse gases from the Seine hydrosystem characterized by a high population rate and intensive agriculture. At the regional scale of the Seine basin, CO_2 emissions (in CO_2 eq.) accounted for 6.4 and 9.5 times the amount of CH_4 and N_2O emissions, respectively, in good agreement with the ~10 times found at the global scale.

We showed that the hydrological drainage network of the Seine River was oversaturated in GHGs (CO_2, CH_4, and N_2O) with respect to their atmospheric concentrations. GHG emissions from the Seine hydrosystem accounted for only 3.7% of the total GHGs emitted from the basin as a whole. GHG emissions from the hydrosystem were also dominated by CO_2 emissions (95.3% of the 3.7%) and were interpreted as controlled by soil leaching and groundwater discharges in small SOs and by wastewater effluents along the main stem of the Seine River. Of the 73% of the GHG emissions originating from the nonagricultural sector, CO_2 emissions contributed 98%, and most came from the Ile-de-France region. For the agricultural sector, the 23.3% of GHG emissions mainly comprised CH_4 and N_2O – 51% and 33%, respectively – while CO_2 emissions accounted for only 16%.

In the future, modeling different scenarios for climate change or changes in anthropic pressure in the Seine basin (including agricultural practices and energy consumption) could enable us to propose actions to minimize the emissions of these greenhouse gases.

4.6. Annex

4.6.1. Annex 4-1. Lithology (Albinet, 1967) and stream orders (Strahler, 1952; 1957) in the Seine basin.

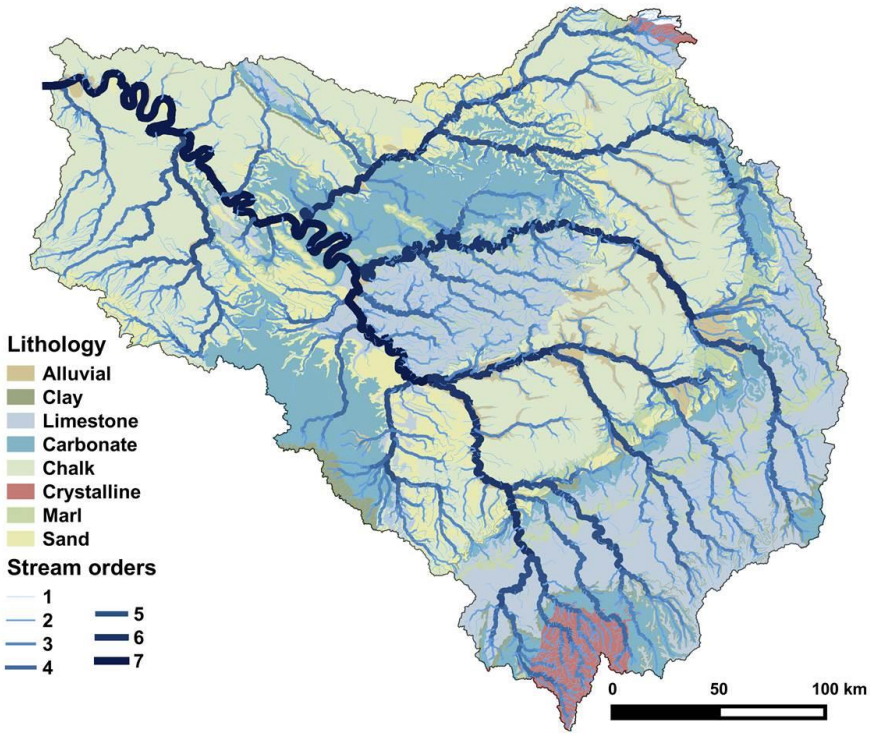

Fig. 4-9 Map of the lithology (Albinet, 1967) and stream orders (Strahler, 1952; 1957) in the Seine basin.

4.6.2. Annex 4-2. Relationships between direct and indirect pCO2.

A relationships was established between direct and indirect pCO_2 measurements (n=108) for the Seine River basin (Marescaux et al., 2018) to reduce pCO_2 indirect calculation bias (see Abril et al., 2015).

$$\boldsymbol{corrected\, p_{CO_2}} = \mathbf{10}^{\left(\frac{\boldsymbol{log}\left(\boldsymbol{calculated\, p_{CO_2}}\right) - \mathbf{0.51}}{\mathbf{0.85}}\right)} \text{ (Marescaux et al., 2018a)}$$

where calculated pCO_2 is partial pressure of carbon dioxide (ppmv) calculated from pH, total alkalinity, and water temperature using the CO2SYS software (Pierrot et al., 2006). The carbonate dissociation constants (K1 and K2) applied are from Millero, (1979) with zero salinity. CO_2 solubility is from Weiss, (1974).

4.6.3. Annex 4-3 Spatial and seasonal variations in gas transfer velocities (k) of CO2, CH4 and N2O

The difference in GHG concentrations between the atmosphere and water surfaces, and gas transfer velocities, control GHG emissions. Values of gas transfer velocities (*k*) were higher for all GHGs for small Strahler order (SOs) than for high SOs (Fig. 2). Our *k* calculations (Eq. 3) are directly related to slope, water velocity and water temperature. Consequently, *k* trends according to Strahler order were in more in agreement with the steeper slopes of the small headwater streams than with those of the main streams. Seasonal patterns and gas transfer velocity values were similar for CO_2 and N_2O, with higher *k* in winter for small SOs than in summer, while the opposite patterns were observed for SOs 5–7. This resulted from the increase in water flow and water velocity in winter that affected *k* values more strongly in small SOs than in main streams, whereas in summer, higher water temperatures led to higher *k* in higher SOs than upstream. However, the *k* of CH_4 showed a different pattern with lower *k* in summer whatever the SO. Indeed, *k* depends on water temperature sensitivities of the Schmidt number of the different gases.

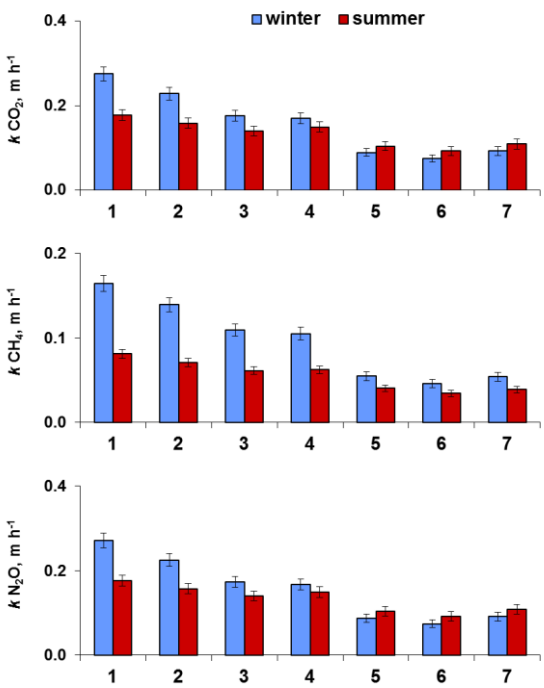

Fig. 4-10 Gas transfer velocity for CO2, CH4, N2O calculated according to the fifth equation in table 2 in Raymond et al. (2012) as a function of stream order (SO) in the Seine basin in winter (blue) and in summer (red). Whiskers are standard deviations between observed GHG concentrations

4.6.4. Annex 4-4 Greenhouse gas concentrations ([GHG]) and fluxes (fGHG) with associated standard deviations and 95% confidence intervals averaged by season and by stream order.

			[GHG]	sd	95% C.I.			fGHG	sd	95% C.I.	
					<	>				<	>
CH_4, µgC l^{-1}	summer	1	0.63	0.15	0.32	0.94	CH_4, kgC d^{-1}	34	9	16	52
		2	1.74	0.34	1.07	2.42		78	16	45	111
		3	1.47	0.37	0.74	2.21		64	17	29	98
		4	2.25	0.20	1.85	2.65		102	12	78	126
		5	1.20	0.17	0.87	1.53		49	8	32	66
		6	1.43	0.13	1.17	1.69		56	8	40	73
		7	3.47	0.36	2.76	4.18		171	25	121	221
	winter	1	0.60	0.09	0.43	0.78		65	11	44	87
		2	0.81	0.15	0.51	1.12		68	14	40	97
		3	0.75	0.08	0.59	0.90		55	7	41	69
		4	1.03	0.22	0.60	1.46		77	18	41	113
		5	0.45	0.09	0.26	0.64		22	6	11	34
		6	0.88	0.09	0.71	1.06		45	7	32	59
		7	1.51	0.34	0.82	2.18		100	26	48	152
$N\text{-}N_2O$, µgN l^{-1}	summer	1	1.22	0.18	0.86	1.58	$N\text{-}N_2O$, kgN d^{-1}	117	26	66	168
		2	0.79	0.12	0.55	1.03		51	13	24	78
		3	0.55	0.05	0.45	0.64		27	7	13	41
		4	0.54	0.06	0.41	0.66		30	9	12	48
		5	0.50	0.04	0.42	0.57		27	7	12	41
		6	0.75	0.11	0.52	0.98		56	16	24	89
		7	3.10	0.26	2.57	3.63		400	61	279	521
	winter	1	1.65	0.29	1.08	2.23		250	59	131	368
		2	0.59	0.05	0.49	0.69		31	9	13	49
		3	0.61	0.06	0.48	0.73		29	9	11	48
		4	0.53	0.04	0.44	0.62		20	7	5	35
		5	0.96	0.46	0.05	1.87		53	42	-32	138
		6	0.56	0.13	0.31	0.81		16	12	-8	40
		7	2.07	0.27	1.53	2.62		202	43	116	287
CO_2, µgC l^{-1}	summer	1	3449	112	225	225	CO_2, MgC d^{-1}	351	21	310	661
		2	2114	53	107	106		191	11	168	360
		3	1959	51	101	102		175	11	152	327
		4	1548	39	79	79		145	9	127	272
		5	1465	37	73	73		130	11	108	238
		6	1731	52	104	103		162	16	130	293
		7	2292	57	114	114		287	24	238	525
	Winter	1	2168	72	144	144		545	29	487	1032
		2	2410	67	134	134		321	16	288	609
		3	2095	56	112	110		236	13	211	447
		4	1633	43	86	86		173	10	154	328
		5	1689	47	94	93		131	10	110	241
		6	2001	55	111	110		154	14	126	280
		7	2362	59	118	118		240	19	203	443

4.6.5. Annex 4-5 Results of the statistical differences between mean of greenhouse gas concentrations by stream order.

		Stream orders						
	CO_2	1	2	3	4	5	6	7
Stream orders	1		p < 0.05*	p < 0.05*	p < 0.05*	p < 0.05*	p < 0.05*	p < 0.05*
	2			p < 0.05*	p < 0.05*	p < 0.05*	p < 0.05*	p > 0.05
	3				p < 0.05*	p < 0.05*	p > 0.05	p < 0.05*
	4					p > 0.05	p < 0.05*	p < 0.05*
	5						p < 0.05*	p < 0.05*
	6							p < 0.05*
	7							
	CH_4	1	2	3	4	5	6	7
	1		p > 0.05	p < 0.05*	p < 0.05*	p < 0.05*	p < 0.05*	p < 0.05*
	2			p > 0.05	p > 0.05	p > 0.05	p > 0.05	p < 0.05*
	3				p < 0.05*	p > 0.05	p > 0.05	p < 0.05*
	4					p > 0.05	p > 0.05	p < 0.05*
	5						p > 0.05	p < 0.05*
	6							p < 0.05*
	7							
	N_2O	1	2	3	4	5	6	7
	1		p < 0.05*	p < 0.05*	p < 0.05*	p < 0.05*	p < 0.05*	p < 0.05*
	2			p > 0.05	p > 0.05	p > 0.05	p > 0.05	p < 0.05*
	3				p > 0.05	p > 0.05	p > 0.05	p < 0.05*
	4					p > 0.05	p < 0.05*	p < 0.05*
	5						p > 0.05	p < 0.05*
	6							p < 0.05*
	7							

4.6.6. Annex 4-6 Exact locations, mean and standard deviations of water quality parameters (chlorophyll a (Chl. a), total alkalinity, pH, dissolved oxygen (O2), and dissolved silica (DSi)) of the sampling stations located along the main stem of the basin.

	Coordinates (EPSG 3857)	km (Paris = 0)	Chl. a (µg/l)		Water temperature (°C)		Alkalinity (mmole l^{-1})		pH (-)		O_2 (mg l^{-1})		DSi (mg l^{-1})	
Name of the sampling station			*mean*	*SD*	*mean*	*SD*	*mean*	*SD*	*mean*	*SD*	*mean*	*SD*	*mean*	*SD*
Tancarville	49°28'21.2"N 0°27'51.5"E	337.00	33.20	22.18	17.05	2.4	4.17	0.42	8.09	0.18	7.41	0.74	3.31	0.90
Caudebec	49°31'13.0"N 0°44'50.1"E	310.50	14.22	10.05	17.73	2.0	4.14	0.41	8.05	0.21	7.48	0.71	3.07	1.10
Duclair	49°28'47.3"N 0°52'34.0"E	278.00	11.63	12.30	17.61	2.5	4.05	0.51	7.96	0.21	7.22	1.09	3.06	1.24
Bouille	49°21'07.8"N 0°56'03.6"E	259.70	12.20	14.17	17.88	2.3	3.99	0.66	7.94	0.18	7.14	0.80	2.97	1.32
Bas Dock	49°26'36.9"N 1°03'51.9"E	251.30	28.06	64.35	17.75	2.4	4.06	0.65	8.11	0.40	7.75	0.93	3.23	1.27
Oissel	49°20'13.8"N 1°05'36.4"E	229.40	24.53	50.89	18.00	2.3	4.01	0.61	8.02	0.23	8.20	0.83	2.83	1.39
Elbeuf	49°17'36.9"N 1°00'35.0"E	218.97	26.59	51.02	18.00	2.4	3.95	0.65	8.03	0.24	8.56	1.09	2.88	1.33
Poses	49°18'35.9"N 1°14'10.9"E	202.00	21.57	42.48	18.26	2.5	3.99	0.52	7.98	0.23	8.44	1.40	2.78	1.34
Vernon	49°05'44.9"N 1°29'15.9"E	150.00	15.76	31.64	17.99	2.9	3.90	0.66	7.93	0.24	8.13	0.57	2.78	1.29
Porcheville	48°57'59.4"N 1°46'35.3"E	101.00	8.39	10.53	17.96	2.8	4.05	0.47	7.88	0.26	7.23	0.87	2.80	1.24
Poissy	48°56'12.3"N 2°02'19.6"E	76.00	6.14	6.54	17.85	2.9	4.06	0.45	7.84	0.19	7.72	0.99	2.86	1.32
Conflans	48°59'19.2"N 2°04'55.2"E	70.00	3.51	3.33	18.24	2.9	3.68	0.42	7.85	0.21	7.12	1.28	2.52	1.16
Maison Laffite	48°56'41.1"N 2°09'30.7"E	48.00	4.57	3.72	18.12	3.0	3.72	0.46	8.05	0.39	7.43	1.01	2.25	1.11
Saint Maurice	48°49'00.4"N 2°25'11.9"E	0.00	19.58	52.80	17.50	3.2	4.18	0.39	8.17	0.26	9.52	2.16	2.25	1.11
Neuilly sur Marne	48°51'13.0"N 2°31'57.9"E	-30.00	10.15	19.12	17.43	2.9	4.29	0.39	8.17	0.21	8.94	1.50	2.32	1.19
Annet	48°54'59.0"N 2°43'08.1"E	-50.00	9.19	16.06	17.18	2.8	4.31	0.38	8.17	0.17	8.97	1.11	2.22	1.10
Sammeron	48°58'10.8"N 3°19'15.0"E	-120.00	6.80	8.53	17.16	3.1	3.97	0.39	8.16	0.17	8.89	0.84	1.82	0.85
Saulchery (Nogent l'Artaud)	49°04'31.7"N 3°38'12.5"E	-150.00	4.76	4.49	17.17	3.0	3.93	0.35	8.12	0.30	8.64	0.97	1.65	0.76
Dormans	48°59'43.0"N 4°14'38.1"E	-180.00	4.68	3.48	17.16	3.3	3.69	0.45	8.11	0.26	8.58	0.74	1.44	0.59
Matougues	48°37'20.9"N 4°42'01.9"E	-260.00	3.12	1.53	16.49	3.3	3.62	0.53	8.04	0.17	8.60	0.97	1.28	0.62
Moncetz l'Abbaye	48°38'49.0"N 4°39'12.7"E	-335.00	5.06	3.36	16.23	3.7	3.47	0.59	8.12	0.18	8.95	1.22	0.98	0.56
Arrigny	48°37'20.9"N 4°42'01.9"E	-337.00	7.15	6.95	16.30	4.0	3.34	0.79	8.03	0.52	8.63	1.70	1.08	0.59
Larzicourt	48°37'47.2"N 4°42'34.0"E	-340.00	5.83	3.96	15.11	2.7	4.17	0.43	8.15	0.39	8.69	1.46	1.21	0.81

Acknowledgements

The C-CASCADES (https://c-cascades.ulb.ac.be/) project of which this study was a part, received funding from the European Union's Horizon 2020 research and innovation programme under the Marie Sklodowska-Curie grant agreement No. 643052. Audrey Marescaux benefitted from a PhD grant. The PIREN-Seine programme and the HydroGES project are also greatly acknowledged for their support. Many thanks are due to Abdelkader Azougui, Sébastien Bosc, Anunciacion Martinez Serrano, and Benjamin Mercier for their kind participation in the fieldwork and for their assistance with chemical analyses in the lab. Goulven Laruelle is also acknowledged for his help with statistical analyses. Vincent Thieu (assistant-professor at the University Pierre and Marie Curie, Paris) and Josette Garnier (Research Director at the CNRS, *Centre National de la Recherche Scientifique*, France) are co-supervisors of the PhD candidate. We thank the four anonymous reviewers for their constructive comments.

Affiliations

Sorbonne Universités, Université Pierre et Marie Curie, Centre National de la Recherche Scientifique, Institut Pierre Simon Laplace, UMR 7619 METIS, Paris, France

Author contribution statement

All the authors contributed to the design of the study. JG and VT are co-supervisors of the PhD. AM participated as a PhD student in the field campaigns and chemical analyses in the laboratory. AM wrote the first draft of the manuscript, and all co-authors helped interpret the data and write the article.

Corresponding authors: Audrey Marescaux**, Audrey.maresaux@sorbonne-universite.fr**

Competing interests: The authors declare no competing personal or financial interests.

Data availability

The datasets generated during the current study are available from the corresponding author on reasonable request (Audrey.marescaux@sorbonne-universite.fr).

Chapter n°5

Long term changes in greenhouse gas emissions of French agriculture and livestock (1852- 2014): from traditional agriculture to conventional intensive systems

Josette Garnier[1], Julia Le Noë[1], Audrey Marescaux[1], Alberto Sanz-Cobena[2], Luis Lassaletta[2], Marie Silvestre[3], Vincent Thieu[1], Gilles Billen[1]

[1]Sorbonne Université, CNRS, Institut Pierre Simon Laplace, UMR 7619 METIS, Paris, France

[2] CEIGRAM. Universidad Politécnica de Madrid, ETSI Agrónomos, Madrid, Spain

[3]Sorbonne Université, CNRS, FIRE FR3020, Paris,, France

Article accepted in Science of the Total Environment (2019),

https://doi.org/10.1016/j.scitotenv.2019.01.048.

Graphical abstract

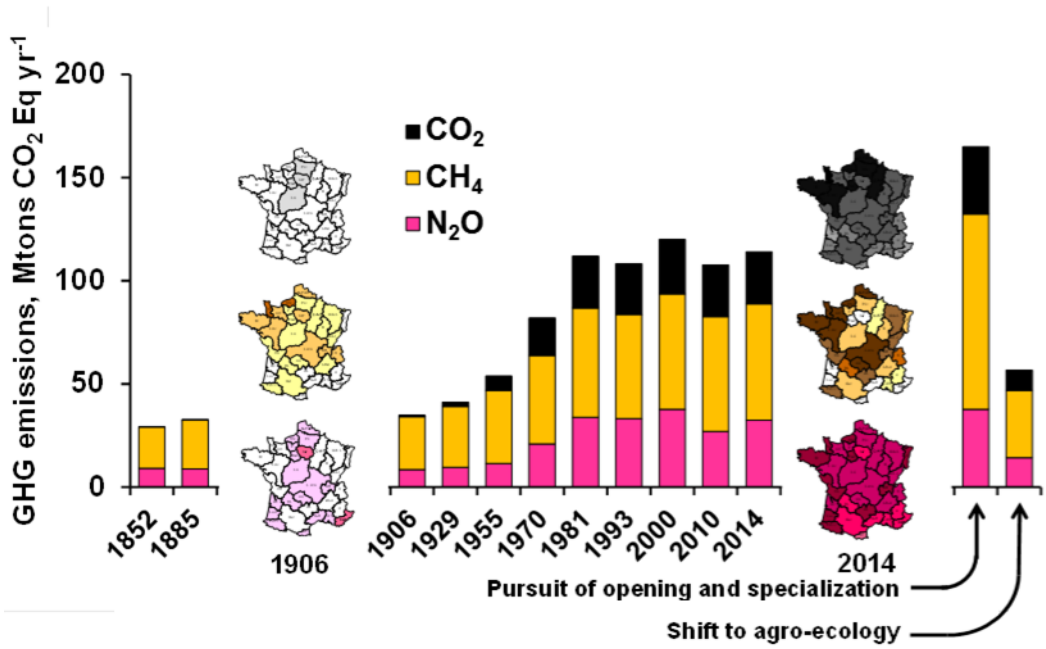

Highlights

- French GHG emissions from agricultural and forest sectors were estimated
- A long-term trajectory (1852–2014) was reconstructed for N_2O, CH_4, CO_2
- GHG emissions have grown 4-fold since 1852, to 120000 CO_2 Eq yr^{-1} in the 2000s
- GHG emissions have only stabilised, in spite of agro-environmental measures
- Deep changes in the agro-food system would reduce agricultural GHG emissions

Abstract

France was a traditionally agricultural country until the first half of the 20th century. Today, it is the first European cereal producer, with cereal crops accounting for 40% of the agricultural surface area used, and is also a major country for livestock breeding with 25% of the European cattle livestock. This major socioecological transition, with rapid intensification and specialisation in an open global market, has been accompanied by deep environmental changes. To explore the changes in agricultural GHG emissions over the long term (1852–2014), we analysed the emission factors of N_2O from field experiments covering major land uses, in a gradient of fertilisation and within a range of temperature and rainfall, and used CH_4 emission coefficients for livestock categories, in terms of enteric and manure management, considering the historical changes in animal excretion rates. We also estimated indirect CO_2 emissions, rarely accounted for in agricultural emissions, using coefficients found in the literature for the dominant energy consumption items (fertiliser production, field work and machinery, and feed import). From GHG emissions of ~30,000 ktons CO_2 Eq yr^{-1} in 1852, reaching 54,000 ktons CO_2 Eq yr^{-1} in 1955, emissions more than doubled during the 'Glorious thirties' (1950–1980), and peaked around 120,000 ktons CO_2 Eq yr^{-1} in the early 2000s. For the 2010–2014 period, French agriculture GHG emissions stabilised at ~114,000 ktons CO_2 Eq yr^{-1}, distributed into 49% methane (CH_4), 22% carbon dioxide (CO_2) and 29% nitrous oxide (N_2O). A regional approach through 33 regions in France shows a diversity of agriculture reflecting the hydro-ecoregion distribution and the agricultural specialisation of local areas. Exploring contrasting scenarios at the 2050 horizon suggests that only deep changes in the structure of the agro-food system would double the reduction of GHG emissions by the agricultural sector.

Keywords: French agriculture, GHG emissions, historical reconstruction, spatial distribution, scenario analysis

5.1. Introduction

Atmospheric greenhouse gas (GHG) concentrations such as carbon dioxide (CO_2), methane (CH_4) and nitrous oxide (N_2O) have rapidly increased, especially since the mid-20th century, as shown by ice core and modern data (IPCC 2006- Eggleston, 2006). At the global scale, agricultural activities and land use changes accounted for 24% of the total emissions (IPCC 2006- Eggleston, 2006) (not including indirect emissions such as those linked to fertilizer manufacture). For the European Union (EU-28), agricultural emissions are considered as the second largest GHG contributors after fossil fuel combustion (respectively, 10% vs. 78% of total EU emissions, amounting 4,300 million tons CO_2 equivalent, in 2016) (EEA, 2018). For France (out of the 520 million tons CO_2 equivalent yr^{-1}, GHG from agriculture and fossil fuel combustion represented 19% vs. 71%, respectively in 2010, with a decreasing trend since the Kyoto protocol (CITEPA, 2012). Fugitive emissions from fuels represented only 1% of the total GHG emissions, industrial processes accounted for about 3.7% and wastes for 4.8% (CITEPA, 2012). Surprisingly, according to CITEPA, whereas 66% and 87% of CH_4 and N_2O emissions are issued from French agriculture, agriculture is not considered as a source of CO_2, its emissions being included in others sectors (machinery, chemicals, …). Therefore, the role of agriculture in overall GHG emissions, including direct and indirect CO_2 emissions linked to fossil fuel-driven farming practices still present a number of uncertainties (Lemke et al., 2007).

The control factors of agricultural N_2O, CH_4 and CO_2 emissions differ greatly from each other. Nitrous oxide fluxes are often reported to be associated with mineral fertiliser applications (Bouwman, 1996; Skiba et al., 1996; Smith et al., 1997; ENA, 2011- Sutton et al., 2011), particularly on wet non-saturated soils (Clayton et al., 1994; Aguilera et al., 2013), but manure and other organic fertilisers also contribute to N_2O emissions (Aguilera et al., 2013). Methane (CH_4) fluxes come essentially from livestock (Moss et al., 2000; Vermorel et al., 2008; Springmann et al., 2018), manure management and enteric fermentation (particularly ruminants), although some soils can be a CH_4 sink through CH_4 oxidation (Boeckx and Van Cleemput, 2001), a capacity that managed agricultural soils have partly lost due to nitrogen fertiliser application, which is unfavourable to methane oxidizing micro-organisms (Ojima et al., 1993; Dobbie and Smith, 1996). In contrast, paddy soils could be net emitters of this gas. While net soil CO_2 emissions result from the balance between humified

organic matter input and mineralisation or leaching, CO_2 emissions by agriculture stem more from CO_2 emitted from the fossil fuel use related to fertiliser manufacture, use of machinery for farm work and feed imports (Gingrich et al., 2007; Dyer et al., 2010; Aguilera et al., 2015). How these different control factors combine with each other to determine the variations in time and space of GHG emissions by agricultural systems remains a question that is difficult to answer.

France is currently the world's fourth largest agricultural exporter (www.fao.org/faostat), with a rather diversified mosaic of regional agricultural systems. It therefore constitutes a good case study for analysing the relationships between the structural characteristics of agriculture and its GHG emissions.

Based on the concepts of socio-ecological trajectories (Fischer-Kowalski and Haberl, 2008) and territorial ecology (Barles, 2010; Barles, 2017), the long-term trends of the French agro-food system have been described by Le Noë et al. (2018) in terms of N, P and C fluxes over the period from 1852 to 2014. A gradual intensification and specialisation of regional systems was shown, all characterised by integrated crop and livestock farming until the beginning of the 20th century, toward either specialised cropping systems fueled by synthetic fertilisation or intensive livestock farming highly dependent on external feed imports (Le Noë et al., 2018). Within the country, the Seine watershed is one emblematic example of the former specialised cropping systems, while Bretagne is a region of typical intensive livestock farming systems highly disconnected from croplands. Marescaux et al. (2018) established the GHG budget for the Seine Basin, including the hydrosystem network, the agricultural and non-agricultural sectors. Of the approximately 61,000 ktons CO_2 Eq yr^{-1} emitted from the whole Seine Basin, non-agriculture GHGs were shown to dominate the total emissions (73%), while the agricultural sector amounted to 23% and emissions by rivers reached 4%. The agricultural emissions found for the Seine Basin were 30% higher than those provided by official French GHG emission inventories.

The first aim of this paper is to establish a spatially distributed long-term budget of GHG emissions by the French agricultural sector, based on previous studies on GHGs (Garnier et al., 2009; Garnier et al., 2013; Marescaux et al., 2018).

A major issue behind this effort is to identify the effect of the structural changes from mixed crop and livestock farming systems to specialised systems on the GHG emissions account.

Indeed, the shift of agricultural and livestock management practices which occurred with mechanisation and intensification are expected to cause increased GHG emissions. Moreover, specific emission rates of CO_2, CH_4, N_2O are expected to depend either on crop or livestock typologies. Another objective is to determine the levers for future mitigation of N_2O, CH_4 and CO_2 emissions by agricultural practices. In this line, we explored two contrasting scenarios recently developed by Billen et al. (2018): (i) continuing the current trends of specialisation into either cropping systems based on chemically synthesised inputs or intensive livestock farming highly dependent on feed import; and (ii) shifting to organic farming and reconnection of crop and livestock farming, while reducing the animal proteins in human diets by half. These two prospective scenarios of French agriculture are tested in order to evaluate to which extent less intensive agriculture and livestock breeding can allow a reduction of GHG emissions.

5.2. Material and methods

5.2.1. Major physiographic and agricultural characteristics of France

France is a heterogeneous country with a mountainous region in the South-East and low relief in the West (Bretagne) as well as large sedimentary plains in the lower part of the Seine, Loire and Garonne rivers flowing to the Atlantic façade. From north to south, there is a climate gradient: temperate, oceanic, temperate warm, and Mediterranean climatic zones (Fig.5-1a). These regions are dominated by field crops in the South-West and North-West parts of the country, with Bretagne dominated by intensive livestock farming (Fig.5-1b). The rest of France (in the South-East) is either characterised by large vineyard domains in the areas bordering the Mediterranean Sea or in the Rhone alluvial corridor, and by varied mixed crop and livestock in the mountainous regions (the Alps, the Jura and the Massif Central). With 33 regions defined by aggregation of the 94 metropolitan départements (Le Noë et al., 2017), we defined three supra-regions, with a similar surface area, with homogenous agricultural patterns and climate for each: (i) the Seine Basin, due to its intensive cereal cropping agriculture and temperate climate, (ii) the oceanic-temperate Great West, including the Bretagne region and the lower Loire basin with intensive livestock, and the Great South-West covering the Garonne basin, with a temperate warm climate, particularly conducive to growing maize for feed purposes (Fig.5-1c).

5.2.2. Reconstruction of past land use and agricultural system

The GRAFS approach for characterising the agricultural structure over the long term

The GRAFS approach (Generalized Representation of Agro-Food System), firstly developed and applied on a global scale (Billen et al., 2013; Billen et al., 2014; Lassaletta et al., 2014b) to local scales (Garnier et al., 2016) for nitrogen (N) circulation, was enlarged to phosphorus (P) (Garnier et al., 2015) and now to N, P and carbon (C) (Le Noë et al., 2017). Briefly, the GRAFS approach describes the agro-food system of a given geographical area by considering four main compartments exchanging nutrient flows: cropland, grassland, livestock system and local population. The potential losses to the environment associated with these exchanges have been estimated for hydrosystems (Garnier et al., 2015, 2016, 2018), but not yet for losses to the atmosphere. This functional representation links arable land productivity, semi-natural or managed grassland that contributes to livestock feeding, and finally, human food

requirements. The agro-food system is driven by (i) nutrient inputs to the soil (synthetic and/or organic fertilisation, atmospheric deposition [hereafter referred to as exogenous fertilisation] as well as symbiotic fixation), (ii), the size of the livestock and its feed requirement and (iii) the size of the human population and its dietary preferences, including feed and food imports/exports. The GRAFS approach does not take into account forested areas.

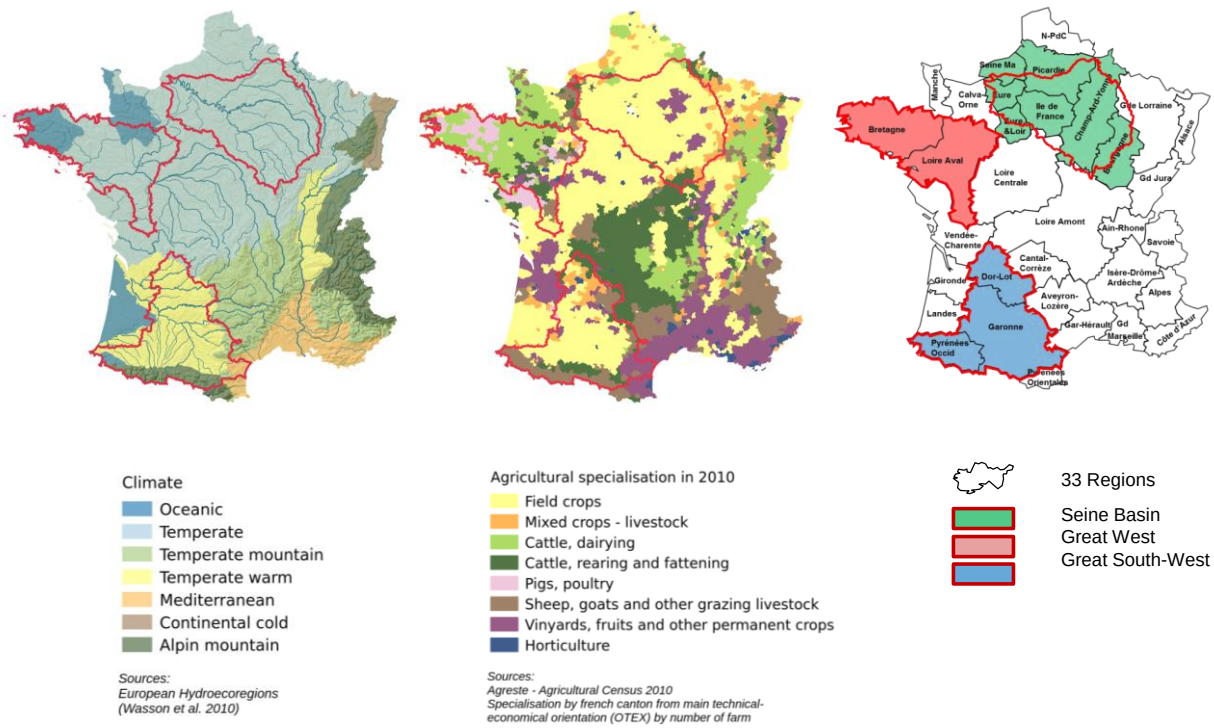

Fig.5-1. General characteristics for France of a. climate from hydroecoregion; b. agricultural patterns; c. homogenous agricultural regions (33) and perimeter of three supra-regions chosen for their identical surface area and their trend for agricultural specialisation.

Based on the long-term agricultural statistics available at the scale of the 94 French administrative “département” units for metropolitan France (equivalent to the European Union NUTS3 statistical division) and additional data gathering (e.g. the forested areas below), the GRAFS approach was documented for 22 dates from 1852 to 2014, and for the 33 French regions (Le Noë et al., 2017; 2018), (Fig.5-1).

Past evolution of forested areas

The surface forest and wooded areas were documented by "département" for the years 1929 (Ministère Agriculture – Enquête Agricole), 1946, 1950, 1955, 1960 and 1965 (Ministère Agriculture – SAA). All years were available from 1970 to 1988 based on data provided by Agreste-SSP. The recent years from 1989 to 2014 were retrieved from the AGRESTE database on agricultural statistics (https://stats.agriculture.gouv.fr/disar-web/). For France, whereas the total surface areas amounted to 10.67 10^6 ha in 1929, examining the chronicle by Cinotti (1996)for the 19th century showed values around 9.3 10^6 ha in 1850 (compared to the 10.67 10^6 ha in 1929) and a linear trend for the intermediate dates, 1885 and 1906. The same changes were applied to the 33 regions, for the dates before 1929.

5.2.3. Reconstruction of greenhouse gas emissions

As a whole, the GHG budget of the agriculture sector can be estimated as the result of N_2O emissions from cropped soils, grassland and forest, CH_4 released from livestock production (enteric fermentation and manure management) and CO_2 emitted from fossil fuel directly used by farming practices as well as indirectly for manufacture and transport of agricultural inputs. Due to their specific origin, each of these GHG emissions required an adapted methodology. Agricultural soil C sequestration has been estimated elsewhere and will be compared to GHG emissions (Le Noë et al., 2018).

Reconstruction of N_2O emissions

To infer N_2O emissions back to 1852 at the scale of the 33 regions of France, on the basis of the recent knowledge gained from field measurements, we first established an empirical relationship linking yearly N_2O emissions to mineral and organic fertilisation, temperature and rainfall, and then assumed that this relationship could be extrapolated to past situations within the timeframe of this study (e.g., Bouwman, 1996).

For N_2O emissions, a literature review from Garnier et al. (2009) and Cayuela et al. (2017) was completed for a total of 208 yearly cropland N_2O emissions values and their associated explicative variables, namely N fertiliser (organic and mineral) inputs, annual mean temperature and rainfall. A similar set of data was gathered for 138 cases of grasslands. For forests, we found 38 cases for N_2O emissions that were only associated with temperature and rainfall data, since they had not been fertilised. Additional early field measurements from the

Seine watersheds were also included in this analysis (Benoit et al., 2015; Garnier et al., unpublished data). The complete data set is presented in the supplementary material.

We searched the best fit parameters for the following relationship:

$$N_2O_{em} = (a + b\ N_{inp}^{d}) * (Rain/Rain_{ref})^{c} * Q_{10}^{T/10} \qquad \text{Eq. 1}$$

where N_2O emissions (N_2O_{em}) and N inputs (N_{inp}) are in kg N_2O-N ha^{-1} yr^{-1}, rainfall (Rain) in mm yr^{-1} and temperature (T) in °C (Table 5-1), and a, b, c, $Rain_{ref}$, d and Q_{10} are parameters to be calibrated within a range of realistic values.

This relationship assumes a power function for the relationship with N inputs and rainfall, and a classical Q10 exponential relationship with temperature.

Table 5-1. a. Summary of the data gathered for establishing relationships between N_2O emissions and its controlling factors, *n*=394, number of data. Relationships, and associated parameter values: b. for cropland and grassland and c. for forest. NRMSE and bias are calculated for evaluation of the fitted relationships.

a.

N=394	**Nb of values**	**N inputs, kgN ha^{-1} yr^{-1}**	**Rainfall, mm yr^{-1}**	**Temperature, °C**	**N2O emission, kgN-N_2O ha^{-1} yr^{-1}**
Cropland	208	0-450	327-1250	2.75-18.5	0.01-11.0
Grassland	138	0-753	400-1837	1.0-16.0	-0.5-18.9
Forest	48	0	607-1239	3.6-10.1	0.17-4.9

b.

$$N_2O_{em} = (a + b\ N_{inp}^{d}) * (Rain/Rain_{ref})^{c} * Q_{10}^{T/10}$$

	units	**value**	**± step**
a	kgN/ha/yr	0.15	0.05
b	dimless	0.016	0.001
c	dimless	1.0	0.05
d	dimless	1.2	0.1
$Rain_{ref}$	mm/yr	1000	100
Q_{10}	dimless	1.2	0.2

nRMSE = 14%
bias = 5%

c.

$$N_2O_{em} = a * (Rain/Rain_{ref})^{c} * Q_{10}^{T/10}$$

	units	**value**	**± step**
a	kgN/ha/yr	1.9	0.05
c	dimless	1	0.1
$Rain_{ref}$	mm/yr	1400	100
Q_{10}	dimless	1.2	0.2

nRMSE = 23%
bias = 10%

Since most grassland was fertilised, no significant difference was found between cropland and grassland so that the two data series were merged. Regarding forests, Ninputs are restricted to atmospheric deposition and a specific relationship was established (Table 5-1).

The six parameter values (a, b, c, d, $Rain_{ref}$ and Q10) were determined by a systematic optimisation procedure searching the combination of parameter values providing the best fit of the calculated emissions to the observed N_2O emission values. The resulting relationship fits the data with an acceptable % bias and Normalised RMSE (root mean square error normalised against the range of observed values) (Table 5-1). Further details on the procedure are provided in Supplementary Material (SM2).

These relationships were applied to cropland and grassland on one hand and to forest on the other hand for each region and 22 dates from 1852 to 2014. Temperature and rainfall were reconstructed from EOPS data for the 1950–2017 period (Version 17, 0.25 degrees resolution (https://www.ecad.eu/download/ensembles/download.php) and spatially averaged by French "département" (NUTS-3 equivalent). For the period prior to 1950, temperature and rainfall data were downloaded for 28 towns spread over the country, back to the dates available in the past, between 1850 and 2017 (http://meteo-climat-bzh.dyndns.org/mete100-1783-2018-3-tn-1-0-0.php). To avoid any discrepancy between the two series, the anomaly for each town was calculated compared to the mean over the long-term period and then added to the mean calculated for the 1950–2017 period. The values prior to 1950 for the towns were then assigned to their respective regions. The same procedure was applied for both temperature and rainfall. The average differences between the two data series for the 1950-2017 period for all 33 regions is close to zero (i.e., no systematic bias) with a standard deviation of 15%, for temperature and rainfall.

Reconstruction of CH_4 emissions

CH_4 emissions were estimated based on livestock numbers and specific emission factors for each animal and age class category, corrected for past variations in excretion rates.

Current CH_4 emission factors (kg-CH_4 $head^{-1}$ $year^{-1}$) from enteric fermentation and manure storage and management were taken from Garnier et al. (2013 in Table 1SM) compiled principally from Vermorel et al. (2008), IPCC 1997 - Houghton et al. (1997) and Zhou et al. (2007). An emission factor for humans was also taken into account, following (Crutzen et al., 1986).

These CH_4 emissions concerned five animal sub-categories for cattle, three for sheep, three for pig, five for poultry, while goat, horse and rabbit represented one category each. Knowing the number of heads per category and the associated manure produced, the total amount of CH_4 emitted by livestock was calculated using the corresponding specific emission factors.

Livestock numbers per category were taken directly from agricultural statistics (Agreste, 2013, or Gallica: https:/gallica.bnf.fr, last accessed November 2018) when these numbers were not available from Agreste). However, the evolution of animal size and physiology changed over the period studied (Chatzimpiros, 2011) and this must be taken into account. Historical variations of excretion rates of the major livestock categories were established by Le Noë et al. (2018, SM1 & SM2) (Table 5-2). The correction factors found during the period for the animal categories reported in Table 5-2 were also used for their corresponding sub-categories. For poultry and rabbit, no change was considered over time.

Table 5-2. Empirical relationship for calculating excretion rates (y, in kgN head^{-1} yr^{-1}) of cattle, sheep, pig and horses as a function of time (t, in year) over the period 1850-2014, and corresponding values of the parameters b, a, a', tmax and dt, calibrated against historical and current animal excretion data (from Le Noë et al., 2018).

General formula : $y = b + a (t – 1850) + a' \exp [- (t – t_{max})^2 / dt^2]$

	b	**a**	**a'**	**t_{max}**	**dt**
	kgN head^{-1} yr^{-1}	kgN head^{-1} yr^{-1}	yr	yr	yr
Cattle	45	0.05	65	2010	40
Sheep	4	0.02	9	2020	45
Pig	56	0.034	-	-	-
Horse	480	0.3	-	-	-

Reconstruction of CO_2 emissions

Current CO_2 emissions by direct or indirect fossil fuel combustion by the agricultural sector were calculated using the official French CLIMAGRI approach (Doublet, 2011), based on CO_2 emission factors calculated for mechanised field work and livestock activities, as well as for synthetic fertiliser manufacture. The coefficients used are gathered in Table 5-3.

Table 5-3. Coefficient applied for the calculations of CO_2 emissions according to major emitter sectors. N fertilisers and P fertilisers concern the production of fertilisers actually used, feed to livestock is the imported feed, machinery corresponds to the manufacture of agricultural equipment, energy for cropland, grassland and livestock, the fuel or electricity necessary for fieldwork and for livestock breeding (from Doublet et al., 2011). UAA: utilised agricultural area; LU: livestock unit.

Major sectors emitting CO_2	Units	Coefficients
Fertilisers N	tonC-CO2/tonN	1.12
Fertilisers P	tonC-CO2/tonP	0.46
Feed to livestock	tonC-CO2/tonN imported	1.339
Machinery	tonC-CO2/ha/yr	0.026
Energy for cropland	tonC-CO2/ha UAA/yr	0.077
Energy for grassland	tonC-CO2/ha UAA/yr	0.055
Energy for livestock	tonC-CO2/LU/yr	0.056

The coefficients related to mechanisation (fossil fuel combustion for machinery, field work in cropland and grasslands, and livestock management and feed to livestock) were applied pro-rata to the usable agricultural area or the total livestock units for each region, and extrapolated to the past taking into account the degree of mechanisation of each region. The proxy for establishing this degree of mechanisation was based on the observed evolution of the numbers of horses between 1906 (zero mechanisation) and 1980 (100% mechanisation) (Table 5-3 and Fig. 5-2).

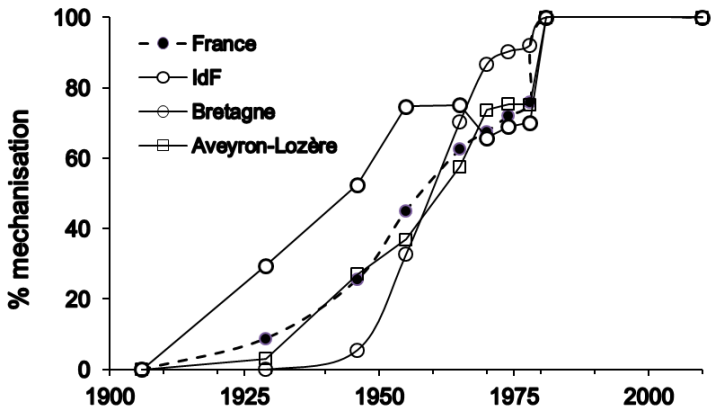

Fig. 5-2. Evolution of the coefficient of mechanisation from 1906 (zero mechanisation) to 1980 (100% mechanisation) as calculated from changes in the number of horses for each of the 33 regions. The coefficient is given here for France and three contrasted regions. Agriculture modernisation appeared earlier in Ile-de-France.

5.2.4. Exploring scenarios

The two contrasting scenarios recently developed by Billen et al. (2018) are explored herein in terms of GHG emissions for their divergent assumptions: one continuing the trends of **O**pening to distant markets and **S**pecialisation into either cropping systems based on synthesised external inputs or intensive livestock farming (O/S), the other with an agricultural system shifting to **A**utonomy through organic farming, crop and livestock **R**econnection and a **D**emitarian diet (A/R/D). The O/S scenario reflects a main stream vision mainly driven by the desire for economic growth, very present in the official discourse, which is accompanied by the strengthening of territorial specialisation in a globalised economy, the continuation of agricultural intensification and the concentration of the population in large cities. On the contrary, the A/R/D scenario assumes a radical rupture towards agro-ecology (Billen et al., 2018a) and organic farming, searching for the autonomy of farmers with respect to agricultural inputs such as N fertilisers and animal feed, and reduction of the share of animal protein in the human diet as recommended by, for example, WHO for health reasons and Springmann et al. (2018) for environmental reasons, all trends already detectable although far from being fully underway. We here assumed reducing the animal proteins in human diets by half following the so-called demitarian diet (see the Barsac declaration, in 2009; https://en.wikipedia.org/wiki/Demitarian). Both scenarios were tested for the 2040 horizon and we therefore considered an increase of 1.5°C for both scenarios in addition to the 1.5°C already observed since the end of the 19th century. We kept the rainfall as it is at present because no general trend has been observed, in spite of yearly oscillations over the studied period. These projections are well in the ranges of those reported in Jouzel et al. (2014) for France for 2050, with four different models. Changes in rainfall might be more visible at the seasonal scale, not investigated here, with wetter winters and drier summers, and increased occurrence of extreme weather events in all seasons. Regarding fertilisation, both the O/S and A/R/D scenarios follow current environmental regulations, external synthetic fertilisers will be used according to a yield objective for the former, while the latter banish the use of mineral fertilisers (and pesticides) replaced by biological nitrogen fixation and possibly by on-farm and recirculated external organic inputs. In both scenarios, the livestock species structure was kept identical to the current one (2004–2014) for the regions that already had livestock.

5.2.1. Uncertainty analysis

The GHG emission values calculated as described above result from complex calculations based on basic statistical data (fertilisation rates, livestock number, etc.) and a number of parameters (coefficient of statistical relationships, emission factors, etc.), both subject to a certain level of uncertainty. In order to assess how these uncertainties propagates to the final emission estimates, a bootstrap procedure was carried out, as developed by Le Noë et al. (2018), under Microsoft Excel and associated VBA macros. Shortly, after having stated the confidence interval of all primary data and parameters (typically 10-20% uncertainty was assumed), thousand independent estimations of the GHG emissions were computed with a random draw of each of these data and parameters according to a Monte Carlo sampling within a Gaussian distribution inside the confidence interval. The uncertainty on the final GHG emissions was calculated as the standard error of the mean of these thousand replicates.

5.3. Results

5.3.1. Long-term trends of the control variables of GHG emissions

Temperature. A 1.5°C increase of mean annual temperature was observed between the mid-19th century and the last decade for all of France, mainly from 1980 when the average temperature exceeded 10°C (Fig. 5-3). The same trend was observed for the three selected regions, the Great South-West being closer to the overall average and the Great West showing the largest difference (+0.3°C) (Fig. 5-3). The coldest and warmest regions are, respectively, Alpes (7°C) and Grand Marseille (13°C) in the South-East of France. Regionally, whereas the temperature increase was >1.7°C in the East, South and South-West of France, with, respectively, a continental and Mediterranean climate, other mountainous regions (Jura, Savoie, Pyrénées) and oceanic temperate (Bretagne), showed an increase of 1.1°C.

Rainfall. Average rainfall over the period studied (1852–2014) was 805 mm yr^{-1} for the whole of France, more or less 100 mm yr^{-1} for the Great South-West (935 mm yr^{-1}) and Seine basin (703 mm yr^{-1}), respectively, whereas rainfall in the Great West averaged 746 mm yr^{-1} (Fig. 5-3). The wettest regions (>1000 mm yr^{-1}) were Savoie, Pyrénées Occidentales and Landes and the driest was Ile-de-France (~600 mm yr^{-1}). No clear trend was observed over the long term, but wet and dry years alternated (Fig. 5-3).

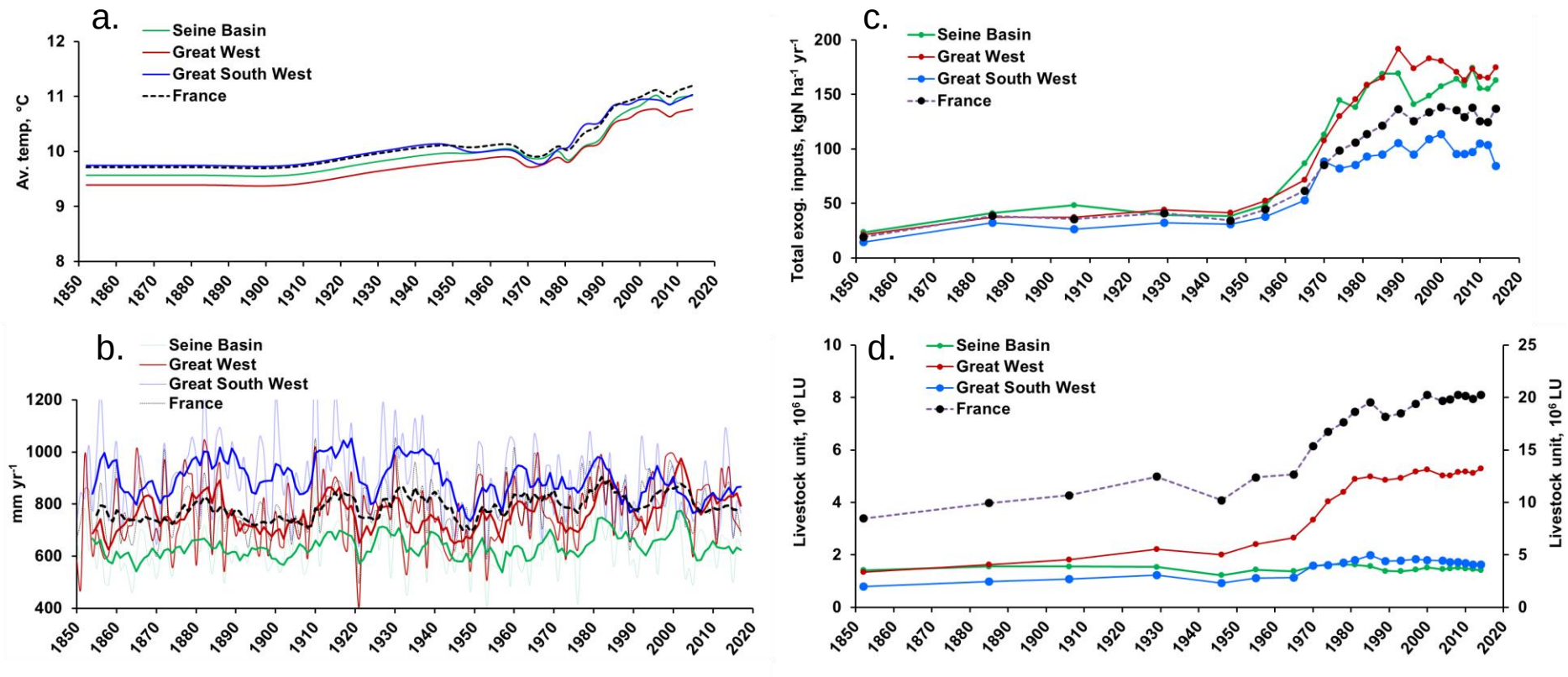

Fig. 5-3. Long-term evolution (1850–2014) for France and the three supra-regions selected in the annual average of a. temperature; b. rainfall. Long-term evolution of major indicators of agriculture in France and the three supra-regions selected for the 22 dates analysed; c. total exogenous N inputs; d. livestock size in terms of livestock units (LU). Left axis is for the three regions of interest and right axis is for the entire France.

Exogenous fertiliser. This accounts for total N inputs (synthetic, manure and deposition), excluding biological nitrogen fixation. From the 1850s until 1965, fertilisation increased from 20 to 60 kgN ha^{-1} yr^{-1}, and more in the early 1970s when half of the regions received 100 kgN ha^{-1} yr^{-1}. The inputs plateaued from the late 1980s at about 135 kgN ha^{-1} yr^{-1} at the national scale. The Northern part of France firstly increased its fertilisation, especially for the fertile soil of Ile-de-France and Nord-Pas-de-Calais, with values exceeding 150 kgN ha^{-1} yr^{-1} in the 1980s (Fig. 5-3). There were few regions where fertilisation remained below 100 kgN ha^{-1} yr^{-1} until now (Savoie, Alpes, Côte d'Azur in South-East France, and Garonne, Pyrénées Orientales in the South-West), mostly mountainous areas. In these regions, mineral fertilisation was less than half the total exogenous N inputs. Before 1965, fertilisation was essentially based on manure.

The same trend was found for the three selected regions, the Seine Basin and Great West fertiliser trajectory being above the average, and the Great South-West below (Fig. 5-3).

Livestock. Livestock density, expressed in livestock units (LU, i.e. equivalent to an animal excreting 85 kg N yr^{-1}) per ha of agricultural surface, increased slowly in all French regions until the mid-20th century. The increase was more pronounced in the 1950–1980 period, except in those regions specialising in stockless crop farming, such as the Seine Basin (Fig. 5-3Fig. 5-4). The Great West, specialising in intensive livestock farming, dependent on feed import, showed the highest increase in livestock density (Le Noë et al., 2018). Differences among regions stabilised after the 1990s (Fig. 5-4).

5.3.2. Agricultural features

We chose three dates (1906 as a reference for traditional agriculture in France, 1970 characterising the beginning of modernisation and 2014 for evidencing the results of specialisation). These agricultural features are mapped for all 33 regions.

Cereal crop production and livestock density. The specificity of the French regions was already in place in the early 20th century with the northern half of France producing 10–25 kgN ha^{-1} yr^{-1} embedded in the harvested grain, similar to two other regions in the South (West: Garonne; East: Grand Marseille). Ile-de-France already distinguished itself as the most productive (Fig. 5-4a). At this time in 1906, the regions with the highest livestock density were generally associated with those with high cereal production, showing the importance of the crop–livestock connection at that time. Specialisation had already appeared in 1970, with an intensification of cereal production in the Seine Basin and a rise in livestock breeding most particularly in Bretagne and Loire Amont. In 2014, the decoupling between crop production and livestock is striking: one map is almost the opposite of the other (Fig. 5-4b).

Percentage of permanent grassland and forest. Except in the Seine Basin, grassland was present over the entire country in 1906, occupying up to 60–80% of the total agricultural area in the South-Eastern quadrant of France (Fig. 5-4c), and in some other regions with (Manche) or without (Pyrénées) high livestock density. In the 1970s, this trend was accentuated, whereas in 2014 grassland was regressing everywhere. The overall forest area increased in proportion throughout the 20th century but more in the South-East of France and the South-Western border of the Massif Central (Fig. 5-4d).

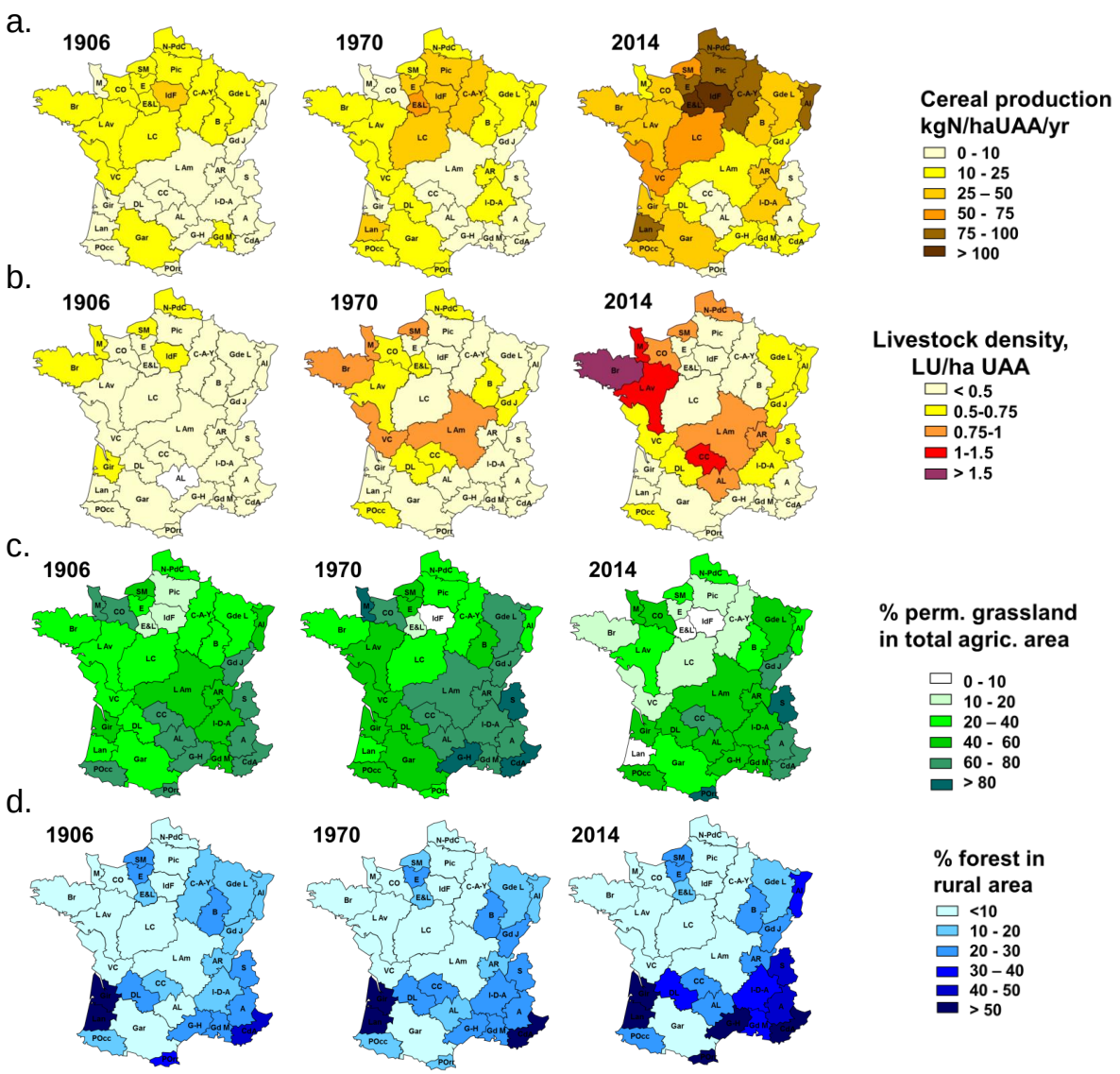

Fig. 5-4. Maps of regional distributions in France for three dates (1906, 1970, 2014) representative of major time periods: a. cereal production; b. livestock density; c. percentage of permanent grassland in total agricultural area; d. percentage of forest in rural area (i.e. cropland + grassland + forest). UAA, utilised agriculture area.

A: Alpes; Al: Alsace; AL: Aveyron-Lozère; AR: Ain-Rhône; B: Bourgogne; Br: Bretagne; C-A-Y: Champagne-Ardennes-Yonne; CC: Cantal-Corrèze; CdA: Côte d'Azur; CO: Calvados-Orne; DL: Dordogne-Lot; E: Eure; E&L: Eure-et-Loire; Gar: Garonne; Gd J: Grand Jura; Gd M: Grand Marseille; Gde L: Grande Lorraine; G-H: Gard-Hérault; Gir: Gironde; I-D-A: Isère-Drôme-Ardèche; IdF: Ile de France; L Am: Loire Amont; L Av: Loire Aval; Lan: Landes; LC: Loire Centrale; M: Manche; N-PdC: Nord Pas-de-Calais; Pic: Picardie; Pocc: Pyrénées Occidentales; POr: Pyrénées Orientales; S: Savoie; VC: Vendée-Charentes.

5.3.3. Distribution of GHG emissions over the long term

N_2O. By construction, N_2O emissions by cropland, grassland and forested areas (the sum of their surface areas forms the rural area, in km²) reflect the long-term spatial and temporal variations in temperature, rainfall and fertilisation of agricultural land. The highest value (75–125 kg N-N_2O km^{-2} yr^{-1}) found for Ile-de-France in 1906 was typically related to its early use of mineral fertilisers (Fig. 5-5a), whereas the values for Côte d'Azur would be more a combination of fertilisation and temperature/rainfall. The same can be said for the North of France region on the one hand and the South and Center of France regions on the other hand, for the 50- to 75-kg N-N_2O km^{-2} yr^{-1} category. For a majority of regions, N_2O emissions showed a great increase in the 1970s, recently reaching or exceeding 250 kg N-N_2O km^{-2} yr^{-1} in 2014, i.e. doubling over the 20th century.

CH_4. The distribution of C-CH_4 emissions in time and space, even more than the livestock density map, clearly reflects the patterns of intensification and specialisation that persisted for the whole period studied (Fig. 5-5b). In brief, a large ring of high emissions was emerging in 1906 around the Seine Basin and was accentuated in 1970 and even more in 2014, when livestock density was reduced giving way to intensive cropping. From emission values generally lower than 2000 kgC-CH_4 km^{-2} yr^{-1} in 1906, they increased to above 6000 kgC-CH_4 km^{-2} yr^{-1} in the regions specialising in intensive livestock farming.

CO_2. The highest emissions of CO_2 in 1906 are directly linked to the small amount of fossil fuels used for mineral fertilisers because no mechanisation and no feed import were considered (Fig. 5-5c). The 1970 map resulted from the post Second World War (WWII) increase of all items taken into account in the calculation (fertiliser production, fossil fuels used for field work, machinery and feed import) the proportion of which was modulated from one region to another according to their rate of modernisation and specialisation. For example, in 1970 feed import concerned essentially Bretagne, Nord-Pas-de-Calais and Loire Centrale, also affected by high fertilisation and mechanisation. In 2014 the highest emissions in Bretagne typically related to increasing feed imports from South America (Billen et al., 2011; Le Noë et al., 2016).

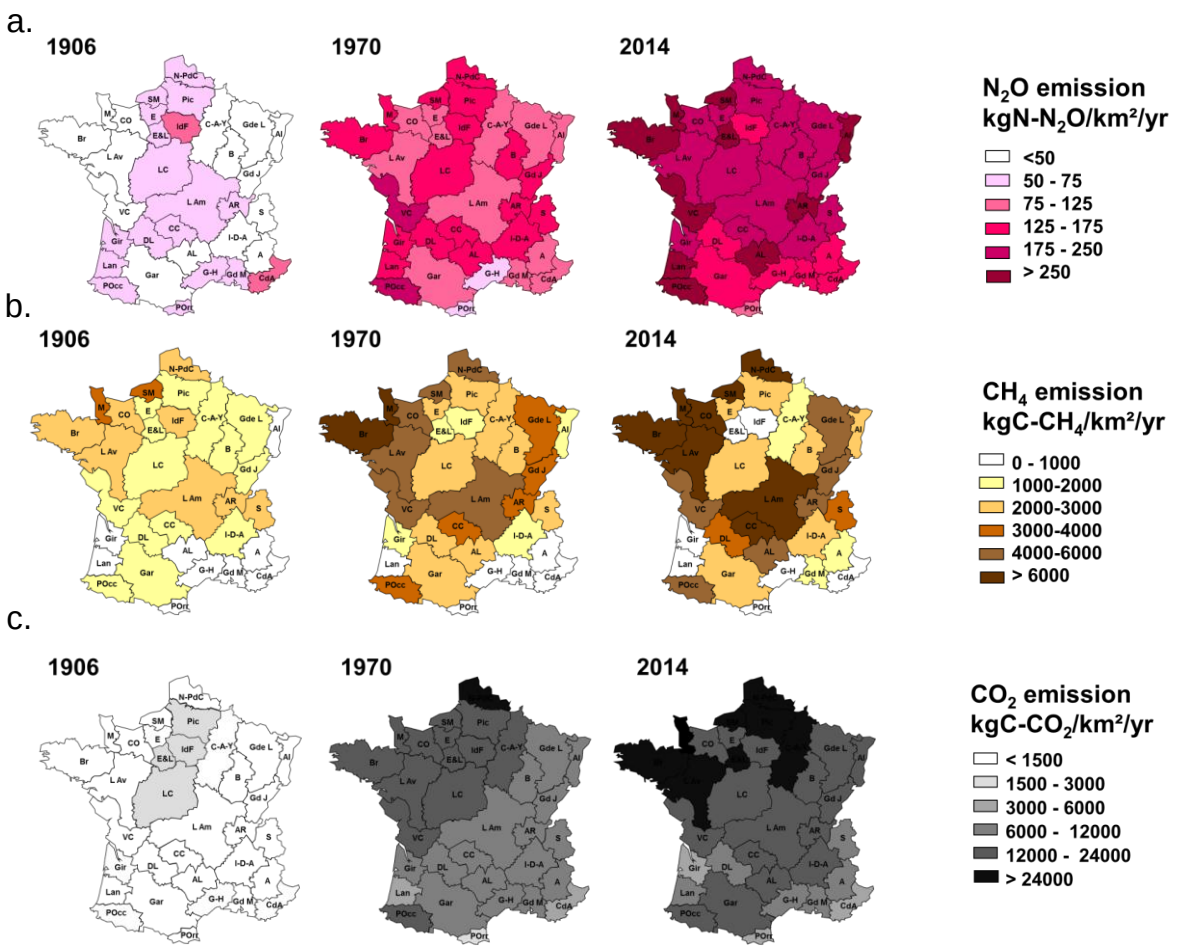

Fig. 5-5. Maps of regional distributions in France for three dates (1906, 1970, 2014) representative of major time periods of GHG emissions per km^2 of rural areas and per year: a. N_2O; b. CH_4; c. CO_2. See legend of Figure 4 for the names of the regions.

5.3.4. Estimating GHGs under contrasted scenarios

For the O/S scenarios all GHG emissions would increase considerably (Fig. 5-6). The approximately 20% increase of N_2O emissions for the entire French territory would not be related to nitrogen synthetic fertilisers, which are not increasing significantly owing to environmental regulations, but rather to manure application in livestock farming regions (Billen et al., 2018a). The Seine Basin, as well as other regions such as Alsace and Landes, emptied of their livestock under extreme specialisation into stockless crop farming, would emit only very low CH_4 while the rest of France would show as high emissions as the most current emitting regions (> 6000 kgC-CH_4 km^{-2} yr^{-1} (Fig. 5-6) because they have reached the maximum authorised livestock density (European Nitrate Directive (91/676/CEE), i.e. 2 LU ha^{-1} of agricultural area). CO_2 emissions would concomitantly increase mostly in breeding

areas, due to feed imports, necessary after a loss in grassland and increased livestock density, in addition to C-CO_2 from fuel consumption and fertiliser production.

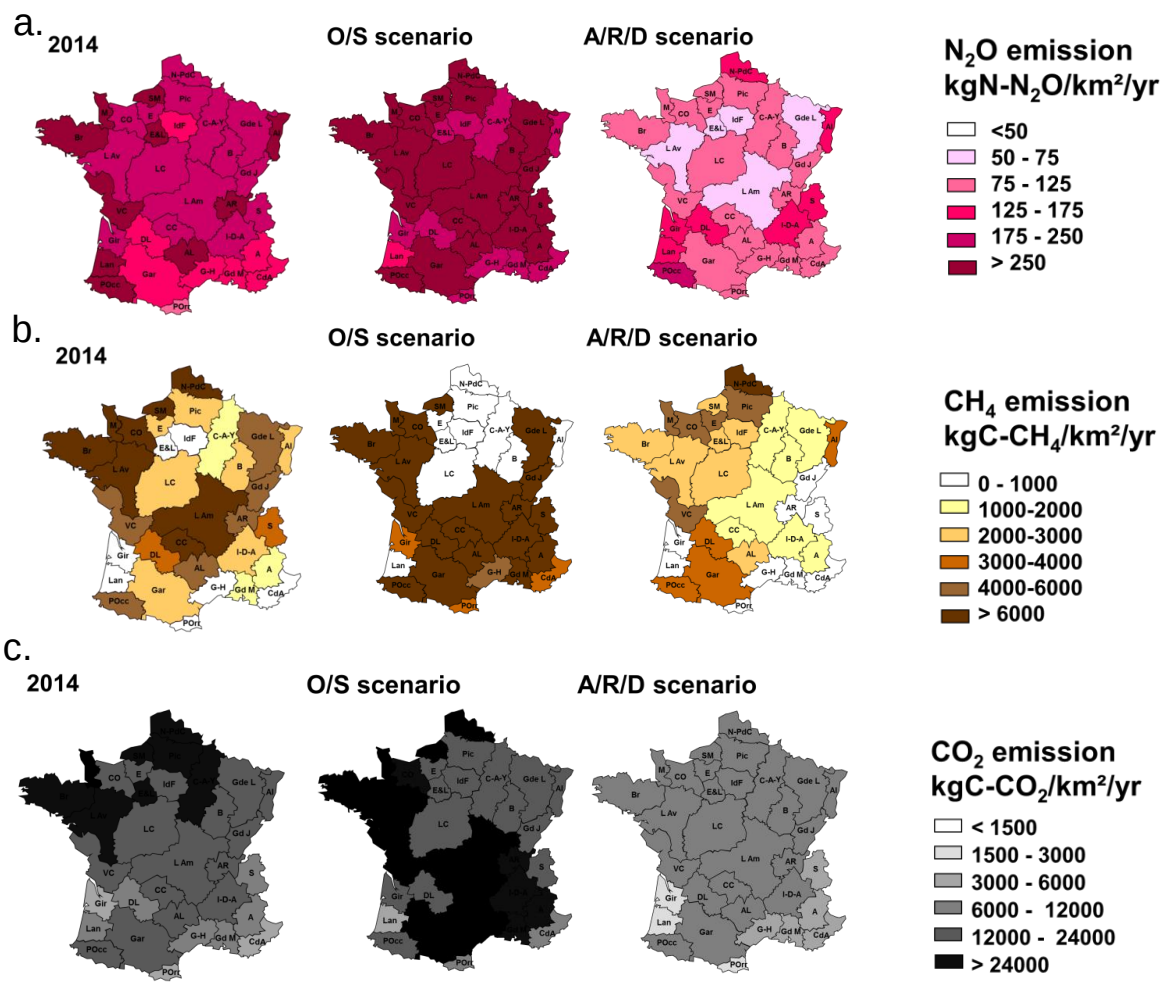

Fig. 5-6. Maps of regional distributions in France for present (2014) and for two prospective scenarios (O/S: opening and specialisation and A/R/D) of GHG emissions per km^2 and per year: a. N_2O; b. CH_4; c. CO_2. See legend of Figure 4 for the names of the regions.

Under the A/R/D scenario, the reduction of GHG emissions would allow a "return" to the emissions before the heavy industrialisation of the 1970s and even 1955 (see Fig. 5-7) depending on the regions. The A/R/D scenario showed that (i) autonomy with respect to synthetic mineral fertilisers would significantly reduce N_2O emissions, (ii) the decrease in animal loading to meet local feed autonomy would lower CH_4 emissions and (iii) CO_2 emissions would be also considerably lowered due to lack of both synthetic fertiliser use and feed imports (Fig. 5-6). This would allow France to achieve GHG emission targets committed to within the COP-21.

The results of these two scenarios for the three GHGs were put into perspective with their respective historical trajectory for the whole nation and for the three regions selected to distinguish the origin of emissions. We thus corroborate our choice of the three dates illustrating three periods: 1906 for its traditional agriculture (until 1955), the 1970s for this period's transitional status, and 2014, typical of intensive production and specialisation since the 1980s.

Whatever the date, croplands were the major N_2O emitters compared to forests and grasslands, especially in the Seine Basin and the Great West (Fig. 5-7), whereas the O/S scenario would not significantly change the pattern and the level of N_2O emissions for these two emblematic specialised regions. The Great South-West, assumed to develop high livestock density, hence imported feed, while optimising its crop production in this scenario, would not only increase N_2O but all three GHG emissions. Concerning CH_4, enteric fermentation dominated CH_4 emission, which overall accounted for 70% of the total, and manure (30%) increased in proportion in the O/S scenario for the Great West, traditionally livestock oriented, but also in the Great South-West, as shown by the fourfold increased CH_4 emissions. For CO_2, concomitantly and consequently, imported feed was the dominant emitter sector in the Great West, which would remain so in the O/S scenario, differently from the Great South-West which, as for cropping, revealed its potential for more livestock, and imported feed, with more CO_2 emissions (Fig. 5-7).

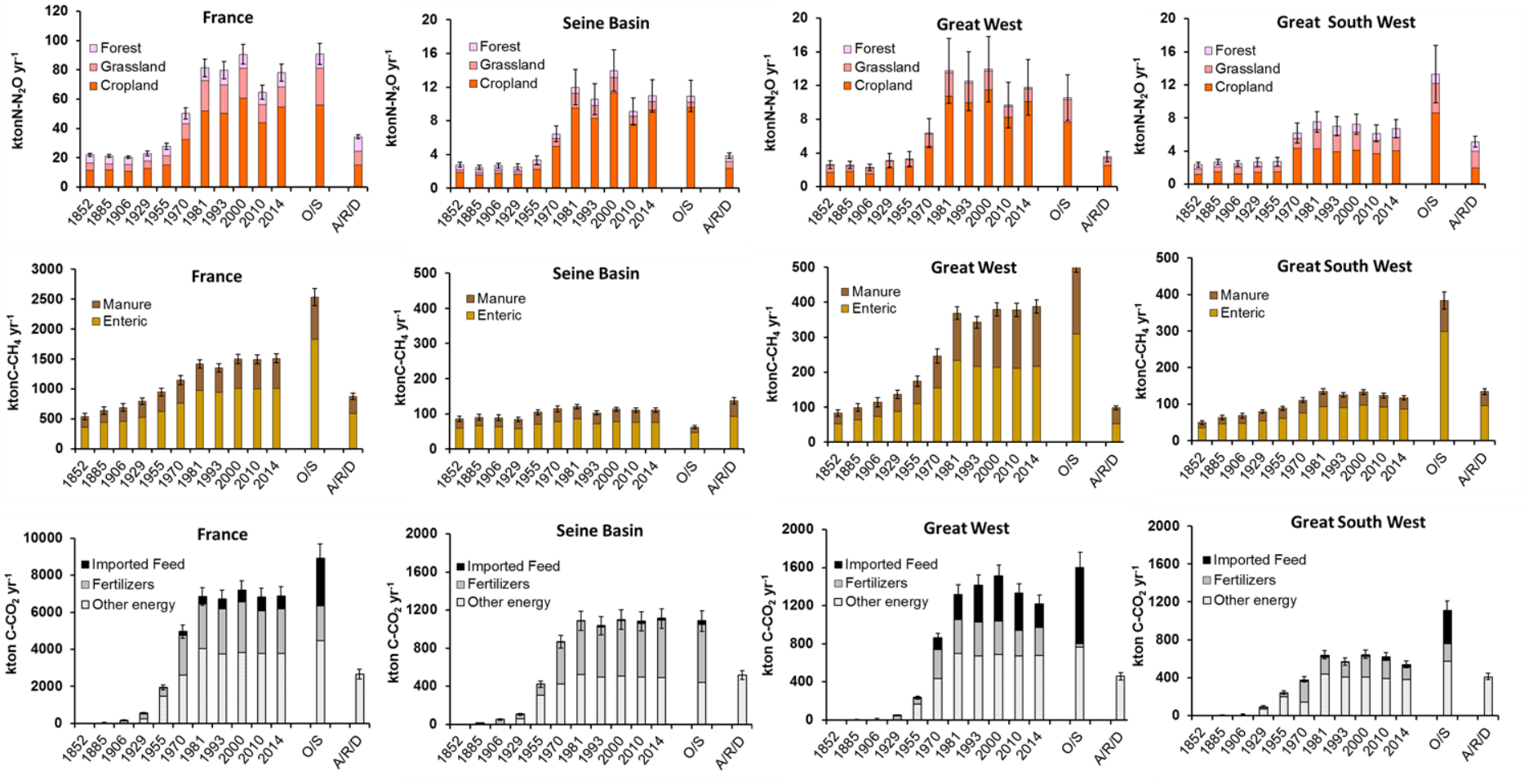

Fig. 5-7. Long-term evolution (1852–2014) for France (a.) and the three selected supra-regions (b., c., d.) in annual average of N_2O, CH_4 and CO_2 from top to bottom. N_2O is represented for the three major land uses (forest, grassland and cropland), CH_4 for manure and enteric emissions, and CO_2 as energy for imported feed, fertiliser production and other energy, including field work, machinery and livestock breeding. Error bars provide uncertainties as calculated by the Monte Carlo analysis.

5.3.5. Comparative agricultural GHG emissions in CO_2 equivalent

The GHG emission can be calculated in a single unit (CO_2 equivalent, CO_2 Eq) by multiplying the global warming potential (GWP) of the different sources with their respective emissions. CO_2 taken as a reference has a GWP of 1, whereas N_2O and CH_4 GWPs are, respectively, 265 and 28 times the CO_2 GWP using the 100-year GWP (IPCC, 2014). Total agricultural emissions for France amounted to 113,939 ktons CO_2 Eq yr^{-1} for the 2010s, with 49% CH_4, 29% N_2O and 22% CO_2 (Fig. 5-8a; Table 5-4). Regarding the three selected regions, similar in area, the Great West emissions were twice those of the other two, with the highest proportion in CH_4 (59%). N_2O emission dominated in the intensively cropped Seine Basin (37%) and CH_4 in the Great South-East (48%). Whereas the O/S scenario would increase overall GHG emissions almost 1.5 times for France, the increase would be about 1.2 for the Seine Basin and the Great West, but emissions would explode for the Great South-West with a 2.5-fold increase. With no mineral fertilisation and extensive livestock breeding, the A/R/D scenario would lower emissions by 50% for France, 36% and 76% for the Seine Basin and the Great West, respectively, but emissions for the Great South-West would only decrease by 11% (Fig. 5-8 b–d; Table 5-4). Note that, taking into account a 20-year GWP, i.e., 265 for N_2O and 84 for CH_4 (IPCC, 2014), would double the total emissions at the scale of France, CH_4 then representing about 75% of the total for the 2010-2014 period, and up to 80% for both scenarios.

When expressed per km² of surface area, agricultural GHG emissions ranged from 148 to 408 tCO_2 eq km^{-2} yr^{-1} for the Great South West and Great West regions respectively, the GHG for the Seine Basin being close to the national value (Table 5-4). For comparison, agricultural GHG emissions were 3.4, 2.4, 1.3 times higher than the French ones for the Netherlands, Belgium and Germany, but 2.0, 1.8, 1.7, 1.6 times lower for Spain, Romania, Austria and Slovenia, respectively (EAA, 2018).

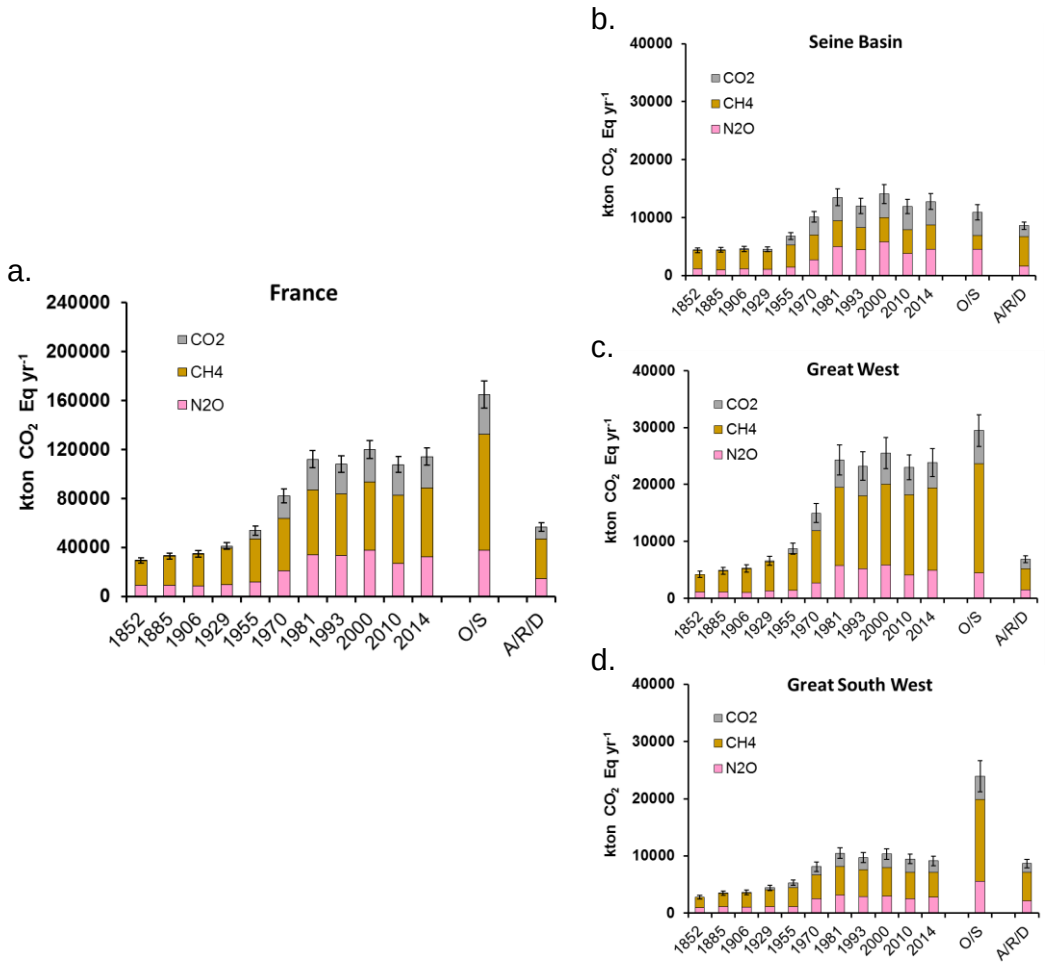

Fig. 5-8. Long-term evolution (1852–2014) for France (a.) and the three selected supra-regions (b., c., d.) in annual average of N_2O, CH_4 and CO_2, expressed in CO2 equivalents per year. Error bars provide uncertainties as calculated by the Monte Carlo analysis.

Table 5-4. Total GHG emissions from agriculture in France and in the three supra-regions considered, given in CO_2 equivalent. Specific GHG emissions ($tCO_2\ km^{-2}\ yr^{-1}$) are provided for comparison. Relative contributions of N_2O, CH_4 and CO_2 are also shown.

CO_2 Eq		**2000-2014**	**O/S scn**	**A/R/D scn**
France	% N_2O	28	23	25
540498 km²	% CH_4	49	57	58
	% CO_2	22	20	17
	$ktCO_2\ yr^{-1}$	**113939**	**165010**	**56678**
	$tCO_2\ km^{-2}\ yr^{-1}$	**211**	**305**	**105**
Seine Basin	% N_2O	37	42	20
69713 km²	% CH_4	32	21	62
	% CO_2	31	37	18
	$ktCO_2\ yr^{-1}$	**12909**	**10872**	**8246**
	$tCO_2\ km^{-2}\ yr^{-1}$	**185**	**156**	**118**
Great West	% N_2O	20	15	23
59109 km²	% CH_4	59	65	57
	% CO_2	21	20	19
	$ktCO_2\ yr^{-1}$	**24123**	**29471**	**6397**
	$tCO_2\ km^{-2}\ yr^{-1}$	**408**	**499**	**108**
Great South-West	% N_2O	29	23	25
65437 km²	% CH_4	48	60	59
	% CO_2	23	17	17
	$ktCO_2\ yr^{-1}$	**9662**	**23937**	**8582**
	$tCO_2\ km^{-2}\ yr^{-1}$	**148**	**366**	**131**

5.4. Discussion

Greenhouse gas emission estimates are known to be highly uncertain, due to the complexity of their controlling factors at the local scale and the difficulty of measuring them on-site as well as due to the lack of uniform information on how highly diverse farming practices may impact net GHG balances. Consequently, the scientific community is encountering problems formalising mechanistic models to estimate GHG emissions (e.g. NOE, DNDC, Gu et al., 2014; Gilhespy et al., 2014; Zimmermann et al., 2018), for upscaling local emissions measurements to larger scales, from local areas to countries. Since the level of detail needed for a wide regional and long-term estimation could make the modelling unfeasible, the approach used here is more a budgeting one, based on activity data from agricultural census

and emission factors determined on a rather detailed analysis of the controlling factors of N_2O and CH_4. For these two GHGs, our calculations allow linking plot-scale measurements or animal physiology to the regional and country scale. CO_2 emission estimates are still rough, although explicitly taking into account several contributions, mostly upstream of the production system, but in line with the Climagri approach for France (Doublet, 2011) and other studies (e.g. Canada, Dyer and Desjardins, 2009, and Spain, Aguilera et al., 2015).

5.4.1. Controlling factors of GHG emissions

To explore strategies to reduce GHGs from agriculture, identifying, quantifying and understanding the factors which control their producing processes, from biotic to abiotic, from microbial to industrial, are challenging.

N_2O. In temperate systems, denitrification is considered the major microbial process at the origin of N_2O emissions in soils, mostly under temperate and highly humid conditions(Benoit et al., 2015; Vilain et al., 2014; Gu et al., 2014). In contrast, nitrification plays an important role in Mediterranean and semi-arid regions (e.g., Sanz-Cobena et al., 2012; Aguilera et al., 2013). The factors affecting denitrification in soils have been largely reported in the literature (see Tiedje, 1988; Groffman, 1991; De Klein et al., 2001, for example). Following Saggar et al. (2013), who distinguished two types of controlling factors, namely (i) soils and plant factors (crops, soil mineral nitrogen, pH, water content and oxygen, carbon availability, C:N ratios) and (ii) environmental factors (temperature, rainfall, drying/wetting vs freezing/thawing), the variables we considered for our prediction relationships (N input, land use and climatic conditions [temperature and rainfall]) covered these two types of factors. Generally considered to be the major controlling factors of N_2O production in soils, under both nitrifying and denitrifying conditions (e.g. Snyder et al., 2009; Schmitz et al., 2012; Kirschbaum et al., 2012; Sanz-Cobena et al., 2017), these variables are the best documented in the literature for achieving such a long-term study.

Our approach is a step further in the use of the Tier 1 emission factor (IPCC 2006- Eggleston, 2006), which has been found too coarse for correctly representing N_2O emissions possibly underestimated in wet areas (Lu et al., 2006 and reference herein) but overestimated in Mediterranean regions (Aguilera et al., 2013; Cayuela et al., 2017). The approach we developed here is advantageous for its low requirement in complex agronomic data, given that

temperature and rainfall are routinely surveyed everywhere and fertilisation commonly quoted in agricultural statistics.

However, taking into account the annual scale of our study, pulses of N_2O emissions cannot be represented as observed after fertiliser applications (Bouwman, 1996; Hénault et al., 1998; Laville et al., 2011; Plaza-Bonilla et al., 2014; Benoit et al., 2015; Recio et al., 2018), rainy events (Zheng et al., 2000; Lu et al., 2006; Beare et al., 2009) and during freeze and thaw periods and rewetting in semi-arid regions (Vilain et al., 2010 ; Lu et al., 2015 ; Wertz et al., 2016; Sanchez-Martín et al., 2010). However, the N_2O emissions data gathered here were selected for their annual representativeness, thus already integrating seasonal variability. Spatial and long-term variations can be expected through the heterogeneous distribution in both rainfall and temperature in the country (cf. Fig.5-1a) and fertiliser applications depending on soil characteristics, which condition the technical orientations of the farms (cf. Fig.5-1b). N_2O emissions related to manure management were not taken into account in the calculations), because they account for only a few percent of GHGs emitted from livestock, i.e., 2.94% in CO_2 Eq according to the review by Zervas and Tsiplakou (2012).

CH_4. Methanogenesis is a microbial process producing CH_4 mainly under anaerobic conditions. Enteric fermentation by grazing animals is the major process producing CH_4, although losses from manure management is far from negligible, far above the net CH_4 flux in the soil. Although agricultural soils can be a sink for this GHG, as a result of the balance between methanogenesis and methanotrophy (microbial CH_4 consumption) (Dutaur and Verchot, 2007; Kirschbaum et al., 2012), this function of oxidation by soils has been reduced with the intensive use of fertilisers. Ammonium inputs, increasing nitrifying activity, would exclude methanotrophs from their ecological niche, which even when fertilisation ceases would not quickly recover (Lemke et al., 2007; Ball et al., 2002; Boeckx and Van Cleemput, 2001; Schnell and King, 1994). In addition, soil cultivation and change in soil structure would restrict diffusion sites, thus affecting CH_4 oxidation (Dobbie and Smith, 1996). Experimental measurements in the Seine Basin showed that CH_4 removal could account for 5.6% of the emissions by livestock (Garnier et al., 2013b). The CH_4 depletion rate was the highest for grassland soils (1.27 mg C m^{-2} d^{-1}) followed by forest (0.7 mg C m^{-2} d^{-1}) and cropland (0.4 mg C m^{-2} d^{-1}). Interestingly, the riparian zones, which were alternatively a source or a sink, overall emitted 0.1 mg C m^{-2} d^{-1} methane.

Considering the low proportion of CH_4 removal by soils compared to the emissions from livestock, even when it was half as much on average than currently for the long 1850–1950 period, we can consider that neglecting soil sink would not lead to overestimation of CH_4 emission in the past. Further CH_4 sink would account for about 2% of N_2O emissions from soils in CO_2 equivalents (Boeckx and Van Cleemput, 2001).

Enteric fermentation was estimated here to be responsible for 70% of CH_4 emissions in France, 30% originating from manure management, with a similar proportion over the time period studied, resulting in a proportion of enteric fermentation lower than the figure provided globally as being responsible for 83% of CH_4 emissions (Zervas and Tsiplakou, 2012). As reported by these authors, ruminant CH_4 production may depend on many factors including diet (fibrous content of the ration), enteric flora, while more generally CH_4 production is influenced by farm management and the farm production system.

In this study, we did not intend to finely characterise CH_4 production from livestock as reported in the study mentioned above (and references therein) but rather used the IPCC Tier 3 guidelines (IPCC 1997 - Houghton et al., 1997), according to specific emissions (enteric and manure) for 19 categories of livestock and related to animal body weight over the period studied (see Methods section).

CO_2. An increasing greenhouse effect is currently dominated by the increase in CO_2 concentration derived from fossil-fuel consumption, clearly the compound responsible for the enhanced greenhouse effect (Forster et al., 2007). At the scale of the Seine Basin, CO_2 emissions account for 79% of the total emissions (agricultural and non-agricultural), 72% of which come from non-agricultural sectors (Marescaux et al., 2018b). Similar figures were provided by CITEPA for France (i.e. 78% and 75%, respectively, in 2014 (https://www.citepa.org/fr/activites/inventaires-des-emissions/secten). Regarding the three GHGs, the CITEPA figures showed an approximately 20% underestimation for the agricultural sector (90,000 ktons CO_2 eq.yr^{-1} versus 114,000 ktons CO_2 eq.yr^{-1} here), due to an underestimation of CO_2, fertiliser production, and machinery manufacture, for example, accounted for in the industrial sector rather than the agricultural sector.

The coefficients from Doublet (2011) (Table 5-3) are quite comparable with other approaches (Bochu, 2006; Aguilera et al., 2015). For all of France, we showed that a large amount of CO_2 emissions (35%) is linked to the energy supply for production of commercial chemicals. CO_2

emissions from feed to livestock accounted for 10% for France, but 20% for the specialised Great West. These emissions are generally ignored in most studies, including national inventories. “Other energy” (i.e. fuel for farm fieldwork, electricity for on-farm operations and energy for machinery appeared to be the largest emitter sector (55%). Farm machinery manufacturing energy, a significant part of total CO_2 emissions (13% in 2014 with spatial differences) from agriculture has been roughly taken into account in this paper, but could be included in future research with greater detail (taking into account for example the number of tractors and their power, etc.). This percentage is lower than the farm machinery percentage reported for US corn farms for all Canada, accounting for 15% of the direct CO_2 emissions in the US (Patzek, 2003) and 19% in Canada (Dyer and Desjardins, 2009).

5.4.2. Past long-term changes in GHG emissions: practice and land use changes

Agriculture in France until the late 19th and early 20th centuries was characterised by a traditional family-based agriculture, with low external requirements (mechanisation, electrical power, etc.). Whereas the number of farms was around 5.5 million during the second-half of the 19th century, this number decreased to 2.3 million in 1955, with an increase in the size of farms, although small ones still dominated. During this period, only slow changes occurred in terms of the indicators selected, however (see Fig. 5-3, exogenous fertilisers and livestock including horses). Accordingly, N_2O and CO_2 emissions remained rather stable while CH_4 increased slowly, due to a slow but general increase of livestock density within integrated crop–livestock farming systems.

A second period can be identified after WWII when indirect energy inputs in agriculture started with the war materials industry and chemicals were reoriented to agricultural goods (e.g., fertiliser production through the Haber-Bosch process) and intensification of tractor manufacturing (and other agricultural machinery) . This initiated 3 decades of continuous growth with cheap fossil energy and expanding global food markets (Dyer and Desjardins, 2009). French farms decreased in number by a factor of five by 1980 (i.e. 1 million), intensified their production, with a strong dependence on mechanisation, industrial fertilisers, pesticides and imported feed. GHGs reached their maximum in the early 1990s, when the Rio conference (1992) alerted the world to the strong deterioration of the environment, including GHG emissions.

Despite continuing intensification and specialisation, the third period, from the mid-1990s to the present, showed a stabilisation in GHG emissions and even a tendency to decrease (N_2O especially, see Fig. 5-7Fig. 5-8). Even before the Rio conference (1992), the use of mineral fertilisers – a major driver for N_2O emissions – was reduced in France (see Lassaletta et al., 2014), since the nitrate directive (91/676/CEE) was promulgated for water resource protection. At this time, the data show that ruminants were reduced by 10%, slightly more in the specialised Great West in livestock breeding (17%). During this period, the number of farms still decreased (664 000 in 2000, 452 000 in 2013), with small farms the most affected (Agreste, 2013). Between 1993 and 2014, we calculated a net loss of 1.2 million ha (1.53 million ha lost as permanent grassland and 0.33 million ha gained in cropland, with forested areas stable during this time).

Land use changes are reported to have modified the flux of CO_2, CH_4 and N_2O through altered biogeochemical processes (Forster et al., 2007; Houghton et al., 2012; Kirschbaum et al., 2012; Tate, 2015). For example, according to Kim and Kirschbaum, (2015), conversion from natural forest to cropland or grassland would increase net emissions by 7.3±0.6 or 5.9±0.3 t CO_2 eq ha^{-1} y^{-1}, respectively, while conversion of cropland or grassland to secondary forest would decrease emissions by 5.3±0.9 or 3.6±0.7 t CO_2 eq ha^{-1} y^{-1}, i.e. figures on the same order of magnitude, although the delay in losses/recoveries might not be similar.

Between 1929 and 2014, 3.3 and 1.8 million ha of permanent grassland and cropland, respectively, have changed use whereas 7.7 million ha were gained as forested area, representing a total loss of 2.6 million ha of these total rural areas. We considered 1929 as the first date of French border stability after the Alsace and Lorraine regions were reattributed to France in 1918. Most of these land use changes were implicitly taken into account in our calculations. However, the possible loss of sink function by soils for CH_4 under increased fertilisation was not accounted for (Boeckx and Van Cleemput, 2001). We also did not consider wetlands as possible CH_4 emitters, which were lost after their conversion to agricultural and other land uses (Zedler and Kercher, 2005; Verhoeven and Sorrell, 2010).

5.4.3. Contrasted scenarios for a possible future

The scenarios (Billen et al., 2018a) explored here for GHG emissions were inspired from prospective documents elaborated at different regional, national and European levels (Poux et al., 2005; Solagro, 2014; Poux and Aubert, 2018) and also took into account other published results for the global scale (Schmitz et al., 2012; Erb et al., 2016; Muller et al., 2017).

The pursuit of intensification and specialisation in the O/S scenario, despite taking into account the current regulations, would, at a national scale, increase GHG emissions as a whole, but also each of the three GHGs considered separately. Some regional differences would appear however. Whereas increased N_2O emissions would be generalised over the 33 regions, CO_2 and especially CH_4 would be lower in the regions dedicated to cereal production, with no livestock as predicted for the Seine Basin. In most other regions, livestock would increase CH_4 and its associated feed production would impact CO_2, in accordance with the approach. This scenario, although credible taking into account the current trends of opening the agro-food system (Le Noë et al., 2016), would not be desirable for the environment, and specifically here for GHG warming, as stated by the last, recently published in the IPCC report (2018). This economic desire for growth, which is highly dependent on the international market, facilitating trade exchanges, is fully present in political discourse. This vision of the future of French agriculture devoted to cereal exportation driven by powerful food sectors, animal production oriented to milk powder export in industrial breeding farms and a human diet with a high ratio of animal proteins is in line with many documents coming from professional farmer organisations as well as Harbour Authorities (CRAN, 2006; Dreal, 2014; Benhalima, 2015; HAROPA, 2015). Furthermore, the emergence of the bio-fuel industries (mainly ethanol from sugar beet and biodiesel from rapeseed) is a paradigm that agriculture will have to face in future decades, even for energy consumption of the farm itself. It is worth mentioning that in this O/S scenario, the livestock structure was kept constant, since French livestock is traditionally dominated by cattle, despite a trend, at the global scale, to shift animal production from ruminants to non-ruminants, which could possibly reduce CH_4 emissions and CO_2 from feed (Westhoek et al., 2014).

Contrary to this vision of France fully involved in globalisation, the A/R/D scenario (Billen et al., 2018a) amplifies the weak signals observed in recent years, showing the emergence of a new relationship to nature for a sustainable development, from which proactive policies could emerge. Due to several food crises (e.g. the mad cow problems in 1996, dioxin contamination

in 1999, the *Escherichia coli* outbreak in 2011, among the most publicised events), increasing numbers of consumers are demanding healthy food products. At the same time, farmers exposed to chemical products are concerned by health issues, victims either themselves or family members and neighbours.

In this context, the A/R/D scenario explores alternative agro-food systems which (i) generalise organic farming practices banning exogenous mineral fertilisers and pesticides, (ii) favour local supply and (iii) decrease animal protein consumption in the diet, while reducing food waste. Although not fully realistic over the short term, this scenario becomes desirable for the health of people and the environment. For this scenario total production of plant and animal products are reduced, but this reduction is compensated by a reduction in the demand associated with dietary changes (see Billen et al., 2018a). The A/R/D scenario, despite requiring a deep structural change of the agro-food system, shows a significant reduction of GHGs, i.e. 50% for the French agricultural sector compared to the 2010–2014 period, more than one-third of the total reduction advocated. Interestingly, this scenario, beneficial in terms of GHGs, has also been shown to improve water quality and to prevent the risk of coastal eutrophication (Desmit et al., 2018; Garnier et al., 2018).

5.4.4. Weaknesses and strengths of the approach

Agricultural statistics have been rather well documented in France since the mid-19th century, at the scale of the French “départements” (Poisvert et al., 2017; Le Noë et al., 2018; see also Garnier et al., 2014, 2016 for local studies), and hence the entire country (Harchaoui and Chatzimpiros, 2018), and provide realistic pictures of the changes occurring in the agricultural sectors for indicators such as fertiliser inputs, crop production, livestock units, etc.

The estimate of GHGs from these data is more ambitious given that no statistics exist for the past at this regional resolution. The task was the most difficult for N_2O due to variability in the emission factors even for the present. Indeed, direct N_2O emissions in agricultural fields occur essentially with great spatial and temporal variabilities related to many factors (soil parameters, crop species, agricultural practices, rainfall and water management, amount and type of fertilisation, etc.; Lu et al., 2006; Bouwman et al., 2013; Cayuela et al., 2017). Here, taking into account the accompanying N_2O data in the literature, and the data available over the long term, previous N_2O data mining (Garnier et al., 2009) was enlarged for the main land uses (forest, grassland and cropland), gathering temperature, rainfall and fertilisation, three

major variables that were analysed for the past. Even though soil parameters were often documented in the papers examined, they were not included due to the lack of a homogeneous description in the studies considered. Because grassland studies, similar to cropland, reported fertiliser applications either though external inputs or grazing animals, N_2O emissions for these two land uses were grouped under the same relationship. The relationship for forests was established with fewer data. Overall the evaluation of both relationships in terms of NRMSE and bias is quite good.

Regarding CH_4, the uncertainties may be more related to changes in the size of the animals over time, modifying the figures documenting CH_4 emissions from enteric fermentation and manure management for the present. By applying a factor of change on the basis of a reconstruction of excretion for the major types of animals, we can consider that CH_4 emissions from livestock farming must be robust for the past. CH_4 emissions and oxidation from soils were not taken into account given that soils are known to be low emitters (Garnier et al., 2013; Kandel et al., 2018), which must be true for the period studied, because ecosystems such as wetlands, ponds, etc. had already been considerably reduced in the landscape, for health issues and for conversion of these lands into cultivated areas (Zedler and Kercher, 2005; Verhoeven and Sorrell, 2010).

The estimates for CO_2 are more indicative, because we only took into account its emissions related to field and on-farm work, fertiliser use, CO_2 emissions from machinery and CO_2 emissions linked to feed imports, applying coefficients reported in the literature based on a full material flow analysis (Doublet, 2011; see also Aguilera et al., 2015).

However, the approach allows reflecting regional differences and, differently from an overall national estimate, provides a variable range of GHGs related to the details of specific characteristics and possible transitions for each region.

For the whole of France, our approach fits rather well with the national agricultural inventories (Doublet, 2011) reporting ~114,000 ktons CO_2 eq. yr^{-1} (2010–2014) emitted from agriculture versus ~103,000 ktons CO_2 eq. yr^{-1} (for 2006); the percentages we found for N_2O, CH_4 and CO_2 (29%, 49% and 22%, respectively) can be compared with the 39%, 44% and 17%, respectively, found in Doublet (2011). Interestingly, carbon sequestration by agricultural soils, amounting to 6,200 ktons CO_2 eq. yr^{-1} for France (Le Noë et al., 2018), accounts for only ~5% of our GHG emissions.

5.5. Conclusions

An analysis of the controlling factors of GHG emissions (land use, rainfall, temperature) together with the GRAFS approach gathering key variables of the agro-food system at any temporal and spatial resolution (fertilisers, livestock, crop production, etc.) made it possible to estimate N_2O, CH_4, CO_2 emissions at the scale of France's 33 agricultural regions.

The period studied, from 1852 to 2014, showed that the increase of GHGs can be divided into three major periods: (i) a long period from 1852 to 1955 with family mixed crop–livestock farming systems still in effect, small in size with very little mechanisation, with emissions increasing from ~30 000 to 54,000 ktons CO_2 Eq yr^{-1}; (ii) a second period of modernisation of French agriculture after WWII, with an increasing dependence on mechanisation, industrial fertilisers, pesticides and imported feed, favoured by fossil energy at a relatively low monetary cost and expanding global food markets, a period corresponding the maximum of GHG emissions, which reached 110,000 ktons CO_2 Eq yr^{-1} in the 1990s and 120,000 CO_2 ktons Eq yr^{-1} in the early 2000s; (iii) and then stabilisation (around 114,000 ktons CO_2 Eq yr^{-1} for 2010–2014) related to the abandonment of government policies directly aimed at intensification, and their replacement by environmental regulations after the Rio conference (1992 - UNCED, 1992) and the following protocols (e.g., Kyoto in 1997-UNFCCC, 1997), which prompted the countries of the world to control or decrease their GHG emissions to avoid the adverse effects of climate change. Progressive spatial specialisation was observed as early as 1906, with regions already characterised by cereal production in the Northern half of France, and in the South-West, others by livestock, such as Bretagne in the West, and still others with a typically low proportion of grasslands, such as in the Seine Basin. This specialisation had an influence on the distribution of emissions in terms of intensity and compounds.

The contrasting scenarios explored showed that a 50% reduction of GHG emissions in the agriculture sector could be achieved with a deep change in the structure of the agro-food system, whereas the pursuit of the present trends of specialisation and intensification associated with international trade, even applying the current environmental regulations, could increase the current GHG emissions by a factor of 1.5.

Acknowledgements

The study was conducted within the framework of several scientific projects, C-Cascades (funded by Horizon 2020 research and innovation program under the Marie Sklodowska-Curie grant agreement No. 643052), HydroGES (financed by the Agency for the Environment and Mastery of Energy, ADEME) and Escapade (supported by the National Agency for Research, ANR). The PIREN-Seine programme and the Fédération Ile-de-France de Recherche pour l'Environnement (FIRE) are also acknowledged for their support. L. Lassaletta acknowledges support from MINECO, Spain, co-funded by the European Commission ERDF (Ramon y Cajal fellowship, RYC-2016-20269).

Supplementary material of this article can be retrieved at:
https://doi.org/10.1016/j.scitotenv.2019.01.048.

.

General conclusion and perspectives

In line with our objectives, this PhD research enabled a better understanding of environmental factors controlling carbon dioxide (CO_2) concentrations in the human-impacted basin of the temperate Seine hydrosystem (i.e., breakdown, discharge, and dissolved organic carbon, among others). These factors were documented based on field work and supplemented with collection and processing of databases in order to incorporate a new inorganic carbon model in the Riverstrahler model. This upgraded version of the model takes into account the inorganic carbon cycle and its interactions with other biogeochemical cycles and the dynamics of aquatic microorganisms.

These improvements, which make it possible to estimate gaseous CO_2 emissions from the river drainage network, were then enhanced as part of a coupled river-estuary modeling approach, leading to the first organic and inorganic carbon budget along the aquatic continuum of the Seine River, based on a joint deterministic modeling of aquatics processes. These CO_2 emissions were compared to other riverine greenhouse gas (GHG) emissions (CH_4-methane, and N_2O-nitrous oxide) as well as agricultural and urban GHG emissions. The fluxes emitted from the basin are included in a recent historical review of agricultural GHG emissions since 1850.

The Seine River: a supersaturated system

Despite the fact that the Seine watershed is now well documented and has benefited from the 30-year Piren-Seine program (a privileged interdisciplinary scientific environment), partial pressure of CO_2 (pCO_2) had never previously been investigated.

The field campaigns undertaken in winter, spring flood, summer-autumn (2016) and spring (2017) in streams draining croplands, forests, grasslands, urban areas, and wetlands showed supersaturation of CO_2 in water with respect to atmospheric equilibrium. Undersaturation of CO_2 was observed only in the Marne reservoir where higher residence time promotes particle sedimentation that reduces turbidity and enhances primary production along with CO_2 consumption.

According to our measurements, groundwaters were significantly more concentrated than streams or rivers. Analysis of pCO_2 controlling factors also showed pCO_2 to be significantly correlated with dissolved organic carbon (DOC) whereas higher instream concentrations were linked to higher organic carbon contents in soils (wetlands and grasslands). These controls of pCO_2 by hydro-climatic and organic soils factors were clearly illustrated by the flood event flushes during the growing season when DOC (spring flood DOC median: 11.44 mgC l^{-1}) and pCO_2 (spring flood median: 3297 ppm) reached their highest values.

In addition to our own measurements, the processing of data from French national monitoring stations of the quality of surface water (Qualit'Eau), groundwater (ADES) or water discharge (Banque Hydro) in the basin represented an important effort. These data confirmed that pCO_2 was significantly correlated with hydro-climatic conditions with seasonal concentrations increasing from winter to summer-autumn related to increased temperature and reduced water discharge. The data also showed that pCO_2 in headwater streams in the upstream parts of the drainage network and the main stem of the Seine River are equally supersaturated in CO_2.

It was also possible to analyze the pCO_2 from a temporal perspective that highlighted recent changes in the Seine River basin and the associated anthropogenic pressures. Long term changes in pCO_2 observed over the 1970–2015 period appear to be controlled by the increase in effluent released from wastewater treatment plants (WWTPs). Indeed, the long-term annual pCO_2 values in the urbanized main stream of the Seine River strictly mirror variations in releases of urban organic matter by the largest WWTPs of the Paris conurbation. The pCO_2 at the outlet of the basin increased between 1970 and 1990 due to the intensification of

wastewater collection. Subsequently, in response to the Urban Wastewater Directive (1991/271/EC) and the Water Framework Directive (WFD, 2000/60/EC), the increase in the number of WWTPs in the Paris agglomeration, and the improvement of processes for treating the OM of discharged effluent, reduced pCO_2 downstream from the main WWTP of the basin. However despite this major reduction in anthropogenic organic carbon inputs, the Seine River remains supersaturated in CO_2.

A modeling approach for quantifying the sources and the fate of pCO_2 in the hydrosystem

A modeling approach at the scale of an entire drainage network requires summarizing a number of different datasets describing both the model inputs, namely: geomorphology, discharge, inputs from diffuse and points sources among the major constraints. Besides nitrogen –N-, phosphorus –P-, silica –Si-, all these constraints needed to be documented in terms of carbon, from inorganic to organic carbon, and from particulate to dissolved carbon. Characterization of diffuse inputs led to a spatially explicit assignment of the mean values of total alkalinity (TA) and dissolved inorganic carbon (DIC) mean values according to homogenous groundwater entities, and land use (for organic carbon only). For point sources, WWTP releases were also characterized with TA and DIC based on a single weighted mean according to our measurements and the WWTP treatment capacity. Collaboration with Veolia Water France, Veolia Research and Innovation and with the "*Syndicat interdépartemental pour l'assainissement de l'agglomération parisienne*" (French acronym - SIAAP), enabled us to collect data from various WWTPs. Such data are rarely measured, but were essential for this work. The gas transfer velocities implemented were retrieved from the literature and adapted to the morphological characteristics of the Seine River.

In parallel with the construction of the model input databases, the core of the biogeochemical model was supplemented with the coding of new formalisms (TA and DIC concentrations evolving according to biogeochemical processes of microorganisms; solubility, water density and pH calculations; CO_2 exchange at the water interface, etc.) and the associated parameters. Once both the mathematical formalizations, and the input constraints were completed, the simulations performed by the model represented both spatial (kilometric) and temporal (10-day time steps) variations in carbon (organic and inorganic) in relation with the dynamics of nutrients and microorganisms that were also simulated throughout the entire hydrological network.

For the recent period (2010-2013) and despite the large uncertainties concerning simulated CO_2 and the variability of observed CO_2 concentrations, the spatial dynamics of CO_2 was simulated in the right range when looking at mean CO_2 concentrations by Strahler orders, and along the main stem. Along the main steam, the simulated trend was in agreement with observations, with peaks downstream from the discharge of effluents from the main WWTPs of the basin. Concerning seasonal dynamics, the model has succeeded in correctly capturing the variability of DIC and TA concentrations that decrease in summer related to the support of low-water by reservoirs. Indeed, reservoirs showed lower concentrations of TA, DIC and were undersaturated in CO_2.

This modeling approach with a detailed description of instream processes enabled quantification of the aquatic metabolism of the basin. Simulated photosynthesis and heterotrophic planktonic respiration increased with Strahler stream orders, as expressed in the river concept continuum. Simulated benthic respiration was higher upstream where biomass associated with streambeds is fed by the subsurface flows that supply nutrients and oxygen and remove metabolic waste than downstream. In addition to the supersaturation of the hydrosystem in CO_2 described based on field campaigns and long term data analyses, net ecosystem production remained negative in the entire basin, highlighting the net heterotrophy of the basin for the recent period simulated.

This new improvement of the pyNuts-Riverstrahler model also makes it possible to calculate the inorganic and organic carbon budgets in the Seine River basin. On average over the period 2010-2013, calculated inputs of DIC reached 17,484 kgC km^{-2} yr^{-1} while in the OC budget, they were ten times lower at 1606 kgC km^{-2} yr^{-1}. The important contribution of the Seine aquifer to the IC flux supplied by groundwater appeared to dominate flows from the subsurface (respectively 57% vs. 34% of total IC inputs), while for OC, the groundwater contributions were lower than the subsurface ones (14% vs. 54% of total OC fluxes). This is due to high OC concentrations in the topsoil and degradation to IC during transfer in deeper layers. The main DIC outputs were DIC exports to the estuary (69%) and outgassing (30%). The outgassing per mirror surface of the river of 108 ± 31 mol C m^{-2} yr^{-1} is in the range of estimates reported in other studies (ranging from 5.8 to 334 mol C m^{-2} yr^{-1} (Li et al., 2013 and references herein, e.g. Butman and Raymond, 2011). Concerning OC, 65% of OC supplied to the river (including both particulate and dissolved forms) were exported to the estuary. Proportionally, instream processes were more important in the OC budget (8% - net primary

production and nitrification) than in the IC budget (less than 2% - net primary production, denitrification, heterotrophic respiration).

Towards the land-to sea continuum

The coupling of the riverine pyNuts-Riverstrahler with the estuarine C-GEM biogeochemical models for the first time allowed simulation of pCO_2 and CO_2 evasion from headwaters to mouth of the estuary of an entire hydrosystem. In the Seine, coupling the models enabled calculation of the outgassing of the estuary at 101 Gg C yr^{-1}. While representing 34% of the river mirror area of the basin, the estuary contributes ~23% of the degassing of the entire hydrosystem. The organic carbon fraction increases up to the SAV WWTP due to anthropogenic pressure and then decreases downstream and in the estuary.

CO_2 compared with the two other major GHGs (N_2O and CH_4) in the Seine Basin

The estimation of CO_2 outgassing from the Seine hydrosystem was compared to that of the other GHG emissions (CH_4, and N_2O). The same behaviors with peaks in concentrations downstream from the main WTTP of the basin were observed. In CO_2 equivalent, GHG emissions from the Seine hydrosystem, estimated at 2276 Gg CO_2eq yr^{-1}, were dominated by 95.3% CO_2 (with 44% emitted from small Strahler stream orders 1 to 2) while N_2O and CH_4 accounted for 4.4% and 0.3%, respectively. Comparatively, emissions from agricultural areas amounting to 14,295 Gg CO_2eq yr^{-1} represented 23.3% of the total GHG emissions, including agricultural and non-agricultural emissions from the basin, and from the Seine hydrosystem. These agricultural emissions can be broken down into 51% from CH_4, 33% from N_2O, and 16% from CO_2.

Agricultural emissions were taken into account in a historical reconstruction of GHG emissions in France since 1850. This study focused on three time periods. The first period (1852 to 1955), was characterized by small barely mechanized family mixed crop-livestock farming systems, during which GHG emissions for France increased from 30,000 to 50,000 Gg CO_2 eq yr^{-1}. The second time period (1955-2000) was characterized by the modernization of French agriculture after the World War II concomitantly with the expansion of the global food market, and the availability of fossil energy at relatively low cost. The end of this second period covers the increase in mechanization, the use of industrial fertilizers and pesticides, and imports of animal feed which resulted in GHG emissions reaching 120,000 GgCO_2 eq. yr^{-1}. The third period from the early 2000s to 2017, showed stabilization of GHG emissions at

114,000 $GgCO_2$ eq. yr^{-1}(2010-2014), thanks to the Rio conference (1992) and the following protocols (e.g., Kyoto in 1997) that encouraged the replacement of state intensification policies by environmental regulations aimed at decreasing GHG emissions to avoid the effects of climate change. Then two contrasted agricultural scenarios for the horizon 2040 were compared revealing that the present trend of the agro-food system with specialization and intensification associated with international trade would increase agricultural emissions by a factor of 1.5; whereas a structural change in agro-food system could lead to a 50% reduction in agricultural GHG emissions.

Future works

This work on the Seine River provided evidence for the need for further measurements at the land-water interface, which would help better understand carbon cycling in the land to ocean aquatic continuum (LOAC). Indeed, the aerobic degradation of DOC was identified as a factor controlling pCO_2, and DOC concentrations instream were related to organic carbon leaching from soil stocks. Consequently, the link between soil organic carbon content and instream DOC could be studied by measuring DOC in drainpipes, characterizing the quality of organic carbon, in terms of biodegradability. Simultaneously, measurements in drainpipes should enable better characterization of TA and DIC lateral concentrations in subsurface flow, which, associated groundwater flow, represent the diffuse sources of inorganic carbon taken into account in pyNuts-Riverstrahler model.

Isotopic measurements δ^{13}C-DOC/POC or δ^{13}C-DIC analyses would be useful to identify and quantify the different sources of pCO_2 in the Seine River. For example, the difference in isotopic signatures can separate terrestrial DOC derived from DOC originating from in stream vegetation (Bade et al., 2007). Regarding DIC, CO_2 from soil respiration has the same isotopic signature as organic matter, related to the signature of photosynthesis (C4 or C3 plants) while HCO_3^- from weathering of carbonate rocks with soil CO_2 has a distinct signature (Dubois et al., 2010).

In addition to the characterization of organic matter and the identification of its origin, other field measurements are required to better estimate pCO_2 and infer CO_2 evasion. Indeed direct measurements of gas transfer velocity (k) in small streams and larger rivers in a large basin should help determine appropriate k values and make it possible to propose a new formulation to help reduce uncertainties in GHG emissions estimates.

Beyond the inorganic carbon module of pyNuts-Riverstrahler, phytoplankton modeling parameters also need to be reviewed within the range of values reported experimentally to better capture the seasonality of algal development.

Another outcome of this study would be modeling CH_4 and N_2O, parallel to CO_2. While formulations of the CH_4 and N_2O are already included in the modeling approach, their levels and variations in the hydrosystem remain to be validated. Whereas validation data are available in the river, from headwaters to the estuary, further work is necessary to document the constraints, again in terms of point and diffuse sources. Modeling the three GHG emissions would then make it possible to simulate different scenarios for example, to explore climate change (discharges) impacts or changes in anthropic pressures in the Seine basin (improved wastewater treatment versus deterioration due to urban concentration, agricultural practices, changes in land use, etc.). Finally, such modeling could help identify and propose actions to minimize emissions of these GHG gases, by providing quantitative figures on GHG emissions and by highlighting the importance of aquatic systems as an active component of the land-to-ocean continuum.

Bibliography

Abril, G., Borges, A.V., 2004. Carbon dioxide and methane emissions from estuaries, in: Springer (Ed.), Greenhouse Gases Emissions from Natural Environments and Hydroelectric Reservoirs: Fluxes and Processes. Berlin, pp. 187–207.

Abril, G., Bouillon, S., Darchambeau, F., Teodoru, C.R., Marwick, T.R., Tamooh, F., Ochieng Omengo, F., Geeraert, N., Deirmendjian, L., Polsenaere, P., Borges, A. V., 2015a. Technical Note: Large overestimation of pCO2 calculated from pH and alkalinity in acidic, organic-rich freshwaters. Biogeosciences 12, 67–78. doi:10.5194/bg-12-67-2015

Abril, G., Commarieu, M.-V., Sottolichio, A., Bretel, P., Guérin, F., 2009. Turbidity limits gas exchange in a large macrotidal estuary. Estuar. Coast. Shelf Sci. 83, 342–348. doi:10.1016/j.ecss.2009.03.006

Abril, G., Etcheber, H., Borges, A. V., Frankignoulle, M., 2000. Excess atmospheric carbon dioxide transported by rivers into the Scheldt estuary. Comptes Rendus l'Academie Sci. - Ser. IIa Sci. la Terre des Planetes 330, 761–768. doi:10.1016/S1251-8050(00)00231-7

Abril, G., Guérin, F., Richard, S., Delmas, R., Galy-Lacaux, C., Gosse, P., Tremblay, A., Varfalvy, L., Dos Santos, M.A., Matvienko, B., 2005. Carbon dioxide and methane emissions and the carbon budget of a 10-year old tropical reservoir (Petit Saut, French Guiana). Global Biogeochem. Cycles 19, 1–16. doi:10.1029/2005GB002457

Abril, G., Martinez, J.-M., Artigas, L.F., Moreira-Turcq, P., Benedetti, M.F., Vidal, L., Meziane, T., Kim, J.-H., Bernardes, M.C., Savoye, N., Deborde, J., Souza, E.L., Albéric, P., Landim de Souza, M.F., Roland, F., 2014. Amazon River carbon dioxide outgassing fuelled by wetlands. Nature 505, 395–398. doi:10.1038/nature12797

Abril, G., Richard, S., Guérin, F., 2006. In situ measurements of dissolved gases (CO2 and CH4) in a wide range of concentrations in a tropical reservoir using an equilibrator. Sci. Total Environ. 354, 246–251. doi:http://dx.doi.org/10.1016/j.scitotenv.2004.12.051

Agence de l'eau Seine Normandie, 1978. Les bassins de la Seine et des cours d'eau normands. Ressources d'eau et données hydrologiques.

Agreste, 2013. Agreste-Recensements agricoles 1988, 2000, 2010 et enquête structure 2013. [WWW Document]. URL http://agreste.agriculture.gouv.fr/IMG/pdf/Gaf15p019-021.pdf (accessed 11.6.18).

Aguilera, E., Guzman, G., Alonso, A., 2015. Greenhouse gas emissions from conventional and organic cropping systems in Spain. II. Fruit tree orchards. Agron. Sustain. Dev. 35, 725–737. doi:10.1007/s13593-014-0267-9

Aguilera, E., Lassaletta, L., Sanz-Cobena, A., Garnier, J., Vallejo, A., 2013. The potential of organic fertilizers and water management to reduce N2O emissions in Mediterranean climate cropping systems. A review. Agric. Ecosyst. Environ. doi:10.1016/j.agee.2012.09.006

Aissa-Grouz, N., Garnier, J., Billen, G., 2016. Long trend reduction of phosphorus wastewater loading in the Seine: determination of phosphorus speciation and sorption for modeling algal growth. Environ. Sci. Pollut. Res. 1–14. doi:10.1007/s11356-016-7555-7

Aissa-Grouz, N., Garnier, J., Billen, G., Mercier, B., Martinez, A., 2015. The response of river nitrification to changes in wastewater treatment (The case of the lower Seine River downstream from Paris). Ann. Limnol. - Int. J. Limnol. 51, 351–364. doi:10.1051/limn/2015031

Aksoy, E., Yigini, Y., Montanarella, L., 2016. Combining soil databases for topsoil organic carbon mapping in Europe. PLoS One 11, 1–17. doi:10.1371/journal.pone.0152098

Albinet, M., 1967. Piézométrie moyennes eaux de 1967 : Carte hydrogéologique du bassin de Paris au 1/500 000, Editions B. ed.

Alin, S.R., Rasera, M.M.D.F.F.L., Salimon, C.I., Richey, J.E., Holtgrieve, G.W., Krusche, A. V., Snidvongs, A., 2011b. Physical controls on carbon dioxide transfer velocity and flux in low-gradient river systems and implications for regional carbon budgets. J. Geophys. Res. 116, 17. doi:G01009 10.1029/2010jg001398

Almajhdi, F.N., Al-Qudari, A.Y., Hussain, Z., 2013. Differential expression of transforming growth factor-β1 and HBx enhances hepatitis B virus replication and augments host immune cytokines and chemokines. Ann. Hepatol. 12, 408–415. doi:10.1017/CBO9781107415324.015

Almeida, R.M., Pacheco, F.S., Barros, N., Rosi, E., Roland, F.F.F., 2017. Extreme floods increase CO2 outgassing from a large Amazonian river. Limnol. Oceanogr. 62, 989–999. doi:10.1002/lno.10480

Alshboul, Z., 2016. Water management practices and anthropogenic carbon sources alter the patterns of CH 4 and CO 2 emissions from inland waters. doi:10.1021/acs.est.5b01525.)

Alshboul, Z., Encinas-Fernández, J., Hofmann, H., Lorke, A., Encinas-ferna, J., Hofmann, H., Lorke, A., Encinas-Fernández, J., Hofmann, H., Lorke, A., 2016. Export of dissolved methane and carbon dioxide with effluents from municipal wastewater treatment plants. Environ. Sci. Technol. 0. doi:10.1021/acs.est.5b04923

Arndt, S., Lacroix, G., Gypens, N., Regnier, P., Lancelot, C., 2011. Nutrient dynamics and phytoplankton development along an estuary-coastal zone continuum: A model study. J. Mar. Syst. 84, 49–66. doi:10.1016/j.jmarsys.2010.08.005

Arndt, S., Regnier, P., 2007. A model for the benthic-pelagic coupling of silica in estuarine ecosystems: Sensitivity analysis and system scale simulation. Biogeosciences 4, 331–352. doi:10.5194/bg-4-331-2007

Arndt, S., Regnier, P., Vanderborght, J.P., 2009. Seasonally-resolved nutrient export fluxes and filtering capacities in a macrotidal estuary. J. Mar. Syst. 78, 42–58. doi:10.1016/j.jmarsys.2009.02.008

Arnold, J.G., Allen, P.M., 1999. Automated methods for estimating baseflow and ground water recharge from streamflow records. J. Am. Water Resour. Assoc. 35, 411–424. doi:10.1111/j.1752-1688.1999.tb03599.x

Arrouays, D., Deslais, W., Badeau, V., 2001. The carbon content of topsoil and its geographical distribution in France. Soil use Manag. 17, 7–11. doi:10.1079/SUM200053

Attali, J., 2010. Paris et la mer. La Seine est capitale, Fayard. ed.

Aufdenkampe, A.K., Mayorga, E., Raymond, P.A., Melack, J.M., Doney, S.C., Alin, S.R., Aalto, R.E., Yoo, K., 2011. Riverine coupling of biogeochemical cycles between land, oceans, and atmosphere. Front. Ecol. Environ. 9, 53–60. doi:10.1890/100014

Aumont, O., Ethé, C., Tagliabue, A., Bopp, L., Gehlen, M., 2015. PISCES-v2: An ocean biogeochemical model for carbon and ecosystem studies. Geosci. Model Dev. 8, 2465–2513. doi:10.5194/gmd-8-2465-2015

Bade, D.L., Carpenter, S.R., Cole, J.J., Pace, M.L., Kritzberg, E., Van De Bogert, M.C., Cory, R.M., McKnight, D.M., 2007. Sources and fates of dissolved organic carbon in lakes as determined by whole-lake carbon isotope additions. Biogeochemistry 84, 115–129. doi:10.1007/s10533-006-9013-y

Ball, B.C., McTaggart, I.P., Watson, C.A., 2002. Influence of organic ley-arable management and afforestation in sandy loam to clay loam soils on fluxes of N2O and CH4in Scotland. Agric. Ecosyst. Environ. 90, 305–317. doi:10.1016/S0167-8809(01)00207-9

Barillier, A., Garnier, J., 1993. Influence of Temperature and Substrate Concentration on Bacterial Growth Yield in Seine River Water Batch Cultures. Appl. Environ. Microbiol. 59, 1678–1682.

Barles, S., 2017. Écologie territoriale et métabolisme urbain : quelques enjeux de la transition socio-écologique. Rev. d'économie régionale urbaine 5, 819–836.

Barles, S., 2010. Society, energy and materials: The contribution of urban metabolism studies to sustainable urban development issues. J. Environ. Plan. Manag. 53, 439–455. doi:10.1080/09640561003703772

Barles, S., 2007. Feeding the city: Food consumption and flow of nitrogen, Paris, 1801-1914. Sci. Total Environ. 375, 48–58. doi:10.1016/j.scitotenv.2006.12.003

Barros, N., Cole, J.J., Tranvik, L.J., Prairie, Y.T., Bastviken, D., Huszar, V.L.M., Del Giorgio, P., Roland, F., 2011. Carbon emission from hydroelectric reservoirs linked to reservoir age and latitude. Nat. Geosci. 4, 593–596. doi:10.1038/ngeo1211

Bastviken, D., Cole, J., Pace, M., Tranvik, L., 2004. Methane emissions from lakes: Dependence of lake characteristics, two regional assessments, and a global estimate. Global Biogeochem. Cycles 18, 1–12. doi:10.1029/2004GB002238

Bastviken, D., Tranvik, L.J., Downing, J., Crill, J. a, M, P., Enrich-prast, A., 2011. Freshwater Methane Emissions Offset the Continental Carbon Sink. Science (80-.). 331, 50. doi:10.1126/science.1196808

Batjes, N.H., 2014. Total carbon and nitrogen in the soils of the world. Eur. J. Soil Sci. 65, 10–21. doi:10.1111/ejss.12114_2

Battin, T.J., Kaplan, L. a., Findlay, S., Hopkinson, C.S., Marti, E., Packman, A.I., Newbold, J.D., Sabater, F., 2009a. Biophysical controls on organic carbon fluxes in fluvial networks. Nat. Geosci. 2, 595–595. doi:10.1038/ngeo602

Battin, T.J., Luyssaert, S., Kaplan, L. a., Aufdenkampe, A.K., Richter, A., Tranvik, L.J., 2009b. The boundless carbon cycle. Nat. Geosci. 2, 598–600. doi:10.1038/ngeo618

Bauer, J.E., Cai, W., Raymond, P.A., Bianchi, T.S., Hopkinson, C.S., Regnier, P.A.G., 2013. The changing carbon cycle of the coastal ocean. Nature 504, 61–70. doi:10.1038/nature12857

Baulch, H.M., Schiff, S.L., Maranger, R., Dillon, P.J., 2011. Nitrogen enrichment and the emission of nitrous oxide from streams 25. doi:10.1029/2011GB004047

Beare, M.H., Gregorich, E.G., St-Georges, P., 2009. Compaction effects on CO2 and N2O production during drying and rewetting of soil. Soil Biol. Biochem. 41, 611–621. doi:10.1016/j.soilbio.2008.12.024

Beaulieu, J.J., Shuster, W.D., Rebholz, J.A., 2010. Nitrous oxide emissions from a large, impounded river: The Ohio river. Environ. Sci. Technol. 44, 7527–7533. doi:10.1021/es1016735

Beaulieu, J.J., Tank, J.L., Hamilton, S.K., Wollheim, W.M., Hall, R.O., Mulholland, P.J., Peterson, B.J., Ashkenas, L.R., Cooper, L.W., Dahm, C.N., Dodds, W.K., Grimm, N.B., Johnson, S.L., McDowell, W.H., Poole, G.C., Valett, H.M., Arango, C.P., Bernot, M.J., Burgin, A.J., Crenshaw, C.L., Helton, A.M., Johnson, L.T., O'Brien, J.M., Potter, J.D., Sheibley, R.W., Sobota, D.J., Thomas, S.M., 2011. Nitrous oxide emission from denitrification in stream and river networks. Proc. Natl. Acad. Sci. U. S. A. 108, 214–219. doi:10.1073/pnas.1011464108

Beck, M.B., 1987. Water quality modeling: A review of the analysis of uncertainty. Water Resour. Res. 23, 1393–1442. doi:10.1029/WR023i008p01393

Benhalima, M., 2015. Analyse du système agro-alimentaire de la région Nord-Pas de Calais et ses enjeux sur l'eau. Etudes et Documents n° 125. Commissariat Général au Développement Durable. [WWW Document]. URL http://www.developpement-durable.gouv.fr/IMG/pdf/ED125.pdf (accessed 11.6.18).

Benoit, M., Garnier, J., Billen, G., 2015a. Temperature dependence of nitrous oxide production of a luvisolic soil in batch experiments. Process Biochem. 50, 79–85. doi:10.1016/j.procbio.2014.10.013

Benoit, M., Garnier, J., Billen, G., Tournebize, J., Gréhan, E., Mary, B., 2015b. Nitrous oxide emissions and nitrate leaching in an organic and a conventional cropping system (Seine basin, France). Agric. Ecosyst. Environ. 213, 131–141. doi:10.1016/j.agee.2015.07.030

Bianchi, T.S., Garcia-Tigreros, F., Yvon-Lewis, S.A., Shields, M., Mills, H.J., Butman, D., Osburn, C., Raymond, P., Shank, G.C., DiMarco, S.F., Walker, N., Reese, B.K., Mullins-Perry, R., Quigg, A., Aiken, G.R., Grossman, E.L., 2013. Enhanced transfer of terrestrially derived carbon to the atmosphere in a flooding event. Geophys. Res. Lett. 40, 116–122. doi:10.1029/2012GL054145

Billen, G., 1991. Proteins degradation in aquatic environments., in: Chröst, R. (Ed.), Microbial Enzymes in Aquatic Environments. pp. 122–142.

Billen, G., Chesterikoff, A., Garban, B., Garnier, J., Hanset, P., Meybeck, M., Miquelis, A., Ollivon, D., Pourriot, R., Servais, P., Thibert, S., 1992. Eutrophisation de la Marne : état 1991. Rapport final d'étude réalisée par l'Agence de l'eau Seine-Normandie.

Billen, G., Garnier, J., 2000. Nitrogen transfers through the Seine drainage network : a budget based on the application of the ' Riverstrahler ' model. Hydrobiologia 139–150.

Billen, G., Garnier, J., Ficht, A., Cun, C., 2001a. Modeling the Response of Water Quality in the Seine River Estuary to Human Activity in its Watershed Over the Last 50 Years. Estuaries 24, 977–993. doi:10.2307/1353011

Billen, G., Garnier, J., Ficht, A., Cun, C., Curie, M., Anti-pollution, C., Billen, G., Garnier, J., Ficht, A., Cun, C., 2001b. Modeling the Response of Water Quality in the Seine River Estuary to Human Activity in its Watershed Over the Last 50 Years. Estuaries 24, 977–993.

Billen, G., Garnier, J., Hanset, P., 1994. Modelling phytoplankton development in whole drainage networks: the RIVERSTRAHLER Model applied to the Seine river system. Hydrobiologia 289, 119–137. doi:10.1007/BF00007414

Billen, G., Garnier, J., Lassaletta, L., 2013. The nitrogen cascade from agricultural soils to the sea: Modelling nitrogen transfers at regional watershed and global scales. Philos. Trans. R. Soc. B Biol. Sci. 368. doi:10.1098/rstb.2013.0123

Billen, G., Garnier, J., Mouchel, J.-M., Silvestre, M., 2007. The Seine system: introduction to a multidisciplinary approach of the functioning of a regional river system. Sci. Total Environ. 375, 1–12. doi:10.1016/j.scitotenv.2006.12.001

Billen, G., Garnier, J., Némery, J., Sebilo, M., Sferratore, a, Barles, S., Benoit, P., Benoît, M., 2007. A long-term view of nutrient transfers through the Seine river continuum. Sci. Total Environ. 375, 80–97. doi:10.1016/j.scitotenv.2006.12.005

Billen, G., Garnier, J., Silvestre, M., 2015. A simplified algorithm for calculating benthic nutrient fluxes in river systems. Ann. Limnol. - Int. J. Limnol. 51, 37–47. doi:10.1051/limn/2014030

Billen, G., Lassaletta, L., Garnier, J., 2014. A biogeochemical view of the global agro-food system: Nitrogen flows associated with protein production, consumption and trade. Glob. Food Sec. 3, 209–219. doi:10.1016/j.gfs.2014.08.003

Billen, G., Le Noë, J., Garnier, J., 2018a. Two contrasted future scenarios for the French agro-food system. Sci. Total Environ. 637–638, 695–705. doi:10.1016/j.scitotenv.2018.05.043

Billen, G., Ramarson, A., Thieu, V., Théry, S., Silvestre, M., Pasquier, C., Hénault, C., Garnier, J., 2018b. Nitrate retention at the river–watershed interface: a new conceptual modeling approach. Biogeochemistry 139, 31–51. doi:10.1007/s10533-018-0455-9

Billen, G., Servais, P., 1989. Modélisation des processus de degradation de la matière organique en milieux aquatiques, in: Al., B.M. et (Ed.), Microorganismes Dans Les Systèmes Océaniques. p. 447.

Bochu, J., 2006. Consommation et efficacité énergétique de différents systèmes de production agricoles avec la méthodologie PLANETE. Fourrages 186, 165–177.

Boden, T.A., Marland, G., Andres, R.J., 2013. Global, Regional, and National Fossil-Fuel CO2 Emissions. Carbon Dioxide Inf. Anal. Center, Oak Ridge Natl. Lab. U.S. Dep. Energy, Oak Ridge, Tenn., U.S.A. 53, 1689–1699. doi:10.3334/CDIAC/00001_V2013

Bodmer, P., Heinz, M., Pusch, M., Singer, G., Premke, K., 2016. Carbon dynamics and their link to dissolved organic matter quality across contrasting stream ecosystems. Sci. Total Environ. 553, 574–586. doi:10.1016/j.scitotenv.2016.02.095

Boeckx, P., Van Cleemput, O., 2001. Estimates of N2O and CH4 fluxes from agricultural lands in various regions in Europe. Nutr. Cycl. Agroecosystems 60, 35–47. doi:10.1023/A:1012604032377

Borges, A.V., Delille, B., Schiettecatte, L.-S., Gazeau, F., Abril, G., Frankignoulle, M., 2004. Gas transfer velocities of CO2 in three European estuaries (Randers Fjord, Scheldt, and Thames). Limnol. Oceanogr. 49, 1630–1641. doi:10.4319/lo.2004.49.5.1630

Borges, A. V., 2005. Do we have enough pieces of the jigsaw to integrate CO2fluxes in the coastal ocean? Estuaries. doi:10.1007/BF02732750

Borges, A. V., Abril, G., Darchambeau, F., Teodoru, C.R., Deborde, J., Vidal, L.O., Lambert, T., Bouillon, S., 2015a. Divergent biophysical controls of aquatic CO2 and CH4 in the World's two largest rivers. Sci. Rep. 5, 15614. doi:10.1038/srep15614

Borges, A. V., Darchambeau, F., Lambert, T., Bouillon, S., Morana, C., Brouyère, S., Hakoun, V., Jurado, A., Tseng, H.C., Descy, J.P., Roland, F.A.E., 2018. Effects of agricultural land use on fluvial carbon dioxide, methane and nitrous oxide concentrations in a large European river, the Meuse (Belgium). Sci. Total Environ. 610–611, 342–355. doi:10.1016/j.scitotenv.2017.08.047

Borges, A. V., Darchambeau, F., Teodoru, C.R., Marwick, T.R., Tamooh, F., Geeraert, N., Omengo, F.O., Guérin, F., Lambert, T., Morana, C., Okuku, E., Bouillon, S., 2015b. Globally significant greenhouse-gas emissions from African inland waters. Nat. Geosci. 8, 637–642. doi:10.1038/ngeo2486

Borges, A. V., Delille, B., Frankignoulle, M., 2005. Budgeting sinks and sources of CO2in the coastal ocean: Diversity of ecosystem counts. Geophys. Res. Lett. 32, 1–4. doi:10.1029/2005GL023053

Borges, A. V., Schiettecatte, L.S., Abril, G., Delille, B., Gazeau, F., 2006. Carbon dioxide in European coastal waters. Estuar. Coast. Shelf Sci. 70, 375–387. doi:10.1016/j.ecss.2006.05.046

Borges, A. V, Morana, C., Bouillon, S., Servais, P., Descy, J.-P., Darchambeau, F., 2014. Carbon Cycling of Lake Kivu (East Africa): Net Autotrophy in the Epilimnion and Emission of CO2 to the Atmosphere Sustained by Geogenic Inputs. PLoS One 9, e109500. doi:10.1371/journal.pone.0109500

Borrelli, P., Van Oost, K., Meusburger, K., Alewell, C., Lugato, E., Panagos, P., 2018. A step towards a holistic assessment of soil degradation in Europe: Coupling on-site erosion with sediment transfer and carbon fluxes. Environ. Res. 161, 291–298. doi:10.1016/j.envres.2017.11.009

Bouwman, A.F., 1996. Direct emission of nitrous oxide from agricultural soils. Nutr. Cycl. Agroecosystems 46, 53–70. doi:10.1007/BF00210224

Bouwman, A.F., Beusen, A.H.W., Griffioen, J., Van Groenigen, J.W., Hefting, M.M., Oenema, O., Van Puijenbroek, P.J.T.M., Seitzinger, S., Slomp, C.P., Stehfest, E., 2013. Global trends and uncertainties in terrestrial denitrification and N2O emissions. Philos. Trans. R. Soc. B Biol. Sci. 368. doi:10.1098/rstb.2013.0112

Boyer, J.N., Stanley, D.W., Christian, R.R., 1994. Dynamics of NH4+ and NO3- Uptake in the Water Column of the Neuse River Estuary, North Carolina. Estuaries 17, 361. doi:10.2307/1352669

Breón, F.M., Broquet, G., Puygrenier, V., Chevallier, F., Xueref-Remy, I., Ramonet, M., Dieudonné, E., Lopez, M., Schmidt, M., Perrussel, O., Ciais, P., 2015. An attempt at estimating Paris area CO2 emissions from atmospheric concentration measurements. Atmos. Chem. Phys. 15, 1707–1724. doi:10.5194/acp-15-1707-2015

Broullón, D., Pérez, F.F., Velo, A., Hoppema, M., Olsen, A., Takahashi, T., Key, M., González-dávila, M., Tanhua, T., Jeansson, E., Kozyr, A., Steven, M.A.C., 2018. A global monthly climatology of total alklalinity: a neurol network approach. Earth Syst. Sci. Data Discuss 2, 1–31.

Burgos, M., Ortega, T., Forja, J.M., 2017. Temporal and spatial variation of N2O production from estuarine and marine shallow systems of Cadiz Bay (SW, Spain). Sci. Total Environ. 607–608, 141–151. doi:10.1016/j.scitotenv.2017.07.021

Butman, D., Raymond, P. a., 2011. Significant efflux of carbon dioxide from streams and rivers in the United States. Nat. Geosci. 4, 839–842. doi:10.1038/ngeo1294

Cai, W.-J., Wang, Y., 1998. The chemistry, fluxes, and sources of carbon dioxide in the estuarine waters of the Satilla and Altamaha Rivers, Georgia. Limnol. Oceanogr. 43, 657–668. doi:10.4319/lo.1998.43.4.0657

Cai, W.J., 2011. Coastal Ocean Carbon Paradox: CO2 Sinks or Sites of Terrestrial Carbon Incineration. Ann. Rev. Mar. Sci. 3.

Campeau, A., Lapierre, J., Vachon, D., Del Giorgio, P. a, 2014. Regional contribution of CO2 and CH4 fluxes from the fluvial network in a lowland boreal landscape of Québec. Global Biogeochem. Cycles 28, 57–69. doi:10.1002/2013GB004685.Received

Causse, J., Billen, G., Garnier, J., Henri-des-Tureaux, T., Olasa, X., Thammahacksa, C., Latsachak, K.O., Soulileuth, B., Sengtaheuanghoung, O., Rochelle-Newall, E., Ribolzi, O., 2015. Field and modelling studies of Escherichia coli loads in tropical streams of montane agro-ecosystems. J. Hydro-environment Res. doi:10.1016/j.jher.2015.03.003

Cayuela, M.L., Aguilera, E., Sanz-Cobena, A., Adams, D.C., Abalos, D., Barton, L., Ryals, R., Silver, W.L., Alfaro, M.A., Pappa, V.A., Smith, P., Garnier, J., Billen, G., Bouwman, L., Bondeau, A., Lassaletta, L., 2017. Direct nitrous oxide emissions in Mediterranean climate cropping systems: Emission factors based on a meta-analysis of available measurement data. Agric. Ecosyst. Environ. 238, 25–35. doi:10.1016/j.agee.2016.10.006

Cébron, A., Garnier, J., 2005. Nitrobacter and Nitrospira genera as representatives of nitrite-oxidizing bacteria: Detection, quantification and growth along the lower Seine River (France). Water Res. 39, 4979–4992. doi:10.1016/j.watres.2005.10.006

Chatzimpiros, P., 2011. Les Empreintes Environnementales de l ’ Approvisionnement Alimentaire : 366.

Chen, C.T.A., Borges, A. V., 2009. Reconciling opposing views on carbon cycling in the coastal ocean: Continental shelves as sinks and near-shore ecosystems as sources of atmospheric CO2. Deep. Res. Part II Top. Stud. Oceanogr. 56, 578–590. doi:10.1016/j.dsr2.2009.01.001

Chen, C.T.A., Huang, T.H., Chen, Y.C., Bai, Y., He, X., Kang, Y., 2013. Air-sea exchanges of coin the world’s coastal seas. Biogeosciences 10, 6509–6544. doi:10.5194/bg-10-6509-2013

Chu, C.R., Jirka, G.H., 2003. Wind and Stream Flow Induced Reaeration. J. Environ. Eng. 129, 1129–1136. doi:10.1061/(ASCE)0733-9372(2003)129:12(1129)

Ciais, P., Sabine, C., Bala, G., Bopp, L., Brovkin, V., Canadell, J., Chhabra, A., DeFries, R., Galloway, J., Heimann, M., Jones, C., Quéré, C. Le, Myneni, R.B., Piao, S., Thornton, P., 2013. Carbon and Other Biogeochemical Cycles, in: Stocker, T.F., Qin, D., G.-K. Plattner, Tignor, M., Allen, S.K., Boschung, J., Nauels, A., Xia, Y., Bex, V., Midgle, P.M. (Eds.), Climate Change 2013 - The Physical Science Basis Contribution of Working Group I to the Fifth Assessment Report of the Intergovernmental Panel on Climate Change. Cambridge, United Kingdom and New York, NY, USA, pp. 465–570. doi:10.1017/CBO9781107415324.015

Cinotti, B., 1996. Evolution des surfaces boisées en France depuis le début du XIXème siècle. Rev. For. Française XL VIII, 547–562. doi:10.4267/2042/5359

CITEPA, 2012. Rapport national d’inventaire pour la France au titre de la convention cadre des nations unies sur le changement climatique et du protocole de Kyoto. Rapport CCNUCC / Mars.

CITEPA, 2005. Inventaire départementalisé des émissions de polluants atmosphériques en Franc en 2000.

Clayton, H., Arah, J.R.M., Smith, K.A., 1994. Measurement of nitrous oxide emissions from fertilized grassland using closed chambers. J. Geophys. Res. Atmos. 99, 16599–16607. doi:10.1029/94JD00218

Cole, J.J., Caraco, N.F., 2001. Emissions of nitrous oxide (N2O) from a tidal, freshwater river, the Hudson River, New York. Environ. Sci. Technol. 35, 991–996. doi:10.1021/es0015848

Cole, J.J., Prairie, Y.T., Caraco, N.F., McDowell, W.H., Tranvik, L.J., Striegl, R.G., Duarte, C.M., Kortelainen, P., Downing, J.A., Middelburg, J.J., Melack, J., 2007. Plumbing the Global Carbon Cycle: Integrating Inland Waters into the Terrestrial Carbon Budget. Ecosystems 10, 172–185. doi:10.1007/s10021-006-9013-8

Conrad, R., 1999. Contribution of hydrogen to methane production and control of hydrogen concentrations in methanogenic soils and sediments. FEMS Microbiol. Ecol. doi:10.1016/S0168-6496(98)00086-5

CRAN, 2006. Chambre Régionale d'Agriculture de Normandie (2006). 2020 : Que mangerons-nous? [WWW Document]. URL www.normandie.chambagri.fr/eco_prosp.asp (accessed 11.6.18).

Crawford, J.T., Loken, L.C., Stanley, E.H., Stets, E.G., Dornblaser, M.M., Striegl, R.G., 2016. Basin scale controls on CO2 and CH4 emissions from the Upper Mississippi River. Geophys. Res. Lett. 43, 1973–1979. doi:10.1002/2015GL067599.Received

Crusius, J., Wanninkhof, R., 2003. Gas transfer velocities measured at low wind speed over a lake. Limnol. Oceanogr. 48, 1010–1017. doi:10.4319/lo.2003.48.3.1010

Crutzen, P.J., Aselmann, I., Seiler, W., 1986. Methane production by domestic animals, wild ruminants, other herbivorous fauna, and humans. Tellus B 38 B, 271–284. doi:10.1111/j.1600-0889.1986.tb00193.x

Cugier, P., Billen, G., Guillaud, J.F., Garnier, J., Ménesguen, a., 2005a. Modelling the eutrophication of the Seine Bight (France) under historical, present and future riverine nutrient loading. J. Hydrol. 304, 381–396. doi:10.1016/j.jhydrol.2004.07.049

Cugier, P., Billen, G., Guillaud, J.F., Garnier, J., Ménesguen, A., 2005b. Modelling the eutrophication of the Seine Bight (France) under historical, present and future riverine nutrient loading. J. Hydrol. 304, 381–396. doi:10.1016/j.jhydrol.2004.07.049

Culberson, C.H., 1980. Calculation of the in situ pH of seawater. Limnol. Oceanogr. 25, 150–152. doi:10.4319/lo.1980.25.1.0150

Curie, F., Gaillard, S., Ducharne, A., Bendjoudi, H., 2007. Geomorphological methods to characterise wetlands at the scale of the Seine watershed. Sci. Total Environ. 375, 59–68. doi:10.1016/j.scitotenv.2006.12.013

Datry, T., Foulquier, A., Corti, R., von Schiller, D., Tockner, K., Mendoza-Lera, C., Clément, J.C., Gessner, M.O., Moleón, M., Stubbington, R., Gücker, B., Albariño, R., Allen, D.C., Altermatt, F., Arce, M.I., Arnon, S., Banas, D., Banegas-Medina, A., Beller, E., Blanchette, M.L., Blanco-Libreros, J.F., Blessing, J.J., Boëchat, I.G., Boersma, K.S., Bogan, M.T., Bonada, N., Bond, N.R., Brintrup Barría, K.C., Bruder, A., Burrows, R.M., Cancellario, T., Canhoto, C., Carlson, S.M., Cauvy-Fraunié, S., Cid, N., Danger, M., de Freitas Terra, B., de Girolamo, A.M., de la Barra, E., Del Campo, R., Diaz-Villanueva, V.D., Dyer, F., Elosegi, A., Faye, E., Febria, C., Four, B., Gafny, S., Ghate, S.D., Gómez, R., Gómez-Gener, L., Graça, M.A.S., Guareschi, S., Hoppeler, F., Hwan, J.L.,

Jones, J.I., Kubheka, S., Laini, A., Langhans, S.D., Leigh, C., Little, C.J., Lorenz, S., Marshall, J.C., Martín, E., McIntosh, A.R., Meyer, E.I., Miliša, M., Mlambo, M.C., Morais, M., Moya, N., Negus, P.M., Niyogi, D.K., Papatheodoulou, A., Pardo, I., Pařil, P., Pauls, S.U., Pešić, V., Polášek, M., Robinson, C.T., Rodríguez-Lozano, P., Rolls, R.J., Sánchez-Montoya, M.M., Savić, A., Shumilova, O., Sridhar, K.R., Steward, A.L., Storey, R., Taleb, A., Uzan, A., Vander Vorste, R., Waltham, N.J., Woelfle-Erskine, C., Zak, D., Zarfl, C., Zoppini, A., 2018. A global analysis of terrestrial plant litter dynamics in non-perennial waterways. Nat. Geosci. 1–7. doi:10.1038/s41561-018-0134-4

Datry, T., Larned, S.T., Tockner, K., 2014. Intermittent rivers: A challenge for freshwater ecology. Bioscience 64, 229–235. doi:10.1093/biosci/bit027

Davidson, E.A., 1991. Soil Water Content and the Ratio of Nitrous Oxide Emitted from Soil, in: Biogeochemistry of Global Change : Radiatively Active Trace Gases : Selected Papers from the Tenth International Symposium on Environmental Biogeochemistry, San Francisco, August 19-24, 1991 / [Edited by R.S. Oremland]. pp. 369–386. doi:10.1007/978-1-4615-2812-8_20

Davis, J.R., Koop, K., 2006. Eutrophication in Australian rivers, reservoirs and estuaries - A southern hemisphere perspective on the science and its implications. Hydrobiologia. doi:10.1007/s10750-005-4429-2

De Klein, C.A.M., Sherlock, R.R., Cameron, K.C., van der Weerden, T.J., 2001. Nitrous oxide emissions from agricultural soils in New Zealand-a review of current knowledge and directions for future research. J. R. Soc. New Zeal. 31, 543–574. doi:10.1080/03014223.2001.9517667

Deemer, B.R., Harrison, J.A., Li, S., Beaulieu, J.J., Delsontro, T., Barros, N., Bezerra-Neto, J.F., Powers, S.M., Dos Santos, M.A., Vonk, J.A., 2016. Greenhouse gas emissions from reservoir water surfaces: A new global synthesis. Bioscience 66, 949–964. doi:10.1093/biosci/biw117

Denfeld, B.A., Frey, K.E., Sobczak, W. V., Mann, P.J., Holmes, R.M., 2013. Summer CO2 evasion from streams and rivers in the Kolyma river basin, north-east Siberia. Polar Res. 32, 1–15. doi:10.3402/polar.v32i0.19704

Denman, K.L., Brasseur, G., Chidthaisong, A., Ciais, P., Cox, P.M., Dickinson, R.E., Hauglustaine, D., Heinze, C., Holland, E., Jacob, D., Lohmann, U., Ramachandran, S., Dias, P.L. da S., Wofsy, S.C., Zhang, X., 2007. Couplings Between Changes in the Climate System and Biogeochemistry., in: Solomon, S., Qin, D., Manning, M., Chen, Z., Marquis, M., Averyt, K.B., Tignor, M., Miller, H.L. (Eds.), Climate Change 2007: The Physical Science Basis. Contribution of Working Group I to the Fourth Assessment Report of the Intergovernmental Panel on Climate Change. Nature Publishing Group, Cambridge, United Kingdom and New York, NY, USA, pp. 499–588.

Dentener, F., Stevenson, D., Cofala, J., Mechler, R., Amann, M., Bergamaschi, P., Raes, F., Derwent, R., 2005. The impact of air pollutant and methane emission controls on tropospheric ozone and radiative forcing: CTM calculations for the period 1990-2030. Atmos. Chem. Phys. 5, 1731–1755. doi:10.5194/acp-5-1731-2005

Desmit, X., Thieu, V., Billen, G., Campuzano, F., Dulière, V., Garnier, J., Lassaletta, L., Ménesguen, A., Neves, R., Pinto, L., Silvestre, M., Sobrinho, J.L., Lacroix, G., 2018. Reducing marine eutrophication may require a paradigmatic change. Sci. Total Environ. 635, 1444–1466. doi:10.1016/j.scitotenv.2018.04.181

Dickson, A., Goyet, C., DOE, Dickson, A., Goyet, C., 1992. Handbook of methods for the analysis of the various parameters of the carbon dioxide system in sea water. DOE Handb. 1994, 22. doi:ORNL/CDIAC-74

Dinsmore, K.J., Billett, M.F., 2008. Continuous measurement and modeling of CO2 losses from a peatland stream during stormflow events. Water Resour. Res. 44, 1–11. doi:10.1029/2008WR007284

Dinsmore, K.J., Billett, M.F., Dyson, K.E., 2013. Temperature and precipitation drive temporal variability in aquatic carbon and GHG concentrations and fluxes in a peatland catchment. Glob. Chang. Biol. 19, 2133–2148. doi:10.1111/gcb.12209

Division Physical Sciences, NOAA Earth System Research Laboratory, n.d. CO2 Scripps program [WWW Document]. Phys. Sci. Div. URL (accessed 10.27.16).

Dobbie, K.E., Smith, K.A., 1996. Comparison of CH4 oxidation rates in woodland, arable and set aside soils. Soil Biol. Biochem. 28, 1357–1365. doi:10.1016/S0038-0717(96)00152-6

Doney, S.C., Lindsay, K., Caldeira, K., Campin, J.M., Drange, H., Dutay, J.C., Follows, M., Gao, Y., Gnanadesikan, A., Gruber, N., Ishida, A., Joos, F., Madec, G., Maier-Reimer, E., Marshall, J.C., Matear, R.J., Monfray, P., Mouchet, A., Najjar, R., Orr, J.C., Plattner, G.K., Sarmiento, J., Schlitzer, R., Slater, R., Totterdell, I.J., Weirig, M.F., Yamanaka, Y., Yool, A., 2004. Evaluating global ocean carbon models: The importance of realistic physics. Global Biogeochem. Cycles 18. doi:10.1029/2003GB002150

Doublet, S., 2011. CLIMAGRI : bilan énergies et GES des territoires ruraux, la ferme France en 2006 et 4 scénarios pour 2030. Rapport ADEME [WWW Document]. URL http://www.ademe.fr/sites/default/ files/assets/documents/climagri-la-ferme-france-en-2006-et-4-scenarios-pour-2030.pdf. (accessed 11.6.18).

Drake, T.W., Raymond, P.A., Spencer, R.G.M., 2017. Terrestrial carbon inputs to inland waters: A current synthesis of estimates and uncertainty. Limnol. Oceanogr. Lett. doi:10.1002/lol2.10055

Dreal, H., 2014. Scénarios prospectifs de développement de la Vallée de Seine à l'horizon 2040. Etude. [WWW Document]. URL http://www.normandie.developpement-durable.gouv.fr/prospective-vallee-de-la-seine-2040-a250.html (accessed 11.6.18).

Duarte, C.M., Prairie, Y.T., 2005. Prevalence of heterotrophy and atmospheric CO2 emissions from aquatic ecosystems. Ecosystems 8, 862–870. doi:10.1007/s10021-005-0177-4

Dubois, K.D., Lee, D., Veizer, J., 2010. Isotopic constraints on alkalinity, dissolved organic carbon, and atmospheric carbon dioxide fluxes in the Mississippi River. J. Geophys. Res. Biogeosciences 115, n/a-n/a. doi:10.1029/2009JG001102

Ducharne, a, Baubion, C., Beaudoin, N., Benoit, M., Billen, G., Brisson, N., Garnier, J., Kieken, H., Lebonvallet, S., Ledoux, E., Mary, B., Mignolet, C., Poux, X., Sauboua, E., Schott, C., Théry, S., Viennot, P., 2007. Long term prospective of the Seine River system: confronting climatic and direct anthropogenic changes. Sci. Total Environ. 375, 292–311. doi:10.1016/j.scitotenv.2006.12.011

Ducharne, A., 2008. Importance of stream temperature to climate change impact on water quality. Hydrol. Earth Syst. Sci. 12, 797–810. doi:10.5194/hess-12-797-2008

Ducharne, A., Ledoux, E., 2003. Influence du changement climatique sur l'hydrologie du bassin de la Seine. VertigO 4, 1–58. doi:10.4000/vertigo.3845

Duchemin, E., Lucotte, M., Canuel, R., Chamberland, A., 1995. Production of the greenhouse gases CH4 and CO2 by hydroelectric reservoirs of the boreal region. Global Biogeochem. Cycles 9, 529–540. doi:10.1029/95GB02202

Dutaur, L., Verchot, L. V., 2007. A global inventory of the soil CH4 sink. Global Biogeochem. Cycles 21, 1–9. doi:10.1029/2006GB002734

Dyer, J.A., Desjardins, R.L., 2009. A review and evaluation of fossil energy and carbon dioxide emissions in Canadian agriculture. J. Sustain. Agric. doi:10.1080/10440040802660137

Dyer, J.A., Kulshreshtha, S.N., McConkey, B.G., Desjardins, R.L., 2010. An assessment of fossil fuel energy use and CO2emissions from farm field operations using a regional level crop and land use database for Canada. Energy 35, 2261–2269. doi:10.1016/j.energy.2010.02.013

EEA, 2018. Annual European Union greenhous gas inventory 1990-2016 and inventory report 2018. EEA Tech. Rep. Submission, 955. doi:10.2800/92220

EEA, 2012. Copernicus Land Monitoring Service - Corine Land Cover (CLC), Copernicus Land Monitoring Service - Corine Land Cover. doi:https://www.eea.europa.eu/data-and-maps/data/copernicus-land-monitoring-service-corine

Eggleston, S., 2006. IPCC Guidelines for National Greenhouse Gas Inventories: Agriculture, Forestry and Other Land Use. Institute for Global Environmental Strategies (IGES).

Emiroglu, O., Cicek, A., Arslan, N., Aksan, S., Rüzgar, M., 2010. Boron concentration in water, sediment and different organisms around large borate deposits of Turkey. Bull. Environ. Contam. Toxicol. 84, 427–431. doi:10.1007/s00128-010-9961-8

Erb, K.H., Lauk, C., Kastner, T., Mayer, A., Theurl, M.C., Haberl, H., 2016. Exploring the biophysical option space for feeding the world without deforestation. Nat. Commun. 7. doi:10.1038/ncomms11382

Etheridge, D.M., Steele, L.P., Langenfelds, R.L., Francey, R.J., Barnola, J.M., Morgan, V.I., 1996. Natural and anthropogenic changes in atmospheric CO2 over the last 1000 years from air in Antarctic ice and firn. J. Geophys. Res. 101, 4115–4128. doi:10.1029/95JD03410

Finlay, J.C.. b, 2003. Controls of streamwater dissolved inorganic carbon dynamics in a forested watershed. Biogeochemistry 62, 231–252. doi:10.1023/A:1021183023963

Fischer-Kowalski, M., Haberl, H., 2008. Socioecological Transitions and Global Change: Trajectories of Social Metabolism and Land Use. Landsc. Ecol. 1003–1005. doi:10.1007/s10113-008-0078-0

Flipo, N., Labarthe, B., Pryet, A., Baratelli, F., Goblet, P., 2016. Echanges nappe-rivière à l'échelle du bassin de la seine, Technical report, PIREN Seine, in: Dans Interfaces Nappe-Rivière, Rapport de Synthèse 2011-2015.

Follows, M.J., Ito, T., Dutkiewicz, S., 2006. On the solution of the carbonate chemistry system in ocean biogeochemistry models. Ocean Model. 12, 290–301. doi:10.1016/j.ocemod.2005.05.004

Forster, P., Ramaswamy, V., Artaxo, P., Berntsen, T., Betts, R., Fahey, D.W., Haywood, J., Lean, J., Lowe, D.C., Myhre, G., Nganga, J., Prinn, R., Raga, G., Schulz, M., von Dorland, R., 2007. Chapter 2: Changes in atmospheric and radiative forcing., in: Solomon, S., Qin, D., Manning, M., Chen, Z., Marquis, M., Averyt, K.B., Tignor, M., Miller, H.L. (Eds.), Climate Change 2007: The Physical Science Basis. Contribution of Working Group I to the Fourth Assessment Report of the Intergovernmental Panel on Climate Change. Cambridge, United Kingdom and New York, NY, USA, pp. 129–234. doi:10.1103/PhysRevB.77.220407

Frankignoulle, M., Abril, G., Borges, A. V., Bourge, I., Canon, C., Delille, B., Libert, E., Théate, J.-M., 1998. Carbon Dioxide Emission from European Estuaries. Science (80-.). 282, 434–436. doi:10.1126/science.282.5388.434

Frankignoulle, M., Borges, A., Biondo, R., 2001. A new design of equilibrator to monitor carbon dioxide in highly dynamic and turbid environments. Water Res. 35, 1344–1347. doi:10.1016/S0043-1354(00)00369-9

Frankignoulle, M., Borges, A.V., 2002. Direct and Indirect pCO 2 Measurements in a Wide Range of pCO 2 and Salinity Values (The Scheldt Estuary). Aquat. Geochemistry 267–273.

Frey, K.E., McClelland, J.W., 2009. Impacts of permafrost degradation on arctic river biogeochemistry. Hydrol. Process. doi:10.1002/hyp.7196

Galy-Lacaux, C., Delmas, R., Jambert, C., Dumestre, J.F., Labroue, L., Richard, S., Gosse, P., 1997. Gaseous emissions and oxygen consumption in hydroelectric dams: A case study in French Guyana. Global Biogeochem. Cycles 11, 471–483. doi:10.1029/97GB01625

Garnier, J., Anglade, J., Benoit, M., Billen, G., Puech, T., Ramarson, A., Passy, P., Silvestre, M., Lassaletta, L., Trommenschlager, J.M., Schott, C., Tallec, G., 2016. Reconnecting crop and cattle farming to reduce nitrogen losses to river water of an intensive agricultural catchment (Seine basin, France): Past, present and future. Environ. Sci. Policy 63, 76–90. doi:10.1016/j.envsci.2016.04.019

Garnier, J., Billen, G., 2007. Production vs. respiration in river systems: an indicator of an "ecological status". Sci. Total Environ. 375, 110–24. doi:10.1016/j.scitotenv.2006.12.006

Garnier, J., Billen, G., 1994. Ecological interactions in a shallow sand-pit lake (Lake Créteil, Parisian Basin, France): a modelling approach. Hydrobiologia 275–276, 97–114. doi:10.1007/BF00026703

Garnier, J., Billen, G., Cébron, A., 2007. Modelling nitrogen transformations in the lower Seine river and estuary (France): Impact of wastewater release on oxygenation and N2O emission. Hydrobiologia 588, 291–302. doi:10.1007/s10750-007-0670-1

Garnier, J., Billen, G., Coste, M., 1995. Seasonal succession of diatoms and Chlorophyceae in the drainage network of the Seine River: Observation and modeling. Limnol. Oceanogr. 40, 750–765. doi:10.4319/lo.1995.40.4.0750

Garnier, J., Billen, G., Even, S., Etcheber, H., Servais, P., 2008. Organic matter dynamics and budgets in the turbidity maximum zone of the Seine Estuary (France). Estuar. Coast. Shelf Sci. 77, 150–162. doi:10.1016/j.ecss.2007.09.019

Garnier, J., Billen, G., Hannon, E., Fonbonne, S., Videnina, Y., Soulie, M., 2002. Modelling the Transfer and Retention of Nutrients in the Drainage Network of the Danube River. Estuar. Coast. Shelf Sci. 54, 285–308. doi:10.1006/ecss.2000.0648

Garnier, J., Billen, G., Némery, J., Sebilo, M., 2010a. Transformations of nutrients (N, P, Si) in the turbidity maximum zone of the Seine estuary and export to the sea. Estuar. Coast. Shelf Sci. 90, 129–141. doi:10.1016/j.ecss.2010.07.012

Garnier, J., Billen, G., Palfner, L., 1999a. Understanding the oxygen budget and related ecological processes in the river Mosel: The RIVERSTRAHLER approach. Hydrobiologia 410, 151–166. doi:10.1023/A:1003894200796

Garnier, J., Billen, G., Sanchez, N., Leporcq, B., 2000. Ecological Functioning of the Marne Reservoir (Upper Seine Basin, France). Regul. Ri6ers Res. Mgmt 16, 51–71. doi:doi: 10.1002/(SICI)1099-1646(200001/02)16:1%3C51::AID-RRR571%3E3.0.CO;2-I

Garnier, J., Billen, G., Servais, P., 1992a. Physiological characteristics and ecological role of small and large sized bacteria in a polluted river (Seine River, France). Arch. Hydrobiol. Beih. Ergebn. Limnol. 37, 83–94.

Garnier, J., Billen, G., Vilain, G., Benoit, M., Passy, P., Tallec, G., Tournebize, J., Anglade, J., Billy, C., Mercier, B., Ansart, P., Azougui, A., Sebilo, M., Kao, C., 2014. Curative vs. preventive management of nitrogen transfers in rural areas: lessons from the case of the Orgeval watershed (Seine River basin, France). J. Environ. Manage. 144, 125–34. doi:10.1016/j.jenvman.2014.04.030

Garnier, J., Billen, G., Vilain, G., Martinez, A., Silvestre, M., Mounier, E., Toche, F., 2009. Nitrous oxide (N2O) in the Seine river and basin: Observations and budgets. Agric. Ecosyst. Environ. 133, 223–233. doi:10.1016/j.agee.2009.04.024

Garnier, J., Brion, N., Callens, J., Passy, P., Deligne, C., Billen, G., Servais, P., Billen, C., 2013a. Modeling historical changes in nutrient delivery and water quality of the Zenne River (1790s–2010): The role of land use, waterscape and urban wastewater management. J. Mar. Syst. 128, 62–76. doi:10.1016/j.jmarsys.2012.04.001

Garnier, J., Lassaletta, L., Billen, G., Romero, E., Grizzetti, B., Némery, J., Le, T.P.Q., Pistocchi, C., Aissa-Grouz, N., Luu, T.N.M., Vilmin, L., Dorioz, J.M., 2015. Phosphorus budget in the water-agro-food system at nested scales in two contrasted regions of the world (ASEAN-8 and EU-27). Global Biogeochem. Cycles 29, 1348–1368. doi:10.1002/2015GB005147

Garnier, J., Leporcq, B., Sanchez, N., Phillippon, Garnier, J., Leporcq, B., Sanchez, N., Philippon, 1999b. Biogeochemical mass-balances (C, N, P, Si) in three large reservoirs of the Seine Basin (France). Biogeochemistry 47, 119–146. doi:10.1023/A:1006101318417

Garnier, J., Mounier, E.M., Laverman, A.M., Billen, G.F., 2010b. Potential Denitrification and Nitrous Oxide Production in the Sediments of the Seine River Drainage Network (France). J. Environ. Qual. 39, 449. doi:10.2134/jeq2009.0299

Garnier, J., Némery, J., Billen, G., Théry, S., 2005. Nutrient dynamics and control of eutrophication in the Marne River system: modelling the role of exchangeable phosphorus. J. Hydrol. 304, 397–412. doi:10.1016/j.jhydrol.2004.07.040

Garnier, J., Ramarson, A., Billen, G., Théry, S., Thiéry, D., Thieu, V., Minaudo, C., Moatar, F., 2018. Nutrient inputs and hydrology together determine biogeochemical status of the Loire River (France): Current situation and possible future scenarios. Sci. Total Environ. 637–638, 609–624. doi:10.1016/j.scitotenv.2018.05.045

Garnier, J., Servais, P., Billen, G., 1992b. Bacterioplankton in the Seine River (France) - Impact of the Parisian Urban Effluent. Can. J. Microbiol. 38, 56–64. doi:10.1139/m92-009

Garnier, J., Servais, P., Billen, G., Akopian, M., Brion, N., 2001. Lower Seine River and Estuary (France) Carbon and Oxygen Budgets during Low Flow. Estuaries 24, 964–976. doi:10.2307/1353010

Garnier, J., Vilain, G., Silvestre, M., Billen, G., Jehanno, S., Poirier, D., Martinez, A., Decuq, C., Cellier, P., Abril, G., 2013b. Budget of methane emissions from soils, livestock and the river network at the regional scale of the Seine basin (France). Biogeochemistry 116, 199–214. doi:10.1007/s10533-013-9845-1

Gilhespy, S.L., Anthony, S., Cardenas, L., Chadwick, D., del Prado, A., Li, C., Misselbrook, T., Rees, R.M., Salas, W., Sanz-Cobena, A., Smith, P., Tilston, E.L., Topp, C.F.E., Vetter, S., Yeluripati, J.B., 2014. First 20 years of DNDC (DeNitrification DeComposition): Model evolution. Ecol. Modell. 292, 51–62. doi:10.1016/j.ecolmodel.2014.09.004

Gingrich, S., Erb, K.H., Krausmann, F., Gaube, V., Haberl, H., 2007. Long-term dynamics of terrestrial carbon stocks in Austria: A comprehensive assessment of the time period from 1830 to 2000. Reg. Environ. Chang. 7, 37–47. doi:10.1007/s10113-007-0024-6

Griffith, D.R., Barnes, R.T., Raymond, P.A., 2009. Inputs of fossil carbon from wastewater treatment plants to U.S. Rivers and oceans. Environ. Sci. Technol. 43, 5647–5651. doi:10.1021/es9004043

Groffman, P., 1991. Ecology of nitrification and denitrification in soil evaluated at scales relevant to atmospheric chemistry. Microb. Prod. Consum. Greenh. Gases Methane, Nitrogen Oxides Halomethanes.

Gu, J., Loustau, D., Hénault, C., Rochette, P., Cellier, P., Nicoullaud, B., Grossel, A., Richard, G., 2014. Modeling nitrous oxide emissions from tile-drained winter wheat fields in Central France. Nutr. Cycl. Agroecosystems 98, 27–40. doi:10.1007/s10705-013-9593-6

Guerrini, M.-C., Mouchel, J.-M., Meybeck, M., Penven, M.J., Hubert, G., Muxart, T., 1998. Le bassin de la Seine : la confrontation du rural et de l'urbain, in: Meybeck, M., de Marsily, G., Fustec, E. (Eds.), La Seine En Son Bassin. Fonctionnement Écologique d'un Système Fluvial Anthropisé. pp. 29–73.

Guo, L., He, Q., 2011. Freshwater flocculation of suspended sediments in the Yangtze River, China. Ocean Dyn. 61, 371–386. doi:10.1007/s10236-011-0391-x

Gutz, I.G.R., 2012. CurTiPot – pH and Acid–Base Titration Curves: Analysis and Simulation freeware, version 3.0 [WWW Document]. URL http://www.iq.usp.br/gutz/Curtipot_.html

Gypens, N., Borges, a. V., Lancelot, C., 2009. Effect of eutrophication on air-sea CO2 fluxes in the coastal Southern North Sea: A model study of the past 50 years. Glob. Chang. Biol. 15, 1040–1056. doi:10.1111/j.1365-2486.2008.01773.x

Gypens, N., Lacroix, G., Lancelot, C., Borges, a. V., 2011. Seasonal and inter-annual variability of air-sea CO2 fluxes and seawater carbonate chemistry in the Southern North Sea. Prog. Oceanogr. 88, 59–77. doi:10.1016/j.pocean.2010.11.004

Gypens, N., Lancelot, C., Borges, A. V., 2004. Carbon dynamics and CO2 air-sea exchanges in the eutrophied coastal waters of the Southern Bight of the North Sea: a modelling study. Biogeosciences 1, 147–157. doi:10.5194/bg-1-147-2004

H. W. Streeter, B. Phelps, 1925. A study of the pollution and natural purification of the Illunois River. III: factors concerning the phenomena of oxidation and reaeration. Public Health Bulletin (Wash. D. C). 146. doi:10.1002/ange.19290420217

Habets, F., Boé, J., Déqué, M., Ducharne, A., Gascoin, S., Hachour, A., Martin, E., Pagé, C., Sauquet, E., Terray, L., Thiéry, D., Oudin, L., Viennot, P., 2013. Impact of climate change on the hydrogeology of two basins in northern France. Clim. Change 121, 771–785. doi:10.1007/s10584-013-0934-x

Habets, F., Boone, A., Champeaux, J.L., Etchevers, P., Franchistéguy, L., Leblois, E., Ledoux, E., Le Moigne, P., Martin, E., Morel, S., Noilhan, J., Seguí, P.Q., Rousset-Regimbeau, F., Viennot, P., 2008. The SAFRAN-ISBA-MODCOU hydrometeorological model applied over France. J. Geophys. Res. Atmos. 113, 1–18. doi:10.1029/2007JD008548

Halbedel, S., Koschorreck, M., 2013. Regulation of CO2 emissions from temperate streams and reservoirs. Biogeosciences 10, 7539–7551. doi:10.5194/bg-10-7539-2013

Hall, R.O., 2016. Metabolism of Streams and Rivers: Estimation, Controls and Application. Stream Ecosyst. a Chang. Environ. 151–180.

Han, P., Li, Y., Yang, X., Xue, L., Zhang, L., 2017. Effects of aerobic respiration and nitrification on dissolved inorganic nitrogen and carbon dioxide in human-perturbed eastern Jiaozhou Bay, China. Mar. Pollut. Bull. 124, 449–458. doi:10.1016/j.marpolbul.2017.07.055

Hannon, E., Boyd, P.W., Silvoso, M., Lancelot, C., 2001. Modeling the bloom evolution and carbon flows during SOIREE: Implications for future in situ iron-enrichments in the Southern Ocean. Deep. Res. Part II Top. Stud. Oceanogr. 48, 2745–2773. doi:10.1016/S0967-0645(01)00016-9

Harchaoui, S., Chatzimpiros, P., 2018. Energy, Nitrogen, and Farm Surplus Transitions in Agriculture from Historical Data Modeling. France, 1882-2013. J. Ind. Ecol. doi:10.1111/jiec.12760

Harned, H.S., Davis, R.J., Jr., R.D., 1943. The ionization constant of carbonic acid in water and the solubility of carbon dioxide in water and aqueous salt solutions from 0 to 50°. J. Am. Chem. Soc. 65, 2030–2037.

Harned, H.S., Scholes, S.R., 1941. The Ionization Constant of HCO3- from 0 to 50°. J. Am. Chem. Soc. 63, 1706–1709. doi:10.1021/ja01851a058

HAROPA, 2015. Projets stratégiques HAROPA 2030 [WWW Document]. URL http://www.haropaports.com/ projets_strategiques/ (accessed 8.20.11).

Harrison, J.A., Matson, P.A., Fendorf, S.E., 2005. Effects of a diel oxygen cycle on nitrogen transformations and greenhouse gas emissions in a eutrophied subtropical stream. Aquat. Sci. 67, 308–315. doi:10.1007/s00027-005-0776-3

Hartmann, D.L., Klein Tank, A.M.G., Rusticucci, M., Alexander, L. V, Brönnimann, S., Charabi, Y.A.R., Dentener, F.J., Dlugokencky, E.J., Easterling, D.R., Kaplan, A., Soden, B.J., Thorne, P.W., Wild, M., Zhai, P., 2013. Observations: Atmosphere and surface, in: Climate Change 2013 the Physical Science Basis: Working Group I Contribution to the Fifth Assessment Report of the Intergovernmental Panel on Climate Change. pp. 159–254. doi:10.1017/CBO9781107415324.008

He, B., Kanae, S., Oki, T., Hirabayashi, Y., Yamashiki, Y., Takara, K., 2011. Assessment of global nitrogen pollution in rivers using an integrated biogeochemical modeling framework. Water Res. 45, 2573–2586. doi:10.1016/j.watres.2011.02.011

Hénault, C., Devis, X., Lucas, J.L., Germon, J.C., 1998. Influence of different agricultural practices (type of crop, form of N-fertilizer) on soil nitrous oxide emissions. Biol. Fertil. Soils 27, 299–306. doi:10.1007/s003740050437

Hlaváčová, E., Rulík, M., Čáp, L., Mach, V., 2006. Greenhouse gas CO2, CH4, N2O) emissions to the atmosphere from a small lowland stream in Czech Republic. Arch. für Hydrobiol. 165, 339–353. doi:10.1127/0003-9136/2006/0165-0339

Ho, D.T., Coffineau, N., Hickman, B., Chow, N., Koffman, T., Schlosser, P., 2016. Influence of current velocity and wind speed on air-water gas exchange in a mangrove estuary. Geophys. Res. Lett. 43, 3813–3821. doi:10.1002/2016GL068727.Received

Ho, D.T., Ferrõn, S., Engel, V.C., Larsen, L.G., Barr, J.G., 2014. Air-water gas exchange and CO2 flux in a mangrove-dominated estuary. Geophys. Res. Lett. 41, 108–113. doi:10.1002/2013GL058785

Hotchkiss, E.R., Hall, R.O., Sponseller, R., Butman, D., Klaminder, J., Laudon, H., Rosvall, M., Karlsson, J., 2015. Sources and control of CO2 emissions change with the size of sreams and rivers. Nat. Geosci. 8. doi:10.1038/ngeo2507

Houghton, J.T. (ed. ., Filho, L.G. (ed. . M., Lim, B. (ed. ., Treanton, K. (ed. ., Mamaty, I. (ed. ., 1997. Revised 1996 IPCC guidelines for national greenhouse gas inventories. v. 1: Greenhouse gas inventory reporting instructions.- v. 2: Greenhouse gas inventory workbook.- v.3: Greenhouse gas inventory reference manual, Bracknell. ed.

Houghton, R.A., House, J.I., Pongratz, J., Van Der Werf, G.R., Defries, R.S., Hansen, M.C., Le Quéré, C., Ramankutty, N., 2012. Carbon emissions from land use and land-cover change. Biogeosciences 9, 5125–5142. doi:10.5194/bg-9-5125-2012

Hu, M., Chen, D., Dahlgren, R.A., 2016. Modeling nitrous oxide emission from rivers: a global assessment. Glob. Chang. Biol. 22, 3566–3582. doi:10.1111/gcb.13351

Huang, W., Bi, Y., Hu, Z., Zhu, K., Zhao, W., Yuan, X., 2015. Spatio-temporal variations of GHG emissions from surface water of Xiangxi River in Three Gorges Reservoir region, China. Ecol. Eng. 83, 28–32. doi:10.1016/j.ecoleng.2015.04.088

Huntington, T.G., Balch, W.M., Aiken, G.R., Sheffield, J., Luo, L., Roesler, C.S., Camill, P., 2016. Climate change and dissolved organic carbon export to the Gulf of Maine. J. Geophys. Res. Biogeosciences 121, 2015JG003314. doi:10.1002/2015JG003314

Huotari, J., Haapanala, S., Pumpanen, J., Vesala, T., Ojala, A., 2013. Efficient gas exchange between a boreal river and the atmosphere. Geophys. Res. Lett. 40, 5683–5686. doi:10.1002/2013GL057705

Huttunen, J.T., Alm, J., Liikanen, A., Juutinen, S., Larmola, T., Hammar, T., Silvola, J., Martikainen, P.J., 2003. Fluxes of methane, carbon dioxide and nitrous oxide in boreal lakes and potential anthropogenic effects on the aquatic greenhouse gas emissions. Chemosphere 52, 609–621. doi:10.1016/S0045-6535(03)00243-1

IFEN, 2012. Corine Land Cover. Base de données géographiques de l'occupation du sol. Orléans, France.

INSEE, 2015. French National Institute of Statistics and Economic Studies, Recensement de la population 2015.

IPCC, 2018. Global warming of 1.5 °C (SR15) Summary for Policymakers. 2018.

Jia, Z., Liu, T., Xia, X., Xia, N., 2016. Effect of particle size and composition of suspended sediment on denitrification in river water. Sci. Total Environ. 541, 934–940. doi:10.1016/j.scitotenv.2015.10.012

Jones, J.B., Stanley, E.H., Mulholland, P.J., 2003. Long-term decline in carbon dioxide supersaturation in rivers across the contiguous United States. Geophys. Res. Lett. 30, n/a-n/a. doi:10.1029/2003GL017056

Jones, M.N., 1984. Nitrate reduction by shaking with cadmium. Alternative to cadmium columns. Water Res. 18, 643–646. doi:10.1016/0043-1354(84)90215-X

Joos, F., Bruno, M., Fink, R., Siegenthaler, U., Stocker, T.F., Le Quéré, C., Sarmiento, J.L., 1996. An efficient and accurate representation of complex oceanic and biospheric models of anthropogenic carbon uptake. Tellus, Ser. B Chem. Phys. Meteorol. 48, 397–417. doi:10.1034/j.1600-0889.1996.t01-2-00006.x

Joos, F., Roth, R., Fuglestvedt, J.S., Peters, G.P., Enting, I.G., Von Bloh, W., Brovkin, V., Burke, E.J., Eby, M., Edwards, N.R., Friedrich, T., Frölicher, T.L., Halloran, P.R., Holden, P.B., Jones, C., Kleinen, T., Mackenzie, F.T., Matsumoto, K., Meinshausen, M., Plattner, G.K., Reisinger, A., Segschneider, J., Shaffer, G., Steinacher, M., Strassmann, K., Tanaka, K., Timmermann, A., Weaver, A.J., 2013. Carbon dioxide and climate impulse response functions for the computation of greenhouse gas metrics: A multi-model analysis. Atmos. Chem. Phys. 13, 2793–2825. doi:10.5194/acp-13-2793-2013

Jouzel, J., Ouzeau, G., Déqué, M., Jouini, M., Planton, S., Vautard, R., 2014. Le climat de la France au XXIe siècle, Volume 4, Scénarios régionalisés: édition 2014 pour la métropole et les régions d'outre-mer. Ministère de l'Écologie, du Développement durable et de l'Énergie 62.

Jurado, A., Borges, A. V., Brouyère, S., 2017. Dynamics and emissions of N2O in groundwater: A review. Sci. Total Environ. 584–585, 207–218. doi:10.1016/j.scitotenv.2017.01.127

Kandel, T.P., Lærke, P.E., Elsgaard, L., 2018. Annual emissions of CO2, CH4and N2O from a temperate peat bog: Comparison of an undrained and four drained sites under permanent grass and arable crop rotations with cereals and potato. Agric. For. Meteorol. 256–257, 470–481. doi:10.1016/j.agrformet.2018.03.021

Kempe, S., 1984. Sinks of the anthropogenically enhanced carbon cycle in surface fresh waters. J. Geophys. Res. 89, 4657. doi:10.1029/JD089iD03p04657

Kempe, S., 1982. Long-term records of CO2 pressure fluctuations in fresh waters. Transp. carbon Miner. major world rivers, part 1 91–332.

Khalil, M.A.K., Rasmussen, R.A., Shearer, M.J., 2002. Atmospheric nitrous oxide: Patterns of global change during recent decades and centuries. Chemosphere 47, 807–821. doi:10.1016/S0045-6535(01)00297-1

Kim, D.G., Kirschbaum, M.U.F., 2015. The effect of land-use change on the net exchange rates of greenhouse gases: A compilation of estimates. Agric. Ecosyst. Environ. doi:10.1016/j.agee.2015.04.026

Kirschbaum, M.U.F., Saggar, S., Tate, K.R., Giltrap, D.L., Ausseil, A.G.E., Greenhalgh, S., Whitehead, D., 2012. Comprehensive evaluation of the climate-change implications of shifting land use between forest and grassland: New Zealand as a case study. Agric. Ecosyst. Environ. doi:10.1016/j.agee.2012.01.004

Kroeze, C., Dumont, E., Seitzinger, S., 2010. New Estimates of Global Emissions of N_2O from Rivers and Estuaries. J. Integr. Environ. Sci. 2, 159–165. doi:10.1080/1943815X.2010.496789

Lambert, T., Bouillon, S., Darchambeau, F., Morana, C., Roland, F.A.E., Descy, J.P., Borges, A. V., 2017. Effects of human land use on the terrestrial and aquatic sources of fluvial organic matter in a temperate river basin (The Meuse River, Belgium). Biogeochemistry 136, 191–211. doi:10.1007/s10533-017-0387-9

Lancelot, C., Veth, C., Mathot, S., 1991. Modelling ice-edge phytoplankton bloom in the Scotia-Weddell sea sector of the Southern Ocean during spring 1988. J. Mar. Syst. 2, 333–346. doi:10.1016/0924-7963(91)90040-2

Langerwisch, F., Walz, A., Rammig, A., Tietjen, B., Thonicke, K., Cramer, W., 2016. Climate change increases riverine carbon outgassing, while export to the ocean remains uncertain. Earth Syst. Dyn. 7, 559–582. doi:10.5194/esd-7-559-2016

Laruelle, G.G., Dürr, H.H., Lauerwald, R., Hartmann, J., Slomp, C.P., Goossens, N., Regnier, P.A.G., 2013. Global multi-scale segmentation of continental and coastal waters from the watersheds to the continental margins. Hydrol. Earth Syst. Sci. 17, 2029–2051. doi:10.5194/hess-17-2029-2013

Laruelle, G.G., Goossens, N., Arndt, S., Cai, W.J., Regnier, P., 2017a. Air-water CO2 evasion from US East Coast estuaries. Biogeosciences 14, 2441–2468. doi:10.5194/bg-14-2441-2017

Laruelle, G.G., Landschützer, P., Gruber, N., Ti, J.L., Delille, B., Regnier, P., 2017b. Global high-resolution monthly pCO2 climatology for the coastal ocean derived from neural network interpolation. Biogeosciences 14, 4545–4561. doi:10.5194/bg-14-4545-2017

Laruelle, G.G., Lauerwald, R., Rotschi, J., Raymond, P.A., Hartmann, J., Regnier, P., 2015. Seasonal response of air – water CO2 exchange along the land – ocean aquatic continuum of the northeast North American coast . 1447–1458. doi:10.5194/bg-12-1447-2015

Laruelle, G.G., Regnier, P., Ragueneau, O., Kempa, M., Moriceau, B., Longphuirt, S.N., Leynaert, A., Thouzeau, G., Chauvaud, L., 2009. Benthic-pelagic coupling and the seasonal silic cycle in the bay of brest (France): New insights from a coupled physical-biological model. Mar. Ecol. Prog. Ser. 385, 15–32. doi:10.3354/meps07884

Lassaletta, L., Billen, G., Grizzetti, B., Anglade, J., Garnier, J., 2014a. 50 year trends in nitrogen use efficiency of world cropping systems: The relationship between yield and nitrogen input to cropland. Environ. Res. Lett. 9. doi:10.1088/1748-9326/9/10/105011

Lassaletta, L., Billen, G., Romero, E., Garnier, J., Aguilera, E., 2014b. How changes in diet and trade patterns have shaped the N cycle at the national scale: Spain (1961-2009). Reg. Environ. Chang. 14, 785–797. doi:10.1007/s10113-013-0536-1

Lauerwald, R., Laruelle, G.G., Hartmann, J., Ciais, P., Regnier, P.A.G., 2015. Spatial patterns in CO_2 evasion from the global river network. Global Biogeochem. Cycles 29, 534–554. doi:10.1002/2014GB004941

Laverman, A.M., Garnier, J.A., Mounier, E.M., Roose-Amsaleg, C.L., 2010. Nitrous oxide production kinetics during nitrate reduction in river sediments. Water Res. 44, 1753–1764. doi:10.1016/j.watres.2009.11.050

Laville, P., Lehuger, S., Loubet, B., Chaumartin, F., Cellier, P., 2011. Effect of management, climate and soil conditions on N_2O and NO emissions from an arable crop rotation using high temporal resolution measurements. Agric. For. Meteorol. 151, 228–240. doi:10.1016/j.agrformet.2010.10.008

Le Noë, J., Billen, G., Esculier, F., Garnier, J., 2018. Long-term socioecological trajectories of agro-food systems revealed by N and P flows in French regions from 1852 to 2014. Agric. Ecosyst. Environ. 265, 132–143. doi:10.1016/j.agee.2018.06.006

Le Noë, J., Billen, G., Garnier, J., 2017. How the structure of agro-food systems shapes nitrogen, phosphorus, and carbon fluxes: The generalized representation of agro-food system applied at the regional scale in France. Sci. Total Environ. 586, 42–55. doi:10.1016/j.scitotenv.2017.02.040

Le Noë, J., Billen, G., Lassaletta, L., Silvestre, M., Garnier, J., 2016. Importance of agricultural transport in the biogeochemical cycle of nitrogen in France: Insight into territorial production specialization. Cah. Agric. 25, 0–14. doi:10.1051/cagri/2016002

Le Quéré, C., Moriarty, R., Andrew, R.M., Peters, G.P., Ciais, P., Friedlingstein, P., Jones, S.D., Sitch, S., Tans, P., Arneth, A., Boden, T.A., Bopp, L., Bozec, Y., Canadell, J.G., Chini, L.P., Chevallier, F., Cosca, C.E., Harris, I., Hoppema, M., Houghton, R.A., House, J.I., Jain, A.K., Johannessen, T., Kato, E., Keeling, R.F., Kitidis, V., Klein Goldewijk, K., Koven, C., Landa, C.S., Landschützer, P., Lenton, A., Lima, I.D., Marland, G., Mathis, J.T., Metzl, N., Nojiri, Y., Olsen, A., Ono, T., Peng, S., Peters, W., Pfeil, B., Poulter, B., Raupach, M.R., Regnier, P., Rödenbeck, C., Saito, S., Salisbury, J.E., Schuster, U., Schwinger, J., Séférian, R., Segschneider, J., Steinhoff, T., Stocker, B.D., Sutton, A.J., Takahashi, T., Tilbrook, B., van der Werf, G.R., Viovy, N., Wang, Y.-P., Wanninkhof, R., Wiltshire, A., Zeng, N., 2015. Global carbon budget 2014. Earth Syst. Sci. Data 7, 47–85. doi:10.5194/essd-7-47-2015

Le, T.P.Q., Billen, G., Garnier, J., Chau, V.M., 2014. Long-term biogeochemical functioning of the Red River (Vietnam): past and present situations. Reg. Environ. Chang. 15, 329–339. doi:10.1007/s10113-014-0646-4

Lemke, R.L., Zhong, Z., Campbell, C.A., Zentner, R., 2007. Can pulse crops play a role in mitigating greenhouse gases from North American agriculture?, in: Agronomy Journal. pp. 1719–1725. doi:10.2134/agronj2006.0327s

Li, S., Lu, X.X., Bush, R.T., 2013. CO2 partial pressure and CO2 emission in the Lower Mekong River. J. Hydrol. 504, 40–56. doi:10.1016/j.jhydrol.2013.09.024

Liss, P.S., Merlivat, L., 1986. Air-Sea Gas Exchange Rates: Introduction and Synthesis, in: Buat-Ménard, P. (Ed.), The Role of Air-Sea Exchange in Geochemical Cycling. Springer Netherlands, Dordrecht, pp. 113–127. doi:10.1007/978-94-009-4738-2_5

Looman, A., Maher, D.T., Pendall, E., Bass, A., Santos, I.R., 2017. The carbon dioxide evasion cycle of an intermittent first-order stream: contrasting water–air and soil–air exchange. Biogeochemistry 134, 237–238. doi:10.1007/s10533-017-0347-4

Lorenzen, C., 1967. Determination of chlorophyll and pheopigments:spectrophotometric equations. Limnol. Oceanogr. 12, 343–346. doi:10.4319/lo.1967.12.2.0343

Lower, S.S.K., 1999. Carbonate equilibria in natural waters. Simon Fraser Univ. Chem 1, 1–26. doi:http://dx.doi.org/10.1063/1.555900

Lu, Y., Huang, Y., Zou, J., Zheng, X., 2006. An inventory of N2O emissions from agriculture in China using precipitation-rectified emission factor and background emission. Chemosphere 65, 1915–1924. doi:10.1016/j.chemosphere.2006.07.035

Lu, Z., Du, R., Du, P., Qin, S., Liang, Z., Li, Z., Wang, Y., Wang, Y., 2015. Influences of Land se/Cover types on nitrous oxide emissions during freeze-thaw periods from waterlogged soils in inner Mongolia. PLoS One 10, 1–18. doi:10.1371/journal.pone.0139316

Maavara, T., Lauerwald, R., Regnier, P., Van Cappellen, P., 2017. Global perturbation of organic carbon cycling by river damming. Nat. Commun. 8, 1–10. doi:10.1038/ncomms15347

MacFarling Meure, C., Etheridge, D., Trudinger, C., Steele, P., Langenfelds, R., Van Ommen, T., Smith, A., Elkins, J., 2006. Law Dome CO2, CH4 and N2O ice core records extended to 2000 years BP. Geophys. Res. Lett. 33, 2000–2003. doi:10.1029/2006GL026152

Mackenzie, F.T., De Carlo, E.H., Lerman, A., 2011. Coupled C, N, P, and O Biogeochemical Cycling at the Land-Ocean Interface, Treatise on Estuarine and Coastal Science. Elsevier Inc. doi:10.1016/B978-0-12-374711-2.00512-X

Mackereth, F.J.H., Heron, J., Talling, J.F., 1978. Water Analysis: Some Revised Methods for Limnologists. Ambleside Freshw. Biol. Assoc. doi:10.1007/s00374-013-0801-y

Maeck, A., Delsontro, T., Mcginnis, D.F., Fischer, H., Flury, S., Schmidt, M., Fietzek, P., Lorke, A., 2013. Sediment Trapping by Dams Creates Methane Emission Hot Spots. doi:10.1021/es4003907

Manickam, S., Barbaroux, L., Ottmann, F., 1985. Composition and mineralogy of suspended sediment in the fluvio-estuarine zone of the Loire River, France. Sedimentology 32, 721–741. doi:10.1111/j.1365-3091.1985.tb00484.x

Marescaux, A., Thieu, V., Borges, A.V., Garnier, J., 2018a. Seasonal and spatial variability of the partial pressure of carbon dioxide in the human-impacted Seine River in France. Sci. Rep. 8, 13961. doi:10.1038/s41598-018-32332-2

Marescaux, A., Thieu, V., Garnier, J., 2018b. Carbon dioxide, methane and nitrous oxide emissions from the human-impacted Seine watershed in France. Sci. Total Environ. 643, 247–259. doi:10.1016/j.scitotenv.2018.06.151

Martinez-Cruz, K., Gonzalez-Valencia, R., Sepulveda-Jauregui, A., Plascencia-Hernandez, F., Belmonte-Izquierdo, Y., Thalasso, F., 2017. Methane emission from aquatic ecosystems of Mexico City. Aquat. Sci. 79, 159–169. doi:10.1007/s00027-016-0487-y

Marx, A., Conrad, M., Aizinger, V., Prechtel, A., Van Geldern, R., Barth, J.A.C., 2018. Groundwater data improve modelling of headwater stream CO2outgassing with a stable DIC isotope approach. Biogeosciences 15, 3093–3106. doi:10.5194/bg-15-3093-2018

Marx, A., Dusek, J., Jankovec, J., Sanda, M., Vogel, T., van Geldern, R., Hartmann, J., Barth, J.A.C., 2017. A review of CO2 and associated carbon dynamics in headwater streams: A global perspective. Rev. Geophys. 55, 560–585. doi:10.1002/2016RG000547

McGinnis, D.F., Bilsley, N., Schmidt, M., Fietzek, P., Bodmer, P., Premke, K., Lorke, A., Flury, S., 2016. Deconstructing Methane Emissions from a Small Northern European River: Hydrodynamics and Temperature as Key Drivers. Environ. Sci. Technol. 50, 11680–11687. doi:10.1021/acs.est.6b03268

McMahon, P.B., Dennehy, K.F., 1999. N2O emissions from a nitrogen-enriched river. Environ. Sci. Technol. 33, 21–25. doi:10.1021/es980645n

Meehl, G. A., Stocker, T. F., Collins, W. D., Friedlingstein, P., G., A. T., Gregory, J. M., Kitoh, A., Knutti, R., Murphy, J. M., N., A., Raper, S. C. B., Watterson, I. G., J., W. A., Zhao, Z.-C., 2007. Global Climate Projections, in: Solomon, S., Qin, D., Manning, M., Chen, Z., Marquis, M., Averyt, K.B., Tignor, M., Miller, H.L. (Eds.), Climate Change 2007: The Physical Science Basis. Contribution of Working Group I to Fourth Assessment Report of the Intergovernmental Panel on Climate Change. Cambridge, United Kingdom and New York, NY, USA, p. 996.

Mégnien, C., 1980. Synthèse géologique du bassin de Paris, Mémoires du BRGM Fr. Édition du B.R.G.M.

Meybeck, M., 2006. Origins and behaviors of carbon species in world rivers. Soil Eros. Carbon Dyn. 209–238.

Meybeck, M., 1993. Riverine transport of atmospheric carbon: Sources, global typology and budget. Water, Air, Soil Pollut. 70, 443–463. doi:10.1007/BF01105015

Meybeck, M., 1987. Global chemical weathering of surficial rocks estimated from river dissolved loads. Am. J. Sci. doi:10.2475/ajs.287.5.401

Meybeck, M., Dürr, H.H., Vörösmarty, C.J., 2006. Global coastal segmentation and its river catchment contributors: A new look at land-ocean linkage. Global Biogeochem. Cycles 20. doi:10.1029/2005GB002540

Michard, G., 2008. Can we explain atmospheric carbon dioxide oscillations during the past 400,000 years? Comptes Rendus - Geosci. 340, 483–494. doi:10.1016/j.crte.2008.06.004

Miettinen, H., Pumpanen, J., Heiskanen, J.J., Aaltonen, H., Mammarella, I., Ojala, A., Levula, J., Rantakari, M., 2015. Towards a more comprehensive understanding of lacustrine greenhouse gas dynamics — two-year measurements of concentrations and fluxes of CO 2 , CH 4 and N 2 O in a typical boreal lake surrounded by managed forests. Boreal Env. Res. 20, 75–89.

Mignolet, C., Schott, C., Benoît, M., 2007. Spatial dynamics of farming practices in the Seine basin: Methods for agronomic approaches on a regional scale. Sci. Total Environ. 375, 13–32. doi:10.1016/j.scitotenv.2006.12.004

Millero, F.J., 1979. The thermodynamics of the carbonate system in seawater. Geochim. Cosmochim. Acta 43, 1651–1661. doi:10.1016/0016-7037(79)90184-4

Millero, F.J., Graham, T.B., Huang, F., Bustos-Serrano, H., Pierrot, D., 2006. Dissociation constants of carbonic acid in seawater as a function of salinity and temperature. Mar. Chem. 100, 80–94. doi:10.1016/j.marchem.2005.12.001

Millero, F.J., Poisson, A., 1981. International one-atmosphere equation of state of seawater. Deep Sea Res. Part A, Oceanogr. Res. Pap. 28, 625–629. doi:10.1016/0198-0149(81)90122-9

Minaudo, C., Curie, F., Jullian, Y., Gassama, N., Moatar, F., 2018. QUAL-NET, a high temporal-resolution eutrophication model for large hydrographic networks. Biogeosciences 15, 2251–2269. doi:10.5194/bg-15-2251-2018

Minshall, G.W., Petersen, R.C., Cummins, K.W., Bott, T.L., Sedell, J.R., Cushing, C.E., Vannote, R.L., 1983. Interbiome Comparison of Stream Ecosystem Dynamics. Ecol. Monogr. 53, 1–25. doi:10.2307/1942585

Morelle, J., Schapira, M., Françoise, S., Courtay, G., Orvain, F., Claquin, P., 2018. Dynamics of exopolymeric carbon pools in relation with phytoplankton succession along the salinity gradient of a temperate estuary (France). Estuar. Coast. Shelf Sci. 209, 18–29. doi:10.1016/j.ecss.2018.05.008

Moss, A.R., Jouany, J.-P., Newbold, J., 2000. Methane production by ruminants: its contribution to global warming. Ann. Zootech. 49, 231–253. doi:10.1051/animres:2000119

Mulholland, P.J., Kuenzler, E.J., 1979. Organic carbon export from upland and forested wetland watersheds. Limnol. Oceanogr. 24, 960–966. doi:10.4319/lo.1979.24.5.0960

Muller, A., Schader, C., El-Hage Scialabba, N., Brüggemann, J., Isensee, A., Erb, K.H., Smith, P., Klocke, P., Leiber, F., Stolze, M., Niggli, U., 2017. Strategies for feeding the world more sustainably with organic agriculture. Nat. Commun. 8, 1–13. doi:10.1038/s41467-017-01410-w

Myhre, G., Shindell, D., Bréon, F.-M., Collins, W., Fuglestvedt, J., Huang, J., Koch, D., Lamarque, J.-F., Lee, D., Mendoza, B., Nakajima, T., Robock, A., Stephens, G., Takemura, T., Zhang, H., 2013. Anthropogenic and Natural Radiative Forcing, in: Stocker, T.F., Qin, D., Plattner, G.-K., Tignor, M., Allen, S.K., Boschung, J., Nauels, A., Xia, Y., Bex, V., Midgley, P.M. (Eds.), Climate Change 2013: The Physical Science Basis. Contribution of Working Group I to the Fifth Assessment Report of the Intergovernmental Panel on Climate Change. Cambridge, United Kingdom and New York, NY, USA, pp. 659–740. doi:10.1017/ CBO9781107415324.018

Nakayama, T., 2016. New perspective for eco-hydrology model to constrain missing role of inland waters on boundless biogeochemical cycle in terrestrial aquatic continuum. Ecohydrol. Hydrobiol. 16, 138–148. doi:10.1016/j.ecohyd.2016.07.002

Neal, C., House, W.A., Down, K., 1998. An assessment of excess CO2 partical pressures in natural water based on pH and alkalinity. Sci. Total Environ. 210/211, 173–185.

Nightingale, P.D., Malin, G., Law, C.S., Watson, A.J., Liss, P.S., Liddicoat, M.I., Boutin, J., Upstill-Goddard, R.C., 2000. In situ evaluation of air-sea gas exchange parameterizations usingn ovel conservativea nd volatile tracers. Glob. Biochem. Cycles 14, 373–387.

Nydahl, A.C., Wallin, M.B., Weyhenmeyer, G.A., 2017. No long-term trends in p CO_2 despite increasing organic carbon concentrations in boreal lakes, streams, and rivers. Global Biogeochem. Cycles 31, 985–995. doi:10.1002/2016GB005539

O'Connor, D.J., Dobbins, W.E., 1958. Mechanism of reaeration in natural streams. Trans. Am. Soc. Civ. Eng. 123, 641–684.

Ojima, D.S., Valentine, D.W., Mosier, A.R., Parton, W.J., Schimel, D.S., 1993. Effect of land use change on methane oxidation in temperate forest and grassland soils. Chemosphere 26, 675–685. doi:10.1016/0045-6535(93)90452-B

Öquist, M.G., Wallin, M., Seibert, J., Bishop, K., Laudon, H., 2009. Dissolved Inorganic Carbon Export Across the Soil / Stream Interface and Its Fate in a Boreal Headwater Stream. Environ. Sci. Technol. 43, 7364–7369.

Park, P.K., 1969. Oceanic CO2 system: an evaluation of then methods of investigation. Limnol. Oceanogr. 14, 179–186.

Passy, P., Gypens, N., Billen, G., Garnier, J., Thieu, V., Rousseau, V., Callens, J., Parent, J.-Y., Lancelot, C., 2013. A model reconstruction of riverine nutrient fluxes and eutrophication in the Belgian Coastal Zone since 1984. J. Mar. Syst. 128, 106–122. doi:10.1016/j.jmarsys.2013.05.005

Passy, P., Le Gendre, R., Garnier, J., Cugier, P., Callens, J., Paris, F., Billen, G., Riou, P., Romero, E., 2016. Eutrophication modelling chain for improved management strategies to prevent algal blooms in the Bay of Seine. Mar. Ecol. Prog. Ser. 543, 107–125. doi:10.3354/meps11533

Pataki, D.E., Alig, R.J., Fung, A.S., Golubiewski, N.E., Kennedy, C.A., Mcpherson, E.G., Nowak, D.J., Pouyat, R. V., Lankao, P.R., 2006. Urban ecosystems and the North American carbon cycle. Glob. Chang. Biol. 12, 2092–2102. doi:10.1111/j.1365-2486.2006.01242.x

Patzek, T.W., 2003. Energy Required to Produce Corn. Civil and Environmental Engineering, U.C. Berkeley, March 12, 2003 [WWW Document]. URL http://petroleum.berkeley.edu/patzek/ce24/ce24top.htm (accessed 11.6.18).

Pawellek, F., Veizer, J., 1994. Carbon cycle in the upper Danube and its tributaries: δ13CDIC constraints. Isr. J. Earth Sci. 43, 187–194.

Pedersen, O., Colmer, T.D., Sand-Jensen, K., 2013. Underwater Photosynthesis of Submerged Plants – Recent Advances and Methods. Front. Plant Sci. 4. doi:10.3389/fpls.2013.00140

Pelletier, G.J., Chapra, S.C., Tao, H., 2006. QUAL2Kw - A framework for modeling water quality in streams and rivers using a genetic algorithm for calibration. Environ. Model. Softw. 21, 419–425. doi:10.1016/j.envsoft.2005.07.002

Pierrot, D., Lewis, D.E., Wallace, D.W.R., 2006. MS Excel Program Developed for CO2 System Calculations. ORNL/CDIAC-105a. Carbon Dioxide Inf. Anal. Center, Oak Ridge Natl. Lab. U.S. Dep. Energy, Oak Ridge, Tennessee. doi:10.3334/CDIAC/otg.CO2SYS_XLS_CDIAC105a

Pimentel, D., Harvey, C., Resosudarmo, P., Sinclair, K., Kuiz, D., Mcnair, M., Crist, S., Shpritz, L., Fitton, L., Saffouri, I., Blair, R., 1995. Environmental and economic erosion and conservation costs of soil benefits. Science (80-.). 267, 1117–1123.

Plaza-Bonilla, D., Álvaro-Fuentes, J., Arrúe, J.L., Cantero-Martínez, C., 2014. Tillage and nitrogen fertilization effects on nitrous oxide yield-scaled emissions in a rainfed Mediterranean area. Agric. Ecosyst. Environ. 189, 43–52. doi:10.1016/j.agee.2014.03.023

Poisvert, C., Curie, F., Moatar, F., 2017. Annual agricultural N surplus in France over a 70-year period. Nutr. Cycl. Agroecosystems 107, 63–78. doi:10.1007/s10705-016-9814-x

Polsenaere, P., Abril, G., 2012. Modelling CO2degassing from small acidic rivers using water pCO2, DIC and δ13C-DIC data. Geochim. Cosmochim. Acta 91, 220–239. doi:10.1016/j.gca.2012.05.030

Polsenaere, P., Savoye, N., Etcheber, H., Canton, M., Poirier, D., Bouillon, S., Abril, G., 2013. Export and degassing of terrestrial carbon through watercourses draining a temperate podzolized catchment. Aquat. Sci. 75, 299–319. doi:10.1007/s00027-012-0275-2

Pomerol, C., Feugueur, L.L., 1986. Bassin de Paris: Ile de France, Pays de Bray, Guides géologiques régionaux. Masson, Paris.

Poux, X., Aubert, P.-M., 2018. Une Europe agroécologique en 2050 : une agriculture multifonctionnelle pour une alimentation saine. Iddri.

Poux, X., Narcy, J.-B., Chenat, V., 2005. Agriculture et environnement: 4 scénarios à l'horizon 2025. Groupe de la Bussière. ASCA.

Prairie, Y.T., Alm, J., Beaulieu, J., Barros, N., Battin, T., Cole, J., Del Giorgio, P., DelSontro, T., Guérin, F., Harby, A., Harrison, J., Mercier-Blais, S., Serça, D., Sobek, S., Vachon, D., 2017. Greenhouse Gas Emissions from Freshwater Reservoirs: What Does the Atmosphere See? Ecosystems 1–14. doi:10.1007/s10021-017-0198-9

Prairie, Y.T., Cole, J.J., 2009. Carbon , Unifying Currency. Encycl. Inl. Waters 2, 743–746. doi:http://dx.doi.org/10.1016/B978-012370626-3.00107-1

Prairie, Y.T., Duarte, C.M., 2007. Direct and indirect metabolic CO2 release by humanity. Biogeosciences 4, 215–217. doi:10.5194/bg-4-215-2007

Prasad, M.B.K., Kaushal, S.S., Murtugudde, R., 2013. Long-term pCO2 dynamics in rivers in the Chesapeake Bay watershed. Appl. Geochemistry 31, 209–215. doi:10.1016/j.apgeochem.2013.01.006

Prather, M.J., Holmes, C.D., Hsu, J., 2012. Reactive greenhouse gas scenarios: Systematic exploration of uncertainties and the role of atmospheric chemistry. Geophys. Res. Lett. 39. doi:10.1029/2012GL051440

Prentice, I.C., Farquhar, G.D., Fasham, M.J.R., Goulden, M.L., Heimann, M., Jaramillo, V.J., Kheshgi, H.S., Le Quéré, C., Scholes, R.J., Wallace, D.W.R., 2001. The carbon cycle and atmospheric carbon dioxide, in: Climate Change 2001: The Scientific Basis. pp. 183–237. doi:10.1256/004316502320517344

QGIS Development Team, 2016. QGIS Geographic Information System 2.18. Open Source Geospatial Found.

Qualls, R.G., Haines, B.L., Swank, W.T., Tyler, S.W., 2002. Retention of soluble organic nutrients by a forested ecosystem. Biogeochemistry 61, 135–171. doi:10.1023/A:1020239112586

Quintana-Seguí, P., Le Moigne, P., Durand, Y., Martin, E., Habets, F., Baillon, M., Canellas, C., Franchisteguy, L., Morel, S., 2008. Analysis of near-surface atmospheric variables: Validation of the SAFRAN analysis over France. J. Appl. Meteorol. Climatol. 47, 92–107. doi:10.1175/2007JAMC1636.1

R Core team, 2015. R Core Team. R A Lang. Environ. Stat. Comput. R Found. Stat. Comput. Vienna, Austria. ISBN 3-900051-07-0, URL http//www.R-project.org/.

Raimonet, M., Thieu, V., Silvestre, M., Oudin, L., Rabouille, C., Vautard, R., Garnier, J., 2018. Landward perspective of coastal eutrophication potential under future climate change: The Seine River case (France). Front. Mar. Sci. 5, 1–16. doi:10.3389/fmars.2018.00136

Rajkumar, A.N., Barnes, J., Ramesh, R., Purvaja, R., Upstill-goddard, R.C., 2008. Methane and nitrous oxide fluxes in the polluted Adyar River and estuary , SE India. Mar. Pollut. Bull. 56, 2043–2051. doi:10.1016/j.marpolbul.2008.08.005

Ran, L., Lu, X.X., Liu, S., 2017. Dynamics of riverine CO2 in the Yangtze River fluvial network and their implications for carbon evasion. Biogeosciences 14, 2183–2198. doi:10.5194/bg-14-2183-2017

Rasilo, T., Hutchins, R.H.S., Ruiz-González, C., del Giorgio, P.A., 2017. Transport and transformation of soil-derived CO2, CH4 and DOC sustain CO2 supersaturation in small boreal streams. Sci. Total Environ. 579, 902–912. doi:10.1016/j.scitotenv.2016.10.187

Raymond, P.A., Bauer, J.E., Cole, J.J., 2000. Atmospheric CO<inf>2</inf> evasion, dissolved inorganic carbon production, and net heterotrophy in the York River estuary. Limnol. Oceanogr. 45, 1707–1717. doi:10.4319/lo.2000.45.8.1707

Raymond, P.A., Caraco, N.F., Cole, J.J., 1997. Carbon dioxide concentration and atmospheric flux in the Hudson River. Estuaries 20, 381–390. doi:10.1007/BF02690380

Raymond, P.A., Cole, J.J., 2001. Gas Exchange in Rivers and Estuaries: Choosing a Gas Transfer Velocity. Estuaries 24, 312. doi:10.2307/1352954

Raymond, P.A., Hartmann, J., Lauerwald, R., Sobek, S., McDonald, C., Hoover, M., Butman, D., Striegl, R., Mayorga, E., Humborg, C., Kortelainen, P., Dürr, H., Meybeck, M., Ciais, P., Guth, P., 2013. Global carbon dioxide emissions from inland waters. Nature 503, 355–359. doi:10.1038/nature12760

Raymond, P.A., Saiers, J.E., 2010. Event controlled DOC export from forested watersheds. Biogeochemistry 100, 197–209. doi:10.1007/s10533-010-9416-7

Raymond, P.A., Zappa, C.J., Butman, D., Bott, T.L., Potter, J., Mulholland, P., Laursen, A.E., McDowell, W.H., Newbold, D., 2012. Scaling the gas transfer velocity and hydraulic geometry in streams and small rivers. Limnol. Oceanogr. Fluids Environ. 2, 41–53. doi:10.1215/21573689-1597669

Recio, J., Vallejo, A., Le-Noë, J., Garnier, J., García-Marco, S., Álvarez, J.M., Sanz-Cobena, A., 2018. The effect of nitrification inhibitors on NH3and N2O emissions in highly N fertilized irrigated Mediterranean cropping systems. Sci. Total Environ. 636, 427–436. doi:10.1016/j.scitotenv.2018.04.294

Regnier, P., Arndt, S., Goossens, N., Volta, C., Laruelle, G.G., Lauerwald, R., Hartmann, J., 2013a. Modelling Estuarine Biogeochemical Dynamics: From the Local to the Global Scale. Aquat. Geochemistry 19, 591–626. doi:10.1007/s10498-013-9218-3

Regnier, P., Friedlingstein, P., Ciais, P., Mackenzie, F.T., Gruber, N., Janssens, I. a., Laruelle, G.G., Lauerwald, R., Luyssaert, S., Andersson, A.J., Arndt, S., Arnosti, C., Borges, A. V., Dale, A.W., Gallego-Sala, A., Goddéris, Y., Goossens, N., Hartmann, J., Heinze, C., Ilyina, T., Joos, F., LaRowe, D.E., Leifeld, J., Meysman, F.J.R., Munhoven, G., Raymond, P. a., Spahni, R., Suntharalingam, P., Thullner, M., 2013b. Anthropogenic perturbation of the carbon fluxes from land to ocean. Nat. Geosci. 6, 597–607. doi:10.1038/ngeo1830

Regnier, P., Mouchet, A., Wollast, R., Ronday, F., 1998. A discussion of methods for estimating residual fluxes in strong tidal estuaries. Cont. Shelf Res. 18, 1543–1571. doi:10.1016/S0278-4343(98)00071-5

Regnier, P., O'Kane, J.P., Steefel, C.I., Vanderborght, J.P., 2002. Modeling complex multi-component reactive-transport systems: Towards a simulation environment based on the concept of a knowledge base. Appl. Math. Model. 26, 913–927. doi:10.1016/S0307-904X(02)00047-1

Regnier, P., Steefel, C.I., 1999. A high resolution estimate of the inorganic nitrogen flux from the Scheldt estuary to the coastal North Sea during a nitrogen-limited algal bloom, spring 1995. Geochim. Cosmochim. Acta 63, 1359–1374. doi:10.1016/S0016-7037(99)00034-4

Regnier, P., Wollast, R., Steefel, C.I., 1997. Long-term fluxes of reactive species in macrotidal estuaries: Estimates from a fully transient, multicomponent reaction-transport model, in: Marine Chemistry. pp. 127–145. doi:10.1016/S0304-4203(97)00030-3

Resplandy, L., Keeling, R.F., Eddebbar, Y., Brooks, M.K., Wang, R., Bopp, L., Long, M.C., Dunne, J.P., Koeve, W., Oschlies, A., 2018. Quantification of ocean heat uptake from changes in atmospheric O2 and CO2 composition. Nature 563, 105–108. doi:10.1038/s41586-018-0651-8

Richey, J.E., Melack, J.M., Aufdenkampe, A.K., Ballester, V.M., Hess, L.L., 2002. Outgassing from Amazonian rivers and wetlands as a large tropical source of atmospheric CO2. Nature 416, 617–620. doi:10.1038/416617a

Rocher, V., Azimi, S., 2017. Evolution de la qualité de la Seine en lien avec les progrès de l'assainissement, Johanet. ed. Paris.

Romero, E., Garnier, J., Billen, G., Ramarson, A., Riou, P., Le Gendre, R., 2018a. The biogeochemical functioning of the Seine estuary and the nearby coastal zone: export, retention and transformations. A modelling approach. Limnol. Ocean. . doi:10.1002/lno.11082

Romero, E., Garnier, J., Billen, G., Ramarson, A., Riou, P., Le Gendre, R., 2018b. The biogeochemical functioning of the Seine estuary and the nearby coastal zone: export, retention and transformations. A modelling approach. Limnol. Ocean. . doi:DOI: 10.1002/lno.11082

Romero, E., Le Gendre, R., Garnier, J., Billen, G., Fisson, C., Silvestre, M., Riou, P., 2016. Long-term water quality in the lower Seine: Lessons learned over 4 decades of monitoring. Environ. Sci. Policy 58, 141–154. doi:10.1016/j.envsci.2016.01.016

Roobaert, A., Laruelle, G.G., Landschützer, P., Regnier, P., 2018. Uncertainty in the global oceanic CO2 uptake induced by wind forcing: Quantification and spatial analysis. Biogeosciences 15, 1701–1720. doi:10.5194/bg-15-1701-2018

Saggar, S., Jha, N., Deslippe, J., Bolan, N.S., Luo, J., Giltrap, D.L., Kim, D.G., Zaman, M., Tillman, R.W., 2013. Denitrification and N2O: N2 production in temperate grasslands: Processes, measurements, modelling and mitigating negative impacts. Sci. Total Environ. 465, 173–195. doi:10.1016/j.scitotenv.2012.11.050

Sanchez-Martín, L., Meijide, A., Garcia-Torres, L., Vallejo, A., 2010. Combination of drip irrigation and organic fertilizer for mitigating emissions of nitrogen oxides in semiarid climate. Agric. Ecosyst. Environ. 137, 99–107. doi:10.1016/j.agee.2010.01.006

Sanz-Cobena, A., Lassaletta, L., Aguilera, E., Prado, A. del, Garnier, J., Billen, G., Iglesias, A., Sánchez, B., Guardia, G., Abalos, D., Plaza-Bonilla, D., Puigdueta-Bartolomé, I., Moral, R., Galán, E., Arriaga, H., Merino, P., Infante-Amate, J., Meijide, A., Pardo, G., Álvaro-Fuentes, J., Gilsanz, C., Báez, D., Doltra, J., González-Ubierna, S., Cayuela, M.L., Menéndez, S., Díaz-Pinés, E., Le-Noë, J., Quemada, M., Estellés, F., Calvet, S., van Grinsven, H.J.M., Westhoek, H., Sanz, M.J., Gimeno, B.S., Vallejo, A., Smith, P., 2017. Strategies for greenhouse gas emissions mitigation in Mediterranean agriculture: A review. Agric. Ecosyst. Environ. 238, 5–24. doi:10.1016/j.agee.2016.09.038

Sanz-Cobena, A., Sánchez-Martín, L., García-Torres, L., Vallejo, A., 2012. Gaseous emissions of N2O and NO and NO3-leaching from urea applied with urease and nitrification inhibitors to a maize (Zea mays) crop. Agric. Ecosyst. Environ. 149, 64–73. doi:10.1016/j.agee.2011.12.016

Savenije, H.H.G., 2012. Salinity and tides in alluvial estuaries, 2nd completely revised edition: salinityandtides.com, Open Access.

Savenije, H.H.G., 1992. Lagrangian solution of St. Venant's equations for alluvial estuary. J. Hydraul. Eng. 118, 1153–1163. doi:10.1061/(ASCE)0733-9429(1992)118:8(1153)

Sawakuchi, H.O., Bastviken, D., Sawakuchi, A.O., Krusche, A. V., Ballester, M.V.R., Richey, J.E., 2014. Methane emissions from Amazonian Rivers and their contribution to the global methane budget. Glob. Chang. Biol. 20, 2829–2840. doi:10.1111/gcb.12646

Sawakuchi, H.O., Neu, V., Ward, N.D., Barros, M. de L.C., Valerio, A.M., Gagne-Maynard, W., Cunha, A.C., Less, D.F.S., Diniz, J.E.M., Brito, D.C., Krusche, A. V., Richey, J.E., 2017. Carbon Dioxide Emissions along the Lower Amazon River. Front. Mar. Sci. 4, 1–12. doi:10.3389/fmars.2017.00076

Schade, J.D., Bailio, J., McDowell, W.H., 2016. Greenhouse gas flux from headwater streams in New Hampshire, USA: Patterns and drivers. Limnol. Oceanogr. 61, S165–S174. doi:10.1002/lno.10337

Schlesinger, W.H., 1984. Soil organic matter: a source of atmospheric CO2, in: Woodwell, G.M. (Ed.), The Role of Terrestrial Vegetation in the Global Carbon Cycle: Measurement by Remote Sensing. pp. 111–127.

Schmitz, C., Biewald, A., Lotze-Campen, H., Popp, A., Dietrich, J.P., Bodirsky, B., Krause, M., Weindl, I., 2012. Trading more food: Implications for land use, greenhouse gas emissions, and the food system. Glob. Environ. Chang. 22, 189–209. doi:10.1016/j.gloenvcha.2011.09.013

Schnell, S., King, G.M., 1994. Mechanistic analysis of ammonium inhibition of atmospheric methane consumption in forest soils. Appl. Environ. Microbiol. 60, 3514–3521.

Schubert, D., 2011. Boron Oxides, Boric Acid, and Borates, Kirk-Othmer Encyclopedia of Chemical Technology. doi:10.1002/0471238961.0215181519130920.a01.pub3

Schwarzenbach, G., Meier, J., 1958. Formation and investigation of unstable protonation and deprotonation products of complexes in aqueous solution. J. Inorg. Nucl. Chem. 8, 302–312. doi:10.1016/0022-1902(58)80195-5

Seitzinger, S.P., Kroeze, C., Styles, R. V., 2000. Global distribution of N2O emissions from aquatic systems: Natural emissions and anthropogenic effects. Chemosph. - Glob. Chang. Sci. 2, 267–279. doi:10.1016/S1465-9972(00)00015-5

Servais, P., Billen, G., Garnier, J., Idlafkih, Z., Mouchel, J.M., Seidl, M., Meybeck, M., 1998. Le carbone organique, in: Meybeck, M., De Marsily, G., Futsec, F. (Eds.), La Seine En Son Bassin. Fonctionnement Écologique d'un Système Fluvial Anthropisé. Paris, pp. 483–529.

Servais, P., Billen, G., Goncalves, A., Garcia-Armisen, T., 2007. Modelling microbiological water quality in the Seine river drainage network: past, present and future situations. Hydrol. Earth Syst. Sci. Discuss. 11, 1581–1592. doi:10.5194/hessd-4-1153-2007

Servais, P., Billen, G., Hascoët, M.C., 1995. Determination of the biodegradable fraction of dissolved organic matter in waters. Water Res. 21, 445–450. doi:10.1016/0043-1354(87)90192-8

Servais, P., Billen, G., Hascoët, M.C., 1987. Determination of the biodegradable fraction of dissolved organic matter in waters. Water Res. 21, 445–450. doi:10.1016/0043-1354(87)90192-8

Servais, P., Garnier, J., 1993. Contribution of heterotrophic bacterial production to the carbon budget of the river Seine (France). Microb. Ecol. 25, 19–33. doi:10.1007/BF00182127

Servais, P., Garnier, J., Billen, G., Barillier, A., 1991. Servais, P., Garnier, J., Billen, G., & Barillier, A. (1991). Dégradation de la matière organique et dynamique des bactéries hétérotrophes dans la Seine., in: Vernet, J.P. (Ed.), Comte-Rendu CILEF III. pp. 108–11.

Servais, P., Garnier, J., Demarteau, N., Brion, N., Billen, G., 1999. Supply of organic matter and bacteria to aquatic ecosystems through waste water effluents. Water Res. 33, 3521–3531. doi:10.1016/S0043-1354(99)00056-1

Servais, P., Vives-Rego, J., Billen, G., 1992. Survival and mortality of bacteria in natural environments, in: Fry, J.C., Day, M.J. (Eds.), Release of Genetically Engineered and Other Micoorganisms. pp. 100–119.

Sferratore, A., Billen, G., Garnier, J., Smedberg, E., Humborg, C., Rahm, L., 2008. Modelling nutrient fluxes from sub-arctic basins: Comparison of pristine vs. dammed rivers. J. Mar. Syst. 73, 236–249. doi:10.1016/j.jmarsys.2007.10.012

Six, J., Paustian, K., Elliott, E.T., Combrink, C., 2000. Soil Structure and Organic Matter. Soil Sci. Soc. Am. J. 64, 681. doi:10.2136/sssaj2000.642681x

Skiba, U., McTaggart, I.P.P., Smith, K.A.A., Hargreaves, K.J.J., Fowler, D., 1996. Estimates of nitrous oxide emissions from soil in the UK. Energy Convers. Manag. 37, 1303–1308. doi:10.1016/0196-8904(95)00337-1

Slawyk, G., MacIsaac, J.J., 1972. Comparison of two automated ammonium methods in a region of coastal upwelling. Deep. Res. Oceanogr. Abstr. 19, 521–524. doi:10.1016/0011-7471(72)90019-8

Smith, K.., Mctaggart, I.., Tsuruta, H., 1997. Emissions of N2O and NO associated with nitrogen fertilization in intensive agriculture, and the potential for mitigation. Soil Use Manag. 13, 296–304. doi:10.1111/j.1475-2743.1997.tb00601.x

Smitz, J.S., Everbecq, E., Deliège, J.-F., Descy, J.-P., Wollast, R., Vanderborght, J.P., 1997. PEGASE, une méthodologie et un outil de simulation prévisionnelle pour la gestion de la qualité des eaux de surface. Trib. l'eau.

Snyder, C.S., Bruulsema, T.W., Jensen, T.L., Fixen, P.E., 2009. Review of greenhouse gas emissions from crop production systems and fertilizer management effects. Agric. Ecosyst. Environ. 133, 247–266. doi:10.1016/j.agee.2009.04.021

Solagro, 2014. Afterres 2050. Un scénario soutenable pour l'agriculture et l'utilisation des terres en France à l'horizon 2050 60.

Soussana, J.F., Allard, V., Pilegaard, K., Ambus, P., Amman, C., Campbell, C., Ceschia, E., Clifton-Brown, J., Czobel, S., Domingues, R., Flechard, C., Fuhrer, J., Hensen, A., Horvath, L., Jones, M., Kasper, G., Martin, C., Nagy, Z., Neftel, A., Raschi, A., Baronti, S., Rees, R.M., Skiba, U., Stefani, P., Manca, G., Sutton, M., Tuba, Z., Valentini, R., 2007. Full accounting of the greenhouse gas (CO2, N2O, CH4) budget of nine European grassland sites. Agric. Ecosyst. Environ. 121, 121–134. doi:10.1016/j.agee.2006.12.022

Spawn, S.A., Dunn, S.T., Fiske, G.J., Natali, S.M., Schade, J.D., Zimov, N.S., 2015. Summer methane ebullition from a headwater catchment in Northeastern Siberia. Inl. Waters 5, 224–230. doi:10.5268/IW-5.3.845

Springmann, M., Clark, M., Mason-D'Croz, D., Wiebe, K., Bodirsky, B.L., Lassaletta, L., De Vries, W., Vermeulen, S.J., Herrero, M., Carlson, K.M., Jonell, M., Troell, M., DeClerck, F., Gordon, L.J., Zurayk, R., Scarborough, P., Rayner, M., Loken, B., Fanzo, J., Godfray, H.C.J., Tilman, D., Rockström, J., Willett, W., 2018. Options for keeping the food system within environmental limits. Nature. doi:10.1038/s41586-018-0594-0

Stanley, E.H., Casson, N.J., Christel, S.T., Crawford, J.T., Loken, L.C., Oliver, S.K., 2016. The ecology of methane in streams and rivers: Patterns, controls, and global significance. Ecol. Monogr. 86, 146–171. doi:10.1890/15-1027.1

Stanley, E.H., Powers, S.M., Lottig, N.R., Buffam, I., Crawford, J.T., 2012. Contemporary changes in dissolved organic carbon (DOC) in human-dominated rivers: Is there a role for DOC management? Freshw. Biol. 57, 26–42. doi:10.1111/j.1365-2427.2011.02613.x

Staufer, J., Broquet, G., Bréon, F.M., Puygrenier, V., Chevallier, F., Xueref-Rémy, I., Dieudonné, E., Lopez, M., Schmidt, M., Ramonet, M., Perrussel, O., Lac, C., Wu, L., Ciais, P., 2016. The first 1-year-long estimate of the Paris region fossil fuel CO2 emissions based on atmospheric inversion. Atmos. Chem. Phys. 16, 14703–14726. doi:10.5194/acp-16-14703-2016

Strahler, A.N., 1957. Quantitative Analysis of Watershed Geomorphology. Geophys. Union Trans. 38, 913–920. doi:10.1029/TR038i006p00913

Strahler, A.N., 1952. Hypsometric (area-altitude) analysis of erosional topography. Bull. Geol. Soc. Am. 63, 1117–1142. doi:10.1130/0016-7606(1952)63

Sutton, M., Howard, C., Erisman, J., 2011. The European nitrogen assessment: sources, effects and policy perspectives, Cambridge University Press. doi:10.1017/CBO9780511976988

Tanaka, K., Kriegler, E., Bruckner, T., Georg, H., Knorr, W., Raddatz, T., 2007. Aggregated Carbon Cycle, Atmospheric Chemistry, and Climate Model (ACC2) – description of the forward and inverse modes. Reports Earth Syst. Sci. Max Planck Institue Meteorol. Hambg. 188.

Tate, K.R., 2015. Soil methane oxidation and land-use change - from process to mitigation. Soil Biol. Biochem. doi:10.1016/j.soilbio.2014.10.010

Telmer, K., Veizer, J., 1999. Carbon fluxes, pCO2 and substrate weathering in a large northern river basin, Canada: Carbon isotope perspectives. Chem. Geol. 159, 61–86. doi:10.1016/S0009-2541(99)00034-0

Teodoru, C.R., 2009. Patterns in pCO2 in boreal streams and rivers of northern Quebec , Canada , Global Biogeochem. doi:10.1029/2008GB003404

Teodoru, C.R., Del Giorgio, P.A., Prairie, Y.T., Camire, M., 2009. Patterns in pCO2 in boreal streams and rivers of northern Quebec, Canada. Global Biogeochem. Cycles 23, 1–11. doi:10.1029/2008GB003404

Teodoru, C.R., Nyoni, F.C., Borges, A. V., Darchambeau, F., Nyambe, I., Bouillon, S., 2015. Dynamics of greenhouse gases (CO2, CH4, N2O) along the Zambezi River and major tributaries, and their importance in the riverine carbon budget. Biogeosciences 12, 2431–2453. doi:10.5194/bg-12-2431-2015

Thieu, V., Billen, G., Garnier, J., 2009. Nutrient transfer in three contrasting NW European watersheds: the Seine, Somme, and Scheldt Rivers. A comparative application of the Seneque/Riverstrahler model. Water Res. 43, 1740–54. doi:10.1016/j.watres.2009.01.014

Thieu, V., Silvestre, M., Billen, G., Garnier, J., Passy, P., Lassaletta, L., Gilles, B., Passy, P., Lassaletta, L., 2015. Nutrient transfer in aquatic continuum and delivery to coastal zone: rising up the challenge of a generic application of the Riverstrahler ecological model to the watershed domain of the European North Atlantic Ocean., in: 2nd International Conference: Integrative Sciences and Sustainable Development of Rivers. Lyon - France, p. 2.

Thieu, V., Silvestre, M., G., B., J., G., Passy, P., Lassaletta, L., 2015. Nutrient transfer in aquatic continuum and delivery to coastal zone: rising up the challenge of a generic application of the Riverstrahler ecological model to the watershed domain of the European North Atlantic Ocean, in: 2nd International Conference: Integrative Sciences and Sustainable Development of Rivers. Lyon - France. p. 2.

Tiedje, J.M., 1988a. Ecology of denitrification and dissimilatory nitrate reduction to ammonium. Environ. Microbiol. Anaerobes 179–244. doi:10.1016/j.jacc.2011.09.010

Tiedje, J.M., 1988b. Ecology of denitrification and dissimilatory nitrate reduction to ammonium. Environ. Microbiol. Anaerobes 179–244. doi:10.1016/j.jacc.2011.09.010

Tranvik, L.J., Jansson, M., 2002. Climate change (Communication arizing): Terrestrial export of organic carbon. Nature 415, 861. doi:10.1038/415861a

Tsivoglou, E.C., Neal, L.A., 1976. Tracer Measurement of Reaeration: III. Predicting the Reaeration Capacity of Inland Streams. Water Pollut. Control Fed. 48, 2669–2689. doi:10.2307/25040082

Turner, P.A., Griffis, T.J., Lee, X., Baker, J.M., Venterea, R.T., Wood, J.D., 2015. Indirect nitrous oxide emissions from streams within the US Corn Belt scale with stream order. Proc. Natl. Acad. Sci. 112, 201503598. doi:10.1073/pnas.1503598112

UNCED, 1992. Earth Summit. Agenda 21: The United Nations Programme of Action from Rio. Agenda 21, 351. doi:10.1007/s11671-008-9208-3

UNESCO, 1994. Protocols for the joint global ocean flux study (JGOFS) core measurements. IOC Man. Guid. No.29 180. doi:10013/epic.27912

UNFCCC, 1997. Kyoto Protocol to the United Nations Framework Convention on Climate Change adopted at COP3 in Kyoto.

van Geldern, R., Schulte, P., Mader, M., Baier, A., Barth, J.A.C., 2015. Spatial and temporal variations of pCO2, dissolved inorganic carbon and stable isotopes along a temperate karstic watercourse. Hydrol. Process. 29, 3423–3440. doi:10.1002/hyp.10457

van Heuven, S., Pierrot, D., Rae, J.W.B., Lewis, E., Wallace, D.W.R., 2011. MATLAB Program Developed for CO2 System Calculations. ORNL/CDIAC-105b. ORNL/CDIAC-105b. Carbon Dioxide Inf. Anal. Center, Oak Ridge Natl. Lab. U.S. Dep. Energy, Oak Ridge, Tennessee. doi:10.1017/CBO9781107415324.004

Vanderborght, J.P., Wollast, R., Loijens, M., Regnier, P., 2002. Application of a transport-reaction model to the estimation of biogas fluxes in the Scheldt Estuary. Biogeochemistry 59, 207–237. doi:10.1023/A:1015573131561

Vannote, R.L., Minshall, G.W., Cummins, K.W., Sedell, J.R., Cushing, C.E., 1980. The River Continuum Concept. Can. J. Fish. Aquat. Sci. 37, 130–137. doi:10.1139/f80-017

Venkiteswaran, J.J., Schiff, S.L., Wallin, M.B., 2014. Large carbon dioxide fluxes from headwater boreal and sub-boreal streams. PLoS One 9, 22–25. doi:10.1371/journal.pone.0101756

Verhoeven, J.T.A., Sorrell, B.K., 2010. Plant adaptations and microbial processes in wetlands. Ann. Bot. 105, 127. doi:10.1093/aob/mcp266

Vermorel, M., Jouany, J.P., Eugène, M., Sauvant, D., Noblet, J., Dourmad, J.Y., 2008. Evaluation quantitative des émissions de méthane entérique par les animaux d'élevage en 2007 en France. Prod. Anim. 21, 403–418.

Vilain, G., Garnier, J., Decuq, C., Lugnot, M., 2014. Nitrous oxide production from soil experiments: Denitrification prevails over nitrification. Nutr. Cycl. Agroecosystems 98, 169–186. doi:10.1007/s10705-014-9604-2

Vilain, G., Garnier, J., Passy, P., Silvestre, M., Billen, G., 2012. Budget of N2O emissions at the watershed scale: Role of land cover and topography (the Orgeval basin, France). Biogeosciences 9, 1085–1097. doi:10.5194/bg-9-1085-2012

Vilain, G., Garnier, J., Tallec, G., Cellier, P., 2010. Effect of slope position and land use on nitrous oxide (N2O) emissions (Seine Basin, France). Agric. For. Meteorol. 150, 1192–1202. doi:10.1016/j.agrformet.2010.05.004

Vilain, G., Garnier, J., Tallec, G., Tournebize, J., 2012. Indirect N2O emissions from shallow groundwater in an agricultural catchment (Seine Basin, France). Biogeochemistry 111, 253–271. doi:10.1007/s10533-011-9642-7

Vilmin, L., Flipo, N., Escoffier, N., Groleau, A., 2018. Estimation of the water quality of a large urbanized river as defined by the European WFD: what is the optimal sampling frequency? Environ. Sci. Pollut. Res. 25, 23485–23501. doi:10.1007/s11356-016-7109-z

Vilmin, L., Flipo, N., Escoffier, N., Rocher, V., Groleau, A., 2016. Carbon fate in a large temperate human-impacted river system: Focus on benthic dynamics. Global Biogeochem. Cycles 30, 1086–1104. doi:10.1002/2015GB005271

Vilmin, L., Flipo, N., Fouquet, C. De, Poulin, M., 2015. Science of the Total Environment Pluri-annual sediment budget in a navigated river system : The Seine River (France). Sci. Total Environ. 502, 48–59. doi:10.1016/j.scitotenv.2014.08.110

Volta, C., Arndt, S., Savenije, H.H.G., Laruelle, G.G., Regnier, P., 2014. C-GEM (v 1.0): A new, cost-efficient biogeochemical model for estuaries and its application to a funnel-shaped system. Geosci. Model Dev. 7, 1271–1295. doi:10.5194/gmd-7-1271-2014

Volta, C., Laruelle, G.G., Arndt, S., Regnier, P., 2016a. Linking biogeochemistry to hydro-geometrical variability in tidal estuaries : a generic modeling approach 991–1030. doi:10.5194/hess-20-991-2016

Volta, C., Laruelle, G.G., Regnier, P., 2016b. Regional carbon and CO2budgets of North Sea tidal estuaries. Estuar. Coast. Shelf Sci. 176, 76–90. doi:10.1016/j.ecss.2016.04.007

Vörösmarty, C.J., Meybeck, M., Fekete, B., Sharma, K., Green, P., Syvitski, J.P.M., 2003. Anthropogenic sediment retention: Major global impact from registered river impoundments. Glob. Planet. Change 39, 169–190. doi:10.1016/S0921-8181(03)00023-7

Wallin, M.B., Öquist, M.G., Buffam, I., Billett, M.F., Nisell, J., Bishop, K.H., 2011. Spatiotemporal variability of the gas transfer coefficient (KCO2) in boreal streams: Implications for large scale estimates of CO 2 evasion. Global Biogeochem. Cycles 25. doi:10.1029/2010GB003975

Wang, X., He, Y., Yuan, X., Chen, H., Peng, C., Yue, J., Zhang, Q., Diao, Y., Liu, S., 2017. Greenhouse gases concentrations and fluxes from subtropical small reservoirs in relation with watershed urbanization. Atmos. Environ. 154, 225–235. doi:10.1016/j.atmosenv.2017.01.047

Wanninkhof, R., 1992. Relationship Between Wind Speed and Gas Exchange. J. Geophys. Res. 97, 7373–7382. doi:10.1029/92JC00188

Wanninkhof, R., 1985. Kinetic fractionation of the carbon isotopes 13C and 12C during transfer of CO 2from air to seawater. Tellus B 37B, 128–135. doi:10.1111/j.1600-0889.1985.tb00061.x

Weiss, R.F., 1981. Determinations of carbon dioxide and methane by dual catalyst flame ionization chromatography and nitrous oxide by electron capture chromatography. J. Chromatogr. Sci. 19, 611–616. doi:10.1093/chromsci/19.12.611

Weiss, R.F., 1974. Carbon dioxide in water and seawater: the solubility of a non-ideal gas. Mar. Chem. 2, 203–215. doi:10.1016/0304-4203(74)90015-2

Weiss, R.F., Price, B.A., 1980. Nitrous oxide solubility in water and seawater. Mar. Chem. 8, 347–359. doi:10.1016/0304-4203(80)90024-9

Westhoek, H., Lesschen, J.P., Rood, T., Wagner, S., De Marco, A., Murphy-Bokern, D., Leip, A., van Grinsven, H., Sutton, M.A., Oenema, O., 2014. Food choices, health and environment: Effects of cutting Europe's meat and dairy intake. Glob. Environ. Chang. 26, 196–205. doi:10.1016/j.gloenvcha.2014.02.004

Whitehead, P.G., Williams, R.J., Lewis, D.R., 1997. Quality simulation along river systems (QUASAR): Model theory and development. Sci. Total Environ. 194–195, 447–456. doi:10.1016/S0048-9697(96)05382-X

Wickland, K.P., Neff, J.C., Aiken, G.R., 2007. Dissolved organic carbon in Alaskan boreal forest: Sources, chemical characteristics, and biodegradability. Ecosystems 10, 1323–1340. doi:10.1007/s10021-007-9101-4

Wilke, C.R., Chang, P., 1955. Correlation of diffusion coefficients in dilute solutions. AIChE J. 1, 264–270. doi:10.1002/aic.690010222

Wrage-Mönnig, N., Horn, M.A., Well, R., Müller, C., Velthof, G., Oenema, O., 2018. The role of nitrifier denitrification in the production of nitrous oxide revisited. Soil Biol. Biochem. doi:10.1016/j.soilbio.2018.03.020

Wu, L., Broquet, G., Ciais, P., Bellassen, V., Vogel, F., Chevallier, F., Xueref-Remy, I., Wang, Y., 2016. What would dense atmospheric observation networks bring to the quantification of city CO2emissions? Atmos. Chem. Phys. 16, 7743–7771. doi:10.5194/acp-16-7743-2016

Xia, X., Liu, T., Yang, Z., Michalski, G., Liu, S., Jia, Z., Zhang, S., 2017. Enhanced nitrogen loss from rivers through coupled nitrification-denitrification caused by suspended sediment. Sci. Total Environ. 579, 47–59. doi:10.1016/j.scitotenv.2016.10.181

Yang, C., Telmer, K., Veizer, J., 1996. Chemical dynamics of the "St. Lawrence" riverine system: δDH2O, δ18OH2O, δ13CDIC, δ34Ssulfate, and dissolved87Sr/86Sr. Geochim. Cosmochim. Acta 60, 851–865. doi:10.1016/0016-7037(95)00445-9

Yao, G., Gao, Q., Wang, Z., Huang, X., He, T., Zhang, Y., Jiao, S., Ding, J., 2007. Dynamics of CO2 partial pressure and CO2 outgassing in the lower reaches of the Xijiang River, a subtropical monsoon river in China. Sci. Total Environ. 376, 255–266. doi:10.1016/j.scitotenv.2007.01.080

Yu, Z., Deng, H., Wang, D., Ye, M., Tan, Y., Li, Y., Chen, Z., Xu, S., 2013. Nitrous oxide emissions in the Shanghai river network: Implications for the effects of urban sewage and IPCC methodology. Glob. Chang. Biol. 19, 2999–3010. doi:10.1111/gcb.12290

Zedler, J.B., Kercher, S., 2005. Wetland Resources: Status, Trends, Ecosystem Services, and Restorability. Annu. Rev. Environ. Resour. 30, 39–74. doi:10.1146/annurev.energy.30.050504.144248

Zeebe, R., Wolf-Gladrow, D., 2001. CO2 in Seawater-Equilibrium, Kinetics, Isotopes. Elsevier 100. doi:10.1016/S0422-9894(01)80002-7

Zeng, F.W., Masiello, C.A., 2010. Sources of CO2 evasion from two subtropical rivers in North America. Biogeochemistry 100, 211–225. doi:10.1007/s10533-010-9417-6

Zervas, G., Tsiplakou, E., 2012. An assessment of GHG emissions from small ruminants in comparison with GHG emissions from large ruminants and monogastric livestock. Atmos. Environ. doi:10.1016/j.atmosenv.2011.11.039

Zhao, Y., Wu, B.F., Zeng, Y., 2013. Spatial and temporal patterns of greenhouse gas emissions from Three Gorges Reservoir of China Earth System 1219–1230. doi:10.5194/bg-10-1219-2013

Zheng, X., Wang, M., Wang, Y., Shen, R., Gou, J., Li, J., Jin, J., Li, L., 2000. Impacts of soil moisture on nitrous oxide emission from croplands: A case study on the rice-based agro-ecosystem in Southeast China. Chemosph. - Glob. Chang. Sci. 2, 207–224. doi:10.1016/S1465-9972(99)00056-2

Zhou, J.B., Jiang, M.M., Chen, G.Q., 2007. Estimation of methane and nitrous oxide emission from livestock and poultry in China during 1949-2003. Energy Policy 35, 3759–3767. doi:10.1016/j.enpol.2007.01.013

Zimmermann, J., Carolan, R., Forrestal, P., Harty, M., Lanigan, G., Richards, K.G., Roche, L., Whitfield, M.G., Jones, M.B., 2018. Assessing the performance of three frequently used biogeochemical models when simulating N2O emissions from a range of soil types and fertiliser treatments. Geoderma 331, 53–69. doi:10.1016/j.geoderma.2018.06.004

Zimov, S. a, Schuur, E. a G., 2006. Permafrost and the Global Carbon Budget. Science (80-.). 312, 1612–1613. doi:10.1126/science.1128908

Carbon cycling across the human-impacted Seine River basin:

from the modeling of carbon dioxide outgassing to the assessment of greenhouse gas emissions

Audrey Marescaux

Several recent studies have highlighted significant fluxes of carbon dioxide (CO_2) from inland waters in the global carbon cycling. The first main objective of this thesis was to quantify and understand carbon dynamics in the Seine River basin, which is deeply impacted by human activities. For this purpose a new inorganic carbon (IC) module was implemented in the biogeochemical Riverstrahler model, to simulate spatial and temporal variations in carbon forms in the drainage work. A second major objective was to size both aquatic and terrestrial emissions as a part of a joint assessment of three main GHGs (CO_2, methane –CH_4, and nitrous oxide –N_2O).

Field campaigns in rivers draining various land uses in different hydrological seasons, showed a supersaturation in CO_2 of the Seine hydrosystem leading to CO_2.emissions to the atmosphere. The main factor controlling the CO_2 partial pressure (pCO_2) was the concentration of dissolved organic carbon (DOC) (R^2=0.56, n=119, $p<0.05$), modulated by hydro-climatic conditions and groundwater contribution. In small streams, DOC concentrations were dependent on the soil organic carbon stock. For the main stem, a long-term analysis (1970-2015) showed that pCO_2 tracked urban pollution, decreasing from the 2000s after improvement of wastewater treatment.

The validation of the IC module newly implemented in Riverstrahler showed that IC inputs to the Seine River dominated the overall carbon budget (1138 ktC yr^{-1} on average for the period 2010-2013) of which less than 2% was produced from biogeochemical processes (27 ktC yr^{-1}). In addition, CO_2 outgassing represented 30% of IC outputs while exports to the estuary represented 69% of IC outputs. OC inputs were comparatively lower, accounting only for 104 ktC yr^{-1}. Analysis of the biogeochemical processes of the Seine River showed a negative net ecosystem production (NEP), the river being mostly heterotrophic.

In order to complete the modeling of the fate of carbon in the Seine River, the Riverstrahler model was combined with the estuarine C-GEM model, towards an integrated approach to the Land-to-Ocean Aquatic continuum. Representing 34% of the river mirror area, the estuary thus contributes ~23% of the CO_2 emitted from the whole estuary-river aquatic continuum (estimated at 445 kt C for the year 2010).

In addition, analyses of available institutional databases and measurements of other GHGs (CH_4 and N_2O) enabled estimation of aquatic emissions at 3.7% of the Seine basin total emissions (2,276 ktCO_2 equivalent yr^{-1}), dominated by CO_2 (95.3%), while agricultural (14,295 ktCO_2 equivalent yr^{-1}) and urban emissions (44,713 ktCO_2 equivalent yr^{-1}) accounted for 23.3% and 73.0%, respectively. A historical reconstruction of agricultural emissions for the whole of France (1850-2014) estimated that, among the 114,000 ktCO_2 equivalent yr^{-1} emitted by the agricultural sector, 22% were represented by CO_2, 49% by CH_4 and 29% by N_2O. Finally, two contrasting scenarios were explored (horizon 2040). The first, characterized by the current trend towards specialization and intensification, predicted an almost 1.5-fold increase in agricultural emissions. While the second, characterized by a transition to organic agriculture and dietary change, would reduce current emissions by about 50%.

Keywords: *Carbon cycling, CO_2, GHG emissions, aquatic ecosystem modeling, Seine River basin.*